Alma Mater Studiorum - Università di Bologna

DOTTORATO DI RICERCA IN

FISICA

Ciclo 34

Settore Concorsuale: 02/A2 - FISICA TEORICA DELLE INTERAZIONI FONDAMENTALI

Settore Scientifico Disciplinare: FIS/02 - FISICA TEORICA, MODELLI E METODI MATEMATICI

MODULI STABILISATION AND THE STATISTICS OF LOW-ENERGY PHYSICS IN THE STRING LANDSCAPE

Presentata da: Igor Broeckel

Coordinatore Dottorato

Michele Cicoli

Supervisore

Michele Cicoli

Esame finale anno 2022

Cogito, ergo sum.

-René Descartes

ACKNOWLEDGEMENTS

I would like to thank my collaborators and colleagues: Michele Cicoli, Anshuman Maharana, Kajal Singh, Kuver Sinha, Rouzbeh Allahverdi, Jacek Osinski and Veronica Guidetti, who tought me everything necessary to realize this work.
I am especially grateful to my supervisor Michele Cicoli, this work would not have been possible without his constant support and advice.

I am particularly grateful to my family: Olga, Viktor and Junna. I would not be writing these lines, if it would not have been for them, and of course my friends: Kürbis, Nici, Martin and Ricci.

I am also thanking the Institute of Advanced Studies, my colleagues from the institute and director Dario Braga. The institute created an inspiring academic environment, which allowed me to focus entirely on my studies.

ABSTRACT

In this thesis we present a detailed analysis of the statistical properties of the type IIB flux landscape of string theory. We focus primarily on models constructed via the Large Volume Scenario (LVS) and KKLT and study the distribution of various phenomenologically relevant quantities. First, we compare our considerations with previous results and point out the importance of Kähler moduli stabilisation, which has been neglected in this context so far. We perform different moduli stabilisation procedures and compare the resulting distributions. To this end, we derive the expressions for the gravitino mass, various quantities related to axion physics and other phenomenologically interesting quantities in terms of the fundamental flux dependent quantities g_s, W_0 and $\mathfrak{n}$, the parameter which specifies the nature of the non-perturbative effects. Exploiting our knowledge of the distribution of these fundamental parameters, we can derive a distribution for all the quantities we are interested in. For models that are stabilised via LVS we find a logarithmic distribution, whereas for KKLT and perturbatively stabilised models we find a power-law distribution. We continue by investigating the statistical significance of a newly found class of KKLT vacua and present a search algorithm for such constructions. We conclude by presenting an application of our findings. Given the mild preference for higher scale supersymmetry breaking, we present a model of the early universe, which allows for additional periods of early matter domination and ultimately leads to rather sharp predictions for the dark matter mass in this model. We find the dark matter mass to be in the very heavy range $m_\chi \sim 10^{10} - 10^{11}$ GeV.

Contents

Part I

INTRODUCTION

What is the universe made of? Despite the briefity and simplicity of this question, the answer is still as elusive as it was hundreds of years ago. Interestingly, today's most modern and sophisticated attempts to an answer, are not much different from the very first attempts. In essence the idea is: *It is made of small things.* The ancient greeks incorporated this concept in their explanation of reality, most famously in Plato's *atomism.* According to this idea, the world is build out of four geometrical solids, which represent the elements fire (tetrahedron), air (octahedron), water (icosahedron) and earth (cube). All these geometrical structures can be decomposed in terms of triangles, which allow for the notion of transforming elements into each other.
Surprisingly, the key ingredients for a succesfull description of our world are already present in this simple picture. The first concept is based on the following heuristic argument. If we divide a piece of matter in two parts and keep dividing the remaining parts, logic dictates that we must reach an end eventually. Hence, all matter is made of fundamental building blocks. They are the smallest entities in our universe and have no further substructure. The second idea is that these entities are *mathematical* in their nature. In Plato's picture they are represented as geometrical objects. In the modern viewpoint, as we will see later, the fundamental building blocks are described by *irreducible representations* of the Poincaré group. It is interesting to note that the realization of the deep connection between mathematics and the physical world dates back as early as roughly 400 BC.
The modern form of Plato's atomism is called *Standard Model of Particle Physics* (SM) and will be described in detail in the next section. The successes of the SM are numerous and at this point we want to highlight only one example: the prediction of the anomalous magnetic moment.
The 'classical' prediction for the magnetic moment can be computed with the Dirac equation and is given by $g = 2$. This result, however, differs from the observed value for instance for the electron by a small fraction of a percent [5]. The anomalous part is due to quantum mechanical corrections and can be computed within the framework of *quantum electrodynamics* (QED). By evaluating not only the tree level Feynman diagrams but also higher order loop contributions, it is possible to compute the expected value of the anomalous magnetic moment. The QED prediction agrees with the experimentally meassured value to more than 10 significant digits [5, 6], making it the most accurate theory of all time.

What is the origin of the universe? An equally challenging question that remains difficult to answer. However, the most notable progress in this domain was made in the last century. The development of Einstein's *General Relativity* enabled us to describe the evolution of the universe in astonishing detail. The discovery of the expansion of our universe lead to the best answer we have so far: *It all started with a big bang.*
The now so called *Standard Model of Cosmology*, which will be explored in detail in the next section, describes the universe with incredible precision. The detection of gravitational waves by LIGO and Virgo [7] and the creation of the very first image of

a black hole by the Event Horizon collaboration [8] are only the most recent successes of the model.

Given the great achievments of the Standard Models one could think that there is nothing left to do and we have unveiled the underlying laws of nature. However, despite the success, there are still many open questions. The most prominent and urgent problems are the following:

- *Hierarchy problem*
  Generally speaking a hierarchy problem occurs when the effective value of a physical parameter differs drastically from its fundamental value. The two values are connected via *renormalization*, which essentially is a way to quantify the quantum corrections that modify the fundamental value. For most quantities the values of the effective and fundamental parameters are very close. For some quantites, however, they differ drastically which is an indication for a very delicate and precise cancelation between the higher order loop contributions. This precise cancelation seems very unnatural and demands an explenation.
  In the context of the SM the problem manifests itself in the question why the Higgs mass is not closer to the Planck scale. Given that the Higgs is a scalar particle, it is sensitive to ultraviolett physics, hence one would expect its mass to be at a much higher scale.

- *Number of families*
  As we will see later in more detail, the SM incorporates 3 families of elementary particles. However, this number is put in by hand and not derived.

- *Neutrino mass*
  According to the SM neutrinos are massless particles. However, the observation of neutrino oscillation by the Super-Kamiokande observatory [9], which was awarded with the Nobel prize in 2015, implies massive neutrinos.

- *Cosmological constant problem*
  In 1917, Einstein introduced the cosmological constant term to his field equations in order to allow for an eternally static universe. This term was set such that it would balance out the gravitational dynamics of the universe. However, the observation of the expansion of our universe by Edwin Hubble led to the realization that universe is not static.
  In 1998, it was realized that the universe is expanding in an *accelerated* fashion [10, 11] implying a positive cosmological constant. The most intuitive physical explanation for the cosmological constant is the vacuum energy that can be computed via *quantum field theory* (QFT). According to QFT, the vacuum is filled with quantum fields that represent the particle content of the SM. Despite

being in their ground state, the fields fluctuate around this minimum resulting in a non-zero vacuum energy. Theoretical computations of this quantity result in a value that differs from the observed value by 120 orders of magnitude.

- *Dark matter and dark energy*
  According observations, only roughly 5% of the energy content of our universe is due to baryonic matter. The rest is attributed to *dark energy* (70%) and *dark matter* (25%). The nature of DE and DM is still a mystery.

- *Matter-Antimatter asymmetry*
  The matter-antimatter asymmetry is the observed imbalance of baryonic matter and anti-baryonic matter. In principle, the big bang should have produced an equal amount of matter and antimatter. The asymmetry between these two forms of matter is not explained by the SM.

- *Quantum Gravity*
  Perhaps the biggest challenge in theoretical physics is to formulate a quantum theory of gravity. Standard Einstein gravity is non-renormalizable due to its dimensionfull coupling G, which is Newton's constant. A perturbative expansion in G would require an infinite amount of counter terms, making the theory loose its predictive power. Hence, GR is not suited to be quantized in the standard QFT approach and new paradigm is needed.

In this work we will address some of these problems within the framework of *string theory* (ST), which is the most promising candidate for a unified languange of gravity and quantum mechanics.
In the introduction part, we start with a summary of the standard model of particle physics and the standard model of cosmology. Then, we introduce some basic concepts of string theory that are necessary in order to understand the main part of this work.
In the second part, we present a detailed study of the statistical properties of the solution space of string theory called the *landscape*. We finish by introducing an alternative model for the early universe, which is motivated by our findings and recent experimental observations.

Chapter 1

Standard Model

In this chapter we give a brief introduction to the standard models of particle physics and cosmology. Here, we follow primarily [12, 13, 14, 15, 16] and refer to these references for more information on the presented subjects.

1.1 Particle Physics

Arguebly the most important concept in modern physics is the notion of symmetries. A symmetry is present when physical obersvations and their underlying laws are invariant with respect to the transformation associated with that symmetry. A simple example is *Galilean invariance*, which states that the laws of motion are invariant under rotations and translations.
A closely related idea is the concept of a *conservation law*. It is intuitively clear that if we perform a transformation and the physicial system does not change, that there must be some sort of preservation of information. This intuition manifests itself in the famous *Noether theorem*, which states that for every continous symmetry of the action there exists an associated conservation law. For instance, time translation invariance is associated with conservation of energy and spatial translation invariance is connected to conservation of momentum. The same principle is at the heart of our concept of an elementary particle. We *define* an elementary particle to be an entity which does not change some properties with respect to a particular symmetry. The underlying fundamental symmetry group is called the *Poincare group* and the properties that define an *irreducible representation* of that group are *mass* and *spin*. The fermionic part of the SM, which can be defined in this way, is summarized in the Table 1.1

Generation	Lepton	Quark
1^{st}	electron e-neutrino	up down
2^{nd}	muon μ-neutrino	charm strange
3^{rd}	tau τ-neutrino	top bottom

Table 1.1: Quarks and leptons of the standard model.

We know two different types of fermions, leptons and quarks. Both types exist in different *variations* called *generations* or *families*. The masses of the particles in Table 1.1 increase with the generation number.
The next important ingredient is the notion of *interactions*. Just like the particles themself, the interactions between them are defined in terms symmetries. The symmetry group that is used to build the SM is

$$SU(3)_C \times SU(2)_L \times U(1)_Y. \tag{1.1}$$

The first part of (1.1) describes *quantum chromodynamics* (QCD), whereas the second and third part describe the *electroweak* force. The labels C, L and Y stand for color, left-handed and hypercharge respectively. Each particle in the SM spectrum has a particular transformation property with respect to the symmetry group. Denoting quarks and leptons of different generations as Q_i and L_i we can summarize the transformation properties as follows

$$Q_i \equiv \begin{pmatrix} u_{L_i} \\ d_{L_i} \end{pmatrix} \sim (3, 2, \frac{1}{6}), \quad L_i \equiv \begin{pmatrix} e_{L_i} \\ \nu_{L_i} \end{pmatrix} \sim (1, 2, -\frac{1}{2}) \tag{1.2}$$

$$U_i \equiv u_{R_i} \sim (\bar{3}, 1, \frac{2}{3}) \tag{1.3}$$

$$D_i \equiv d_{R_i} \sim (\bar{3}, 1, -\frac{1}{3}) \tag{1.4}$$

$$E_i \equiv e_{R_i} \sim (1, 1, -1). \tag{1.5}$$

The first number describes the transformation with respect to $SU(3)_C$, the second with respect to $SU(2)_L$ and the third number is the $U(1)_Y$ charge. For instance, this implies that quarks transform as triplets under $SU(3)$, whereas leptons transform as singlets.
Note, we introduced the additional labels L_i and R_i, which stand for *left-handed* and *right-handed* and $i \in \{1, 2, 3\}$ stands for the 3 generations. Parity conservation was long believed to be conserved, but was shown in 1957 [17] to be violated by the weak force. This observation has far reaching consequenses, namely that there is a natural distinction between left and right, i.e. a mirror image of our world is physically different from the original world. In the SM this result is encoded in the following way. The $SU(2)_L$ part of the gauge group distinguishes left- and right-handed particles.

Left-handed particles transform as doublets, whereas right-handed versions of these particles transform as singlets. One important observation, is that there are no right-handed neutrinos in the SM rendering the left-handed versions massless.
In addition to the fermionic particle content the SM also hosts a scalar particle called the *Higgs boson*

$$H \equiv \begin{pmatrix} \phi^+ \\ \phi^0 \end{pmatrix} \sim (1, 2, \frac{1}{2}). \tag{1.6}$$

The Higgs is responsible for the spontaneous symmetry breaking

$$SU(2)_L \times U(1)_Y \to U(1)_{em} \tag{1.7}$$

via the *Higgs mechanism*, which generates mass terms for the SM particles[1].
However, in order for the full SM gauge group to be a consistent local symmetry, we need to introduce gauge bosons. The gauge bosons of the srong interactions are the *gluons* and will be denoted as G^A_μ with $A \in \{1, ..., 8\}$, the $SU(2)$ gauge bosons are written as W^I_μ with $I \in \{1, 2, 3\}$ and the $U(1)_Y$ gauge field is given by B_μ.
The full SM lagrangian is given by

$$\mathcal{L}_{SM} = \mathcal{L}_F + \mathcal{L}_G + \mathcal{L}_Y + \mathcal{L}_\phi. \tag{1.8}$$

The first term encodes the fermionic content of the SM and is given by

$$\mathcal{L}_F = i\bar{\Psi}\gamma^\mu \mathcal{D}_\mu \Psi, \tag{1.9}$$

here the γ^μ are the usual Dirac gamma matrices and we denote all the fermions collectively as

$$\Psi = (Q_i, U_i, D_i, L_i, E_i), \tag{1.10}$$

and $\bar{\Psi}$ is the usual Dirac conjugate. The covariant derivative contains also the bosonic fields in order to ensure gauge invariance

$$\mathcal{D}_\mu = \partial_\mu - ig_s G^A_\mu \lambda^A - i\frac{g}{2} W^I_\mu \tau^I - ig' B_\mu Y_W. \tag{1.11}$$

The $SU(3)_C$, $SU(2)_L$ and $U(1)_Y$ coupling constants are given by g_s, g and g'. In the second term, the λ^A are the Gell-Mann matrices, the generators of the color group. In the third term, the τ^I are the Pauli matrices, the generators of $SU(2)$. In the last term, Y_W is the weak hypercharge.
The second term in (1.8) describes the kinetic part of the gauge fields and is given by

$$\mathcal{L}_G = -\frac{1}{4} G^A_{\mu\nu} G^{\mu\nu A} - \frac{1}{4} W^I_{\mu\nu} W^{\mu\nu I} - \frac{1}{4} B_{\mu\nu} B^{\mu\nu}, \tag{1.12}$$

[1] Neutrinos are an exception in this process.

where the field strengths are defined as

$$G^A_{\mu\nu} = \partial_\mu G^A_\nu - \partial_\nu G^A_\mu + g_s f_{ABC} G^B_\mu G^C_\nu \tag{1.13}$$

$$W^I_{\mu\nu} = \partial_\mu W^I_\nu - \partial_\nu W^I_\mu + g f_{IJK} W^J_\mu W^K_\nu \tag{1.14}$$

$$B_{\mu\nu} = \partial_\mu B_\nu - \partial_\nu B_\mu. \tag{1.15}$$

Note the additional terms proportional to f_{ABC} and f_{IJK}. These are the structure constants of $SU(3)_C$ and $SU(2)_L$, which parametrize their non-abelian property. The third term in (1.8) represents the Yukawa interactions, which parametrize the interaction of the fermions with the Higgs and is responsible for the fermion mass generation

$$\mathcal{L}_Y = h^u_{ij} \bar{Q}_i U_j \tilde{H} + h^d_{ij} \bar{Q}_i D_j H + h^e_{ij} \bar{L}_i E_j H + h.c. \tag{1.16}$$

with $\tilde{H} = i\sigma^2 H^*$ and the Yukawa couplings $h^u_{ij}, h^d_{ij}, h^e_{ij}$. The last part of the SM lagrangian represents the scalar content

$$\mathcal{L}_S = (\mathcal{D}_\mu H)^\dagger \mathcal{D}^\mu H - V(H), \tag{1.17}$$

with the famous Higgs potential

$$V(H) = \mu^2 H^\dagger H + \lambda \left(H^\dagger H\right)^2. \tag{1.18}$$

As mentioned before, this part of the lagrangian is responsible for the mass generations of the SM particles and the spontaneous breaking of the electroweak theory. In order to realize a scenario, which allows for spontaneous symmetry breaking of the electroweak part, we need to set $\mu^2 < 0$ in (1.18). For this potential, the vacuum ist not located at $H = \begin{pmatrix} 0 \\ 0 \end{pmatrix}$. Instead, we have an infinite amount of vacua oriented around the origin. We can chose the so-called *unitary gauge* and set the vacuum to

$$H = H_0 = \frac{1}{\sqrt{2}} \begin{pmatrix} 0 \\ v + h \end{pmatrix}. \tag{1.19}$$

Where h is the fluctuation around the minimum and represents the physical Higgs boson. Combining this Higgs vacuum doublet with the scalar part of the Lagrangian (1.17) and the covariant derivative (1.11), we can work out the expressions and masses for the physical gauge fields W^+, W^-, Z and γ and their interaction with the Higgs. It is straightforward to see that the charged and massive gauge fields W^+ and W^- are a linear combination of W^1 and W^2

$$W^\pm = \frac{1}{\sqrt{2}}(W^1 \mp W^2). \tag{1.20}$$

The massless photon γ and the massive Z boson are a combination of W^3 and B_μ

$$A_\mu = \frac{1}{\sqrt{g^2 + g'^2}} \left(g' W_3 + g B_\mu\right) \tag{1.21}$$

$$Z_\mu = \frac{1}{\sqrt{g^2 + g'^2}} \left(g W_3 - g' B_\mu\right). \tag{1.22}$$

Writing down the kinetic part of (1.17) explicitely, one can see that the photon A_μ is indeed massless due to the lack of a term proportional to $\sim A^2$. The masses for the other gauge bosons turn out to be

$$m_{W^-} = m_{W^+} = \frac{1}{2} v g \tag{1.23}$$

$$m_Z = \frac{1}{2} v \sqrt{g^2 + g'^2}. \tag{1.24}$$

Note, the couplings are free parameters, hence the SM does not predict the masses of the gauge bosons. The measured values are around $m_W = 80.4$ GeV and $m_Z = 91.2$ GeV. The Higgs mass can be read of to be

$$m_h = \sqrt{2\lambda v^2}. \tag{1.25}$$

In 2012, the LHC collaboration announced the discovery of the Higgs boson and presented the measured mass $m_h = 125$ GeV [18].
Regarding the fermions, it is easy to see that terms like

$$-m\bar{\Psi}\Psi = -m\left(\bar{\Psi}_L \Psi_R + \bar{\Psi}_R \Psi_L\right) \tag{1.26}$$

break gauge invariance since left-handed fermions are a doublet under the $SU(2) \times U(1)$ group, while right-handed fermions form a singlet. Hence, we cannot insert fermion mass terms explicitly in the lagrangian. In order to make the mass term invariant we need to add the compelx Higgs doublet

$$\propto \bar{\Psi}_L H \Psi_R. \tag{1.27}$$

This is exactly the type of terms we find in the Yukawa part of the lagrangian (1.16). As in the case with the gauge bosons, setting the Higgs vacuum to (1.19) results in fermionic mass terms and fermion-higgs interactions. Note, the Yukawa couplings are free parameters aswell. Hence, the SM does not give a sharp prediction for the fermion masses.

1.2 Cosmology

One of the most astonishing facts about our universe is also the most apparent one. If we look at the night sky, what we see is mostly black and empty. There are only a few stars that we can observe with the naked eye. If we think about it carefully, this observation is indeed strange. When we stand in a forest and the forest is large enough, no matter where we look, our sight will always be blocked by trees. Hence, if the universe is infinite, static and eternal, then the sky should be covered in stars. Therefore, the darkness of the sky is a first hint for the dynamical nature of our universe. This is the famous *Olbers' paradox*.
Modern cosmology begins with the observation of the expansion of our universe in 1929 by Edwin Hubble. The spectra of galaxies were found to be red-shifted and this red-shift seemed to increase with the galaxies distance. Hubble established a linear relation between the distance of a galaxy and its velocity, which today is known as *Hubble's law* [19].
The fundamental theory of cosmology is Einstein's theory of *General Relativity* formulated in 1915. Alexander Friedmann and George Lemaître derived independently a solution for Einstein's field equations which describes an expanding universe with a flat, positively or negatively curved spatial geometry. Later, Howard Robertson and Arthur Walker showed that the spatial geometry, which was assumed by Friedman and Lemaître are the only homogeneous and isotropic geometries possible, and thereby showing that the Friedmann-Lemaître equations give a complete description of the dynamics of our universe.
If our universe is expanding it is logical to assume[2] that at some finite time in the past all matter was concentrated in one small portion of space. The idea that our universe originated from one single point is called *the Big Bang*. It turns out that we can still observe evidence of this event. It is called the *cosmic microwave background* (CMB) and is the relic of the Big Bang. Eventually, when the universe expanded and consequently cooled down, it reached a temperature when electrons could recombine with the H and He atoms and the unvierse became transparent. The CMB that we observe today is the red-shifted radiation from this event.
Detailed observations of the CMB revealed tiny fluctuations in the spectrum. These fluctuations are believed to be the seeds for the cosmological structure formation. Shortly after the Big Bang, a period of rapid spatial expansion called *Inflation* imprinted tiny quantum fluctuations of the matter fields in the matter density distribution. These fluctuations grew over time via gravitational contraction and gave rise to the rich structures that we observe today.
Let us start by briefly introducing some basic concepts, which will be important later on. If we meassure the spectrum of a distant object such as a galaxy, we find that the observed spectral lines are shifted with respect to the expected spectrum. We define the *redshift* of a galaxy as

$$z = \frac{\lambda_0 - \lambda_1}{\lambda_1}. \tag{1.28}$$

[2]However, this conclusion is not imperative.

The intuitive way of understanding the redshift is to think of the expansion of the universe as an expansion of space itself. During the time the emitted photon travels from the galaxy to our telescope, the space in between expands and changes the wavelegth of the photon.
If we want to examine the universe at different times, it is convenient to introduce the so called *scale factor* $a(t)$. The scale factor parametrizes the spatial expansion and is defined such that $a(t) \in [0, 1]$. At Big Bang, the scale factor is $a(0) = 0$ and if t_0 represents the present then $a(t_0) = 1$. The scale factor is related to the redshift by

$$1 + z = \frac{a(t_0)}{a(t_1)}. \tag{1.29}$$

For nearby sources we can perform a Taylor expansion and factor out the scale factor at present time

$$a(t_1) = a(t_0) + (t_1 - t_0) \left.\frac{da(t)}{dt}\right|_{t=t_0} + ... \tag{1.30}$$

$$\approx a(t_0) \left(1 + (t_1 - t_0)H_0\right). \tag{1.31}$$

Here, we defined the *Hubble constant*

$$H_0 \equiv \frac{\dot{a}(t_0)}{a(t_0)}. \tag{1.32}$$

Using the relation between the redshift and the scale factor we get $z = H_0(t_1 - t_0) + ...$ For small distances and in units where $c = 1$ we have that $(t_1 - t_0) = d$ is just the physical distance. Hence, we obtain

$$z \simeq H_0 d, \tag{1.33}$$

which is the famous Hubbel's law.
Next, we will introduce some important concepts from GR and derive the Friedmann-Lemaître equations. We will use these equation in order to analyze the evolution of the universe by identifying different periods in time that were dominated by different energy sources. In the main part of this work we will present a string theory inspired model that will modify this standard picture and suggest an alternative scenario for the evolution of the universe.
In special and general relativity we treat space and time on equal footing. Hence, we denote a spacetime point x^μ as a 4-vector. The first entry $x^0 = ct$ is the time component and x^i with $i \in [1, 2, 3]$ are the spatial components. In flat space the metric is called *Minkowski metric* and is given by

$$g_{\mu\nu} = \begin{pmatrix} -1 & 0 & 0 & 0 \\ 0 & 1 & 0 & 0 \\ 0 & 0 & 1 & 0 \\ 0 & 0 & 0 & 1 \end{pmatrix} \tag{1.34}$$

We will also adapt the standard convention where we use greek indices for the full 4-vector and latin indices for the spatial part. In addition, we use *Einstein's summation convention*, i.e. we perform a summation over indices that appear twice in an expression. We can define the so-called *world line* of an observer as the spatial location as a function of time $x^i(t)$. Taking the derivative of this expression with respect to time, we can obtain the 3-velocity

$$v^i(t) = \frac{dx^i(t)}{dt}. \tag{1.35}$$

In order to define the 4-velocity we need to introduce the *proper time* τ, which is the time that an observer would meassure on his/her watch. We can define the 4-velocity as

$$u^\mu = \frac{dx^\mu(t)}{d\tau}. \tag{1.36}$$

The energy-momentum 4-vector follows from the 4-velocity as

$$p^\mu = mu^\mu, \tag{1.37}$$

where m is the mass. If we have a collection of particles that are moving in space, we can regard this colletion as a gas and define the so-called *energy-stress tensor* $T^{\mu\nu}$, which is the Noether current associated with spacetime translations. The conventional way to classify matter in this context is, whether it is relativistic or not. Non-relativistic (cold), pressureless matter ist called *dust*. The energy-momentum tensor for dust is

$$T^{\mu\nu} = \rho u^\mu u^\nu, \tag{1.38}$$

where ρ is the particle density. If we choose our coordinate system such that the gas is not moving then the tensor can be written as

$$T^{\mu\nu} = \begin{pmatrix} \rho c^2 & 0 & 0 & 0 \\ 0 & 0 & 0 & 0 \\ 0 & 0 & 0 & 0 \\ 0 & 0 & 0 & 0 \end{pmatrix}. \tag{1.39}$$

If the gas does have pressure, then the energy-momentum tensor is modified and is given by

$$T^{\mu\nu} = \rho u^\mu u^\nu + p\left(g^{\mu\nu} + \frac{1}{c^2}u^\mu u^\nu\right), \tag{1.40}$$

where p is the pressure. Again, choosing a coordinate system where the gas is in rest the energy-momentum tensor becomes

$$T^{\mu\nu} = \begin{pmatrix} \rho c^2 & 0 & 0 & 0 \\ 0 & p & 0 & 0 \\ 0 & 0 & p & 0 \\ 0 & 0 & 0 & p \end{pmatrix}. \tag{1.41}$$

As mentioned before, the energy-momentum tensor is the Noether current associated with spacetime translations. Hence, we can formulate a continuity equation of the form

$$\partial_\nu T^{\mu\nu} = 0. \tag{1.42}$$

General Relativity is primarily a theory that explains and quantifies the curvature of spacetime. The first ingredient in order to be able to write down Einstein's field equations are the so-called *Christoffel symbols*.

$$\Gamma^\alpha_{\beta\gamma} = \frac{1}{2} g^{\alpha\mu} \left(\frac{\partial g_{\mu\gamma}}{\partial x^\beta} + \frac{\partial g_{\mu\beta}}{\partial x^\gamma} - \frac{\partial g_{\beta\gamma}}{\partial x^\mu} \right). \tag{1.43}$$

The Christoffel symbols are the affine connection on our manifold and are used to define concepts like parallel transport, geodesics or covariant derivatives. Most importantly, we can use (1.43) in order to define curvature of our space. We cannot use the Christoffel symbols on their own, since they don't measure only the curvature of spacetime but also the curvature of the coordinate system. That means, that also in a flat space we can have non-zero Christoffel symbols, if we chose a curved coordinate system. However, physics should not depend on the choice of the coordinate system. The object that measures the curvature of space is the so-called *Riemann-Christoffel curvature tensor*

$$R^\alpha_{\sigma\beta\rho} \equiv \partial_\beta \Gamma^\alpha_{\rho\sigma} - \partial_\rho \Gamma^\alpha_{\beta\sigma} + \Gamma^\alpha_{\beta\gamma} \Gamma^\gamma_{\rho\sigma} - \Gamma^\alpha_{\rho\gamma} \Gamma^\gamma_{\beta\sigma}. \tag{1.44}$$

It can be derived by parallel transporting a vector along a closed path. Equation (1.44) contains all the information about the curvature of spacetime. A space is flat if $R^\alpha_{\sigma\beta\rho} = 0$ everywhere. Using the Riemann tensor we can define the famous Einstein equations. To this end we contract two indices of the Riemann tensor to obtain the *Ricci tensor*

$$R_{\alpha\beta} \equiv R^\gamma_{\alpha\gamma\beta}. \tag{1.45}$$

Contracting the remaining two indices we obtain the *scalar curvature*

$$R \equiv g^{\alpha\beta} R_{\alpha\beta}. \tag{1.46}$$

This is the last ingredient that we need to be able to write down the famous Einstein field equations

$$R^{\alpha\beta} - \frac{1}{2} g^{\alpha\beta} R = \frac{8\pi G}{c^2} T^{\mu\nu}. \tag{1.47}$$

Here, G is Newton's constant and c is the speed of light. We can also modify (1.47) by adding a term that accounts for the expansion of space, the cosmological constant Λ

$$R^{\alpha\beta} - \frac{1}{2} g^{\alpha\beta} R = \frac{8\pi G}{c^2} T^{\alpha\beta} - \Lambda g^{\alpha\beta}. \tag{1.48}$$

The Einstein equations formulate the connection between energy and the curvature of space. The presence of energy distorts space and solving the equations we can understand how particles are affected by gravity.
Next, we will derive a solution for (1.48). Given that our unvierse seems to be homogeneous and isotropic, we will use a very particular ansatz for the metric, the FLRW metric

$$ds^2 = dr^2 + f_K(r)^2 \left(d\theta^2 + \sin(\theta)^2 d\phi^2\right). \tag{1.49}$$

The function $f_K(r)$ encodes the curvature in the metric and is given by

$$f_K(r) = \begin{cases} K^{-1/2}\sin(K^{1/2}r), & K > 0 \\ r, & K = 0 \\ K^{-1/2}\sinh(K^{1/2}r), & K < 0 \end{cases}. \tag{1.50}$$

Here, we can see that the value of the *curvature constant* K determines the exact form of the metric and hence the geometry of space. Finally, we can introduce the time dependent scale factor and rewrite the radial coordinate as $r = a(t)x$. Adding also the time component results in

$$ds^2 = -dt^2 + a(t)^2 \left[dx^2 + f_K(x)^2 x^2 d\omega^2\right] \tag{1.51}$$

where we defined $d\omega \equiv d\theta^2 + \sin(\theta)^2 d\phi^2$. We can plug (1.51) in (1.48) and after some steps of algebra we arrive at the *Friedmann equations*

$$\left(\frac{\dot{a}}{a}\right)^2 = \frac{8\pi G}{3}\rho - \frac{Kc^2}{a^2} + \frac{\Lambda}{3} \tag{1.52}$$

$$\frac{\ddot{a}}{a} = -\frac{4\pi G}{3}\left(\rho + \frac{3p}{c^2}\right) + \frac{\Lambda}{3} \tag{1.53}$$

One can combine the two Friedmann equations to obtain the *adiabatic equation*

$$\frac{d}{dt}(\rho a^3 c^2) + p\frac{d}{dt}a^3 = 0 \tag{1.54}$$

and investigate it for two different limit cases.

- **cold matter**
  For the limiting case of cold matter we have

  $$p \ll \rho c^2. \tag{1.55}$$

  Hence, eq. (1.54) simplifies to

  $$\rho \propto \frac{1}{a^3}. \tag{1.56}$$

- **relativistic matter**
  For the second case that we study we have the maximum possible relativistic isotropic preassure

$$p = \frac{\rho c^2}{3}. \tag{1.57}$$

  Using this expression in (1.54) we derive

$$\rho \propto \frac{1}{a^4}. \tag{1.58}$$

In the following we will make the assumption that the universe consists only of these two limiting cases.
Using the first Friedmann equation, we can define the so-called critical density, which specifies the energy density for which the universe would be flat. The first Friedmann equation can be written as

$$H^2 = \frac{8\pi G}{3}\left(\rho_m + \rho_r + \rho_\Lambda\right) - \frac{Kc^2}{a^2}. \tag{1.59}$$

Here, we divided the energy density in different contributions. The energy density due to matter is described by ρ_m and we rewrote the cosmological constant as $\rho_\Lambda = \frac{\Lambda}{8\pi G}$. Defining the critical density as

$$\rho_{crit} = \frac{3H^2}{8\pi G}, \tag{1.60}$$

we see that if the total energy density is equal to (1.60) then $K = 0$, implying that the universe is indeed flat. Since the critical density depends on H, it has different values at different times. Denoting the present Hubble constant as H_0 we can write down the present critical density as

$$\rho_{crit,0} = \frac{3H_0^2}{8\pi G}. \tag{1.61}$$

Using these values we can rewrite the Friedmann equation as

$$H^2 = H_0^2\left(\frac{\rho_m}{\rho_{crit,0}} + \frac{\rho_r}{\rho_{crit,0}} + \frac{\rho_\Lambda}{\rho_{crit,0}}\right) - \frac{Kc^2}{a^2}. \tag{1.62}$$

At this point it is convenient to introduce the dimensionless densities

$$\Omega_m(a) = \frac{\rho_m(a)}{\rho_{crit}(a)} \tag{1.63}$$

$$\Omega_r(a) = \frac{\rho_r(a)}{\rho_{crit}(a)} \tag{1.64}$$

$$\Omega_\Lambda(a) = \frac{\rho_\Lambda(a)}{\rho_{crit}(a)} \tag{1.65}$$

$$\Omega_K(a) = \frac{\rho_K(a)}{\rho_{crit}(a)}. \tag{1.66}$$

In the last expression we also defined the *curvature density*. Combining the equations of state (1.56) and (1.58) with $\Omega_{K,0} = -\frac{Kc^2}{H_0^2}$ we can bring the Friedman equation to its final form

$$H^2 = H_0^2 \left(\frac{\Omega_{r,0}}{a^4} + \frac{\Omega_{m,0}}{a^3} + \frac{\Omega_{K,0}}{a^2} + \Omega_{\Lambda,0} \right). \tag{1.67}$$

One can solve (1.67) numerically or analytically for limiting cases where one energy form dominates. We can distinguish 3 cases: matter domination, radiation domination and Λ-domination.

- **matter domination**
  If we set $\Omega_{m,0} = 1$ and $\Omega_{i,0} = 0$ for $i \neq m$ then we can simplify (1.67) to arrive at

  $$\frac{\dot{a}}{a} = H_0 \frac{1}{a^{3/2}}. \tag{1.68}$$

  If we set $a = 0$ at the time of Big Bang ($t = 0$), we can solve this equation and obtain

  $$a(t) = \left(\frac{3}{2} H_0 t \right)^{2/3}. \tag{1.69}$$

  This solution describes an expanding universe with an expansion rate that is inverse proportional to time. Therefore, the universe is decellerating.

- **radiation domination**
  Similarly, we can set $\Omega_{r,0} = 1$ and $\Omega_{i,0} = 0$ for $i \neq r$ and reduce the Friedmann equation to

  $$\frac{\dot{a}}{a} = H_0 \frac{1}{a^2}. \tag{1.70}$$

  The solution is then given by

  $$a(t) = (2H_0 t)^{1/2}. \tag{1.71}$$

  Again, as in the matter-dominated period, the universe decellerates, since the expansion rate is inversely proportional to time.

- **Λ-domination**
  We repeat the exercise and set $\Omega_{\Lambda,0} = 1$ and $\Omega_{i,0} = 0$ for $i \neq \Lambda$. This time we can simplify the Friedmann equation to

  $$\frac{\dot{a}}{a} = H_0. \tag{1.72}$$

  Interestingly, in this case we do not have a solution for $a = 0$. Instead, we find an exponentially expanding universe

  $$a(t) = e^{H_0 t}. \tag{1.73}$$

The current picture of our universe is such that space is flat, i.e. $\Omega_{K,0} \simeq 0$ [20]. But the universe contains matter, radiation and it is expanding, so it has a non-zero cosmological constant. Our current understanding is such that shortly after the Big Bang the universe underwent a period of rapid expansion called *Inflation*. After Inflation the universe kept expanding and gradualy cooled down. When Inflation ended, the universe was dominated by radiation, afterwhich a period of matter domination followed. Then the universe entered a phase of Λ-domination. In the main part of this work we will present an alternative scenario for the history of our universe. This model will be motived by generic solutions of type IIB string theory.

Chapter 2

Beyond the Standard Model

In the following we will give a brief introduction to string theory and general concepts that are beyond the standard models. We follow primarily [21, 22, 23, 24, 25, 26] and refer to these references for more information on the presented subjects.

2.1 Supersymmetry

In the following we give a brief introduction to supersymmetry. As already mentioned before, the most important concept in modern physics is the notion of a symmetry. The basic spacetime symmetry group of nature is the so-called *Poincaré group*

$$x^\mu \to x'^\mu = \Lambda^\mu_\nu x^\nu + a^\mu. \tag{2.1}$$

Here the matrix Λ represents Lorentz transformations, which leave the metric invariant

$$\Lambda^T \eta \Lambda = \eta. \tag{2.2}$$

Constant translations are parametrized by a^μ. The generators of the Poincaré group define the algebra

$$[P^\mu, P^\nu] = 0 \tag{2.3}$$
$$[M^{\mu\nu}, P^\sigma] = i\left(P^\mu \eta^{\nu\sigma} - P^\nu \eta^{\mu\sigma}\right) \tag{2.4}$$
$$[M^{\mu\nu}, M^{\rho\sigma}] = i\left(M^{\mu\sigma}\eta^{\nu\rho} + M^{\nu\rho}\eta^{\mu\sigma} - M^{\mu\rho}\eta^{\nu\sigma} - M^{\nu\sigma}\eta^{\mu\rho}\right). \tag{2.5}$$

According to the famous *No-Go theorem* of Coleman and Mandula [27], the most general symmetry group of the S-matrix is a direct product of the Poincaré group and some internal symmetry group (such as the SM group). However, Haag, Lopuszanski and Sohnius [28] pointed out that one can generalize the No-Go theorem by including spinor generators Q^A_α with $\alpha = 1, 2$ and $A = 1, ..., \mathcal{N}$ in addition to P^μ and $M^{\mu\nu}$. Here, A denotes the number of susy generators. Due to the fermionic nature of the new generators we generalize the concept of commutators to *graded algebras*. Let O_a be operators of a Lie algebra, then

$$O_a O_b - (-1)^{\eta_a \eta_b} O_b O_a = i C^c_{ab} O_c, \tag{2.6}$$

where the gradings η_a are given by

$$\eta_a = \begin{cases} 0 & : O_a \text{ bosonic generator} \\ 1 & : O_a \text{ fermionic generator} \end{cases}. \tag{2.7}$$

Following from this definition we can derive the additional relations

$$[Q_\alpha, M^{\mu\nu}] = (\sigma^{\mu\nu})_\alpha^\beta \, Q_\beta \tag{2.8}$$
$$[Q_\alpha, P^\mu] = 0 \tag{2.9}$$
$$\{Q_\alpha, Q_\beta\} = 0 \tag{2.10}$$
$$\left\{Q_\alpha, \bar{Q}_\beta\right\} = 2\,(\sigma^\mu)_{\alpha\dot{\beta}}\, P_\mu. \tag{2.11}$$

Here, the matrices $\sigma^{\mu\nu}$ are generators of $SL(2,\mathbb{C})$.
Using the commutation relations we can derive ladder operators for the so-called *supermultiplets*, which are defined in terms of the generators. Supermultiplets are irreducible representations of the supersymmetry algebra and can be split up into sub-states with varying spins via the ladder operators. For instance, in the case of simple $\mathcal{N} = 1$ susy we have the following massless supermultiplets

$\lambda = 0$ **(scalar)**	$\lambda = 1/2$ **(fermion)**
squark	quark
slepton	lepton
Higgs	Higgsino

Table 2.1: Chiral multiplet

$\lambda = 1/2$ **(fermion)**	$\lambda = 1$ **(boson)**
photino	photon
gluino	gluon
Wino, Zino	W,Z

Table 2.2: Vector multiplet

$\lambda = 3/2$ **(fermion)**	$\lambda = 3$ **(boson)**
gravitino	graviton

Table 2.3: Gravity multiplet

The least invasive supersymmetric extension of the SM is called *Minimal Supersymmetric Standard Model* (MSSM). Interestingly, if R-parity is conserved the lightest supersymmetric particle (LSP) is stable. Usually the LSP is neutral (neutralino, higgsino, photino) and is a good dark matter candidate.
In order to write down a Lagrangian that is invariant under supersymmetry tranformations we need to specify two functions, the *Kähler potential* K and the *Superpotential*

W with

$$\mathcal{L} = K(\Phi, \Phi^\dagger)\big|_D + \left(W(\Phi)|_F + h.c.\right). \tag{2.12}$$

Here K and W are functions of the superfield Φ and the subscripts D, F denote that we select only particular terms of these expressions. The simplest chiral superfield Φ can be written as

$$\Phi(x^\mu, \theta^\alpha, \bar{\theta}^{\dot{\alpha}}) = \phi(x) + \sqrt{2}\theta\psi(x) + \theta\theta F(x) + i\theta\sigma^\mu\bar{\theta}\partial_\mu\phi(x) \tag{2.13}$$

$$- \frac{i}{\sqrt{2}}(\theta\theta)\,\partial_\mu\psi(x)\sigma^\mu\bar{\theta} - \frac{1}{4}(\theta\theta)\left(\bar{\theta}\bar{\theta}\right)\partial_\mu\partial^\mu\phi(x). \tag{2.14}$$

Here, the θ's are fermionic coordinates. In addition, one also introduces a so-called *gauge kinetic function* $f(\Phi)$ which is the prefactor of the term in the Lagrangian that describes the kinetic terms of the gauge fields. It is important to note that the Kähler potential is a real function whereas the superpotential is holomorphic. A crucial observation is that the Kählerpotential gets corrected by perturbative and non-perturbative corrections. However, the superpotential enjoys only non-perturbative corrections and the gauge kinetic function feels only first order perturbative corrections and non-perturbative corrections

$$K = \sum_{n=0}^{\infty} K^{(n)} + K^{(np)}, \tag{2.15}$$

$$W = W^{(0)} + W^{(np)}, \tag{2.16}$$

$$f = f^{(0)} + f^{(1)} + f^{(np)}. \tag{2.17}$$

In the main part of this work we will give particular definition of these function appropriate for type IIB models and our particular brane setup.
Since we do not observe supersymmetry it must be a broken symmetry. Note, that string theory does not predict a sharp energy scale at which we can expect to find supersymmetry breaking. However, in Sec. 3 we will see that the landscape shows a logarithmic preference for higher scale susy breaking[1].
A supersymmetric theory transforms bosonic (B) degrees of freedom into fermionic (F) ones and vice versa

$$\delta B \sim F, \qquad \delta F \sim B. \tag{2.18}$$

A reasonable assumption is that the vacuum should preserves the Lorentz symmetry, i.e. $\langle F\rangle_{vac} = 0$ while scalars can have a non-trivial background value $\langle B_{scl}\rangle_{vac} \neq 0$. Hence, in order to preserve the Lorentz symmetry we need $\langle \delta B\rangle = 0$ while $\langle \delta F\rangle|_{scl}$ can be non-zero. In this case the transformation signals spontaneous supersymmetry breaking, i.e. $\langle \delta F\rangle|_{scl}$ is the order parameter of supersymmetry breaking. These

[1] At least for models that are stabilised via LVS. For KKLT models the preference might be power-law.

conditions can be translated into a condition on the supergravity scalar potential

$$V_F = \exp\left(\frac{K}{M_{pl}^2}\right)\left((K^{-1})^{i\bar{j}} D_i W D_{\bar{j}} W^* - 3\frac{|W|^2}{M_{pl}^2}\right). \tag{2.19}$$

Unbroken supersymmetry corresponds to $\langle V_F \rangle \leq 0$. Note, that a dS-background is incompatible with unbroken supersymmetry. One possibility to break supersymmetry is e.g. $\langle F \rangle \neq 0$ in (2.14).

2.2 Inflation

In this section we briefly introduce the concept of *Inflation*. Despite the success of the standard cosmological picture, it has one major problem. It does not explain why the universe is homogeneous and isotropic on large scales as we observe it today. In fact, standard cosmology predicts the opposite. The universe should consist of large causally disconnected patches of space. Hence, each patch should experience a different time evolution.
The theory of Inflation suggests that an early period of accelerated expansion drived the early universe towards a homogeneous and isotropic state. To understand this idea better we need to clarify the concept of a *horizon*. A horizon limits distances at which we can interact with future or past events. Hence, we distinguish between the *particle horizon*, which determines the patch of space that we can observe in the past and the *event horizon*, which defines the patch that we can causally interact with in the future. The greatest comoving distance from which an observer at time t will be able to receive signals travelling with $c = 1$ is given by

$$\begin{aligned}\Delta x(\tau) &= \tau - \tau_i && (2.20)\\ &= \int_{t_i}^{t} \frac{dt}{a(t)} && (2.21)\\ &= \int_{a_i}^{a} \frac{da}{a\dot{a}} && (2.22)\\ &= \int_{\ln a_i}^{\ln a} (aH)^{-1} d\ln a, && (2.23)\end{aligned}$$

here the Big Bang corresponds to t_i or a_i. We observe that the causal structure of the particle horizon can be connected to the evolution of the *comoving Hubble radius* $(aH)^{-1}$. When the universe is dominated by a fluid with the equation of state $w = \frac{P}{\rho}$ we can write the the comoving Hubble radius as

$$(aH)^{-1} = H_0^{-1} a^{\frac{1}{2}(1+3w)}. \tag{2.24}$$

We can solve the horizon problem by assuming a phase of the universe during which the Hubble radius decreased

$$\frac{d}{dt}(aH)^{-1} < 0. \tag{2.25}$$

This condition can be formulated as a requirement on the fluid that dominates the energy density during this period. Its equation of state parameter has to obey

$$1 + 3w < 0. \tag{2.26}$$

The condition of a shrinking Hubble radius can be reformulated or related to other conditions for inflation. For instance, it implies an accelerated expansion $\ddot{a} > 0$ via

$$\frac{d}{dt}(aH)^{-1} = \frac{d}{dt}(\dot{a})^{-1} = -\frac{\ddot{a}}{(\dot{a})^2}. \tag{2.27}$$

Equivalently, we can write

$$\frac{d}{dt}(aH)^{-1} = -\frac{\dot{a}H + a\dot{H}}{(aH)^2} = -\frac{1}{a}(1-\epsilon), \tag{2.28}$$

with the *slow-roll parameter* $\epsilon \equiv -\frac{\dot{H}}{H^2}$. The shrinking Hubble radius then corresponds to

$$\epsilon < 1. \tag{2.29}$$

In order to solve the horizon problem, we want Inflation to last for a long enough period of time. This is achieved by keeping ϵ small for a sufficiently large number of Hubble times. We can quantify this requirement with the parameter

$$\eta \equiv \frac{\dot{\epsilon}}{H\epsilon}. \tag{2.30}$$

For $|\eta| < 1$ the change in ϵ is small and Inflation continues.
Concrete physical models for Inflation can be derived by writing down the parameters ϵ and η in terms of the model defining quantities (e.g. the potential).
Let us give a simple example here and briefly discuss single field inflation. We assume the existence of a single scalar field ϕ called the *inflaton*. The action that dictates the dynamics of the inflaton coupled to gravity is given by

$$S = \int d^4x\sqrt{-g}\left(\frac{1}{2}R + \frac{1}{2}g^{\mu\nu}\partial_\mu\phi\partial_\nu\phi - V(\phi)\right). \tag{2.31}$$

Setting the metric $g_{\mu\nu}$ to the FRW metric and assuming a homogeneous distribution of the inflaton, i.e. $\phi(t,x) \equiv \phi(t)$ the stress-energy tensor takes the form of a perfect fluid (1.41) with the density and pressure

$$\rho = \frac{1}{2}\dot{\phi}^2 + V(\phi) \tag{2.32}$$

$$p = \frac{1}{2}\dot{\phi}^2 - V(\phi). \tag{2.33}$$

Therefore, the resulting equation of state is

$$w_\phi = \frac{\frac{1}{2}\dot{\phi}^2 - V(\phi)}{\frac{1}{2}\dot{\phi}^2 + V(\phi)}. \tag{2.34}$$

From (2.34) we can see that the inflaton can drive an accelerated expansion ($w_\phi < -1/3$) when the potential energy $V(\phi)$ dominates over the kinetic energy. The inflation conditions $\epsilon, |\eta| < 1$ can be related to the inflaton potential by

$$\epsilon_V(\phi) \equiv \frac{M_{pl}^2}{2}\left(\frac{V_{,\phi}}{V}\right)^2 \tag{2.35}$$

$$\eta_V(\phi) \equiv M_{pl}^2\frac{V_{,\phi\phi}}{V}. \tag{2.36}$$

The parameters ϵ_V and η_V are called *potential slow-roll parameters* and inflation ends when

$$\epsilon_V(\phi_{end}) \approx 1. \tag{2.37}$$

The number of e-folds during inflation is given by

$$N(\phi) = \ln \frac{a_{end}}{a}. \tag{2.38}$$

In order to solve the horizon and flatness problem the total number of e-folds has to exceed about $N_{tot} > 60$.
One of the tasks of string phenomenology is to provide a UV embedding of these ideas and give a derivation and physical explanation of the inflaton.

2.3 String Theory

One of the main motivations for string theory is to find a theory of *Quantum Gravity*. Although, Einstein's General Relativity is in excellent agreement with experiment, it fails on small scales. When we try to quantize the metric field we observe infinities. Hence, we say that General Relativity is *non-renormalizable*. But even if it would be renormalizable, like the QFT's we use in the SM, it would be only an effective theory which is valid up to the cut-off scale. From this point of view, even the very successfull QFT's like QED, are not very satisfactory. The fact that we observe ultra-violet loop divergencies, implies that there must be a more fundamental theory at higher energy scales.
One candidate for such a UV complete theory is *String Theory* (ST). The basic assumption of ST is simple: *The fundamental objects in nature are not pointlike but 1-dimensional*. Starting with this idea and following the standard procedures of quantization and general coordinate invariance we arrive at a theory that unifies General Relativity and Yang-Mills theories.
The starting point is the famous *Nambu-Goto-action*. It describes the dynamics of a two dimensional object Σ, called the *worldsheet*. It is the stringy equivalent of a *worldline* produced by a 0-dimensional particle. We use two different sets of coordinates in this context. The worldsheet Σ is embedded in a spacetime of not specified dimension d. The coordinates that encode the embedding are $X^\mu(\tau,\sigma) \in \mathbb{R}^{(1,d-1)}$. The second set of coordinates are $\xi^a = (\tau,\sigma)$ with $a = 0,1$, which are the temporal and spatial coordinates on the worldsheet. Note, Σ can have two different topologies due to two different possible topologies of a string. The string can either be *open*, which corresponds to a worldsheet that resembles an actual sheet and the string can be *closed*, which leads to a cylinder-like worldsheet. The string action is given by

$$S_{NG} = -T \int_\Sigma dA, \tag{2.39}$$

where dA is the area element of Σ

$$dA = \sqrt{-\det\left(\frac{\partial X^\mu}{\partial \xi^a}\frac{\partial X^\nu}{\partial \xi^b}\eta_{\mu\nu}\right)}\, d^2\xi, \tag{2.40}$$

and T is the string tension and $\eta_{\mu\nu}$ is the d-dimensional spacetime metric. The string tension is related to the so-called *Regge slope* α' by $T = \frac{1}{2\pi\alpha'}$, which is related to the string length $l_s = 2\pi\sqrt{\alpha'}$. Due to the appearance of the square root in (2.39) quantization is rather difficult. Therefore, it is standard procedure to introduce an auxiliary field $h_{ab}(\xi^a)$, which can be seen as the metric on the worldsheet. Using this new field one can define the *Polyakov action*, which is equivalent to the Nambu-Goto-action

$$S_P = -\frac{T}{2}\int_\Sigma d^2\xi \sqrt{-\det h} h^{ab}(\xi)\partial_a X^\mu(\xi)\partial_b X^\nu(\xi)\eta_{\mu\nu}. \tag{2.41}$$

The conceptual understanding of string theory at this point is the following. The spacetime coordinates $X^\mu(\xi)$ are promoted to dynamical fields on the 2-dimensional worldsheet. Hence, we study d 2-dimensional scalar fields $X^\mu(\xi)$ coupled to the dynamical worldsheet metric $h_{ab}(\xi)$. Therefore, bosonic string theory is equivalent to 2-dimensional gravity coupled to scalar fields.
It is important to note that the Polyakov action enjoys various symmetries. Given the two different interpretations of X^μ, one has to distinguish between spacetime symmetries and symmetries defined on the worldsheet.

- **Spacetime symmetries**
  The Polyakov action enjoys a d-dimensional Poincare-invariance

  $$X^\mu(\xi) \to \Lambda^\mu_\nu X^\nu(\xi) + V^\mu, \quad \Lambda \in SO(1, d-1). \tag{2.42}$$

  Interestingly, from the viewpoint of the 2-dimensional field theory on the worldsheet the Poincare symmetry can be interpreted as a global internal symmetry.

- **Worldsheet symmetries**

  - *Local diffeomorphism invariance*
    The worldsheet coordinates enjoy a reparametrization invariance of the form

    $$\xi^a \to \tilde{\xi}^a(\xi) = \xi^a - \epsilon^a(\xi). \tag{2.43}$$

  - *Weyl invariance*
    The worldsheet is invariant under conformal transformations

    $$h_{ab} \to e^{2\Lambda(\xi)} h_{ab} = h_{ab} + \delta h_{ab} + \mathcal{O}(\Lambda^2). \tag{2.44}$$

    The presence of this symmetry is crucial for the success of string theory and is due to the 2-dimensional nature of the worldsheet.

In order to solve the dynamics described by (2.41), we need to specify the appropriate boundary conditions. We assume that the variation of the fields vanish at the temporal boundary, i.e. $\delta X|^{\text{inf}}_{\tau=-\text{inf}} = 0$. For the closed string the spatial boundaries are trivial due to its periodic nature

$$X^\mu(\tau, \sigma = 0) = X^\mu(\tau, \sigma = l_s). \tag{2.45}$$

Hence, the boundary terms cancel each other out. In the case of open strings, however, we need to specify appropriate boundary conditions, s.t. the variation vanishes. We can chose between

- **Neumann boundary conditions:**

$$\partial_\sigma X^\mu|_{\sigma=0 \text{ and/or } \sigma=l_s} = 0, \tag{2.46}$$

- **Dirichlet boundary conditions:**

$$\delta X^\mu|_{\sigma=0 \text{ and/or } \sigma=l_s} = 0. \tag{2.47}$$

Note, the Dirichlet condition corresponds to a situation where the string end points are fixed in the μ-directions.

After choosing appropriate coordinates we can solve the equations of motion derived from (2.41). For the closed string we obtain a sum of left- and right-moving waves along the string

$$X^\mu = X^\mu_L + X^\mu_R, \tag{2.48}$$

with

$$X^\mu_R(\tau-\sigma) = \frac{1}{2}(x^\mu + c^\mu) + \frac{1}{2}\frac{2\pi\alpha'}{l_s}p^\mu(\tau-\sigma) + i\sqrt{\frac{\alpha'}{2}}\sum_{n\in\mathbb{Z},n\neq 0}\frac{1}{n}\alpha^\mu_n e^{-\frac{2\pi}{l_s}in(\tau-\sigma)}, \tag{2.49}$$

$$X^\mu_R(\tau+\sigma) = \frac{1}{2}(x^\mu - c^\mu) + \frac{1}{2}\frac{2\pi\alpha'}{l_s}p^\mu(\tau+\sigma) + i\sqrt{\frac{\alpha'}{2}}\sum_{n\in\mathbb{Z},n\neq 0}\frac{1}{n}\tilde{\alpha}^\mu_n e^{-\frac{2\pi}{l_s}in(\tau+\sigma)}. \tag{2.50}$$

Here, $\alpha^\mu_n, \tilde{\alpha}^\mu_n$, are independent right-/left-moving Fourier modes and x^μ is the center-of-mass position at $\tau = 0$.
For the open string we can perform the same computation. However, in this case we can impose different boundary conditions for both string end points: (NN), (DD) and (DN)/(ND). In the case of (NN) boundary conditions we obtain

$$X^\mu(\tau,\sigma) = x^\mu + \frac{2\pi\alpha'}{l_s}p^\mu\tau + i\sqrt{2\alpha'}\sum_{n\in\mathbb{Z},n\neq 0}\frac{1}{n}\alpha^\mu_n e^{-i\frac{\pi}{l_s}n\tau}\cos\left(\frac{n\pi\sigma}{l_s}\right), \tag{2.51}$$

for the (DD) case we find

$$X^\mu(\tau,\sigma) = x^\mu_0 + \frac{1}{l_s}(x^\mu_1 - x^\mu_0)\sigma + \sqrt{2\alpha'}\sum_{n\in\mathbb{Z},n\neq 0}\frac{1}{n}\alpha^\mu_n e^{-i\frac{\pi}{l_s}n\tau}\sin\left(\frac{n\pi\sigma}{l_s}\right), \tag{2.52}$$

and for the mixed case (ND) we obtain

$$X^\mu(\tau,\sigma) = x^\mu + i\sqrt{2\alpha'}\sum_{n\in\mathbb{Z}+\frac{1}{2}}\frac{1}{n}\alpha^\mu_n e^{-i\frac{pi}{l_s}n\tau}\cos\left(\frac{n\pi\sigma}{l_s}\right). \tag{2.53}$$

The fact that the Dirichlet boundary condition fix the string end points introduces the concept of a *Dp-brane*. Dp-branes are dynamical (p+1)-dimensional hypersurfaces of spacetime on which open strings can end. Their excitations are related to the attached open strings. In 10 dimensions the massless open string excitations are $\mathcal{N} = 1$[2] vector multiplets in the adjoint of $SO(32)$. On a Dp-brane one has a $U(1)$

[2]See Sec. 2.1 for more information on supersymmetry.

vector multiplet while on a stack of N branes one has a vector multiplet in the adjoint of $U(N)$. Note, that the gauge theory is localized on the brane.
It turns out that D-branes carry RR-charge

$$Q_e = \int *F_{p+2}, \tag{2.54}$$

$$Q_m = \int F_{p+2}, \tag{2.55}$$

which satisfy the Dirac quantization condition

$$Q_e Q_m = 2\pi n, \quad n \in \mathbb{Z}. \tag{2.56}$$

This can lead to problems on a compact manifold. However, it is possible to avoid these problems via *orientifolds*. It turns out that it is possible to mod out the string background by an isometry ΩG, which includes worldsheet parity Ω that acts as $\Omega : \sigma \to l - \sigma$. If we include a space-time isometry G, which includes an involution σ^*, we can project within the same theory. In a moment we will see that one can define 5 different 10 dimensional manifestations of string theory. One of those theories is called *type IIB*. In this case we have

$$\sigma^*(\Omega_3) = \pm\Omega_3, \qquad \sigma^*(J) = J. \tag{2.57}$$

These transformation can be used to fix coordinates and define orientifold planes. For instance, the plus sign in (2.57) fixes no or two coordinates, which corresponds to O_9 and O_5 orientifold planes, whereas the minus sign fixes one or three coordinates, which corresponds to O_7 and O_3 orientifold planes.
So far, we discussed only the *bosonic* string. However, it turns out that in order to obtain a sensible theory (e.g. no tachyons in the spectrum) we also need to add *fermionic* degrees of freedom. This is achieved by adding a fermionic part to the bosonic string action. Using the worldsheet symmetries in order to pick a particular form of the worldsheet metric (i.e. flat gauge), we can write down the action as

$$S = -\frac{1}{8\pi}\int d^2\xi \frac{2}{\alpha'}\partial_a X^\mu \partial^a X_\mu + 2i\bar{\psi}^\mu_A \gamma^a_{AB}\partial_a \psi_{\mu B}. \tag{2.58}$$

The second term describes the dynamics of two dimensional worldsheet spinors ψ^μ_A. It turns out that the fields X^μ and ψ^μ_A enjoy a so-called *supersymmetry* which was discussed in Sec. 2.1 in more detail. Solving the dynamics of (2.58) and performing a careful quantization procedure, we obtain a crucial consistency condition. Depending on what kind of quantization procedure we choose (canonical, light-cone, path-integral...) the consistency condition manifests itself in a different way, but the physical implication stays the same. *A consistent formulation of superstring theory requires d=10 spacetime dimensions.*
Analyzing the mode expansions of the bosonic and fermionic solutions we can derive the spectrum of the theory. In two spacetime dimensions the superalgebra splits into what is called $(p, q)-$superpsymmetry where p denotes the left-moving supercharges

and q the right-moving supercharges. In 10 dimensions and for $(1,1)-$supersymmetry the worldsheet hosts two inequivalent theories called *type IIA* and *type IIB*. Both theories are $\mathcal{N}=2$ supersymmetric but type IIA is non-chiral whereas type IIB is chiral. If we change the supersymmetry to $(0,1)$ on Σ, then we find three inequivalent theories, *type I*, *heterotic* $SO(32)$ and *heterotic* $E_8 \times E_8$. Type I theories include closed and open strings and all three are $\mathcal{N}=1$ supersymmetric. The spectrum of type IIA and type IIB theories in 10 dimonesions is summarized in Table 2.4.

	Type IIA	**Type IIB**
NS-NS	$G_{(M,N)}, B_{[M,N]}, \phi$	$G_{(M,N)}, B_{[M,N]}, \phi$
R-R	C_1, C_3	l, C_2, C_4^*
NS-R	$\Psi_{M+}, \Psi_{M-}, \lambda_+, \lambda_-$	$\Psi^{1,2}_{M+}, \lambda^{1,2}_-$

Table 2.4: Spectrum of type IIA/IIB theories.

Here, C_p are antisymmetric tensors in p indices. The fields $G_{(M,N)}$ and $B_{[M,N]}$ are the Graviton and the so-called Kalb-Ramond field. The field ϕ is the dilaton, which is related to the string coupling via $g_s \sim e^{\langle\phi\rangle}$. The gravitino is denoted by $\Psi_{M\pm}$, where $\pm$ indicates the 10d chirality and λ is the dilatino. The labels NS (Neveu-Schwarz) and R (Ramond) denote different ways of expanding the fermionic fields.
In this work we are primarily interested in type IIB string theory, due to its better moduli stabilization properties. However, it turns out that all 5 theories are related via so-called *dualities*. Dualities can be view as transformations that relate weakly and strongly coupled systems, in the sense that they transform the couplings like $g \to 1/g$. Since all 5 manifestations of string theory are related by various dualities, they are all connected via a more fundamental underlying theory called *M-theory*. The deep structure of M-theory is not fully understood.

2.4 Compactification

Let us now come back to the observation that consistency of the quantization procedure requires the existence of 10 spacetime dimensions. Since we observe only 4-dimensional spacetime, with 1 temporal and 3 spatial dimensions, we need to find a way to explain the remaining 6 dimensions. The idea is, that these extra dimensions are *compactified* on an internal manifold. The intuition behind this statement is the following: the extra dimensions are too small to be observed. We clarify this concept with the example of *Kaluza-Klein compactification* [29].
We consider a field theory in $D = d + 1$ spacetime dimensions. We choose the d'th dimension to be 'rolled up on a circle', i.e. for the coordinate x^d we have the following periodic relation

$$x^d = x^d + 2\pi R, \tag{2.59}$$

where R is the radius of the circle. The circle S^1, on which x^d now 'lives', is called the *internal space*. This scenario typically has 3 consequences:

- The spectrum hosts a so-called *Kaluza-Klein tower* of massive states in $(D-1)$ dimensions. To see this, let us introduce two sets of labels. Let $M, N = 0, 1, ..., D-1, D$ and $\mu\nu = 0, 1, ..., D-1$. Now, let us consider a free massless scalar in D dimensions

  $$\partial_M \partial^M \Phi(x^M) = 0. \tag{2.60}$$

  In order to respect the periodicity of the d'th dimension, Φ must also be periodic in x^d. The most general ansatz is

  $$\Phi(x^M) = \sum_{n=-\infty}^{\infty} \phi_n(x^\mu) e^{i\frac{n}{R}x^d}. \tag{2.61}$$

  Plugging the ansatz into (2.60) yields

  $$\partial_\mu \partial^\mu \phi_n(x^\mu) = \frac{n^2}{R^2}\phi_n(x^\mu) \quad \forall n. \tag{2.62}$$

  We observe that the n'th Fourier mode $\phi_n(x^\mu)$ appears as a scalar field of mass $m_n^2 = \frac{n^2}{R^2}$. The set of all these massive scalars is called the Kaluza-Klein tower of states. Note, the zero-mode ϕ_0 is massless and independend of x^d.
  In order to obtain a low-energy effective field theory from the full dimensional theory we take the limit $R \to 0$. In this case the mass of the lowest-lying state $m_1^2 \to \infty$ and the KK tower disappears from the low-energy spectrum. Hence, at energies $E \ll \frac{1}{R}$ the theory looks $(D-1)$-dimensional.

- We find an extra $U(1)$ symmetry in $(D-1)$ dimensions.

- We find massless scalar fields called *moduli fields* in $(D-1)$ dimensions. These fields typically parametrize the geometric properties of the internal manifold. One crucial observation is that moduli fields are not constrained by a potential. Hence, they are massless scalars and would correspond to unobserved fifth forces. In order to make contact with our 4-dimensional world it is crucial to generate a potential for these fields and make them massive.

Following the same logic we can apply compactification in string theory. Here, the compactification ansatz is of the form

$$\mathcal{M}^{1,9} = \mathcal{M}^{1,3} \times \mathcal{M}^6, \tag{2.63}$$

with $\mathcal{M}^{1,3}$ being a maximally symmetric 4-dimensional space, i.e. deSitter or Anti-deSitter, while $\mathcal{M}^6$ is the 6-dimensional internal manifold. For this case we can write the free Klein-Gordon equation as

$$(\Box_{1,3} + \Delta_6)\, \phi(x, y) = 0. \tag{2.64}$$

Here, $x \in \mathcal{M}^{1,3}$ and $y \in \mathcal{M}^6$. The two differential operators act on the respective variables. We can expand $\phi(x, y)$ in terms of the eigenfunctions of the wave-operator Δ_6

$$\phi = \sum_n \phi^{(n)}(x)\theta^{(n)}(y). \tag{2.65}$$

Combining (2.64) and (2.65) we obtain

$$\left(\Box_{1,3} + m^{2(n)}\right) \phi^{(n)}(x) = 0, \tag{2.66}$$

where $m^{2(n)}$ are the eigenvalues of $\theta^{(n)}(y)$. The scale of m is related to the so-called *Kaluza-Klein scale*

$$m \sim \frac{1}{l_{KK}}, \qquad V_6 \sim l_{KK}^6, \tag{2.67}$$

where V_6 is the volume of the internal manifold. It is important to note, that although the 10-dimensional theory is unique (up to dualities), its 4-dimensional manifestation is not. Every 4-dimensional effective theory obtained from the full 10-dimensional theory by compactification corresponds to a choice of vacuum, i.e. to a dynamical solution of the 10-dimenional theory. The set of 4-dimensional solutions of string theory is called the *landscape of string vacua*. Part of the string spectrum are gauge potentials C_{p-1} with a field strength $F_p = dC_{p-1}$. It turns out that the field strength can have non-trivial background values called *background fluxes*. Different ways of realizing the fluxes enlarges the number of consistent vacua tremendously and is the origin for the landscape of string vacua.
It can be shown that for a consistent compactification procedure the internal manifold needs to be a *Calabi-Yau 3-fold*. Let us briefly discuss the main properties of such

an object. Almost complext manifolds of even dimension $d = 2n$ are those that are equipped with a real map I from the tangent space to itself

$$I^2 = -1. \tag{2.68}$$

The map I is called *almost complex structure*, as having n $(+i)$ and n $(-i)$ eigenvalues, allows the definition of holomorphic and anti-holomorphic vectors. As an example, let us consider $d = 2$

$$I = \begin{pmatrix} 0 & 1 \\ -1 & 0 \end{pmatrix}. \tag{2.69}$$

The eigenvectors are then given by

$$\frac{\partial}{\partial z} \equiv \frac{\partial}{\partial x^1} + i\frac{\partial}{\partial x^2}, \qquad \frac{\partial}{\partial \bar{z}} \equiv \frac{\partial}{\partial x^1} - i\frac{\partial}{\partial x^2}. \tag{2.70}$$

Given an almost complex structure for the tangent space, one can define the projectors

$$P_{\pm} = \frac{1}{2}\left(1 \mp iI\right), \tag{2.71}$$

which projects onto the holomorphic and anti-holomorphic bundles. An almost complex structure is called a *complex structure* if a holomorphic one-form dz can be *integrated* globally.
A manifold is *symplectic* if there is a globally defined and non-vanishing two-form J such that

$$dJ = 0. \tag{2.72}$$

This defines a symplectic product

$$\langle v, w\rangle_J \equiv J(v, w) = v^m J_{mn} w^n. \tag{2.73}$$

Similarly to complex coordinates z^i for complex manifolds, in symplectic manifolds one can define Darboux coordinates (x^i, y^i) such that

$$J = \sum_{i=1}^{n} dx^i \wedge dy^i. \tag{2.74}$$

Kähler manifolds are complex and symplectic manifolds for which the complex and symplectic structures are compatible. This means that J is $(1,1)$ in terms of I, i.e.

$$J = J_{ij} dz^i \wedge d\bar{z}^{\bar{j}}. \tag{2.75}$$

The complex structure I and the symplectic two-form J together define the metric g via

$$g_{mn} = J_{mp} I^p_n. \tag{2.76}$$

This metric can be derived from a real scalar function K, the *Kähler potential*

$$J_{i\bar{j}} = i g_{ij} = i\partial_i \bar{\partial}_{\bar{j}} K. \tag{2.77}$$

The deformations of the Calabi-Yau metric, which do not destroy the Calabi-Yau conditions correspond to moduli scalars in the low energy effective action.

- $\delta g_{i\bar{j}}$
  These are deformations of the Kähler form and can be written as

$$\delta g_{i\bar{j}} = it^a(x)\omega^a_{i\bar{j}}, \quad a = 1, ..., h^{(1,1)}, \tag{2.78}$$

  where ω_a are harmonic $(1,1)$-forms on Y, which form a basis of $H^{(1,1)}(Y)$. The scalar fields t^a are called *Kähler moduli*. The geometric interpretation of these moduli is that they control the size of 2-cycles of Y.

- δ_{ij}
  These deformations of the complex structure are parametrized by complex moduli z^a, which are in one-to-one correspondence with harmonic $(1,2)$-forms via

$$\delta g_{ij} = \frac{i}{||\Omega||^2}\bar{z}^a(x)\bar{\chi}^a_{i\bar{i}\bar{j}}\Omega^{\bar{i}\bar{j}}_j, \quad a = 1, ..., h^{(1,2)}, \tag{2.79}$$

  here, Ω is the holomorphic $(3,0)$-form and $\bar{\chi}_a$ denotes a basis of $H^{(1,2)}$.

In order to understand the last property of a Calabi-Yau we need to introduce the notion of cohomology classes.
Closed p-forms A_p are p-forms such that $dA_p = 0$, where d is the exterior derivative. Let us call $\mathcal{C}^p(\mathcal{M})$ the space of all closed p-forms. Exact p-forms B_p are such that $B_p = dC_{p-1}$ for some globally defined $(p-1)$-form. Let us call $\mathcal{Z}^p(\mathcal{M})$ the space of all exact forms. Then, the p-th de Rham cohomology H^p is defined by

$$H^p(\mathcal{M}) = \frac{\mathcal{C}^p(\mathcal{M})}{\mathcal{Z}^p(\mathcal{M})}. \tag{2.80}$$

The elements of H^p are equivalence classes of closed forms and are called cohomology classes. The dimension of H^p are called the Betti numbers b_p

$$\dim H^p(\mathcal{M}) = b_p. \tag{2.81}$$

The Betti numbers are so-called topological invariants since they are independent of the metric that we define on the manifold. On a complex manifold one can define cohomology classes for (p,q)-forms. Furthermore, one can define another cohomology called the *Dolbeault cohomology*, which is analogous to the de Rham cohomology but with the exterior derivative d replaced by the holomorphic derivative ∂. On Kähler manifolds both cohomologies coincide

$$H^{p,q}_d = H^{p,q}_\partial = H^{p,q}_{\bar{\partial}}. \tag{2.82}$$

The dimensions of these cohomology classes are denoted by the *Hodge numbers* $h^{p,q}$. An important cohomology class is the one that hosts the Ricci two-form

$$\mathfrak{R} \equiv R_{mnpq}J^{pq}dx^m \wedge dx^n. \tag{2.83}$$

This is a closed form on a Kähler manifold and therefore defines a cohomology class, the *first Chern class*

$$c_1 = \frac{1}{2\pi} [\mathfrak{R}] \,. \tag{2.84}$$

Finally, Calabi-Yau manifolds are Kähler manifolds on which the first Chern class is $c_1 = 0$. An important proterty of Calabi-Yau manifolds is that the only non-trivial Hodge numbers are $h^{1,1}$ and $h^{1,2}$. A representative of this cohomology class is the holomorphic 3-form Ω

$$\Omega = \frac{1}{6}\Omega_{ijk} dz^i \wedge dz^j \wedge dj^k. \tag{2.85}$$

Equivalently to the complex structure I, this form tells us what the complex coordinates are.

2.5 Flux compactification

As already mentioned, part of the origin for the landscape of string theory is the possibility to turn on background fluxes. Hence, the concept of *flux compactification* is a crucial ingredient in a realistic string theory model. Type IIB compactification on a Calabi-Yau threefold Y with non-trivial NSNS and RR 3-form field strength backgrounds H_3 and F_3 have been extensively studied [30, 31]. It was shown that the fluxes must obey a certain consistency condition, the Bianchi identities

$$dF_3 = 0, \qquad dH_3 = 0, \tag{2.86}$$

and they should be quantized in the sense

$$\frac{1}{(2\pi)^2\alpha'}\int_\Sigma F_3 \in \mathbb{Z}, \qquad \frac{1}{(2\pi)^2\alpha'}\int_\Sigma H_3 \in \mathbb{Z}, \tag{2.87}$$

for any 3-cycle Σ. An important observation is that, in order to avoid no-go theorems about the existence of configurations of fluxes satisfying the equations of motion, it is necessary to include orientifold 3-planes in the compactification. Hence, we will consider type IIB orientifolds with these objects. The most straightforward way to understand the need for orientifold planes is to investigate the type IIB supergravity Chern-Simons coupling

$$\int_{\mathcal{M}_4\times Y} H_3 \wedge F_3 \wedge C_4, \tag{2.88}$$

where C_4 is the IIB self-dual 4-form gauge potential. This coupling implies that upon compactification the flux background contributes with a positive coefficient N_{flux} to a tadpole for C_4. In addition, fluxes contribute positively to the energy of the configuration, due to the 2-form kinetic terms. The only way to cancel these tadpoles is to introduce objects with negative RR C_4-charge and negative tension, to cancel the RR tadpole and also to compensate the vacuum energy of the configuration. Having $O3$-planes in the configuration, it is natural to consider the possibility of adding N_{Q_3} $D3$-branes as well. Hence, the RR tadpole cancellation constraint becomes

$$N_{Q_3} + N_{flux} + Q_{O3} = 0. \tag{2.89}$$

One can normalize the charge such that a $D3$-brane in covering space has charge $+1$. With this convention a $O3$-plane has charge $-1/2$ an we obtain

$$N_{flux} = \frac{1}{(4\pi^2\alpha')^2}\int_Y H_3 \wedge F_3 = \frac{1}{(4\pi^2\alpha')^2}\frac{i}{2\mathrm{Im}(S)}\int_Y G_3 \wedge \bar{G}_3 \tag{2.90}$$

where

$$G_3 = F_3 + iSH_3. \tag{2.91}$$

Finally, in order to satisfy the equations of motion, the flux combination G_3 must be imaginary self-dual with respect to the Hodge operation defined in terms of the Calabi-Yau metric on Y

$$*G_3 = iG_3. \tag{2.92}$$

This can be seen as the minimization of the scalar potential following from the flux induced superpotential

$$W \sim \int_Y G_3 \wedge \Omega. \tag{2.93}$$

These conditions guarantee the existence of a consistent supergravity solution for the different relevant fields in the configuration, metric and 4-form. Note, eq (2.92) should not be seen as an additional contraint on the fluxes. Rather, for a set of fluxes in a fixed topological sector, eq. (2.92) is a condition on the scalar moduli which determine the internal metric. The scalar potential is minimized at points in moduli space when (2.92) is satisfied, while fluxes induce a positive scalar potential at other points. Hence, introduction of fluxes leads to a natural mechanism to stabilise moduli.

2.6 Large Volume Scenario

One of the bigget challenges in string theory is to provide a consistent and reliable mechanism for moduli stabilisation. Given the fact that these fields are massless, they would introduce unobserved fifth-forces in the low-energy theory. In order to overcome this problem one has to find a mechanism that generates a potential and therefore a mass term for these fields.
One possible approach to this issue is the so-called *Large Volume Scenario* (LVS) [32]. The distinguished feature of this stabilisation mechanism is that one combines non-perturbative effects [33] with perturbative corrections such as α'-corrections. The combination of both effects leads to a geometrical scenario where the internal manifold is exponentially large. If one also considers string loop corrections [34] the set of possible Calabi-Yau manifolds gets extended by manifolds that have a fibred structure.
In this work we will be interested in type IIB Calabi-Yau orientifold compactifications with background fluxes, which preserve $\mathcal{N} = 1$ supersymmetry in 4D. As usual in a supersymmetric theory, the resulting effective low-energy theory is characterised by a Kähler potential K, a superpotential W and a gauge kinetic function f. The scalar potential of the theory takes the standard supergravity form [35]

$$V = e^{K/M_p^2}\left(K^{i\bar{j}} D_i W D_{\bar{j}} \bar{W} - 3\frac{|W|^2}{M_p^2}\right), \tag{2.94}$$

here the index i runs over the axio-dilaton $S = e^{-\phi} + iC_0$, $h^{(1,1)}$ Kähler moduli and $h^{(2,1)}$ complex structure moduli. Where we denote the Kähler moduli as T and the complex structure as U. Without any corrections, the tree-level Kähler potential is given by

$$\frac{K_{\text{tree}}}{M_p^2} = -\ln(S+\bar{S}) - \ln(\mathcal{V}) - \ln\left(-i\int_Y \Omega\wedge\bar{\Omega}\right). \tag{2.95}$$

Here $\mathcal{V}$ is the Calabi-Yau volume in Einstein frame (in units of the string length $l_s = 2\pi\sqrt{\alpha'}$), the holomorphic $(3,0)$-form of the Calabi-Yau is denoted as Ω. The volume is related to the Kählerform via

$$\mathcal{V} = \frac{1}{6}\int_Y J\wedge J\wedge J = \frac{1}{6}k_{ijk}t^i t^j t^k, \tag{2.96}$$

where the numbers k_{ijk} are related to the triple intersection numbers of the Calabi-Yau and the t^i are the 2-cycle volumes. We can relate the 2-cycle volumes with the volume of the Poincaré dual 4-cycles via

$$\tau_i = \frac{\partial\mathcal{V}}{\partial t^i} = \frac{1}{2}\int_Y D_i\wedge J\wedge J = \frac{1}{2}k_{ijk}t^j t^k. \tag{2.97}$$

The scalar part of the chiral superfield that defines the effective 4D action is $T_i = \tau_i + ib_i$, where the axions b_i are components of the RR 4-form C_4 along the 4-cycle

Poincaré dual to D_i.
As we have seen in the previous section, when we turn on background fluxes $G_3 = F_3 + iSH_3$, we generate an effective superpotential of the form

$$W_{\text{tree}} \sim \int_Y G_3 \wedge \Omega. \tag{2.98}$$

This procedure stabilises the axio-dilaton S and the U-moduli. However, without considering any higher order corrections, the Kähler moduli remain massless since W_{tree} does not depend on T_i.
In order to generate mass terms for the Kähler moduli we need to consider corrections. Let us start by discussing non-perturbative corrections to the superpotential W. As we have seen in Sec. 2.1 the non-renormalisation theorem forbids the superpotential to be corrected perturbatively. Typically non-perturbative corrections to W are due to Euclidean D3 brane instatons wrapping 4-cycles (ED3) or due to gaugino condensation in the supersymmetric gauge theories located on D7 branes which wrap internal 4-cycles. We can describe both effects with a superpotential of the form

$$W = \frac{M_p^3}{\sqrt{4\pi}} \left(W_0 + \sum_i A_i e^{-a_i T_i} \right). \tag{2.99}$$

Here, A_i corresponds to threshold effects and can depend on the U moduli and the D3 position moduli but not on T_i. The parameter a_i specifies the nature of the non-perturbative effect. For ED3 branes we have $a_i = 2\pi$ and $a_i = 2\pi/N$ for gaugino condensation in an $SU(N)$ gauge theory. Plugging (2.99) in (2.94) we can determine the correction to the scalar potential due to non-perturbative effects

$$\delta V|_{(np)} = e^{K_0} K_0^{j\bar{i}} \left(a_j A_j a_i \bar{A}_i e^{a_j T_j + a_i \bar{T}_i} - \left(a_j A_j e^{-a_j T_j} \bar{W} \partial_{\bar{i}} K_0 + a_i \bar{A}_i e^{-a_i \bar{T}_i} W \partial_j K_0 \right) \right). \tag{2.100}$$

Here, we have defined $K_0 = -2 \ln \mathcal{V}$.
Let us now discuss the perturbative effects. The Kähler potential gets corrected at each order in the α' expansion. The leading order α' corrections modifies the Kähler potential such that we obtain

$$\frac{K}{M_p^2} = -2 \ln \left(\mathcal{V} + \frac{\xi}{2 g_s^{3/2}} \right) \simeq -2 \ln \mathcal{V} - \frac{\xi}{g_s^{3/2} \mathcal{V}}, \tag{2.101}$$

where the factor ξ is given by $\xi = -\frac{\chi \zeta(3)}{2(2\pi)^3}$. Here χ is the Calabi-Yau Euler number and the Riemann zeta function is $\zeta(3) \simeq 1.2$. Again, combining the corrected Kähler potential with the supergravity scalar potential we obtain the correction to the scalar potential due to α' corrections

$$\delta V|_{\alpha'} = 3 e^{K_0} \hat{\xi} \frac{\left(\hat{\xi}^2 + 7 \hat{\xi} \mathcal{V} + \mathcal{V}^2 \right)}{\left(\mathcal{V} - \hat{\xi} \right) \left(2\mathcal{V} + \hat{\xi} \right)^2} W_0^2 \simeq \frac{3 \xi W_0^2}{4 g_s^{3/2} \mathcal{V}^3}, \tag{2.102}$$

here we defined $\hat{\xi} \equiv \xi/g_s^{3/2}$. In order for the perturbative expansion to be valid we need $\mathcal{V} \gg \hat{\xi} \gg 1$.
The next source of corrections that modify the Kähler potential are string loop corrections. Their form was conjectured to be [36]

$$\delta K|_{g_s} \sim \sum_{i=1}^{h^{(1,1)}} \frac{g_s \mathcal{C}_i^{KK}(U,\bar{U})(a_{il}t^l)}{\mathcal{V}} + \sum_i \frac{\mathcal{C}_i^{W}(U,\bar{U})}{(a_{il}t^l)\mathcal{V}}. \tag{2.103}$$

The first term originates from the exchange of closed strings, which carry Kaluza-Klein momentum, between D7- and D3-branes. It is valid for vanishing open string scalars and is based on the assumption that all $h^{(1,1)}$ 4-cycles of the Calabi-Yau are wrapped by D7-branes. The second term in (2.103) is due to the exchange of winding strings between intersecting stacks of D7-branes. The functions $C_i^{KK}(U,\bar{U})$ and $C_i^{W}(U,\bar{U})$ are unknown. But since these functions do not depend on the Kähler moduli we can regard them as $\mathcal{O}(1)$ constants since the complex structure moduli are already stabilised by the background fluxes. It was shown in [37] that for an arbitrary Calabi-Yau background the leading contribution of (2.103) to the scalar potential vanishes, making the loop corrections sub-leading with respect to α' corrections. Again, combining the corrected Kähler potential with the expression for the supergravity scalar potential we obtain the correction of the scalar potential due to loop corrections

$$\delta V|_{g_s} = \left(\left(g_s \mathcal{C}_i^{KK}\right)^2 a_{ik}a_{ij}K^0_{k\bar{j}} - 2\delta K^W_{(g_s)} \right) \frac{W_0^2}{\mathcal{V}^{\in}}. \tag{2.104}$$

Combining the tree-level expression and the various corrections we can write down the scalar potential

$$V = V_{\text{tree}} + \delta V|_{(np)} + \delta V|_{\alpha'} + \delta V|_{g_s} \tag{2.105}$$

$$= \frac{g_s e^{K_{cs}} M_p^4}{8\pi \mathcal{V}^2} \left[K_0^{j\bar{i}} a_j A_j a_i \bar{A}_i \, e^{-(a_j T_j + a_i \bar{T}_i)} + 4W_0 \sum_i a_i A_i \tau_i \cos(a_i b_i) e^{-a_i \tau_i} \right. \tag{2.106}$$

$$\left. + \left[\frac{3\xi}{g_s^{3/2}} + \sum_i \left(g_s^2 (\mathcal{C}_i^{KK})^2 \left(\frac{1}{2}\frac{t_i^2}{\mathcal{V}} - A^{ii} \right) - 8\frac{\mathcal{C}_i^W}{(a_{il}t^l)} \right) \right] \frac{W_o^2}{4\mathcal{V}} \right]. \tag{2.107}$$

Here, we have defined $A_{ij} \equiv k_{ijk}t^k$.

Part II

STATISTICS OF THE LANDSCAPE

Chapter 3

SUPERSYMMETRY STATISTICS

For several decades, the idea of supersymmetry has been one of the central ideas in both phenomenological and formal aspects of high energy physics. From the point of view of phenomenology, it furnishes an elegant solution to the gauge hierarchy problem and provides natural dark matter candidates. Furthermore, the theory is supported by several sets of data via radiative corrections: gauge coupling unification, the value of the top mass, and the value of the Higgs mass which falls within the window allowed by the Minimal Supersymmetric Standard Model (MSSM). For a detailed discussion of the recent status of supersymmetric phenomenology, see [38] and references therein. From a more formal point of view, supersymmetry plays a key rôle in making string theory a consistent theory of quantum gravity. (Approximately) supersymmetric string compactifications are typically stable, as supersymmetry protects solutions from various instabilities. Supersymmetric partners of the Standard Model (SM) are being actively searched for at the LHC, with null results thus far. Given this, the time is ripe to rethink the following question: At what scale should we expect to find supersymmetry?

It is important to understand if string theory can provide guidance in this regard. The literature on supersymmetry breaking and its mediation in string theory is vast, much of it focused on constructions of specific supersymmetry breaking and MSSM-like sectors (see [39, 40, 41, 42, 43] for a review of these and other aspects of string phenomenology). A complementary line of inquiry, starting with the seminal work [44, 45, 46, 47, 48, 49, 50, 51, 52, 53, 54, 55], has been to frame the question in terms of statistical distributions in the landscape of flux vacua [56]. As described in [47], this program relies on several features of flux compactifications: they are the most well-understood string compactifications with moduli stabilisation and broken supersymmetry and thus provide a fertile arena where quantitative answers may be extracted; there are many vacua that at least roughly match the SM; the number of vacua is so large that statistical solutions make sense; and no single vacuum is favoured by the theory. These studies found a preference for high scale supersymmetry due to a uniform distribution of the supersymmetry breaking scale

[47, 50, 51]. This result has been obtained by taking the distribution of the relevant F-terms to be as given by the dilaton and complex structure F-terms, while the Kähler moduli F-terms have been neglected since these fields are stabilised only beyond tree-level.

In this section we revisit the statistical distribution of the supersymmetry breaking scale in the type IIB flux landscape, paying particular attention to the stabilisation of the Kähler moduli. The motivation for our work comes from the fact that the dilaton and complex structure F-terms, if non-zero, typically give rise to a runaway for the Kähler moduli, unless they are tuned to be small as in a recent dS uplifting proposal [57]. This implies that stable vacua where moduli stabilisation is under control require the dilaton and complex structure F-terms to be suppressed with respect to the F-terms of the Kähler moduli. It is therefore the distribution of the F-terms of the Kähler moduli which determines the statistics of the supersymmetry breaking scale in the landscape.

More precisely, in type IIB flux compactifications the complex structure moduli and the dilaton are fixed supersymmetrically at semi-classical level by 3-form fluxes [30]. As we pointed out above, this supersymmetric stabilisation ensures the absence of instabilities along the Kähler moduli directions which are flat at tree-level due to the well-known 'no-scale' property of the low-energy effective action [58, 59, 60, 61]. At this level of approximation, the cosmological constant vanishes and supersymmetry is broken due to non-zero F-terms of the Kähler moduli. However, due to the no-scale structure, the scale of the gravitino mass is unfixed and the soft terms might be zero (as in models where the SM is realised via D3-branes [62, 63, 64, 65]). The inclusion of no-scale breaking effects, which can come from either perturbative contributions to the Kähler potential or non-perturbative corrections to the superpotential, is therefore crucial to stabilise the Kähler moduli, to fix the supersymmetry breaking scale and to determine the soft terms. Kähler moduli stabilisation thus allows to write the gravitino mass (and consequently the soft terms) in terms of microscopic parameters like flux quanta or the number of D-branes. In turn, exploiting these relations and the knowledge of the distribution of these underlying parameters, one can deduce the distribution of the supersymmetry breaking scale in the landscape.

We will try to perform a systematic study of the interplay between Kähler moduli stabilisation and the statistics of the supersymmetry breaking scale by considering three general scenarios: (*i*) models with purely non-perturbative stabilisation like in KKLT vacua [33]; (*ii*) models where the Kähler moduli are frozen by balancing perturbative against non-perturbative effects as in the Large Volume Scenario (LVS) [32]; and (*iii*) models with purely perturbative stabilisation [66]. We primarily study the distributions focusing on vacua with zero cosmological constant, and do not explore the joint distribution of the cosmological and supersymmetry breaking scale in detail (although in the case of LVS we argue that the distribution of the supersymmetry breaking scale should remain the same for a wide range of values of the cosmological constant, see below).

Interestingly, we find that KKLT and perturbatively stabilised vacua behave similarly since in both cases the gravitino mass is governed by flux-dependent

parameters (as the vacuum expectation value of the tree-level superpotential in KKLT models) which are uniformly distributed. Hence the statistics of supersymmetry breaking obeys a power-law behaviour implying that in these cases high scale supersymmetry is preferred, unless tempered by anthropics [67]. Notice that these results match those derived in [47] since in these cases the F-terms of the Kähler moduli, similarly to the dilaton and complex structure F-terms, turn out to be uniformly distributed.

The situation in LVS models is instead different. In fact, we find that in this case the distribution of the supersymmetry breaking scale is exponentially sensitive to the distribution of the string coupling. Due to the exponential behaviour and the fact that the string coupling is uniformly distributed as a flux-dependent variable, the distribution of the soft terms turns out to be only logarithmic. This dependence gives rise to a large number of vacua with low-energy supersymmetry and reproduces in detail previous expectations following an intuition based on dynamical supersymmetry breaking [68, 69, 70, 71] (although a significant difference is that [68, 69] found a logarithmic distribution even in the case of KKLT, which we do not find).[1]

LVS models are particularly interesting also because they provide examples where a crucial assumption formulated in [47] can be explicitly shown to hold. This is the assumption that the distribution of the supersymmetry breaking scale is decoupled from the one of the cosmological constant. This was justified in [47] by relying on the possible existence of several hidden sector models which contribute to the vacuum energy but not to supersymmetry breaking. In LVS models the depth of the non-supersymmetric AdS vacuum scales as $V_{LVS} \sim -m_{3/2}^3 M_p$, where $m_{3/2}$ is the gravitino mass and M_p the Planck scale. Hence any hidden sector responsible for achieving a nearly Minkowski vacuum contributes to the scalar potential with an F-term that scales as $F_{\rm hid} \sim m_{3/2}^{3/2} M_p^{1/2}$. In turn, in a typical gravity mediation scenario, the contribution to the soft terms from this hidden sector would be suppressed with respect to the gravitino mass since $M_{\rm soft} \sim F_{\rm hid}/M_p \sim \epsilon\, m_{3/2} \ll m_{3/2}$ with $\epsilon = \sqrt{m_{3/2}/M_p} \ll 1$.[2] Note that this implies that the distribution of the supersymmetry breaking scale is the same for all vacua with cosmological constant in the range $\pm V_{LVS}$.

We have therefore shown that, while two alternative statistics of the supersymmetry breaking scale have been advanced before in the literature (power-law distributions by assuming democratic distributions of complex structure F-terms and logarithmic distributions by appealing to dynamical supersymmetry breaking), the different behaviours are neatly categorized by different stabilisation mechanisms. In order to determine if the distribution of the supersymmetry breaking scale is power-law or logarithmic, one should therefore determine the relative preponderance of LVS and KKLT vacua in the type IIB landscape. Given that LVS models do not rely on any tuning of the tree-level superpotential, one would naively expect them to

[1] We refer to [72, 73] for other early studies in this general direction.

[2] An exception to this argument could however come from models where the SM is built via D3-branes at singularities which are sequestered from the sources of supersymmetry breaking in the bulk [63, 65].

arise much more frequently, so favouring a logarithmic distribution of the soft terms. However, a full understanding of this question requires detailed (numerical) studies of the distributions of flux vacua which is well beyond the scope of the present work. For estimates of the number of vacua as a function of the flux superpotential and the string coupling see [74, 75, 76, 77, 78].

We finally point out that the ultimate goal of this line of research is to identify the mass scale of the supersymmetric particles preferred by the string landscape in order to find some guidance for low-energy searches of superpartners. In order to achieve this task, one has not just to understand the distribution of vacua, but has to focus also on *phenomenologically viable* vacua. This means that one should impose additional constraints coming for example from cosmology or from anthropic arguments [67]. For example, in string compactifications both the moduli masses and the soft terms turn out to be of order the gravitino mass. Hence the absence of any cosmological moduli problem [79, 80, 81, 82], which requires moduli masses above $\mathcal{O}(50)$ TeV, tends to push the soft terms considerably above the TeV-scale unless the SM sector is sequestered from supersymmetry breaking (as in some D3-brane models [63, 65].) We leave a detailed study of these additional phenomenological and cosmological constraints for future work.

This chapter is organised as follows. In Sec. 3.1 we first review previous determinations of the statistics of the supersymmetry breaking scale neglecting the Kähler moduli. After explaining why this analysis is incomplete and a more accurate study should take the Kähler moduli into account, we then provide an overview of the three general classes of Kähler moduli stabilisation schemes mentioned above: KKLT [33], LVS [32] and perturbative stabilisation [66]. In Sec. 3.2 we derive in detail the distribution of the supersymmetry breaking scale for each of these three scenarios, while in Sec. 3.3 we discuss the interplay between our results and previous findings in the literature and the implications of our distributions for phenomenology. Our conclusions are presented in Sec. 3.4. Finally App. A.1 presents a discussion of the distribution of the string coupling while App. A.2 summarises the structure of the soft terms in KKLT and LVS models with an MSSM-like sector on either D3 or D7-branes.

3.1 The importance of the Kähler moduli for the SUSY breaking statistics

The statistics of the supersymmetry breaking scale in the landscape has been investigated mainly in the context of type IIB flux compactifications since this is one of the best examples where moduli stabilisation can be achieved with control over the effective field theory. However previous studies focused only on the contribution to supersymmetry breaking from the axio-dilaton and the complex structure moduli, ignoring the dynamics of the Kähler moduli [46, 47, 48, 49, 50, 51]. In what follows we shall instead point out that the Kähler moduli play a crucial rôle in determining the correct statistics of the supersymmetry breaking scale in the landscape.

3.1.1 SUSY breaking statistics neglecting the Kähler moduli

The starting point of our discussion is type IIB string theory compactified on a Calabi-Yau X which, together with an appropriate orientifold involution, can lead to an $N = 1$ supergravity effective action in 4D. One of the nicest features of these compactifications is that one can turn on RR and NSNS 3-form fluxes F_3 and H_3 without destroying the underlying Calabi-Yau structure since the flux backreaction just introduces warping [30]. Moreover, these background 3-form fluxes, which appear in the combination $G_3 = F_3 - iSH_3$, can stabilise the axio-dilaton S and all complex structure moduli U^α (with $\alpha = 1, ..., h^{1,2}(X)$) by generating the following tree-level superpotential [83]:

$$W_{\text{tree}} = \int_X G_3 \wedge \Omega(U)\,, \tag{3.1}$$

where $\Omega(U^\alpha)$ is the holomorphic $(3,0)$-form of the Calabi-Yau X that depends on the U-moduli.

The tree-level Kähler potential which can be obtained from direct dimensional reduction is instead [84]:

$$K_{\text{tree}} = -2\ln\mathcal{V} - \ln\left(S+\bar{S}\right) - \ln\left(-\mathrm{i}\int_X \Omega(U)\wedge\bar{\Omega}(\bar{U})\right)\,, \tag{3.2}$$

where $\mathcal{V}$ is the dimensionless volume of the internal manifold expressed in units of the string length $\ell_s = 2\pi\sqrt{\alpha'} = M_s^{-1}$. The Calabi-Yau volume $\mathcal{V}$ is also a function of the real parts of the Kähler moduli $T_i = \tau_i + \mathrm{i}\theta_i$ (with $i = 1, ..., h^{1,1}(X)$) where the τ_i's control the size of internal divisors while the θ_i's are the axions obtained from the dimensional reduction of the RR 4-form C_4 over the same 4-cycles. For the simplest cases with just a single Kähler modulus, $\mathcal{V} = \tau^{3/2}$.

The scalar potential is obtained by plugging the expressions (3.1) and (3.2) in the general expression of the F-term scalar potential in supergravity (setting $M_p \equiv 1/\sqrt{8\pi\,G_N} = 1$ and neglecting possible contributions coming from D-terms):

$$V_F = e^K\left(K^{i\bar{j}}D_iW\,D_{\bar{j}}\overline{W} - 3|W|^2\right) = K_{i\bar{j}}F^i\overline{F}^{\bar{j}} - 3m_{3/2}^2\,, \tag{3.3}$$

where:

$$F^i = e^{K/2}\,K^{i\bar{j}}D_{\bar{j}}\overline{W} \qquad \text{and} \qquad m_{3/2} = e^{K/2}|W|\,. \tag{3.4}$$

Given that the tree-level Kähler potential (3.2) factorises, the F-term scalar potential (3.3) takes the form (denoting all complex structure and Kähler moduli collectively as U and T respectively):

$$V_{\text{tree}} = |F^S|^2 + |F^U|^2 + |F^T|^2 - 3m_{3/2}^2\,. \tag{3.5}$$

Ref. [47, 50, 51] considered situations where supersymmetry is spontaneously broken at the minima of the scalar potential (3.5) and studied the distribution of the supersymmetry breaking scale taking the distribution of the relevant F-terms to be

that obtained from the analysis for the S and U-moduli. The Kähler moduli have been instead neglected since these moduli are not stabilised by fluxes at tree-level, and so the dynamics that fixes them beyond the tree-level approximation has been assumed to give rise just to small corrections to the leading order picture.

Hence the distribution of supersymmetry breaking vacua has been claimed to be given by [47]:

$$dN(F,\hat{\Lambda}) = \prod d^2F^S\, d^2F^U\, d\hat{\Lambda}\, \rho(F,\hat{\Lambda})\,, \tag{3.6}$$

where $\hat{\Lambda}$ is the depth of the supersymmetric AdS vacuum, $\hat{\Lambda} = 3m_{3/2}^2$, and the F-terms of the T-moduli have been ignored. Requiring in addition a vanishing cosmological constant, one obtains:

$$dN_{\Lambda=0}(F) = \prod d^2F^S\, d^2F^U\, d\hat{\Lambda}\, \rho(F,\hat{\Lambda})\, \delta\left(|F^S|^2 + |F^U|^2 - \hat{\Lambda}\right). \tag{3.7}$$

Ref. [47] makes two claims about the cosmological constant: the first claim is that the distribution of values of the supersymmetric AdS vacuum $\hat{\Lambda} = -\Lambda = e^K\,|W|^2$ is determined by the distribution of the tree-level superpotential (3.1) which is uniformly distributed as a complex variable near zero, and throughout its range is more or less uniform. The second claim is instead that this distribution is relatively uncorrelated with the supersymmetry breaking parameters if the hidden sector which breaks supersymmetry is different from the one which is responsible to obtain a nearly zero cosmological constant.

If one assumes a decoupling of the cosmological constant problem from the question of supersymmetry breaking, then the density function ρ is in fact independent of $\hat{\Lambda}$, leading to:

$$dN_{\Lambda=0}(F) = d^2F\, \rho(F)\,, \tag{3.8}$$

where we have collectively denoted all the F-terms of the axio-dilaton and the complex structure moduli simply as F. Using the vanishing cosmological constant condition $|F|^2 = 3m_{3/2}^2$ and the fact that $d^2F \simeq |F|\, d|F| \simeq m_{3/2}\, dm_{3/2}$, (3.8) reduces to:

$$dN_{\Lambda=0}(m_{3/2}) \simeq \rho(m_{3/2})\, m_{3/2}\, dm_{3/2}\,. \tag{3.9}$$

Given that the gravitino mass is set by the F-terms of the axion-dilaton and the complex structure moduli, and F^S and F^U in type IIB flux vacua turn out to be uniformly distributed as complex variables, [47] considered $\rho(m_{3/2})$ as independent on $m_{3/2}$. In order to keep this discussion more general in view of our results in the case where the T-moduli are included, we consider instead:

$$\rho(m_{3/2}) \sim m_{3/2}^{\beta} \qquad \text{with} \qquad \beta \geq 0\,, \tag{3.10}$$

which implies:

$$dN_{\Lambda=0}(m_{3/2}) \simeq m_{3/2}^{\beta+1}\, dm_{3/2} \qquad \text{with} \qquad \beta \geq 0\,, \tag{3.11}$$

where $\beta = 0$ for the case where the dynamics of the Kähler moduli is neglected [47, 50, 51]. Notice that the result with $\beta = 0$ would indicate a preference for high scale supersymmetry.

3.1.2 SUSY breaking statistics including the Kähler moduli

The importance of the Kähler moduli for the statistics of the supersymmetry breaking scale in the landscape can be easily understood by noticing that the tree-level superpotential (3.1) is independent on the T-moduli due to holomorphy combined with the axionic shift symmetry. Hence the F-terms of the Kähler moduli become $F^T = e^{K/2}\,\overline{W}K^{T\bar{T}}K_{\bar{T}}$ and the scalar potential (3.5) can be rewritten as:

$$V_{\rm tree} = |F^S|^2 + |F^U|^2 + m_{3/2}^2\left(K_{\bar{T}}K^{\bar{T}T}K_T - 3\right). \tag{3.12}$$

A generic property of type IIB vacua which holds for all Calabi-Yau manifolds is the famous 'no-scale' relation $K_{\bar{T}}K^{\bar{T}T}K_T = 3$ which has been recently shown to be a low-energy consequence of the axionic shift symmetry combined with approximate higher dimensional symmetries like scale invariance and supersymmetry [61]. This no-scale property of type IIB vacua has important consequences which we now briefly discuss:

- At tree-level the scalar potential (3.12) reduces to (where $K_{\rm cs}$ denotes the Kähler potential for the U-moduli):

$$V_{\rm tree} = |F^S|^2 + |F^U|^2 = \frac{e^{K_{\rm cs}}}{\mathcal{V}^2\left(S+\bar{S}\right)}\left[|D_S W|^2 + |D_U W|^2\right]. \tag{3.13}$$

  This result shows that any vacuum where either $D_S W \neq 0$ or $D_U W \neq 0$ is unstable since it gives rise to a run-away for the volume mode $\mathcal{V}$ at tree-level. One could envisage a scenario where this run-away is counter-balanced by quantum corrections but when the perturbative expansion is under control these effects are expected to be subdominant by consistency. Hence a stable solution requires $F^S = F^U = 0$.[3] This implies that the statistic of the supersymmetry breaking scale in the landscape should instead be driven by the F-terms of the Kähler moduli.

- At tree-level, the gravitino mass is set by the F-terms of the T-moduli since the no-scale relation implies $|F^T|^2 = 3m_{3/2}^2$. This is contrast with the case where the Kähler moduli are ignored and $m_{3/2}$ is set by the F-terms of S and U-moduli. Thus there is no reason to expect that coefficient β in the distribution of the gravitino mass (3.10) should be zero. Moreover, the Kähler moduli are still flat at tree-level, and so any scale of supersymmetry breaking is equally valid. To set $m_{3/2}$ and to understand its distribution one has therefore to study which corrections to the tree-level action can stabilise the Kähler moduli. We shall show that in a large number of flux vacua (all the LVS examples) F^T is not uniformly distributed, and so $\beta \neq 0$.

[3] See however [57] for dS uplifting models where F^S and F^U are tuned to very small values. These cases are consistent with our claims since they feature $F^S \sim F^U \ll F^T$.

- The gravitino mass does not necessarily fix the scale of the soft supersymmetry breaking terms in the visible sector. In fact, in type IIB models an MSSM-like visible sector can be located on either stacks of D7-branes with non-zero gauge fluxes or on D3-branes at singularities. The tree-level Kähler potential including D7 and D3 matter fields, respectively denoted as ϕ_3 and ϕ_7, is given by (focusing for simplicity on the case with $h^{1,1}(X) = 1$) [85]:

$$K_{\rm tree} = -3\ln\left(T+\bar{T}-\bar{\phi}_3\phi_3\right) - \ln\left(S+\bar{S}-\bar{\phi}_7\phi_7\right) \simeq K_0 + \tilde{K}_3\,\bar{\phi}_3\phi_3 + \tilde{K}_7\,\bar{\phi}_7\phi_7\,,$$

where K_0 denotes the Kähler potential for T and S while $\tilde{K}_3 = 3\left(T+\bar{T}\right)^{-1}$ and $\tilde{K}_7 = \left(S+\bar{S}\right)^{-1}$. On the other hand the visible sector gauge kinetic functions for D7s and D3s at tree-level read:

$$f_3 = S \qquad \text{and} \qquad f_7 = T\,. \tag{3.14}$$

Moreover the general expressions of the soft scalar and gaugino masses in gravity mediation look like:

$$m_0^2 = m_{3/2}^2 - \overline{F}^{\bar{i}} F^j \partial_{\bar{i}}\partial_j \ln\tilde{K} \qquad \text{and} \qquad M_{1/2} = \frac{1}{2\,{\rm Re}(f)}\,F^i\partial_i f\,. \tag{3.15}$$

Using $F^S = 0$ and $F^T = e^{K/2}\,\overline{W}K^{T\bar{T}}K_{\bar{T}}$, we then end up with:

$$\begin{aligned} {\rm D3}: \quad m_0 &= M_{1/2} = 0 \\ {\rm D7}: \quad m_0 &= |M_{1/2}| = m_{3/2}\,. \end{aligned} \tag{3.16}$$

Hence we can clearly see that the soft terms are set by the gravitino mass only for D7s, while for D3s they are suppressed with respect to $m_{3/2}$. We conclude that the inclusion of perturbative and/or non-perturbative corrections to the 4D effective action which break the no-scale structure is crucial for two important tasks: (i) to stabilise the Kähler moduli, which in turn fixes the leading order value of F^T and $m_{3/2}$; (ii) to generate a subleading shift to the tree-level results for F^S and F^T which yield non-zero contributions to m_0 and $M_{1/2}$ for visible sector models on D3-branes.

3.1.3 Overview of type IIB Kähler moduli stabilisation

After having motivated the importance of Kähler moduli stabilisation for understanding the correct distribution of the supersymmetry breaking scale in the type IIB flux landscape, we describe now the main features of three different classes of stabilisation scenarios classified in terms of perturbative and non-perturbative corrections to the 4D low-energy action.

3.1.4 Purely non-perturbative stabilisation: KKLT

Let us start by reviewing the KKLT [33] stabilisation mechanism and identify the relevant parameters. The starting point is to introduce 3-form fluxes which stabilise

the axio-dilaton and all complex structure moduli at $F^S = F^U = 0$ [30]. The next step is to allow for effects like gaugino condensation on D7 branes or Euclidean D3 instantons, both wrapped on internal 4-cycles. Both of these effects lead to non-perturbative corrections to the superpotential that stabilise the Kähler modulus $T = \tau + i\theta$ if the vacuum expectation value of W_{tree} is tuned to exponentially small values. Thus in KKLT models the Kähler potential takes the tree-level expression given in (3.2) while the superpotential is:

$$W = W_0 + A\, e^{-a\, T}\,, \tag{3.17}$$

where W_0 is the vacuum expectation value of the tree-level superpotential (3.1). Moreover $a = 2\pi/\mathfrak{n}$ with $\mathfrak{n} = 1$ for stringy instantons while in the case of more standard field theoretic non-perturbative effects on stacks of D7-branes $\mathfrak{n}$ is related to the number of D7-branes that, together with the orientifold involution, determines the rank of the condensing gauge group (for example for gaugino condensation in a pure $SU(N)$ super Yang-Mills theory $\mathfrak{n} = N$). The scalar potential is obtained by plugging the expressions (3.2) and (3.17) in the general expression of the F-term supergravity scalar potential (3.3). After minimising with respect to the axion θ, one arrives at (with $s = \text{Re}(S)$):

$$V_{KKLT} = \frac{2e^{-2a\tau}a^2A^2}{3s\mathcal{V}^{2/3}}\left(1 + \frac{3}{a\tau}\right) - \frac{2e^{-a\tau}aAW_0}{s\mathcal{V}^{4/3}}\,, \tag{3.18}$$

where $\mathcal{V} = \tau^{3/2}$ is the dimensionless CY volume in units of the string length $\ell_s = 2\pi\sqrt{\alpha'} = M_s^{-1}$. Minimising this potential with respect to the volume we get the relation:

$$e^{a\langle\tau\rangle} = \frac{2Aa\langle\tau\rangle}{3W_0}\left(1 + \frac{3}{2a\langle\tau\rangle}\right) \simeq \frac{2Aa\langle\tau\rangle}{3W_0} \qquad \Leftrightarrow \qquad \langle\tau\rangle \simeq \frac{1}{a}\,|\ln W_0|\,, \tag{3.19}$$

where we took the limit $a\langle\tau\rangle \gg 1$ where higher instantons corrections to (3.17) can be safely ignored and we considered natural values of the prefactor A of the non-perturbative contribution to W, i.e. $A \sim \mathcal{O}(1)$. Notice that (3.19) leads to two important observations:

1. A minimum at values of $\langle\tau\rangle \gg 1$, where stringy corrections to the effective action can be neglected, can be obtained only if W_0 is tuned to exponentially small values. Notice that such a tuning guarantees also the consistency of neglecting perturbative corrections to K (since they give rise to contribution to V which are proportional to $|W_0|^2$).

2. This vacuum preserves supersymmetry since (3.19) implies $F^T = 0$. Hence, as can be seen from (3.3), the vacuum energy is negative with $V = -3\, m_{3/2}^2$ where in this case $m_{3/2}$ should just be intended as the parameter defined in (3.4) without any reference to the gravitino mass.

A Minkowski or slightly dS vacuum can be obtained by adding to the scalar potential the positive definite contribution coming from D3-branes at the end of a warped throat [33] (another interesting option relies on α' corrections to K [86]). As shown in [87], this requires the addition of a nilpotent superfield in the 4D effective field theory description. The presence of this nilpotent superfield gives rise to a Minkowski vacuum where the relation (3.19) gets modified to:

$$e^{a\langle\tau\rangle} = \frac{2Aa\langle\tau\rangle}{3W_0}\left(1+\frac{5}{2a\langle\tau\rangle}\right). \tag{3.20}$$

Interestingly, (3.19) and (3.20) agree at leading order, and so we can safely consider $\langle\tau\rangle \simeq \frac{1}{a}\,|\ln W_0|$ also at the Minkowski minimum where supersymmetry is broken. In this case the gravitino mass becomes (where the vacuum expectation value of s sets the string coupling, i.e. $s = g_s^{-1}$):

$$m_{3/2} \simeq \sqrt{\frac{g_s}{8\pi}}\frac{|W_0|}{\langle\mathcal{V}\rangle} \simeq \frac{\pi\, g_s^{1/2}}{\mathfrak{n}^{3/2}}\frac{|W_0|}{|\ln W_0|^{3/2}}\,. \tag{3.21}$$

This equation shows clearly that, begin exponentially small, it is W_0 that determines the order of magnitude of $m_{3/2}$. The soft terms in the KKLT scenario can be generated via either gravity or anomaly mediation [87, 88] with the MSSM-like visible sector located on either stacks of D7-branes with non-zero gauge fluxes or on D3-branes at singularities. In both cases, the overall scale of the soft terms $M_{\rm soft}$ is of order the gravitino mass up to a possible 1-loop factor whose presence is model-dependent: $M_{\rm soft} \sim m_{3/2}$.

3.1.5 Perturbative vs non-perturbative effects: LVS

The starting point of LVS models is the same as in KKLT constructions since at tree-level the complex structure moduli and the dilaton are stabilised supersymmetrically by non-zero 3-form fluxes at $F^U = 0$ and $F^S = 0$. At this semi-classical level of approximation, the Kähler moduli are however flat directions due to the underlying no-scale cancellation which is inherited from higher-dimensional rescaling symmetries [61].

The simplest LVS model (see [34, 89, 90, 91] for more general constructions) features 2 Kähler moduli and a CY volume of the form $\mathcal{V} = \tau_b^{3/2} - \tau_s^{3/2}$ where τ_b is a 'big' divisor controlling the overall volume while τ_s is a 'small' divisor supporting non-perturbative effects, with $\tau_b \gg \tau_s \gg 1$ [32]. If the leading order α' correction to the effective action is included, the Kähler and superpotential of LVS models look like:

$$\begin{aligned} K &= -2\ln\left(\mathcal{V}+\frac{\xi}{2}\left(\frac{S+\bar{S}}{2}\right)^{3/2}\right) - \ln\left(S+\bar{S}\right) - \ln\left(-i\int_X \Omega(U)\wedge\bar{\Omega}(\bar{U})\right) \\ W &= W_0 + A_s\, e^{-a_s T_s}\,, \end{aligned} \tag{3.22, 3.23}$$

with $a_s = 2\pi/\mathfrak{n}$ as in the KKLT case and $\xi \equiv -\frac{\chi(X)\zeta(3)}{2(2\pi)^3}$ where $\chi(X)$ is the CY Euler number and ζ is the Riemann zeta function. Notice that A_s and ξ are both expected to be $\mathcal{O}(1)$ parameters. After setting S and all the U-moduli at their flux-stabilised values and fixing the axionic partner of τ_s at its minimum, the scalar potential (3.3) takes the form:

$$V_{LVS} = \frac{4}{3}\frac{a_s^2 A_s^2 \sqrt{\tau_s} e^{-2a_s\tau_s}}{s\mathcal{V}} - \frac{2a_s A_s |W_0| \tau_s e^{-a_s\tau_s}}{s\mathcal{V}^2} + \frac{3\sqrt{s}\xi |W_0|^2}{8\mathcal{V}^3} \,. \tag{3.24}$$

Minimising the potential we obtain the following conditions on the moduli (with $s = g_s^{-1}$):

$$\langle \mathcal{V} \rangle \simeq \frac{3\sqrt{\langle \tau_s \rangle}\,|W_0|}{4a_s A_s} e^{a_s \langle \tau_s \rangle} \qquad \text{and} \qquad \langle \tau_s \rangle \simeq \frac{1}{g_s}\left(\frac{\xi}{2}\right)^{2/3} . \tag{3.25}$$

Let us again stress two important points which follow from (3.25):

1. In LVS models, it is the smallness of g_s that guarantees that the effective field theory is under control. In fact, if the string coupling is such that perturbation theory does not break down, i.e. $g_s \lesssim 0.1$, stringy corrections to the 4D action can be safely ignored since both τ_b and τ_s are much larger than the string scale. Hence these models can exist for natural values of the flux-generated superpotential W_0 with $W_0 \sim \mathcal{O}(1-10)$.

2. The LVS vacuum is AdS with $V_{\rm LVS} \sim -m_{3/2}^3$ and non-supersymmetric with the largest F-term given by $F^{T_b} \sim \tau_b m_{3/2}$. Hence the Goldstino is the fermionic partner of T_b in the corresponding $N = 1$ chiral superfield. This is eaten up by the gravitino which acquires a non-zero mass.

As in KKLT models, an additional positive definite contribution to the scalar potential has to be added in order to obtain a Minkowski solution. Several 'uplifting' mechanisms have been proposed and the main ones involve anti-branes [33], T-branes [92], hidden sector non-perturbative effects [93] or non-zero F-terms of the dilaton and complex structure moduli [57]. The important observation here is that all these mechanisms modify the relations in (3.25) only at subleading order. Hence we can consider (3.25) a good analytic estimate also for the location of the Minkowski minimum. Thus the gravitino mass becomes:

$$m_{3/2} \simeq \sqrt{\frac{g_s}{8\pi}}\frac{|W_0|}{\langle \mathcal{V} \rangle} \simeq c_1 \frac{g_s}{\mathfrak{n}} e^{-\frac{c_2}{g_s \mathfrak{n}}} , \tag{3.26}$$

where c_1 and c_2 are $\mathcal{O}(1)$ parameters given by:

$$c_1 = \frac{\sqrt{8\pi}A_s}{3}\left(\frac{2}{\xi}\right)^{1/3} \qquad \text{and} \qquad c_2 = 2\pi\left(\frac{\xi}{2}\right)^{2/3} . \tag{3.27}$$

Contrary to KKLT scenarios where the value of $m_{3/2}$ was determined by W_0, (3.26) shows clearly that in LVS models the scale of the gravitino mass is set by the

string coupling. Another difference between KKLT and LVS models, is that in LVS constructions the contribution to the soft terms from anomaly mediation is always loop-suppressed with respect to the contribution from gravity mediation (since similar cancellations in both mediation mechanisms take place due to the underlying no-scale property of these vacua). Moreover, in LVS models, the overall scale of the soft terms depends crucially on the fact that the SM is realised on either D7 or D3-branes [63, 65, 94, 95]:

$$\text{D7}: \; M_{\rm soft} \sim m_{3/2} \qquad\qquad \text{D3}: \; M_{1/2} \sim m_{3/2}^2 \quad \text{and} \quad m_0 \sim m_{3/2}^p \,, \tag{3.28}$$

where p can be either $p = 2$ or $p = 3/2$ depending on the mechanism considered to obtain a Minkowski vacuum [65].

3.1.6 Purely perturbative stabilisation: α' vs g_s effects

Let us now describe Kähler moduli stabilisation based just on perturbative corrections to the effective action [66]. As shown in [94], when W_0 takes natural $\mathcal{O}(1-10)$ values and no blow-up modes like the 'small' modulus τ_s of LVS models are present, non-perturbative effects are subdominant with respect to perturbative corrections in either α' or g_s.

The main perturbative corrections to K which yield non-zero contributions to the scalar potential are (for an more detailed discussion of these effects see [96, 61]): $\mathcal{O}(\alpha'^3)$ corrections at tree-level in g_s have been computed and open string 1-loop effects at both $\mathcal{O}(\alpha'^2)$ and $\mathcal{O}(\alpha'^4)$ have also been computed. In the simplest case of a single Kähler modulus, these corrections to K take the form [97, 98, 99, 36]:

$$K_{g_s^0\alpha'^3} = -\frac{\xi}{g_s^{3/2}\mathcal{V}} \,, \qquad K_{g_s^2\alpha'^2} = g_s \, \frac{b(U)}{\mathcal{V}^{2/3}} \,, \qquad K_{g_s^2\alpha'^4} = \frac{c(U)}{\mathcal{V}^{4/3}} \,. \tag{3.29}$$

The parameters $b(U)$ and $c(U)$ are in general unknown functions of the complex structure moduli (and open string moduli as well) which have been computed explicitly only for simple toroidal orientifolds like $\mathbb{T}^6/(\mathbb{Z}_2 \times \mathbb{Z}_2)$ [99]. They are however expected to be $\mathcal{O}(1-10)$ numbers in absence of fine tuning. Interestingly, the $\mathcal{O}(g_s^2\alpha'^2)$ corrections to K proportional to $b(U)$ experience an 'extended no-scale' cancellation [37], and so they contribute to the scalar potential only at $\mathcal{O}(g_s^4\alpha'^4)$. Hence we can neglect them since for $g_s \lesssim 0.1$ they are subleading with respect to the correction to K proportional to $c(U)$.

After minimising the scalar potential with respect to the axio-dilaton and the complex structure moduli by solving $D_S W = D_U W = 0$, the potential for the Kähler modulus is given by:

$$V = g_s \, \frac{|W_0|^2}{\mathcal{V}^3} \left(-\frac{3|\xi|}{8 g_s^{3/2}} + \frac{c(U)}{\mathcal{V}^{1/3}} \right) , \tag{3.30}$$

where we have considered a negative value of the coefficient ξ in order to get a

minimum.[4] Minimising with respect to $\mathcal{V}$ we obtain a non-supersymmetric (since $F^T \neq 0$) AdS vacuum at:

$$\langle \mathcal{V} \rangle \simeq 26\, g_s^{9/2} \left(\frac{c}{|\xi|} \right)^3 . \tag{3.31}$$

Let us make again two important considerations:

1. The parameter controlling the string loop expansion is g_s while the α' expansion is controlled by $\mathcal{V}^{-1/3}$. Hence perturbation theory does not break down if $g_s \ll 1$ and $\mathcal{V} \gg 1$. The first of these two conditions can be satisfied by an appropriate choice of 3-form fluxes which stabilise $\mathrm{Re}(S) = g_s^{-1}$. On the other hand, the second condition, as can be seen in (3.31), requires the parameter c to be tuned such that $c \sim g_s^{-(3/2+q)} \gg 1$ with $q > 0$ (for $|\xi| \sim \mathcal{O}(1)$). In fact, plugging this relation in (3.31) one obtains $\langle \mathcal{V} \rangle \simeq 26\, g_s^{-3q} \gg 1$ for $g_s \ll 1$. Given that $c = c(U)$ is a function of the complex structure moduli which are fixed in terms of flux quanta, we expect this tuning to be possible in the string landscape by scanning through different combinations of flux quanta.

2. The minimum in (3.31) is non-supersymmetric, since $F^T \neq 0$, and AdS since $\langle V \rangle \simeq -0.1\, c\, g_s\, |W_0|^2\, \langle \mathcal{V} \rangle^{-10/3}$.

The vacuum energy can be set to zero via the same uplifting mechanisms mentioned for KKLT and LVS models which are expected to yield only subleading corrections to the location of the minimum in (3.31). Hence the gravitino mass turns out to be:

$$m_{3/2} \simeq \sqrt{\frac{g_s}{8\pi}} \frac{|W_0|}{\langle \mathcal{V} \rangle} \simeq \lambda \frac{|W_0|}{g_s^4\, c^3} \qquad \text{with} \qquad \lambda \sim \mathcal{O}(10^{-2}) . \tag{3.32}$$

In this case it is the tuned parameter c which controls the order of magnitude of the gravitino mass. The generation of the soft terms in these models with purely perturbative stabilisation of the Kähler moduli has not been studied. However we expect them to have the same behaviour as in (3.28) for LVS models since the contribution from anomaly mediation should feature a leading order cancellation due to the no-scale structure also in this case where therefore the soft terms are generated from gravity mediation.

3.2 SUSY breaking statistics with Kähler moduli stabilisation

In Sec. 3.1 we have first explained why a proper understanding of the statistics of the supersymmetry breaking scale in the type IIB flux landscape necessarily requires

[4] Notice that $\xi < 0$ would require $h^{1,2} < h^{1,1}$ which for $h^{1,1} = 1$ would work only for rigid CY manifolds without complex structure moduli, i.e. for $h^{1,2} = 0$. However the potential (3.30) could also describe a more general situation with $h^{1,1} \gg 1$ where all Kähler moduli scale in the same way, i.e. $\tau_i \sim \mathcal{V}^{2/3}\ \forall i = 1, ..., h^{1,1}$.

the inclusion of the Kähler moduli, and we have then illustrated the key-features of the main Kähler moduli stabilisation mechanisms based on different combinations of perturbative and non-perturbative corrections to the 4D effective field theory. In this section we shall instead determine the actual distribution of the gravitino mass, i.e. the actual value of the coefficient β in (3.10), for each of these scenarios separately.

3.2.1 LVS models

Let us start our analysis of the distribution of the gravitino mass by focusing first on LVS models since they do not require any tuning of the tree-level flux superpotential. In these scenarios the minimum and $m_{3/2}$ are given respectively by (3.25) and (3.26). Notice that $m_{3/2}$ in (3.26) does not depend on $|W_0|$ contrary to the expression (3.21) of the gravitino mass in KKLT models which is mainly determined by $|W_0|$.

Varying the gravitino mass with respect to the flux-dependent parameter g_s and the integer parameter $\mathfrak{n}$ which encodes the nature of non-perturbative effects, and working in the limit $a_s\tau_s \gg 1$ where the instanton expansion is under control, i.e. for $c_2 \gg g_s\mathfrak{n}$, we obtain:

$$\begin{aligned} dm_{3/2} &= \frac{\partial m_{3/2}}{\partial g_s}\, dg_s + \frac{\partial m_{3/2}}{\partial \mathfrak{n}}\, d\mathfrak{n} \simeq c_2\, \frac{m_{3/2}}{(g_s\mathfrak{n})^2}\, (\mathfrak{n}\, dg_s + g_s\, d\mathfrak{n}) \\ &\simeq m_{3/2} \left[\ln\left(\frac{M_p}{m_{3/2}}\right)\right]^2 (\mathfrak{n}\, dg_s + g_s\, d\mathfrak{n})\,, \end{aligned} \tag{3.33}$$

where in the last step we have introduced Planck units and we have approximated $m_{3/2} \sim M_p\, e^{-\frac{c_2}{g_s\mathfrak{n}}}$.

As discussed in App. and recently in [100], the distribution of the string coupling can be considered as approximately uniform[5], implying $dg_s \simeq dN$. On the other hand, the distribution of the rank of the condensing gauge group in the string landscape is still poorly understood.[6] Ref. [101] estimated the largest value of $\mathfrak{n}$ as a function of the total number of Kähler moduli, counted by the topological number $h^{1,1}$, but did not study how the number of vacua varies in terms of $\mathfrak{n}$. Moreover the F-theory analysis of [101] is based on the assumption that the formation of gaugino condensation in the low-energy 4D theory is not prevented by the appearance of unwanted matter fields.

In fact, as shown in [102, 103], F-theory sets severe constraints on the form of 'non-Higgsable' gauge groups which guarantee that the low-energy theory features a pure super Yang-Mills theory undergoing gaugino condensation. Even if simple gauge groups like $SU(2)$ or $SU(3)$ are allowed, they do not survive in the weak coupling type IIB limit since they arise only from non-trivial (p, q) 7-branes that do not admit

[5] In A.1 we numerically study this distribution for rigid Calabi-Yaus while ref. [100] focused on Calabi-Yaus where a discrete symmetry leaves effectively just 1 complex structure modulus. We both find a uniform distribution. The analysis for general Calabi-Yaus remains challenging, for this case we provide arguments based on our results for rigid Calabi-Yaus.

[6] We are thankful to R. Savelli, R. Valandro and A. Westphal for illuminating discussions on this point.

a perturbative description in terms of D7-branes. The only type IIB case allowed for pure super Yang-Mills is $SO(8)$ which corresponds to $\mathfrak{n} = 6$. This fits with the fact that all explicit type IIB Calabi-Yau orientifold models which have been constructed so far, feature exactly an $SO(8)$ condensing gauge group [104, 105, 106, 75, 107].

A non-perturbative superpotential can however arise also in a hidden gauge group with matter fields, even if there are constraints on the numbers of flavours and colours [108]. Chiral matter can always be avoided by turning off all gauge fluxes on D7-branes but vector-like states are ubiquitous features of type IIB models obtained as the $g_s \to 0$ limit of F-theory constructions. Given that the interplay between vector-like states and the generation of a non-perturbative superpotential has not been studied in the literature so far, it is not clear yet if $\mathfrak{n}$ can only take two values, i.e. $\mathfrak{n} = 1$ for ED3s and $\mathfrak{n} = 6$ for a pure $SO(8)$ theory, or an actual $\mathfrak{n}$-distribution is indeed present in the string landscape. Even if we do not have a definite answer to this question at the moment, we can however argue that, if an actual $\mathfrak{n}$-distribution exists, the number of states N is expected to decrease when $\mathfrak{n}$ increases since D7-tadpole cancellation is easier to satisfy for smaller values of $\mathfrak{n}$. We shall therefore take a phenomenological approach and assume $dN \sim -\mathfrak{n}^{-r}\, d\mathfrak{n}$ with $r > 0$. Therefore (3.33) reduces to:

$$dm_{3/2} \simeq \mathfrak{n}\, m_{3/2} \left[\ln\left(\frac{M_p}{m_{3/2}}\right)\right]^2 \left[1 - \frac{c_2\, \mathfrak{n}^{r-2}}{\ln\left(\frac{M_p}{m_{3/2}}\right)}\right] dN\,. \tag{3.34}$$

For $0 < r \leq 2$, the distribution of $m_{3/2}$ is therefore driven mainly by the distribution of the string coupling:

$$\frac{dN}{dm_{3/2}} \simeq \frac{1}{\mathfrak{n}\, m_{3/2}} \left[\ln\left(\frac{M_p}{m_{3/2}}\right)\right]^{-2} \qquad \Rightarrow \qquad N_{LVS}(m_{3/2}) \sim \ln\left(\frac{m_{3/2}}{M_p}\right)\,, \tag{3.35}$$

where we neglected subleading logarithmic corrections.[7] Comparing this results with (3.11), we realise that in LVS models $\beta = -2$, and so we end up with the following the distribution of the gravitino mass:

$$\boxed{\rho_{LVS}(m_{3/2}) \;\sim\; \frac{1}{\mathfrak{n}\, m_{3/2}^2} \left[\ln\left(\frac{M_p}{m_{3/2}}\right)\right]^{-2}}\,. \tag{3.36}$$

On the other hand, for $r > 2$, the distribution of the number of D7-branes starts to play a rôle in the distribution of $m_{3/2}$ when $\mathfrak{n}$ is large. However, except for different subdominant logarithmic corrections, the leading order expression for the number of states as a function of the gravitino mass would still be given by (3.35). It is reassuring to notice that our result is independent on the exact form of the unknown $\mathfrak{n}$-distribution.[8]

[7] Notice that the result is unchanged if the distribution of the dilaton is taken to be power-law.

[8] This is true unless N decreases exponentially when $\mathfrak{n}$ increases but this behaviour looks very unlikely.

Notice that the result (3.34) applies also to the distribution of the soft terms. In fact, as summarised in (3.28) and as reviewed more in detail in App. A.2, the gravitino mass can generically be written in terms of the energy scale associated to the soft terms as $m_{3/2} \simeq M_{\rm soft}^{1/p}$ where for D7-branes $p = 1$, while for D3-branes $p = 2$ for gaugino masses and $p = 2$ or $p = 3/2$ for scalar masses depending on the 'uplifting' mechanism. Thus in LVS models also the distribution of the soft masses turns out to be logarithmic:

$$N_{LVS}(M_{\rm soft}) \sim \frac{1}{p} \ln\left(\frac{M_{\rm soft}}{M_p}\right) . \tag{3.37}$$

This result is particularly important for models where the visible sector is realised on stacks of D3-branes since in this case the visible sector gauge coupling is set by g_s which is therefore fixed by the phenomenological requirement of reproducing the observed visible sector gauge coupling. Hence the distribution of $m_{3/2}$ (or equivalently $M_{\rm soft}$) is entirely determined by the distribution of $\mathfrak{n}$. For this scenario, it would be very interesting to know if a non-perturbative superpotential can indeed be generated also in the presence of vector-like matter. If this does not turn out to be the case, then the value of the gravitino mass in LVS models with the visible sector on D3-branes can only take two values (setting the string coupling of order the GUT coupling $g_s = \alpha_{GUT} = 1/25$, $A_s \sim \mathcal{O}(1-10)$ and $\xi = 1$):

- **ED3-instantons**: in this case $\mathfrak{n} = 1$ and:

$$m_{3/2} = g_s\, c_1\, e^{-\frac{c_2}{g_s}} \sim \mathcal{O}(10^{-26} - 10^{-27})\,\text{GeV} . \tag{3.38}$$

- **Pure** $SO(8)$: in this case $\mathfrak{n} = 6$ and:

$$m_{3/2} = g_s \frac{c_1}{6}\, e^{-\frac{c_2}{6\, g_s}} \sim \mathcal{O}(10^{9} - 10^{10})\,\text{GeV} . \tag{3.39}$$

Notice that the ED3-case would be viable only for models where supersymmetry is broken by brane construction, so that the soft terms are at the string scale which is however around the TeV-scale. The extremely low value of $m_{3/2}$ might be helpful to control corrections to the vacuum energy coming from loops of bulk states [89]. The pure $SO(8)$ case instead corresponds to a more standard situation where however TeV-scale soft terms could be achieved only via sequestering effects [63, 65].

3.2.2 KKLT models

Let us now study the distribution of the gravitino mass in KKLT models where the minimum and $m_{3/2}$ are given respectively by (3.19) and (3.21). Varying the gravitino mass with respect to the two flux-dependent parameters g_s and $|W_0|$, and the integer parameter $\mathfrak{n}$, we obtain:

$$dm_{3/2} \simeq m_{3/2}\left(\frac{d|W_0|}{|W_0|} + \frac{1}{2}\frac{dg_s}{g_s} - \frac{3}{2}\frac{d\mathfrak{n}}{\mathfrak{n}}\right) , \tag{3.40}$$

where we neglected the subleading variation of the logarithm. Following the arguments given in Sec. 3.2.1 and in App. A.1, we assume a uniform distribution of the string coupling, i.e. $dN \simeq dg_s$, and a phenomenological scaling of the distribution of $\mathfrak{n}$ of the form $dN \simeq -\mathfrak{n}^{-r}\, d\mathfrak{n}$. Moreover the distribution of W_0 as a complex variable is also uniform [50], resulting in $dN \simeq |W_0| d|W_0|$. Thus (3.40) reduces to:

$$\begin{aligned} dm_{3/2} &\simeq m_{3/2}\left(\frac{1}{|W_0|^2}+\frac{1}{2g_s}+\frac{3}{2}\,\mathfrak{n}^{r-1}\right) dN \\ &\simeq \frac{M_p^2}{m_{3/2}}\left[\frac{g_s}{\mathfrak{n}^3|\ln W_0|^3}+\frac{\epsilon^2}{2}\left(\frac{1}{g_s}+3\mathfrak{n}^{r-1}\right)\right] dN\,, \end{aligned} \tag{3.41}$$

where $\epsilon \equiv m_{3/2}/M_p$. In order to trust the effective field theory description we need to require $\epsilon \ll 1$, which implies that the distribution of the gravitino mass is dominated by the first term in (3.41), i.e. by the distribution of the flux superpotential:

$$\frac{dN}{dm_{3/2}} \simeq \left(\frac{\mathfrak{n}^3|\ln W_0|^3}{g_s}\right)\frac{m_{3/2}}{M_p^2} \simeq \frac{m_{3/2}}{M_p^2} \qquad \Rightarrow \qquad N_{KKLT}(m_{3/2}) \sim \left(\frac{m_{3/2}}{M_p}\right)^2 . \tag{3.42}$$

Comparing this results with (3.11), we realise that in KKLT models $\beta = 0$, in agreement with previous predictions [47]. Thus we end up with the following the distribution of the gravitino mass:

$$\boxed{\rho_{KKLT}(m_{3/2}) \sim \frac{1}{M_p^2}\left(\frac{\mathfrak{n}^3|\ln W_0|^3}{g_s}\right) \sim \text{const.}} \tag{3.43}$$

As reviewed App. A.2, in KKLT models the soft terms are proportional to the gravitino mass (up to a possible 1-loop suppression factor for visible sector models on D3-branes). Therefore (3.42) and (3.43) give also the distribution of the soft terms in KKLT models.

3.2.3 Perturbatively stabilised models

Let us now study the distribution of the gravitino mass in perturbatively stabilised models where the minimum and $m_{3/2}$ are given respectively by (3.31) and (3.32). Varying the gravitino mass with respect to the three flux-dependent parameters g_s, $|W_0|$ and c, we obtain:

$$dm_{3/2} \simeq m_{3/2}\left(\frac{d|W_0|}{|W_0|}-4\,\frac{dg_s}{g_s}-3\,\frac{dc}{c}\right), \tag{3.44}$$

As discussed in [50] and in App. A.1, both g_s and W_0 are expected to be uniformly distributed, and so we take $dN \simeq dg_s$ and $dN \simeq |W_0| d|W_0|$. Moreover, as stressed in Sec. 3.1.6, the coefficient c is a function of the complex structure moduli which are fixed in terms of flux quanta, and so it is naturally expected to be of order $c \sim \mathcal{O}(1-10)$. However the minimum in (3.31) lies at $\mathcal{V} \gg 1$ only if the flux

quanta are tuned such that $c \sim g_s^{-(3/2+q)} \gg 1$ with $q > 0$. Given that this is a tuned situation, we expect the number of vacua at $c \gg 1$ to be suppressed with respect to the region with $c \sim \mathcal{O}(1-10)$. This behaviour is well described by a distribution of c with a phenomenological scaling of the form $dN \simeq -c^{-k}\, dc$ with $k > 0$. Using all these relations, (3.44) becomes:

$$\begin{aligned} dm_{3/2} &\simeq m_{3/2}\left(\frac{1}{|W_0|^2} - \frac{4}{g_s} + 3\,c^{k-1}\right) dN \\ &\simeq m_{3/2}\left(3\,c^{k-1} - \frac{4}{g_s}\right) dN\,, \end{aligned} \tag{3.45}$$

where we focused on the region with $|W_0| \sim \mathcal{O}(1-10)$ and $g_s \lesssim 0.1$. Notice that for such a small value of the string coupling and $0 < k \leq 1$, the second term in (3.45) would dominate over the first one. However this is a regime where the distribution of the coefficient c would be almost uniform, and so c would be in the regime $c \sim \mathcal{O}(1-10)$ where the effective field theory is not under control. We focus therefore on $k > 1$ where the distribution of c starts to deviate from begin uniform, signaling that c is tuned to large values. In this case the distribution of the gravitino mass is dominated by the first term in (3.45) and becomes:

$$\frac{dN}{dm_{3/2}} \simeq \frac{1}{m_{3/2}\; c^{k-1}} \simeq \left(\frac{g_s^4}{|W_0|}\right)^{\frac{(k-1)}{3}} \frac{1}{M_p} \left(\frac{m_{3/2}}{M_p}\right)^{\frac{(k-4)}{3}}\,, \tag{3.46}$$

which implies:

$$N_{PERT}(m_{3/2}) \sim \left(\frac{m_{3/2}}{M_p}\right)^{\frac{(k-1)}{3}}\,. \tag{3.47}$$

Comparing this results with (3.11), we realise that in perturbatively stabilised models $\beta = (k-7)/3$. Hence we end up with the following distribution of the gravitino mass:

$$\boxed{\rho_{PERT}(m_{3/2}) \;\sim\; \frac{1}{M_p^2}\left(\frac{m_{3/2}}{M_p}\right)^{\frac{(k-7)}{3}}}\,. \tag{3.48}$$

This result is qualitatively similar to the one of KKLT models (which are reproduced exactly for $k = 7$), showing that scenarios where the Kähler moduli are stabilised by perturbative effects favour higher values of the gravitino mass. This behaviour is somewhat expected since these models, similarly to KKLT, can yield trustable vacua only relying on tuning the underlying parameters. This tuning, in turn, reflects itself on the preference for larger values of $m_{3/2}$. As mentioned in Sec. 3.1.6, in perturbatively stabilised models the soft terms are expected to be proportional to the gravitino mass, and so (3.47) and (3.48) give also the distribution of the soft terms in these models.

3.3 Discussion

In this section we summarise our results and discuss them in the context of the original results of [46, 47, 48, 49, 50, 51], as well as the subsequent results obtained in [68, 69, 70, 71].

3.3.1 Interplay with previous results

Firstly, we have stressed in Sec. 3.1 that Kähler moduli stabilisation is a critical requirement for a proper treatment of the statistics of supersymmetry breaking. The reason is that a stable solution requires the F-terms of the axio-dilaton and the complex structure moduli to be suppressed with respect to the F-terms of the Kähler moduli. The statistics of supersymmetry breaking is thus entirely driven by the F-terms of the Kähler moduli at their stabilised values.

As we have shown, the no-scale structure at tree level has important consequences for the statistics of supersymmetry breaking. It implies that in order to obtain vacua where the α' and g_s expansions are under control, terms in the effective action which are part of separate expansions have to be balanced against each other (see [96] for a detailed discussion of this point). For example, in LVS we find that α' corrections associated with the overall volume are balanced against a non-perturbative correction associated with a blow-up modulus. In KKLT, on the other hand, non-perturbative effects are balanced against an exponentially small flux superpotential. This implies that the stabilisation mechanism pushes us to particular regions in moduli space – in LVS the overall volume is large, while in KKLT $|W_0|$ is inevitably small – where the gravitino mass takes specific values.

This has important implications for the statistics of soft terms which in gravity mediation are determined by $m_{3/2}$. As we have seen in Sec. 3.2, different stabilisation mechanisms predict different distributions of the gravitino mass (and hence the soft terms) in the landscape. This is due to the fact that different no-scale breaking effects used to fix the Kähler moduli lead to a different dependence of $m_{3/2}$ on the flux-dependent microscopic parameters W_0, g_s and c whose distribution (together with the one of $\mathfrak{n}$) ultimately governs the statistics of the soft terms, as is evident from (3.33), (3.40) and (3.45). In particular, we found that in LVS models the distributions of the gravitino mass and soft terms are logarithmic, as shown in (3.35) and (3.37). On the other hand, for KKLT and perturbative stabilisation, the distributions are power-law, as shown in (3.42) and (3.47). The difference in behaviour comes from the fact that in the LVS case one has from (3.26):

$$m_{3/2} \sim M_p \, e^{-\frac{1}{g_s}} \,, \tag{3.49}$$

which, when combined with the fact that g_s is uniformly distributed as shown in App. A.1, yields a logarithmic distribution for $m_{3/2}$. For KKLT, one has instead from (3.21):

$$m_{3/2} \sim |W_0| \, M_p \,, \tag{3.50}$$

which results in a power-law distribution of the gravitino mass since since $|W_0|$ is uniformly distributed. A similar reasoning applies in the case of perturbative stabilisation.

Interestingly, we note that both power-law [47, 50, 51] as well as logarithmic distributions [68, 69, 70, 71] have been obtained by different groups in the literature, albeit for reasons different from the ones we have derived. The power-law distribution of gravitino masses in (3.42) and (3.47) for KKLT and perturbatively stabilised vacua reproduces the results of [47, 50, 51] which were based on the assumption of a democratic distribution of complex structure F-terms caused by the uniform distribution of $|W_0|$, as we have reviewed in Sec. 3.1.1. In KKLT and perturbatively stabilised vacua, the supersymmetry breaking scale is instead determined by the F-terms of the Kähler moduli but we obtain the same behaviour given that in these two Kähler stabilisation schemes they are also governed dominantly by $|W_0|$. On the other hand, the logarithmic distributions (3.35) and (3.37) of LVS models reproduce the results of [68, 69, 70, 71] whose derivation was based on the general nature of dynamical supersymmetry breaking: if the scale of supersymmetry breaking is given by $m_{3/2} \sim M_p\, e^{-8\pi^2/g^2}$ with a flat distribution in the coupling g^2, then $m_{3/2}$ would obey a logarithmic distribution. Indeed, this expectation is exactly reproduced by the expression (3.49) for the gravitino mass in LVS models since in type IIB compactifications the gauge coupling g of a hidden sector supporting non-perturbative effects which break supersymmetry dynamically scales as $g^2 \sim g_s$.

Determining which distribution, power-law or logarithmic, is more representative of the structure of the flux landscape therefore translates into the question of which vacua with stabilised Kähler moduli arise more frequently. Given that LVS models can be realised for natural values of the vacuum expectation value of the flux superpotential, $|W_0| \sim \mathcal{O}(1-10)$, while KKLT models can be constructed only via tuning $|W_0|$ to exponentially small values (similar considerations about tuning of the underlying parameters apply also to perturbatively stabilised vacua), we tend to conclude that the distribution of the scale of supersymmetry breaking seems to be logarithmic. However, more detailed studies are needed in order to find a precise definite answer to this important question (see [74, 75, 76, 77, 78] for initial studies on the determination of the number of vacua as a function of $|W_0|$ and g_s).

Finally, we would like to make a few comments discussing our results in the context of the cosmological constant. The explicit analysis carried out in the previous section focused on solutions with zero cosmological constant and so far we considered the joint distribution of the supersymmetry breaking scale and the cosmological constant. As we have mentioned before, soft masses for the SM sector are typically predominantly determined by a small set of non-vanishing F-terms and D-terms in the theory. On the other hand, the cosmological constant receives contributions from *all* F and D-terms, many of which can be sequestered from the SM sector and make subdominant contributions to supersymmetry breaking. This has two implications: (*i*) to compute distributions of the cosmological constant one needs to have a knowledge of all the uplift contributions, which is generally challenging; and (*ii*) since a large number of contributions to the cosmological constant do not

affect the soft masses, one can expect the distribution of the cosmological constant to be independent of the distribution of the soft masses. LVS models are a neat example where the decoupling between the statistics of supersymmetry breaking and the cosmological constant emerges clearly. In fact, combining the expression (3.24) of the scalar potential of LVS models with the location of the minimum (3.25), it is easy to see that the depth of the non-supersymmetric AdS vacuum is:

$$V_{LVS} \sim -\frac{|W_0^2|}{\mathcal{V}^2} \sim -m_{3/2}^3 M_p \,. \tag{3.51}$$

This implies that any hidden sector whose dynamics is responsible for dS uplifting has to provide a contribution to the scalar potential whose order of magnitude is:

$$V_{\rm up} \sim |F_{\rm hid}|^2 \sim m_{3/2}^3 M_p \,. \tag{3.52}$$

In turn this hidden sector generates a contribution to the soft terms via gravity mediation which is suppressed with respect to the gravitino mass:

$$\delta M_{\rm soft} \sim \frac{F_{\rm hid}}{M_p} = m_{3/2}\sqrt{\frac{m_{3/2}}{M_p}} \ll m_{3/2} \,. \tag{3.53}$$

Hence, if the F-terms of other hidden sectors (like for example the F-term of the Kähler modulus controlling the volume of the 4-cycle wrapped by the SM stack of D7-branes) generate soft terms of order $m_{3/2}$, the contribution from $F_{\rm hid}$ is clearly negligible. Notice that this implies that the distribution of the supersymmetry breaking scale is the same at least for all vacua with cosmological constant in the range $\pm V_{LVS}$. Of course, the distribution could change if we consider vacua with much higher values of the cosmological constant.

3.3.2 Implications for phenomenology

We now turn to a brief discussion of the implications of our findings for low energy phenomenology. The ATLAS collaboration has provided 95% CL search limits for gluino pair production within various simplified models using data sets that vary from 36-139 fb^{-1} at $\sqrt{s} = 13$ TeV [109]. The approximate bound from these searches is that $m_{\tilde{g}} \gtrsim 2.2$ TeV. The limits coming from CMS are comparable [110]. Searches for top squark pair production yield the limit $m_{\tilde{t}} \gtrsim 1$ TeV [111, 112].

We have found that the statistics of type IIB flux vacua generally prefers a draw towards high scale supersymmetry: a mild logarithmic draw in the case of LVS, and a strong power-law draw in the case of KKLT and perturbatively stabilised vacua. Given the current limits on gluinos and squarks, can one surmise that it is this statistical draw that is being played out at experiments?

Of course, the problem with this interpretation is that high scale supersymmetry breaking leads to fine-tuning issues for the mass of the Higgs, obviating, at least from the low-energy perspective, the introduction of supersymmetry as a solution to the gauge hierarchy problem in the first place. The severity of this issue may

be quantified by the choice of suitable fine-tuning measures. In other words, since stringy naturalness (the bias towards a property favored by vacuum statistics, in this case, high scale supersymmetry breaking) leads one to posit heavier superpartners, this tendency should somehow be mitigated by a fine-tuning penalty as one goes to higher scales. But which fine-tuning measure should one use, and how much penalty should one impose?

The widely adopted Barbieri-Giudice measure [113] is defined as $\Delta_{BG} \equiv \max_i |\frac{\partial \ln m_Z^2}{\partial \ln p_i}|$ with, for example, $\Delta_{BG} < 10$ corresponding to $\Delta_{BG}^{-1} = 10\%$ fine-tuning. The p_i are the fundamental parameters of the theory, while m_Z denotes the mass of the Z boson. Taking the parameters to be the various soft terms and μ parameter from the mSUGRA/CMSSM model and requiring 10% fine-tuning, one obtains upper limits of $m_{\tilde{g}} \sim 400$ GeV [38]. Most other superpartners are also close to the weak scale (defined as $m_{\rm weak} \simeq m_{W,Z,h} \sim 100$ GeV). It is thus clear from the Barbieri-Giudice measure that supersymmetry is already very finely tuned from LHC data. From the perspective of the landscape, one can impose a penalty on Δ_{BG} for vacua with very high scale supersymmetry breaking (while also allowing for the fine-tuning indicated by data) but it is not entirely clear what the penalty should be or how to motivate it.

An alternative approach is to use anthropic arguments to motivate fine-tuning penalties on vacua with high scale supersymmetry breaking [67, 114, 115].[9] The atomic principle [117] comes closest in relevance in this context. It can be incorporated within the fine-tuning measure introduced in [118], whose starting point is the expression for the mass of the Z boson in supersymmetry: $m_Z^2/2 \simeq -m_{H_u}^2 - \mu^2 - \Sigma_u^u(\tilde{t}_{1,2})$ (for details and exact expressions, we refer to the original paper and [38]). Here, Σ_u^u contains the various radiative corrections [119]. The fine-tuning penalty in this case posits that no single contribution in the expression for m_Z can be too much larger than any other. This is quantified by the measure Δ_{EW} which is the maximum among the quantities on the right hand side divided by the $m_Z^2/2$.

It is now clear how the atomic principle naturally plays into the fine-tuning measure Δ_{EW}. Given that the mass of the Z boson is bounded by the atomic principle, one obtains an anthropic bound on the scale of the superpartners stemming from their contributions to the radiative corrections encapsulated in Σ_u^u. Indeed, requiring that the mass of the Z boson should not exceed its measured value by a factor of 4 imposes $\Delta_{EW} \lesssim 30$, which in turn translates into upper bounds on superpartner masses entering through the radiative corrections Σ_u^u.

One thus has a logarithmic or power-law distribution of vacua biasing towards high supersymmetry breaking scales, tempered by a penalty of $\Delta_{EW} \lesssim 30$ coming from the atomic principle. For power-law distributions, this leads to several predictions for superpartner masses that may be probed at the HL-LHC. For example, the statistical distribution for gluinos and top squarks are peaked around 4 TeV and 1.5 TeV, respectively. Suggestively, the Higgs mass appears to be peaked around 125 GeV for power-law distributions. A logarithmic distribution from the landscape, on the other hand, would imply that a low scale of supersymmetry breaking is reasonably

[9] Indeed, the landscape is already a fertile arena where such arguments have been used in the past, most famously in the context of the cosmological constant problem [44, 116].

probable, perhaps without relying too strongly on anthropic arguments. The value of the weak scale may simply be a mild accident in that case. We leave a more detailed treatment of the phenomenology of the logarithmic case for future work.

3.4 Conclusions

Understanding the distribution of the supersymmetry breaking scale in string vacua is an important question which can potentially have deep phenomenological implications. In this paper, we have revisited this question in the context of IIB flux vacua. In the first part of the paper, we argued that the details of Kähler moduli stabilisation are absolutely necessary to study the distribution of the supersymmetry breaking scale. We then went on to study the distribution of the supersymmetry breaking scale (primarily focusing on vacua with zero cosmological constant) in three scenarios for Kähler moduli stabilisation: (*i*) models with purely non-perturbative stabilisation like in KKLT vacua; (*ii*) models where the Kähler moduli are frozen by balancing perturbative against non-perturbative effects as in LVS models; and (*iii*) models with purely perturbative stabilisation. For KKLT and models with perturbative stabilisation we found a power law distribution, while for LVS we found a logarithmic distribution. The logarithmic distribution is particularly interesting as it could well mean that we should remain optimistic about discovering superpartners in collider experiments.

Let us mention that our results for the distribution of the supersymmetry breaking scale in the type IIB flux landscape are based on the fact that $|W_0|$ and g_s are uniformly distributed.[10] While in the literature there is a lot of evidence in favour of this assumption (as we also have shown for the distribution of the string coupling for rigid Calabi-Yaus), more detailed numerical studies are needed in order to confirm the validity of this behaviour for the general case. This investigation is crucial also to determine which distribution, power-law or logarithmic, is predominant in the flux landscape since the distribution of the vacuum expectation value of the flux-generated superpotential is a key input for determining the relative preponderance of KKLT and LVS vacua. Furthermore, the results of [120] imply that knowledge of the distribution of W_0 is central to developing a detailed understanding of the distribution of the cosmological constant.

This work opens up several interesting directions for future research. Firstly, it is important to carry out a detailed study along the lines of [38] to understand the phenomenological implications of the logarithmic distribution. In order to make contact with observations it will be crucial to incorporate also bounds arising from the cosmological context (such as the cosmological moduli problem). Our analysis has focused on a small (but highly attractive from the point of view of phenomenology) corner of the string landscape, i.e type IIB flux compactifications on Calabi-Yau orientifolds. It will be interesting to carry out an analysis in the same spirit as this paper in other corners of the landscape.[11] A related but very challenging question is

[10] The result for LVS is unchanged as long as the distribution for g_s is a power-law.

[11] Even within the context of type IIB, it will be interesting to explore the constructions in

to investigate if early universe cosmology gives us a natural measure on the space of solutions in string theory.

[121] which naturally have a high scale of supersymmetry breaking, even if the visible sector phenomenology is not well developed in this setting. Another aspect of the IIB landscape that we have not explored is the effect of warped throats. Since warped throats are a generic feature in IIB flux compactifications [30, 122, 123], they could well have an important effect on the statistics of the scale of supersymmetry breaking.

Chapter 4

AXION STATISTICS

The Peccei-Quinn mechanism is without any doubt the most elegant solution to the strong CP problem. It postulates the existence of an anomalous global $U(1)_{\rm PQ}$ symmetry which is spontaneously broken at f_a. The corresponding Goldstone boson is the so-called QCD axion a which enjoys a continuous shift symmetry. QCD instantons lift the axionic direction and provide a minimum where CP is conserved. The QCD axion develops a mass of order $m_a \sim \Lambda^2_{QCD}/f_a$ and naturally contributes to the dark matter (DM) abundance. The phenomenologically allowed window for the axion decay constant f_a is given by $10^9\,{\rm GeV} \lesssim f_a \lesssim 10^{12}\,{\rm GeV}$, where the lower bound is due to astrophysical and direct observations while the upper bound comes from the requirement to avoid DM overproduction if the initial misalignment angle takes natural $\mathcal{O}(1)$ values.

This scenario for the solution of the strong CP problem relies on some assumptions which have to be checked in a UV complete embedding. Some crucial questions which need to be answered are: (i) What is the origin of the axion shift symmetry?; (ii) What dynamics breaks $U(1)_{\rm PQ}$ spontaneously and sets the value of f_a?; (iii) Is f_a related to other important physical quantities like the Planck scale M_p, the string scale M_s, the GUT scale M_{GUT}, the Kaluza-Klein scale M_{KK} or the scale of soft supersymmetry breaking terms $M_{\rm soft}$?; (iv) what dynamics breaks $U(1)_{\rm PQ}$ explicitly and sets the value of m_a?; (v) Is m_a generated by QCD instantons or by other effects?: (vi) How many axion-like particles (ALPs) can arise from UV physics?; (vii) What is the allowed range of f_a and m_a for these ALPs?

Several studies performed during the last 15 years revealed that string theory can provide a successful answer to many, if not all, of the previous questions [124, 125, 126, 127]. However, as mentioned in the introduction, string theory admits a plethora of 4D solutions which goes under the name of string *landscape*. Even if all 4D string vacua share some generic features about axion physics, the number of axions and the corresponding values of f_a and m_a take different values in different string vacua. In order to make contact with observations, it is therefore crucial to perform a statistical analysis of the distribution in the string landscape of phenomenologically relevant quantities like f_a and m_a which determine the axion DM abundance.

As stressed in chapter 3 where we derived the distribution of the supersymmetry

breaking scale in the string landscape, these statistical studies need to be based on a solid understanding of moduli stabilisation. In the case of axion physics, the motivation is the following. We shall focus on the type IIB flux compactifications which provide a well-defined subset of the string landscape. A model-independent origin of 4D axions is provided by the higher-dimensional gauge form C_4 which gives rise to pseudoscalars with a continuous shift symmetry when reduced on internal 4-cycles Σ_4^i: $\theta_i = \int_{\Sigma_4^i} C_4$. These axions are the imaginary parts of the Kähler moduli $T_i = \tau_i + \mathrm{i}\,\theta_i$ whose real parts τ_i control the volume of Σ_4^i in string units. Due to a combination of supersymmetry, scale invariance and the axionic shift symmetry, at tree-level each T_i is a flat direction [61]. The axionic directions θ_i are lifted by instantons which preserve only a discrete shift symmetry. On the other hand, the saxions τ_i can be stabilised either at perturbative or at non-perturbative level. Let us comment on the implications of these two situations for axion physics:

- If a given saxion τ is fixed by non-perturbative physics as in KKLT models [33], the stabilisation is at leading order supersymmetric, implying $m_\theta \sim m_\tau \sim m_{3/2}$. Given that the absence of any cosmological moduli problem requires $m_\tau \gtrsim \mathcal{O}(50)$ TeV [81] and $m_{3/2}$ sets the mass of the superpartners which cannot be lower than the TeV-scale, in this case the axion θ is generically very heavy, and so cannot play the role of the QCD axion [127].

- If τ is stabilised by perturbative physics (such as α' and/or string loop corrections to the Kähler potential), at this level of approximation $m_\tau \sim m_{3/2}$ while $m_\theta = 0$. In the regime where the effective field theory (EFT) is under control, i.e. where non-perturbative contributions are exponentially suppressed with respect to perturbative terms, instanton effects will lift θ while inducing negligible corrections to the stabilisation of τ. This would produce the mass hierarchy $m_\theta \ll m_\tau \sim m_{3/2}$ which identifies θ as a promising QCD axion candidate with $\theta \simeq a/f_a$.

Besides focusing on models where τ is fixed at perturbative level, the other conditions to be checked to get a viable QCD axion are that θ couples to the QCD sector coming from stacks of D7-branes,[1] and that stringy instantons generate a mass $m_{\theta,\mathrm{str}}$ for θ which is smaller than the one developed by QCD instantons, i.e. $m_{\theta,\mathrm{str}} \ll \Lambda_{QCD}^2/f_a$.

If all these conditions are satisfied, one has still to derive the value of f_a which determines all the main phenomenological properties of the QCD axion: its mass, its couplings and its contribution to the DM abundance. Depending on the topology of the 4-cycle Σ_4, f_a can be either of order M_{KK} for bulk cycles, or of order M_s for blow-up modes [125, 127]. In a given moduli stabilisation framework, these two fundamental scales can be explicitly written down in terms of the underlying parameters (like the string coupling g_s and the vacuum expectation value of the tree-level superpotential W_0) which depend on flux quanta. By exploiting the known

[1] Notice that when the QCD sector lives on D3-branes at singularities, C_4-axions are eaten up by anomalous $U(1)$ and the QCD axion arises from open string modes [128].

distributions of g_s and W_0 in the flux landscape [50], one can therefore derive the distribution of f_a. We shall perform this analysis by focusing on the Large Volume Scenario (LVS) [32, 34] which fixes some Kähler moduli at perturbative level, and find that f_a features a logarithmic distribution.

We shall consider two possible realisations of the QCD axion: (i) axions associated to blow-up modes, and (ii) axions associated to bulk cycles. In case (i) f_a is independent on the Standard Model (SM) gauge coupling, while in case (ii) the decay constant is fixed around the GUT scale by the requirement of reproducing the observed visible sector gauge coupling α_{SM}. Hence, once we focus on phenomenologically relevant vacua with $\alpha_{SM}^{-1} \sim \mathcal{O}(10\text{-}100)$, only axions associated to blow-up modes feature a logarithmic distribution of f_a. However we consider this to be the generic situation for vacua where the EFT is under control since axions from bulk cycles require an anisotropic shape of the extra dimensions which corresponds to a tuned situation for moduli stabilisation. The reason is the interplay between two conflicting conditions: the low-energy 4D EFT can be trusted only for large values of the internal Calabi-Yau (CY) manifold, while $\alpha_{SM}^{-1} \sim \mathcal{O}(10\text{-}100)$ implies that the 4-cycle supporting the SM brane system cannot be too large.

This result confirms the naive expectation that a generic 4D string model is characterised by a QCD axion with a GUT scale decay constant which would overproduce DM if the initial misalignment angle $\theta_{\rm in}$ is not tuned close to zero. However it also shows that string vacua with a QCD axion with an intermediate scale f_a and an $\mathcal{O}(1)$ value of $\theta_{\rm in}$ are not so rare since the number of flux vacua grows with f_a only as a logarithm, instead of a power-law.

Interestingly, in chapter 3 we found that also the distribution of the gravitino mass in the flux landscape is logarithmic,[2] providing the intriguing indication that most, if not all, of the phenomenologically interesting quantities in the string landscape might feature a logarithmic distribution. Once the distributions of more than one phenomenological quantity are known, it is important to look at potential correlations among them. In our case, we find that vacua with an intermediate scale f_a are also characterised by TeV-scale soft-terms, as typical of LVS models [94].

Let us finally mention that a generic CY gives rise to many Kähler moduli in the 4D EFT. If several of them are stabilised by perturbative effects, only one of them will play the role of the QCD axion while all the others would behave as ALPs which tend to be ultra-light in the regime where the computational control over the EFT is solid. These ALPs have interesting applications to DM [131], dark radiation [132, 133, 134, 135] and astrophysics [136, 137]. We shall therefore derive also the distribution in the flux landscape of the decay constants, the mass spectrum and the DM contribution of stringy ALPs, finding again a logarithmic dependence.

One may wonder whether our findings provide a trustable representation of the generic situation for axion physics in the flux landscape since they are based on the LVS framework while other moduli stabilisation mechanisms at perturbative

[2] To be more precise, in [1] we concluded that the distribution of the gravitino mass is logarithmic in LVS models and power-law in KKLT scenarios. However recent explicit constructions of KKLT models [76, 129, 130] might indicate a logarithmic distribution also for the KKLT case.

level have been proposed [66]. However recent studies of the Kähler cone of CY manifolds with a large number of Kähler moduli $h^{1,1}$ revealed that, in the regime where the volume of each holomorphic curve is larger than the string scale so that the α' expansion is under control, the overall volume in string units grows as $\mathcal{V} \gtrsim (h^{1,1})^7$ [138]. This clearly implies that for a generic CY with $h^{1,1} \sim \mathcal{O}(100)$, the EFT can be under control only if the moduli are fixed at $\mathcal{V} \gtrsim \mathcal{O}(10^{14})$. Given that only LVS models yield an exponentially large CY volume which can naturally account for such a large value of $\mathcal{V}$, we believe that the genericity of our results is rather robust. Ref. [90] presented an explicit LVS moduli stabilisation procedure which can lead to an exponentially large CY volume for arbitrarily large $h^{1,1}$ exploiting instantons on del Pezzo divisors and $\mathcal{O}(\alpha'^3)$ corrections at $\mathcal{O}(F^2)$ and $\mathcal{O}(F^4)$ (where F denotes an F-term). This moduli stabilisation scenario leads to several ultra-light axions in agreement with the expectation of [138].

Moreover, ref. [139, 140] derived the distributions of the axion decay constants and masses for different values of $h^{1,1}$ but at a given point in the moduli space, focusing in particular on the tip of the so-called stretched Kähler cone, i.e. the point closest to the origin which allows to keep the EFT under control. Interestingly, they found that the mean value of f_a decreases as $h^{1,1}$ increases. Our results are complementary to the ones of [139, 140] since we included moduli stabilisation and worked out the distribution of f_a and m_a as a function of flux quanta, i.e. moving in the moduli space at fixed $h^{1,1}$. The results of [139, 140] can be integrated with ours since they provide the boundaries of the region in moduli space where the EFT is under control and our logarithmic distributions can be trusted, i.e. our logarithmic distributions are valid for $f_a \lesssim f_{a,\max}(h^{1,1})$ or $m_a \lesssim m_{a,\max}(h^{1,1})$ with $f_{a,\max}(h^{1,1})$ and $m_{a,\max}(h^{1,1})$ as given in [139, 140] as a function of the number of Kähler moduli $h^{1,1}$.

Similar considerations apply to the comparison of our findings with the ones of [141] which noticed that, in the presence of $N \gg 1$ ALPs which are effectively massless, there is just a linear combination of them which couples to photons. Ref. [141] derived the distribution of the corresponding ALP-photon coupling $g_{a\gamma\gamma}$ as a function of N (with $N \sim h^{1,1}$) at a fixed point in moduli space, choosing again the tip of the stretched Kähler cone. For type IIB flux vacua, they found $g_{a\gamma\gamma}(N) \sim 10^{-21}\, N^4\, \text{GeV}^{-1}$ which, according to our previous considerations, can be considered as a lower bound for a logarithmic distribution of $g_{a\gamma\gamma}$ as a function of different flux vacua at fixed N, when moduli stabilisation is taken into account along the lines of this work.

This chapter is organised as follows. In Sec. 4.1 we discuss in depth the interplay between axion physics and moduli stabilisation. We first describe in detail an example with $h^{1,1} = 4$ where the QCD axion can arise from either a bulk or a blow-up cycle, and then we discuss a more general example with arbitrarily large $h^{1,1}$. In Sec. 4.2 we derive the distribution in the type IIB flux landscape of several quantities of axion physics relevant for phenomenology: decay constants, masses, DM abundance, axion couplings to gauge bosons and axion dark radiation in Fibre Inflation models [142, 143, 144, 145, 90, 146, 147, 148]. We discuss our results and present our

conclusions in Sec. 4.3. Three appendices are devoted to provide technical details: App. B.1 gives the details of the axion canonical normalisation; App. B.2 provides a few benchmark points which reproduce the observed fuzzy DM abundance for ultra-light stringy ALPs; App. B.3 shows the distribution of additional quantities relevant for phenomenology, like moduli masses and the reheating temperature from moduli decay, which also feature a logarithmic distribution in the flux landscape.

4.1 Axions and moduli stabilisation

As explained in Sec. 4, axions can be light (i.e. much lighter than the gravitino and the soft terms) only if supersymmetry is broken and the corresponding saxions are fixed at perturbative level. Moreover models with a large number of Kähler moduli require a huge CY volume to keep control over the α' expansion. These two considerations single out type IIB LVS models as the best framework to study the interplay between axion physics and moduli stabilisation.

We shall now describe moduli stabilisation for a toy-model which can feature up to 3 light axions. This model is, at the same time, simple enough to perform moduli stabilisation in full detail, and rich enough to be a good representative of a more generic situation. In fact, it has 1 axion which becomes as heavy as the gravitino because of non-perturbative stabilisation, 1 ultra-light bulk axion which plays the role of an ALP, and 2 QCD axion candidates arising from the reduction of C_4 over a bulk or a local 4-cycle.

4.1.1 The geometry

The total number of Kähler moduli is $h^{1,1}(X) = 4$ and the CY X features a K3 or T^4 divisor D_1 fibred over a $\mathbb{P}^1$ base contained in a second divisor D_2, and two additional rigid divisors D_3 and D_4 with only self-intersections. The Kähler form can be expanded in a basis of $(1,1)$-forms as $J = t_1\hat{D}_1 + t_2\hat{D}_2 - t_3\hat{D}_3 - t_4\hat{D}_4$ where the t_i are 2-cycle volumes and the negative signs have been chosen to ensure that all 2-cycle volumes are positive (in particular those dual to rigid divisors). The only non-vanishing intersection numbers are k_{122}, k_{333} and k_{444}. Explicit examples with these properties can be found in [149, 143, 144]. Thus the CY volume form looks like:

$$\mathcal{V} = \frac{1}{6}\int_X J\wedge J\wedge J = \frac{1}{2}k_{122}\,t_1t_2^2 - \frac{1}{6}k_{333}\,t_3^3 - \frac{1}{6}k_{444}\,t_4^3\,. \tag{4.1}$$

The 4-cycle moduli $\tau_i = \frac{1}{2}\int_X \hat{D}_i\wedge J\wedge J$ become:

$$\tau_1 = \frac{1}{2}k_{122}t_2^2\,,\qquad \tau_2 = k_{122}t_1t_2\,,\qquad \tau_3 = \frac{1}{2}k_{333}\,t_3^2\,,\qquad \tau_4 = \frac{1}{2}k_{444}\,t_4^2\,. \tag{4.2}$$

These relations can be inverted and $\mathcal{V}$ can be written in terms of 4-cycle moduli as:

$$\mathcal{V} = \alpha\left(\sqrt{\tau_1}\tau_2 - \gamma_3\tau_3^{3/2} - \gamma_4\tau_4^{3/2}\right), \tag{4.3}$$

where $\alpha = \frac{1}{\sqrt{2k_{122}}}$, $\gamma_3 = \frac{2}{3}\sqrt{\frac{k_{122}}{k_{333}}}$ and $\gamma_4 = \frac{2}{3}\sqrt{\frac{k_{122}}{k_{444}}}$.

Before dwelling on the details of moduli stabilisation, let us outline the main features of this representative model. We assume that the SM is built on stacks of D7-branes wrapping a 4-cycle in the geometric regime. As typical of LVS models, the internal volume is stabilised at exponentially large values. On the other hand, the 2 blow-up modes τ_3 and τ_4 are fixed at small values, and so the volume can be approximated as $\mathcal{V} \simeq \alpha\sqrt{\tau_1}\tau_2$. Given that $\mathcal{V}$ is controlled by 2 moduli, we can consider 2 different regimes in moduli space:

1. **Isotropic limit with SM on a local cycle:** In this case $\tau_1 \sim \tau_2 \gg \tau_3 \sim \tau_4$. Both τ_1 and τ_2 are exponentially large, and so none of them can be wrapped by the SM D7-stack since the corresponding gauge coupling $\alpha_{SM}^{-1} = \tau_i$, $i = 1, 2$, would be hyper-weak. Hence the SM lives on a D7-stack wrapping the local divisor D_3. τ_4 and θ_4 are fixed by instantons which make both of them as heavy as the gravitino. τ_1 and τ_2 are fixed by a combination of α' and g_s effects, and so the corresponding axions θ_1 and θ_2 are ultra-light ALPs. τ_3 is stabilised by a combination of D-terms, F-terms of matter fields and string loops. The associated axion θ_3 plays the role of the QCD axion with a decay constant of order M_s which is around the intermediate scale for TeV-scale soft terms.

2. **Anisotropic limit with SM on a bulk cycle:** In this case $\tau_2 \gg \tau_1 \sim \tau_3 \sim \tau_4$. τ_1 and τ_2 are again frozen by perturbative corrections to the Kähler potential, and τ_3 by non-perturbative contributions to the superpotential. Contrary to the previous case, τ_3 is instead stabilised by non-perturbative physics. Given that τ_1 is hierarchically smaller than τ_2, the underlying CY has an anisotropic shape with 2 extra dimensions much larger than the other 4. Thus the SM can live on the bulk divisor D_1. θ_1 becomes the QCD axion with a decay constant set by the Kaluza-Klein scale associated to the fibre divisor D_1 which turns out to be of order the GUT scale. The mass of θ_3 and θ_4 is around $m_{3/2}$, whereas θ_1 plays again the role of an ultra-light ALP.

4.1.2 Moduli stabilisation: leading results

The model-independent closed string moduli involve the axion dilaton $S = e^{-\phi} + iC_0$, $h^{1,2}(X)$ complex structure moduli U_a, and $h^{1,1}(X) = 4$ Kähler moduli $T_i = \tau_i + \mathrm{i}\,\theta_i$. Dimensional reduction yields the following tree-level Kähler potential:[3]

$$K_{\text{tree}} = -2\ln\mathcal{V} - \ln\left(S + \bar{S}\right) + \ln\left(-i\int_X \Omega\wedge\bar{\Omega}\right). \tag{4.4}$$

S and the U-moduli are fixed at tree-level by turning on the 3-form flux $G_3 = F_3 + iSH_3$ which generates the superpotential:

$$W_{\text{tree}} = \int_X G_3\wedge\Omega(U)\,, \tag{4.5}$$

[3]Here and in the following we set $M_p = 1$ but we will reinsert the correct powers of M_p in the main results.

where $\Omega(U)$ is the U-dependent holomorphic $(3,0)$-form of X. The complex structure moduli and the axio-dilaton develop a mass of order $m_{3/2}$, and so the associated axions are too heavy to be relevant for low-energy phenomenology.

Because of the no-scale cancellation, the T-moduli remain flat at semi-classical order. These directions are lifted by including non-perturbative corrections to (4.5) and perturbative corrections to (4.4). Focusing just on the Kähler sector and including only the leading order α' effects and instanton contributions, K and W become:

$$K = -2\ln\left(\mathcal{V} + \frac{\xi}{2g_s^{3/2}}\right), \qquad W = W_0 + A_4\, e^{-\mathfrak{a}_4 T_4}\,, \tag{4.6}$$

where $\xi = -\frac{\chi(X)\zeta(3)}{2(2\pi)^3}$ with $\chi(X)$ the Euler number of X and $\zeta(3) \simeq 1.2$, W_0 is the vacuum expectation value of (4.5), $A_4 \sim \mathcal{O}(1)$ and $\mathfrak{a}_4 = 2\pi$ for an ED3 wrapping D_4, while $\mathfrak{a}_4 = 2\pi/\mathfrak{n}_4$ for gaugino condensation on a stack of $\mathfrak{n}_4$ D7-branes on D_4.

Plugging (4.6) into the standard form of the 4D $N=1$ supergravity F-term scalar potential, we end up with (up to an overall S and U-dependent factor):

$$V = \frac{8}{3\alpha^2}\mathfrak{a}_4^2 A_4^2 \frac{\sqrt{\tau_4}}{\mathcal{V}}\, e^{-2\mathfrak{a}_4\tau_4} + 4\mathfrak{a}_4 A_4 \tau_4 \cos(\mathfrak{a}_4\theta_4)\frac{W_0}{\mathcal{V}^2} e^{-\mathfrak{a}_4\tau_4} + \frac{3\xi}{4g_s^{3/2}}\frac{W_0^2}{\mathcal{V}^3}\,. \tag{4.7}$$

Minimising (4.7) with respect to the 3 moduli $\mathcal{V}$, τ_4 and θ_4 results in:

$$\langle\mathcal{V}\rangle = \frac{3\alpha}{4\mathfrak{a}_4 A_4}\sqrt{\langle\tau_4\rangle} W_0\, e^{\mathfrak{a}_4\langle\tau_4\rangle}, \qquad \langle\tau_4\rangle = \frac{1}{g_s}\left(\frac{\xi}{2\alpha}\right)^{2/3}, \qquad \langle\theta_4\rangle = (2k+1)\frac{\pi}{\mathfrak{a}_4}\ k\in\mathbb{Z}\,. \tag{4.8}$$

This vacuum is AdS but there exist several mechanisms to uplift it to a dS solution [93, 92, 57, 150]. The order of magnitude of the induced moduli masses is:

$$m_{\tau_4} \simeq m_{\theta_4} \simeq m_{3/2} = \sqrt{\frac{g_s}{2\pi}}\frac{W_0 M_p}{\mathcal{V}}, \qquad m_{\mathcal{V}} \simeq m_{3/2}\sqrt{\frac{m_{3/2}}{M_p}}\,, \tag{4.9}$$

showing that the axion θ_4 becomes too heavy to be relevant for low-energy phenomenology since $m_{3/2}$ sets also the order of magnitude of the soft terms, $M_{\rm soft} \simeq m_{3/2}$, which cannot be below the TeV-scale. At this level of approximation all the other Kähler moduli are still flat.

4.1.3 Moduli stabilisation: subleading results and axion physics

Let us now describe the stabilisation of the remaining Kähler moduli by including additional contributions to K and W which are subdominant with respect to those considered in Sec. 4.1.2. The small parameters controlling the g_s and α' expansions are respectively $e^{\phi} \ll 1$ and $\mathcal{V}^{-1/3} \ll 1$. We shall consider the isotropic and anisotropic limits separately.

4.1.4 Isotropic limit with SM on a local cycle

In this case the SM lives on D7-branes wrapped around the 'small' rigid divisor D_3. Because of the well-known tension between chirality and non-perturbative effects [151], τ_3 cannot be stabilised by instantons, and so θ_3, contrary to θ_4, remains light and can play the role of the QCD axion. Let us see this important issue in detail.

Moduli stabilisation

The total world-volume fluxes on the SM D7-stack and an ED3 instanton (similar considerations apply to gaugino condensation) on D_3 look like:

$$\mathcal{F}_{SM} = f_{SM}\hat{D}_3 + \frac{1}{2}\hat{D}_3 - B\,, \qquad \mathcal{F}_{ED3} = \frac{1}{2}\hat{D}_3 - B\,, \tag{4.10}$$

where $f_{SM} \in \mathbb{Z}$ and the half-integer contributions are due to Freed-Witten anomaly cancellation on non-spin divisors [152, 153]. In order to obtain an $O(1)$ instanton which contributes to W, the B-field has to chosen as $B = \frac{1}{2}\hat{D}_3$ so that $\mathcal{F}_{ED3} = 0$. This, in turn, gives:

$$\mathcal{F}_{SM} = f_{SM}\hat{D}_3\,, \qquad \mathcal{F}_{ED3} = 0\,. \tag{4.11}$$

The number of chiral intersections between the ED3 and the SM D7-stack is then given by:

$$I_{SM-ED3} = \int_X (\mathcal{F}_{SM} - \mathcal{F}_{ED3}) \wedge \hat{D}_3 \wedge \hat{D}_3 = k_{333} f_{SM}\,. \tag{4.12}$$

These zero modes can kill the ED3 contribution to W if they develop vanishing vacuum expectation values, as expected for visible sector fields in order not to break any of the SM gauge symmetries at high energies. In fact, the gauge flux $\mathcal{F}_{SM}$ in (4.11) induces the following $U(1)$-charge for the modulus T_3:

$$q_{T_3} = \int_X \mathcal{F}_{SM} \wedge \hat{D}_3 \wedge \hat{D}_3 = k_{333} f_{SM}\,, \tag{4.13}$$

and W has to be gauge invariant. This implies that the prefactor of the non-perturbative W has also to depend on charged matter fields. Considering for simplicity just a single open string field ϕ, the relevant $U(1)$ transformations are:

$$\delta\phi = \mathrm{i} q_\phi \phi\,, \qquad \delta T_3 = \mathrm{i}\,\frac{q_{T_3}}{2\pi}\,. \tag{4.14}$$

Thus the non-perturbative superpotential (including the possibility of gaugino condensation):

$$W_{ED3} = A_3\, e^{-\mathfrak{a}_3 T_3} \qquad \text{with} \qquad A_3 = A\phi^n \quad \text{and} \quad \mathfrak{a}_3 = \frac{2\pi}{\mathfrak{n}_3}\,, \tag{4.15}$$

transforms under the anomalous $U(1)$ as:

$$\delta W_{ED3} = W_{ED3}\left(n\,\frac{\delta\phi}{\phi} - \frac{2\pi}{\mathfrak{n}_3}\delta T_3\right) = \mathrm{i} W_{ED3}\left(n\, q_\phi - \frac{q_{T_3}}{\mathfrak{n}_3}\right)\,, \tag{4.16}$$

implying that W_{ED3} can be gauge invariant if $n = q_{T_3}/(\mathfrak{n}_3 q_\phi)$. As can be clearly seen from (4.15), $A_3 = 0$ if $\langle\phi\rangle = 0$ (for $n > 0$).

This problem comes along with the following correlated issue. A non-zero gauge flux on the D7-stack generates also a moduli-dependent Fayet-Iliopoulos term of the form [154, 155]:

$$\xi_{SM} = \frac{1}{4\pi\mathcal{V}}\int_X J\wedge\mathcal{F}_{SM}\wedge\hat{D}_3 = -\frac{q_{T_3}}{4\pi}\frac{t_3}{\mathcal{V}} = -\frac{f_{SM}\sqrt{2k_{333}}}{4\pi}\frac{\sqrt{\tau_3}}{\mathcal{V}}\,. \tag{4.17}$$

If $\langle\phi\rangle = 0$, a vanishing D-term potential requires $\xi_{SM} = 0$ which, in turn, implies $\tau_3 \to 0$, causing the collapse of the divisor D_3 to a singularity. This shrinking can be avoided in 2 ways: (i) by considering a slightly different geometry where the 2 rigid divisors D_3 and D_4 intersect each other so that $\xi_{SM} = 0$ would just fix τ_3 in terms of τ_4; (ii) by considering the case where ϕ is a SM gauge singlet (like a right handed sneutrino) which can develop a non-zero vacuum expectation value by D-term cancellation.

In what follows we shall focus on the option (ii) since in the case (i) the anomalous $U(1)$ would become massive by eating up a combination of the θ_3 and θ_4, leaving no light closed string axions to behave as the QCD axion.

The D-term potential reads (taking, without loss of generality, ϕ as a canonically normalised field):

$$V_D = \frac{g_{SM}^2}{2}\left(q_\phi|\phi|^2 + \xi_{SM}\right)^2\,. \tag{4.18}$$

A vanishing D-term potential then fixes the open string field at:

$$\langle|\phi|^2\rangle = \frac{n}{4\pi}\frac{t_3}{\mathcal{V}} = c\,\frac{\sqrt{\tau_3}}{\mathcal{V}} \qquad \text{with} \quad c = \frac{n}{4\pi}\sqrt{\frac{2}{k_{333}}}\,. \tag{4.19}$$

The anomalous $U(1)$ becomes massive by eating up a combination of θ_3 and the phase θ_ϕ of $\phi = |\phi|\,e^{\mathrm{i}\theta_\phi}$. Its mass is given by:

$$M_{U(1)}^2 \simeq g_{SM}^2 M_p^2\left(f_{\rm op}^2 + f_{\rm cl}^2\right), \tag{4.20}$$

where:

$$f_{\rm op}^2 = \langle|\phi|^2\rangle = c\,\frac{\sqrt{\tau_3}}{\mathcal{V}}\,, \tag{4.21}$$

is the decay constant of the open string axion θ_ϕ, while $f_{\rm cl}$ is the decay constant of the closed string axion θ_3. This last quantity can be derived from the kinetic terms:

$$\mathcal{L}_{\rm kin} \supset \frac{1}{4}\frac{\partial^2 K}{\partial\tau_3^2}\partial_\mu\theta_3\partial^\mu\theta_3 = \frac{1}{2}\partial_\mu a\partial^\mu a\,, \tag{4.22}$$

where $a \simeq \theta_3 f_{\rm cl}$ is the canonically normalised axion, implying:

$$f_{\rm cl}^2 = \frac{1}{2}\frac{\partial^2 K}{\partial\tau_3^2} = \frac{1}{8}\sqrt{\frac{k_{122}}{k_{333}}}\frac{1}{\mathcal{V}\sqrt{\tau_3}}\,. \tag{4.23}$$

Comparing (4.21) with (4.23), it is easy to see that $f_{\rm op} \gg f_{\rm cl}$ for $\tau_3 \gg 1$, signaling that the combination of θ_3 and θ_ϕ eaten up by the anomalous $U(1)$ is mostly given by the open string axion θ_ϕ since the largest contribution to $M_{U(1)}$ in (4.20) comes from $f_{\rm op}$ [128]. Thus θ_3 survives in the low-energy theory and can play the role of the QCD axion a. The corresponding saxion τ_3 develops a potential via 2 effects:

1. The F-term potential of the matter field ϕ generated by supersymmetry breaking effects, after writing $|\phi|$ in terms of τ_3 using (4.19):

$$V_{\rm matter} = m_{3/2}^2 |\phi|^2 = c\,\frac{W_0^2\sqrt{\tau_3}}{\mathcal{V}^3}\,. \tag{4.24}$$

2. The potential generated by string loop corrections to the Kähler potential due to the exchange of Kaluza-Klein modes between the D7-stack wrapped around D_3 and O7-planes or D3-branes [99, 36]:

$$V_{\rm loop} = c_{\rm loop}\,\frac{W_0^2}{\mathcal{V}^3\sqrt{\tau_3}}\,, \tag{4.25}$$

   where $c_{\rm loop}$ is expected to be an $\mathcal{O}(1-10)$ coefficient which depends on the U-moduli.

The potential $V_{\rm matter} + V_{\rm loop}$ admits a minimum at $\langle\tau_3\rangle = c_{\rm loop}/c \sim \mathcal{O}(10)$ which reproduces the correct order of magnitude of the SM gauge coupling $g_{SM}^{-2} \simeq \langle\tau_3\rangle$. It can be easily checked that the saxion τ_3 develops a mass of order $m_{3/2}$ similarly to τ_4 and θ_4.

Notice that T_3-dependent instanton corrections to W as in (4.15) would generate a potential of the form (using (4.19) and setting $\theta_\phi = 0$ and $\mathfrak{n}_3 = 1$):

$$V = \frac{32Ac\pi^2}{3\alpha^2}\frac{\tau_3^{(1+n)/2}}{\mathcal{V}^{1+n}}\,e^{-4\pi\tau_3} + 8\pi A c^{n/2}\tau_3^{1+n/4}\cos(2\pi\theta_3)\,\frac{W_0}{\mathcal{V}^{2+n/2}}\,e^{-2\pi\tau_3}\,. \tag{4.26}$$

For $n = q_{T_3}/q_\phi \geq 2$ and $2\pi\tau_3 \gg 1$ (i.e. the limit where higher-order instanton corrections can be neglected), the potential (4.26) is exponentially suppressed with respect to $V_{\rm matter} + V_{\rm loop}$, and so it produces just a tiny shift of the minimum for τ_3. On the other hand, it would generate a mass for θ_3 of order:

$$m_{\theta_3} \simeq \sqrt{K_{33}^{-1}V_{\theta_3\theta_3}} \sim \left(\frac{m_{3/2}}{M_p}\right)^{\frac{n-2}{4}} m_{3/2}\,e^{-\pi\tau_3}\,, \tag{4.27}$$

which for $n \geq 2$, $m_{3/2} \lesssim \mathcal{O}(10^{10})$ GeV and $\tau_3 = \alpha_{SM}^{-1} \simeq 25$ is always subdominant with respect to the contribution from QCD instantons $m_a \simeq \Lambda_{QCD}^2/f_a$ for any possible $f_a \lesssim M_p$. This guarantees that θ_3 is a good QCD axion candidate.

The only saxion which remains to be fixed is the fibre modulus τ_1. This field develops a potential via string loop corrections which experience an 'extended no-scale

cancellation' that suppresses them with respect to the leading α' correction [37]. The resulting scalar potential for τ_1 reads [142]:[4]

$$V_{g_s} = \left(g_s^2 \frac{A}{\tau_1^2} - \frac{B}{\mathcal{V}\sqrt{\tau_1}} \right) \frac{W_0^2}{\mathcal{V}^2} \,, \tag{4.28}$$

where A and B are flux-dependent parameters. The minimum of (4.28) is located at:

$$\langle \tau_1 \rangle = \lambda g_s^{4/3} \langle \mathcal{V} \rangle^{2/3} = \alpha \lambda^{3/2} g_s^2 \langle \tau_2 \rangle \,, \qquad \lambda \equiv \left(\frac{4A}{B} \right)^{2/3} . \tag{4.29}$$

This result has 3 important implications:

1. For $\alpha \simeq \lambda \simeq \mathcal{O}(1)$ and $g_s \simeq \mathcal{O}(0.1)$, τ_1 is roughly of the same order as τ_2, implying that the CY volume is isotropic. Without loss of generality, in what follows we shall consider $\alpha \lambda^{3/2} g_s^2 = 1$, i.e. $\langle \tau_1 \rangle = \langle \tau_2 \rangle$.

2. The scalar potential (4.28) scales as $\mathcal{V}^{-10/3}$, and so for $\mathcal{V} \gg 1$ it is indeed suppressed with respect to the leading order LVS potential (4.7) which scales as $\mathcal{V}^{-3}$.

3. For $\mathcal{V} \gg 1$ the SM cannot live either on τ_1 or on τ_2 since the resulting gauge coupling would be too small. Hence the SM has to be supported by τ_3.

Notice that the axions θ_1 and θ_2 are lifted only by tiny non-perturbative corrections to the superpotential of the form:

$$W \supset A_1 \, e^{-\mathfrak{a}_1 T_1} + A_2 \, e^{-\mathfrak{a}_2 T_2} \,. \tag{4.30}$$

with $A_1 \simeq A_2 \simeq \mathcal{O}(1)$, and $\mathfrak{a}_i = 2\pi/\mathfrak{n}_i$ for $i = 1, 2$. Given that $\tau_1 \simeq \tau_2 \gg 1$, these effects would make θ_1 and θ_2 2 ultra-light, i.e. almost massless, ALPs.

Mass spectrum and decay constants

The mass spectrum of the 3 moduli fixed at leading order, $\mathcal{V}$, τ_4 and θ_4 has been given in (4.9). The mass of the remaining moduli turns out to be:

$$\begin{aligned} m_{\tau_3} &\simeq m_{3/2} \,, \qquad m_{\tau_1} \simeq m_{3/2} \left(\frac{m_{3/2}}{M_p} \right)^{2/3} , \\ m_{\theta_3} &\equiv m_a \simeq \frac{\Lambda_{QCD}^2}{f_{\theta_3}} \,, \qquad m_{\theta_1} \simeq M_p \, e^{-\pi\tau_1/\mathfrak{n}_1} \,, \qquad m_{\theta_2} \simeq M_p \, e^{-\pi\tau_2/\mathfrak{n}_2} \,. \end{aligned} \tag{4.31}$$

Notice that α' effects are under control when $\mathcal{V} \simeq \tau_1^{3/2} \simeq \tau_2^{3/2} \gtrsim 10^3$ since the corresponding expansion parameter is $\mathcal{V}^{-1/3} \lesssim 0.1$. In this regime the 2 ALPs θ_1 and θ_2 are almost massless, $m_{\theta_1} \sim 0$ and $m_{\theta_2} \sim 0$, since their mass would turn out

[4] We neglected loop corrections suppressed by additional powers of $g_s \ll 1$.

to be smaller than the present value of the Hubble constant, $H_0 \simeq 10^{-33}$ eV, for $\mathfrak{n}_1 = \mathfrak{n}_2 = 1$. Larger values of $\mathfrak{n}_1$ and $\mathfrak{n}_2$ can however raise m_{θ_1} and m_{θ_2} above H_0, with interesting application to fuzzy DM [131]. In what follows we shall therefore consider θ_1 and θ_2 as ultra-light.

The decay constants of the QCD axion θ_3 and the 2 ALPs θ_1 and θ_2 can be derived from canonical normalisation and take the generic form (see [127] and App. B.1.1):

$$f_{\theta_i} \equiv \left(\frac{\mathfrak{n}_i}{2\pi}\right) \sqrt{2\lambda_i}\, M_p \,, \tag{4.32}$$

where λ_i is the i-th eigenvalue of the Kähler metric and $\mathfrak{n}_i$ determines the periodicity of the cosine potential which enjoys a discrete shift symmetry (with $\mathfrak{n}_3 = 1$ for the QCD axion). The details of canonical normalisation for this explicit example are provided in App. B.1. The eigenvalues of the Kähler metric (B.5) are given by $\frac{1}{2\tau_2^2}$, $\frac{1}{4\tau_1^2}$ and $\frac{3\alpha\gamma_3}{8}\frac{1}{\mathcal{V}\sqrt{\tau_3}}$, and so the decay constants become:

$$f_{\theta_3} \equiv f_a = \frac{c_3}{\langle\tau_3\rangle^{1/4}}\frac{M_p}{\sqrt{\langle\mathcal{V}\rangle}} \,, \quad f_{\theta_1} = c_1\frac{M_p}{\langle\tau_1\rangle} = c_1\alpha^{2/3}\frac{M_p}{\langle\mathcal{V}\rangle^{2/3}} \,, \quad f_{\theta_2} = c_2\frac{M_p}{\langle\tau_2\rangle} = c_2\alpha^{2/3}\frac{M_p}{\langle\mathcal{V}\rangle^{2/3}} \,, \tag{4.33}$$

where the c_i's are moduli-independent coefficients:

$$c_3 = \frac{\sqrt{3\alpha\gamma_3}}{4\pi} \,, \qquad c_1 = \frac{\mathfrak{n}_1}{2\pi\sqrt{2}} \,, \qquad c_2 = \frac{\mathfrak{n}_2}{2\pi} \,. \tag{4.34}$$

Notice that the QCD axion decay constant scales as the string scale, $f_a \simeq M_s \simeq M_p/\sqrt{\mathcal{V}}$, while the decay constants of the 2 ultra-light ALPs behave as the Kaluza-Klein scale, $f_{\theta_1} \simeq f_{\theta_2} \simeq M_{KK} \simeq M_p/\mathcal{V}^{2/3}$.

The order of magnitude of all these mass scales is set by the overall volume $\mathcal{V}$. An interesting regime in moduli space is the one where $W_0 \sim \mathcal{O}(1-10)$ and $\mathcal{V} \sim \mathcal{O}(10^{14-15})$ which leads to TeV-scale supersymmetry, $M_{\rm soft} \sim m_{3/2} \sim \mathcal{O}(1-10)$ TeV, and a QCD axion decay constant at intermediate scales, $f_a \sim M_s \sim \mathcal{O}(10^{10}-10^{11})$ GeV. Smaller values of the CY volume, like $\mathcal{V} \sim \mathcal{O}(10^3-10^4)$, would push $M_{\rm soft}$ to intermediate scales and f_a around the GUT scale.

Axion couplings to gauge bosons

Other quantities which are relevant for phenomenology are the couplings of the axions to the gauge fields of the visible and hidden sectors. We shall focus just on the couplings of the QCD axion and the 2 ultra-light ALPs which we will express in terms of the corresponding canonically normalised fields $a_3 \equiv a$, a_1 and a_2 (see App. B.1 for the details of canonical normalisation). The visible sector lives on D_3 while the hidden sector involves 2 intersecting stacks of D7-branes wrapped around D_1 and D_2. Knowing that the gauge kinetic function of each sector is given by the corresponding unnormalised Kähler modulus, and denoting the field strengths of the

canonically normalised gauge bosons respectively as $F_{\rm vis}$, F_1 and F_2, we obtain:

$$\mathcal{L}_{\rm ax-gauge} = \frac{a}{f_a}\left[\frac{\lambda_1}{\langle\tau_3\rangle}\,\tilde{F}_{\rm vis}F_{\rm vis} + \frac{\sqrt{\langle\tau_3\rangle}}{\langle\mathcal{V}\rangle}\left(\lambda_2\tilde{F}_1F_1 + \lambda_3\tilde{F}_2F_2\right)\right] + \lambda_4\frac{a_1}{M_p}\tilde{F}_1F_1 + \lambda_5\frac{a_2}{M_p}\tilde{F}_2F_2, \tag{4.35}$$

where the λ_i's are numerical $\mathcal{O}(1)$ coefficients. Notice that the QCD axion a has a stronger than Planckian coupling to the visible gauge bosons while its coupling to hidden sector degrees of freedom is very suppressed. On the other hand, the 2 ALPs have a standard $\mathcal{O}(1/M_p)$ coupling to hidden gauge bosons but they are decoupled from the visible sector. These results are due to the combination of two effects: (i) the visible sector lives on a shrinkable del Pezzo D_3 which has no intersection with the bulk divisors D_1 and D_2; (ii) the axions θ_1 and θ_2 are in practice massless.

4.1.5 Anisotropic limit with SM on a bulk cycle

In LVS scenarios the SM can be realised on a stack of D7-branes wrapped around a bulk cycle only if the underlying geometry has an anisotropic shape. In this case the overall volume can be exponentially large in agreement with a SM gauge coupling which is not too small.

Moduli stabilisation

We focus on the case where the SM lives on the K3 or T^4 fibre D_1. Hence the visible sector gauge coupling is given by $\alpha_{SM}^{-1} = \tau_1 \simeq \mathcal{O}(10\text{-}100)$. Given that $\mathcal{V} \simeq \alpha\sqrt{\tau_1}\tau_2$ is exponentially large, the internal geometry needs to be anisotropic with 2 extra dimensions much larger than the other 4. This can be achieved via the following moduli stabilisation procedure:

- $\mathcal{V}$, τ_4 and θ_4 are stabilised as in (4.8) and the CY volume becomes exponentially large in string units.
- Given that D_3 is not wrapped by the SM D7-stack, the non-perturbative superpotential (4.15) is not suppressed anymore due to chiral intersections with visible sector states. Hence the freezing of τ_3 and θ_3 is completely similar to the stabilisation of τ_4 and θ_4. Contrary to the isotropic scenario, in this case θ_3 acquires a mass of order $m_{3/2}$ and plays no role for low-energy physics.
- The fibre divisor τ_1 is stabilised by string loop corrections as in (4.29) but with $\alpha\lambda^{3/2} = 1$ and $g_s \ll 1$.[5] This results in the following hierarchy:

$$\langle\tau_1\rangle = g_s^2\,\langle\tau_2\rangle \ll \langle\tau_2\rangle\,. \tag{4.36}$$

[5]To be more precise, we envisage a situation similar to the explicit CY cases discussed in [144] where the volume (neglecting blow-up modes) is $\mathcal{V} \simeq \sqrt{\tau_1\tau_2\tilde{\tau}_2}$. Due to the intersection between τ_2 and $\tilde{\tau}_2$, the Fayet-Iliopoulos term induced by gauge fluxes fixes $\tau_2 \propto \tilde{\tau}_2$ for vanishing VEVs of open string fields. An appropriate combination of closed string axions is eaten up by the corresponding anomalous $U(1)$. Substituting $\tau_2 \propto \tilde{\tau}_2$ in $\mathcal{V}$, one obtains effectively the same expression that we are considering: $\mathcal{V} \simeq \sqrt{\tau_1}\tau_2$.

- T_1-dependent non-perturbative corrections to W would be very suppressed due to: (i) the presence of chiral intersections as for T_3-dependent instantons in the isotropic case; (ii) the fact that D_1 is a non-rigid cycle with extra fermionic zero modes which tend to kill instanton contributions. Therefore the closed string axion θ_1 is a perfect QCD axion candidate which becomes massive via standard QCD instantons.

- The remaining closed string axion θ_2 is an almost massless ALP which develops a tiny mass via non-perturbative corrections to W which are exponentially suppressed in terms of the large 4-cycle τ_2.

Mass spectrum and decay constants

The mass of $\mathcal{V}$, τ_4 and θ_4 is again given by (4.9). The mass spectrum of the other moduli instead reads:

$$\begin{aligned} m_{\tau_3} &\simeq m_{\theta_3} \simeq m_{3/2}\,, \qquad m_{\tau_1} \lesssim m_{3/2}\sqrt{\frac{m_{3/2}}{M_p}}\,, \\ m_{\theta_1} &\equiv m_a \simeq \frac{\Lambda^2_{QCD}}{f_{\theta_1}}\,, \qquad m_{\theta_2} \simeq M_p\, e^{-\pi\tau_2/\mathfrak{n}_2}\,. \end{aligned} \tag{4.37}$$

The decay constants of the QCD axion θ_1 and the ALP θ_2 now become:

$$f_{\theta_1} \equiv f_a = c_1\frac{M_p}{\langle\tau_1\rangle} = c_1\alpha_{SM}M_p\,, \qquad f_{\theta_2} = c_2\frac{M_p}{\langle\tau_2\rangle} = c_2\alpha_{SM}g_s^2M_p\,, \tag{4.38}$$

where c_1 and c_2 are again given by (4.34) with $\mathfrak{n}_1 = 1$ for the QCD axion θ_1. Notice that the QCD axion decay constant is proportional to the visible sector gauge coupling since $\alpha_{SM}^{-1} = \langle\tau_1\rangle$ and so $\alpha_{SM}^{-1} \sim \mathcal{O}(10-100)$ implies a GUT-scale decay constant $f_a \simeq M_{GUT}$. Contrary to the isotropic scenario where the SM was supported on a local cycle and the QCD axion decay constant could take different values from M_{GUT} to intermediate scales depending on the value of $\mathcal{V}$, in this case the QCD axion decay constant is fixed at M_{GUT} by the requirement of reproducing the observed value of the SM gauge coupling.

Moreover, for $g_s \lesssim 0.1$ and $\langle\tau_1\rangle \gtrsim 10$, (4.36) yields $\langle\tau_2\rangle \gtrsim 10^3$ which, in turn, implies that the ALP θ_2 is ultra-light, i.e. $m_{\theta_2} \sim 0$. The decay constant of this ALP is set by the Kaluza-Klein scale of the effective 6D theory since:

$$M_{KK}^{6D} \simeq \frac{M_s}{\sqrt{t_1}} \simeq \frac{M_p}{\alpha\tau_2} \simeq f_{\theta_2}\,. \tag{4.39}$$

Interestingly, this scale is one order of magnitude above the gravitino mass since:

$$m_{3/2} \simeq \frac{M_p}{\mathcal{V}} \simeq \sqrt{\alpha_{SM}}\,M_{KK}^{6D} \sim \mathcal{O}(0.1)\,M_{KK}^{6D}\,. \tag{4.40}$$

The decay constant f_{θ_2} can take different values depending on the order of magnitude of τ_2. Varying τ_2 corresponds to varying $\mathcal{V}$ which is mainly controlled by g_s, as can

be seen from (4.8). The string coupling affects also the relation (4.36) where however τ_1 has to remain fixed to get the right SM gauge coupling. This can be achieved by varying W_0 as well. Hence (4.8), (4.36) and $\tau_1 = \alpha_{SM}^{-1} \sim \mathcal{O}(10-100)$ imply an interesting relation between W_0 and g_s (ignoring $\mathcal{O}(1)$ numerical factors):

$$W_0 \sim \left(\frac{\alpha_{SM}^{-1}}{g_s}\right)^{3/2} e^{-\frac{\mathfrak{a}_4}{g_s}} \sim \mathcal{O}(10^3)\, g_s^{-3/2}\, e^{-1/g_s}\,. \tag{4.41}$$

Thus this class of constructions can reproduce the right visible sector gauge coupling only for flux vacua which satisfy the relation (4.41). This implies that larger scales are more natural since $f_{\theta_2} \simeq 10^{14}$ GeV can be obtained for $g_s \simeq \mathcal{O}(0.1)$ and $W_0 \simeq \mathcal{O}(1)$, but $f_{\theta_2} \simeq 10^{12}$ GeV needs $g_s \simeq \mathcal{O}(0.01)$ that would require a severe tuning of W_0 down to values of order $W_0 \simeq \mathcal{O}(10^{-38})$. We conclude that this scenario naturally predicts a QCD axion decay constant around the GUT scale, an almost massless ALP with decay constant around 10^{14} GeV and supersymmetry at intermediate scales.

Axion couplings to gauge bosons

Let us now focus on the coupling of the canonically normalised QCD axion $a_1 \equiv a$ and ALP a_2 to gauge bosons belonging to the visible sector on D_1 and hidden sectors on D_2 and D_3. In fact, SM particles are not charged under the gauge symmetries of the D7-stack wrapping D_3 since D_3 does not intersect with D_1. Similar considerations apply to D_4, and so we shall ignore the possibility of a hidden sector on D_4 since it would have the same features of the hidden sector on D_3. On the other hand, the SM degrees of freedom can be charged under the gauge group on D_2 since there is an intersection among D_1 and D_2. However this would still be a hidden sector since τ_2 is a big cycle, and so the corresponding gauge coupling would be hyper-weak. Thus the relevant couplings are (see App. B.1 for the details of canonical normalisation):

$$\mathcal{L}_{\text{ax-gauge}} = \frac{a}{M_p}\left[\mu_1\, \tilde{F}_{\text{vis}} F_{\text{vis}} + \mu_2 \frac{\langle \tau_3 \rangle^{3/2}}{\langle \mathcal{V} \rangle}\, \tilde{F}_2 F_2 + \mu_3 \left(\frac{m_a}{m_{\theta_3}}\right)^2 \tilde{F}_3 F_3\right] + \mu_4 \frac{a_2}{M_p} \tilde{F}_2 F_2\,, \tag{4.42}$$

where the μ_i's are $\mathcal{O}(1)$ numerical coefficients. Notice that the QCD axion a has a standard Planckian coupling to visible gauge bosons since it arises from a bulk cycle. On the other hand its coupling to the hidden gauge bosons on D_2 is $\mathcal{V}$-suppressed, while a is essentially decoupled from the hidden sector on D_3 since $(m_a/m_{\theta_3})^2 \propto (\Lambda_{QCD}/M_p)^4 \simeq 10^{-76}$. The ALP a_2 features instead an $\mathcal{O}(1/M_p)$ coupling to hidden gauge bosons on D_2 but it is decoupled from the other sectors. These results are again due to the fact that a_2 is essentially massless and D_3 has no intersection with D_1 and D_2.

4.1.6 An example with arbitrary $h^{1,1}$

A generic CY threefold is characterised by hundreds of Kähler moduli, i.e. $h^{1,1} \sim \mathcal{O}(100)$, and so one may wonder whether the axion physics of this more complicated

case would display features similar to the ones of the relatively simple case with $h^{1,1}=4$ analysed above. As we have stresses, this depends on the details of moduli stabilisation. In this section we shall describe how to freeze all Kähler moduli for arbitrary $h^{1,1}$ following [90]. We will obtain an LVS vacuum where $\mathcal{V}$ can be taken large enough to trust the α' expansion.

The only requirement on the geometry is the presence of 2 blow-up modes, the first, D_{SM}, to host the SM and the second, $D_{\rm np}$, to support non-perturbative effects. This condition is not too restrictive since del Pezzo divisors arise very frequently in CY constructions. We shall therefore consider an internal volume of the form:

$$\mathcal{V}=\frac{1}{6}\sum_{i,j,k=1}^{N}k_{ijk}t_it_jt_k-\gamma_{SM}\tau_{SM}^{3/2}-\gamma_{\rm np}\tau_{\rm np}^{3/2}\,,\qquad\text{with}\quad N=h^{1,1}-2\gg 1\,. \tag{4.43}$$

As explained in Sec. 4.1.2, the leading contributions to the scalar potential in a large-$\mathcal{V}$ expansion arise from $\mathcal{O}(\alpha'^3)$ corrections to K and $T_{\rm np}$-dependent non-perturbative corrections to W as in (4.6), which stabilise $\tau_{\rm np}\sim g_s^{-1}$, $\theta_{\rm np}\sim\pi/a_{\rm np}$ and $\mathcal{V}\sim e^{1/g_s}$. Similarly to the isotropic case studied in Sec. 4.1.4, the SM cycle τ_{SM} is instead fixed by the interplay of D-terms, F-terms of matter fields and τ_{SM}-dependent loop corrections. This stabilisation procedure ensures that the internal volume can be exponentially large while $\tau_{SM}=\alpha_{SM}^{-1}\sim\mathcal{O}(10-100)$ can reproduce the observed value of the SM gauge coupling. Moreover the axion θ_{SM} behaves as a perfect QCD axion candidate with a decay constant of order the string scale.

At this level of approximation, there are still $(N-1)$ saxionic and N axionic flat directions (without considering the QCD axion θ_{SM} which we assume to be lifted by QCD instantons). All the $(N-1)$ flat saxions can be lifted by including subdominant α' effects. In 10D the first higher derivative corrections which modify the 4D scalar potential upon dimensional reduction, arise at $\mathcal{O}(\alpha'^3)$ and scale as $G_3^2R^3$. In 4D they generate the term proportional to ξ in (4.7). Additional 10D $\mathcal{O}(\alpha'^3)$ terms scale as $G_3^4R^2$, G_3^6R and G_3^8, and they give rise in 4D to higher F-term contributions to the scalar potential which scale respectively as F^4, F^6 and F^8 [156]. When the superspace derivative expansion is under control [120], these terms represent just negligible corrections to the LVS potential (4.7). However they can be the leading effects to lift any remaining flat direction. In particular, the form of $\mathcal{O}(\alpha'^3)$ F^4 corrections for an arbitrary CY X has been determined to be [156] (ignoring the dependence on del Pezzo moduli):

$$V_{F^4}=\frac{\lambda W_0^4}{\mathcal{V}^4}\sum_{i=1}^{N}\Pi_i t_i\,, \tag{4.44}$$

where $\lambda\propto g_s^{-1/2}$ is a positive coefficient [157] and the Π_i's are $\mathcal{O}(1)$ topological quantities which can be expressed in terms of the second Chern class c_2 as $\Pi_i=\int_X c_2\wedge\hat{D}_i$ [156]. Notice that $\Pi_i\geq 0\;\forall i=1,...,N$ in a basis of the Kähler cone where $t_i\geq 0$. The total potential can thus be written schematically as:

$$V_{\rm tot}=V_{LVS}(\mathcal{V})+V_{F^4}(\mathcal{V},t_i)\,, \tag{4.45}$$

where we have highlighted the moduli-dependence of each contribution. Extremising with respect to the 2-cycle moduli, we obtain:

$$\frac{\partial V_{\rm tot}}{\partial t_i} = \left(\frac{\partial V_{LVS}}{\partial \mathcal{V}} - \frac{4\lambda W_0^4 \Pi_k t_k}{\mathcal{V}^5}\right)\tau_i + \frac{\lambda W_0^4 \Pi_i}{\mathcal{V}^4}\,. \tag{4.46}$$

Using $t_i\tau_i = 3\mathcal{V}$, it is easy to realise that $t_i\partial_{t_i}V_{\rm tot} = 0$ implies:

$$\frac{\partial V_{LVS}}{\partial \mathcal{V}} = \frac{11\lambda W_0^4}{3\mathcal{V}^5}\,\Pi_i t_i\,. \tag{4.47}$$

Plugging this result in (4.46) we find:

$$\frac{\Pi_k t_k}{3\mathcal{V}} = \frac{\Pi_i}{\tau_i} \qquad \forall i = 1, ..., N\,. \tag{4.48}$$

This relation fixes $(N-1)$ moduli in terms of one of them, say τ_N, as:

$$\tau_j = \frac{\Pi_j}{\Pi_N}\,\tau_N\,, \qquad \forall j = 1, ..., N-1\,. \tag{4.49}$$

The positivity of λ and the Π_j's ensures that this is a well-behaved minimum [90]. Substituting (4.49) in (4.43), we obtain:

$$\tau_N = h_N(k_{ijk}, \Pi_i)\,\mathcal{V}^{2/3}\,, \qquad \Rightarrow \qquad \tau_i = h_i(k_{ijk}, \Pi_i)\,\mathcal{V}^{2/3}\,, \qquad \forall i = 1, ..., N\,, \tag{4.50}$$

where $h_i(k_{ijk}, \Pi_i)$ are functions of the intersection numbers and the topological quantities Π_i. The overall volume $\mathcal{V}$ is fixed by solving (4.47) which would yield just a subleading shift of the standard LVS solution (4.8). For $\mathcal{V} \sim e^{1/g_s}$ and $h_i \sim \mathcal{O}(1-10)$ $\forall i$, the minimum (4.50) leads to an isotropic CY where all divisor volumes are large enough to trust the α' expansion.

Given that this stabilisation is purely perturbative, at this level of approximation N axions are still flat. They can be lifted by including non-perturbative corrections to W which however tend naturally to give rise to axion masses below the present Hubble constant for $\mathcal{V} \gtrsim (h^{1,1})^7 \gtrsim 10^{14}$. Let us stress that for such a large value of $\mathcal{V}$ the SM is naturally expected to be supported on a blow-up mode since matching $\tau_* = \alpha_{SM}^{-1} \sim \mathcal{O}(10\text{-}100)$ for a bulk cycle τ_* would need from (4.49) a very unnatural hierarchy between Π_* and Π_N of order 10^{-8} for $\tau_N \sim \mathcal{V}^{2/3} \sim 10^{10}$.

Mass spectrum and decay constants

The mass of the 3 moduli fixed at leading order, $\mathcal{V}$, $\tau_{\rm np}$ and $\theta_{\rm np}$ is given in (4.9). The mass spectrum of the remaining moduli becomes:

$$\begin{aligned} m_{\tau_{SM}} &\simeq m_{3/2}\,, \qquad m_{\tau_j} \simeq m_{3/2}\left(\frac{m_{3/2}}{M_p}\right)^{5/6}\,, \qquad \forall j = 1, ..., N-1\,, \\ m_{\theta_{SM}} &\equiv m_a \simeq \frac{\Lambda_{QCD}^2}{f_{\theta_{SM}}}\,, \qquad m_{\theta_i} \simeq M_p\, e^{-\pi\tau_i/\mathfrak{n}_i} \sim 0\,, \qquad \forall i = 1, ..., N\,, \end{aligned} \tag{4.51}$$

where all the ALPs θ_i's are essentially massless. The decay constants scale as in the isotropic case with $h^{1,1}=4$ analysed in Sec. 4.1.4:

$$f_{\theta_{SM}} \equiv f_a = \frac{c_{SM}}{\langle\tau_{SM}\rangle^{1/4}}\frac{M_p}{\sqrt{\langle\mathcal{V}\rangle}}\,, \qquad f_{\theta_i} = c_i\frac{M_p}{\langle\tau_i\rangle} = \frac{c_i}{h_i}\frac{M_p}{\langle\mathcal{V}\rangle^{2/3}}\,, \quad \forall i=1,...,N\,, \tag{4.52}$$

where c_{SM} and the c_i's are $\mathcal{O}(1)$ moduli-independent coefficients. The decay constant of the QCD axion θ_{SM} scales again as the string scale, whereas the decay constant of each ultra-light ALP is controlled by the Kaluza-Klein scale. Contrary to the case with $h^{1,1}=4$ where values of $\mathcal{V}$ of order $\mathcal{V}\sim\mathcal{O}(10^3-10^4)$ could still be compatible with an EFT under control, for $h^{1,1}\sim\mathcal{O}(100)$ we should focus only on the region $\mathcal{V}\gtrsim\mathcal{O}(10^{14})$. Thus we are naturally led to the region with TeV-scale supersymmetry and an intermediate scale QCD axion decay constant.

Axion couplings

We assume that the SM can be realised with a stack of magnetised D7-branes wrapped around D_{SM}. On the other hand, the 'big' divisors D_i, $i=1,...,N$, can in principle host several hidden sectors. The coupling of the QCD axion and the N ultra-light ALPs to visible and hidden gauge bosons can be derived from the moduli-dependence of the corresponding gauge kinetic functions. Denoting the canonically normalised QCD axion as a, the ALPs as a_i (the results of App. B.1 can be easily generalised to the isotropic case with many bulk Kähler moduli), and the field strengths as $F_{\rm vis}$ and F_i, we end up with:

$$\mathcal{L}_{\rm ax-gauge} = \frac{a}{f_a}\left[\frac{\lambda_{SM}}{\langle\tau_{SM}\rangle}\tilde{F}_{\rm vis}F_{\rm vis} + \frac{\sqrt{\langle\tau_{SM}\rangle}}{\langle\mathcal{V}\rangle}\sum_{i=1}^{N}\tilde{\lambda}_i\tilde{F}_iF_i\right] + \sum_{i=1}^{N}\hat{\lambda}_i\frac{a_i}{M_p}\tilde{F}_iF_i\,, \tag{4.53}$$

where again λ_{SM}, the $\tilde{\lambda}_i$'s and the $\hat{\lambda}_i$'s are numerical $\mathcal{O}(1)$ coefficients. The coupling of the QCD axion a to visible gauge bosons is enhanced with respect to $1/M_p$ while the coupling to hidden degrees of freedom is $\mathcal{V}$-suppressed. This is due again to the fact that D_{SM} is a shrinkable del Pezzo divisor and the vanishing of the mass of the N ALPs.

4.2 Statistics of axion physics in the flux landscape

Building on the results from chapter 3, we investigate the statistical distribution in the type IIB flux landscape of various quantities of axion physics which are phenomenologically interesting. To this end, we first express these quantities in terms of the microscopic parameters, as we did in Sec. 4.1 via moduli stabilisation, and we then exploit their distributions. In particular the shall consider the following distributions for the underlying flux-dependent parameters g_s and W_0, and the rank $\mathfrak{n}$ of the condensing gauge group which generates non-perturbative corrections to the superpotential:

- The distribution of the string coupling g_s is taken to be uniform. This result was explicitly checked in [1] for rigid CY manifolds and is believed to hold for more general cases as well [100]. Hence in the following we shall take $dN \simeq dg_s$ where N is the number of flux vacua.

- Based on the seminal work [50], the tree-level superpotential W_0 is assumed to be uniformly distributed as a complex variable, resulting in $dN \simeq |W_0| d|W_0|$. Note that this distribution might be different in regions where $|W_0|$ is exponentially small since recent constructions of KKLT vacua obtained $|W_0| \sim e^{-1/g_s}$ [76, 129, 130]. However, as explained in Sec. 4, KKLT vacua feature only heavy axions with a mass of order $m_{3/2}$, and so we shall focus just on regions where $|W_0| \sim \mathcal{O}(1\text{-}10)$ where its distribution can be taken as uniform.

- The distribution of the rank of the condensing gauge group $\mathfrak{n}$ in the type IIB flux landscape is still poorly understood. All globally consistent type IIB CY models which have been constructed so far feature contributions to the superpotential which arise from just gaugino condensation in a pure $SO(8)$ sector (corresponding to $\mathfrak{n} = 6$) and ED3 instantons (with $\mathfrak{n} = 1$). It is therefore still unclear if an actual distribution of $\mathfrak{n}$ exists. If so, we argue that it should scale as $dN \simeq -\mathfrak{n}^{-r} d\mathfrak{n}$ with $r > 0$, since the number of flux vacua N is expected to decrease when $\mathfrak{n}$ increases as D7-tadpole cancellation is easier to satisfy for smaller values of $\mathfrak{n}$.

4.2.1 Axion decay constants

Let us start with the axion decay constants. After evaluating the decay constants at the minimum of the scalar potential, we compute their distributions in the flux landscape using the scaling of the number of vacua N with the underlying parameters g_s, W_0 and $\mathfrak{n}$.

Isotropic limit

The axion decay constants in the isotropic limit are given in (4.33). Being exponentially large, the main quantity which controls their distribution is the overall volume $\mathcal{V}$. Using (4.8), we can therefore approximate the axion decay constants as:

$$f_a \sim M_p\, e^{-\frac{c}{g_s \mathfrak{n}_4}}\,, \qquad f_{\theta_1} \sim f_{\theta_2} \sim M_p\, e^{-\frac{4c}{3 g_s \mathfrak{n}_4}} \qquad \text{with} \quad c = \pi \left(\frac{\xi}{2\alpha}\right)^{2/3}\,. \tag{4.54}$$

Notice that, at leading order, the decay constants do not depend on W_0. Hence we can vary them with respect to just g_s and $\mathfrak{n}_4$, obtaining:

$$\begin{aligned} df &= \frac{\partial f}{\partial g_s}\, dg_s + \frac{\partial f}{\partial \mathfrak{n}_4}\, d\mathfrak{n}_4 \simeq \frac{f}{(g_s \mathfrak{n}_4)^2}\, (\mathfrak{n}_4\, dg_s + g_s\, d\mathfrak{n}_4) \\ &\simeq f \left[\ln\left(\frac{M_p}{f}\right)\right]^2 (\mathfrak{n}_4\, dg_s + g_s\, d\mathfrak{n}_4)\,, \end{aligned} \tag{4.55}$$

where f can be any of the 3 decay constants, f_a, f_{θ_1} and f_{θ_2}, and in the last step we have introduced Planck units. Using $dg_s \simeq dN$ and $dN \simeq -\mathfrak{n}_4^{-r}\, d\mathfrak{n}_4$ with $r > 0$, (4.55) takes the form:

$$df \simeq \mathfrak{n}_4\, f \left[\ln\left(\frac{M_p}{f}\right)\right]^2 \left[1 - \frac{\tilde{c}\,\mathfrak{n}_4^{r-2}}{\ln\left(\frac{M_p}{f}\right)}\right] dN\,, \tag{4.56}$$

where $\tilde{c} = c$ for f_a and $\tilde{c} = 4c/3$ for f_{θ_1} and f_{θ_2}. Ignoring subdominant logarithmic effects, we therefore obtain that the distributions of the decay constants of both the QCD axion and the 2 ultra-light ALPs scale as:

$$N(f_a) \sim \ln\left(\frac{f_a}{M_p}\right) \qquad \text{and} \qquad N(f_{\theta_i}) \sim \ln\left(\frac{f_{\theta_i}}{M_p}\right), \quad i = 1, 2\,. \tag{4.57}$$

Let us stress 3 important points:

1. Isotropic models with the SM localised on a blow-up cycle feature only a mild logarithmic preference for higher values of the axion decay constants.

2. As can be seen from (4.56), for $f \ll M_p$ and $0 < r \leq 2$, the distribution of f is driven mainly by the distribution of g_s. Moreover the final result (4.57) is unchanged if the distribution of g_s is taken to be power-law.

3. As can be seen again from (4.56), the unknown distribution of $\mathfrak{n}_4$ would start being important only for $r > 2$. However it is reassuring to notice that it would affect only the form of subleading logarithmic corrections to (4.57).

Anisotropic limit

For the anisotropic case the axion decay constants are given in (4.38). As already observed in Sec. 4.1.5, the QCD axion decay constant is fixed around the GUT scale, $f_a \sim M_{GUT}$, by the need to match the correct SM gauge coupling. If this phenomenological condition is dropped, however f_a would feature a logarithmic distribution as in (4.57). The same is true for the distribution of the decay constant of the ALP θ_2. However in this case the phenomenological requirement $\alpha_{SM}^{-1} = \tau_1 \simeq \mathcal{O}(10\text{-}100)$ still leaves some freedom to vary f_{θ_2} in the flux landscape since from (4.38) we have $f_{\theta_2} \simeq n_2 g_s^2 M_{GUT}$. Notice that the ALP decay constant does not depend on W_0 which has however to respect the relation (4.41) to keep $\tau_1 = \alpha_{SM}^{-1}$ constant when g_s is varied. Differentiating f_{θ_2} with respect to g_s and $\mathfrak{n}_2$ we thus obtain:

$$\frac{df_{\theta_2}}{f_{\theta_2}} = \frac{\partial f_{\theta_2}}{\partial g_s}\frac{dg_s}{f_{\theta_2}} + \frac{\partial f_{\theta_2}}{\partial \mathfrak{n}_2}\frac{d\mathfrak{n}_2}{f_{\theta_2}} = 2\,\frac{dg_s}{g_s} + \frac{d\mathfrak{n}_2}{\mathfrak{n}_2}\,. \tag{4.58}$$

Using again $dg_s \simeq dN$ and $dN \simeq -\mathfrak{n}_2^{-r}\, d\mathfrak{n}_2$ with $r > 0$, (4.58) reduces to:

$$df_{\theta_2} \simeq \sqrt{\mathfrak{n}_2}\,\sqrt{f_{\theta_2}\, M_{GUT}}\left(1 - \frac{g_s}{2}\,\mathfrak{n}_2^{r-1}\right) dN\,. \tag{4.59}$$

For $0 < r \leq 1$, $\mathfrak{n}_2 \geq 1$ and $g_s \ll 1$, the second term in brackets in (4.59) is always smaller than unity. This term could instead become larger than 1 for $r > 1$. However, for $g_s \lesssim 0.1$, this would require large values of $\mathfrak{n}_2$ which are hard to realise in explicit examples (the largest value obtained so far is $\mathfrak{n}_2 = 6$ for gaugino condensation in a pure $SO(8)$ gauge theory which would however still yield a second term of $\mathcal{O}(1)$ for $r \leq 3$). We shall therefore consider the term in brackets in (4.59) of order unity, and obtain:

$$N(f_{\theta_2}) \sim \sqrt{\frac{f_{\theta_2}}{M_{GUT}}} \,. \tag{4.60}$$

Let us make 2 important observations:

1. Interestingly, we obtained now a power-law distribution for the ALP decay constant whose scaling is however very similar to the logarithmic case due to the mild square root dependence.

2. The distribution (4.60) holds as long as W_0 can be tuned to satisfy the relation (4.41) which implies $W_0 \sim e^{-1/g_s}$. In the absence of a dynamical mechanism which fixes the flux superpotential in terms of dilaton-dependendent non-perturbative effects, this relation would however not hold anymore when g_s is taken very small. A good estimate for the lowest value of the ALP decay constant for which (4.60) still applies, can be obtained for $g_s \simeq 0.01$ which would give $f_{\theta_2} \gtrsim 10^{12}$ GeV.

Model with arbitrary $h^{1,1}$

As shown in Sec. 4.1.6, the results of the isotropic case with the SM on a blow-up cycle can be generalised to models with an arbitrarily large number of Kähler moduli where all saxions can be explicitly stabilised by α' corrections to the scalar potential. In this case the axion decay constants are given in (4.52), and they scale with the CY volume as in the isotropic case discussed above. Hence we expect again a logarithmic distribution in the type IIB flux landscape as in (4.57):

$$N(f_a) \sim \ln\left(\frac{f_a}{M_p}\right) \qquad \text{and} \qquad N(f_{\theta_i}) \sim \ln\left(\frac{f_{\theta_i}}{M_p}\right), \quad \forall i = 1, ..., N \,. \tag{4.61}$$

Let us comment on the regime of validity of these distributions. They hold at fixed $h^{1,1}$ when moving in the Kähler moduli space by varying microscopic parameters like g_s after the decay constants are written in terms of them thanks to moduli stabilisation. These results are complementary to the ones of [139, 140] (see also [141] for qualitatively similar findings) which found an approximate log-normal distribution for the axion decay constants of a given CY model focusing at the tip of the stretched Kähler cone. Moreover they found that the mean value of the f_{θ_i}'s decreases when $h^{1,1}$ increases.

Given that the tip of the stretched Kähler cone corresponds to the smallest values of the Kähler moduli which are compatible with a controlled α' expansion, and the axion decay constants are inversely proportional to 4-cycle volumes, the values of the

f_{θ_i}'s obtained by [139, 140] represent the largest values of the axion decay constants compatible with a trustable EFT. These values would therefore provide an upper bound for the regime of validity of our logarithmic distributions (4.61) which can be integrated with the results of [139, 140] to describe how the number of flux vacua changes has a function of both f_{θ_i} and $h^{1,1}$.

As an illustrative example, we consider the distribution $N(f, h^{1,1})$ where f is the mean value of the axion decay constants. As derived in [138], the requirement to trust the α' expansion implies that the volume of each 4-cycle grows with $h^{1,1}$ as $\tau_i \gtrsim (h^{1,1})^3 \ \forall i = 1, ..., h^{1,1}$ (at least for basis elements obtained from generators of the cone of effective divisors). On the other side, as we have seen in Sec. 4.1, the axion decay constants scale as $f_{\theta_i} \simeq M_p/\tau_i$. Combining the two results gives a qualitative understanding of the fact the mean value f of the log-normal distribution found in [139, 140] decreases as $h^{1,1}$ increases. Moreover, we can obtain an explicit estimate of the upper bound for our logarithmic distributions:

$$f \lesssim f_{\max}(h^{1,1}) \simeq \frac{M_p}{(h^{1,1})^3}\,, \tag{4.62}$$

where, for a given $h^{1,1}$, f can take different values by moving in the stretched Kähler cone in a way compatible with moduli stabilisation, and $f = f_{\max}$ at the tip. Hence we expect the following distribution for the number of type IIB flux vacua as a function of f and $h^{1,1}$ (see Fig. 4.1):

$$N(f, h^{1,1}) \sim \ln\left(\frac{f}{M_p}\right) \qquad \text{with} \qquad f \lesssim \frac{M_p}{(h^{1,1})^3}\,. \tag{4.63}$$

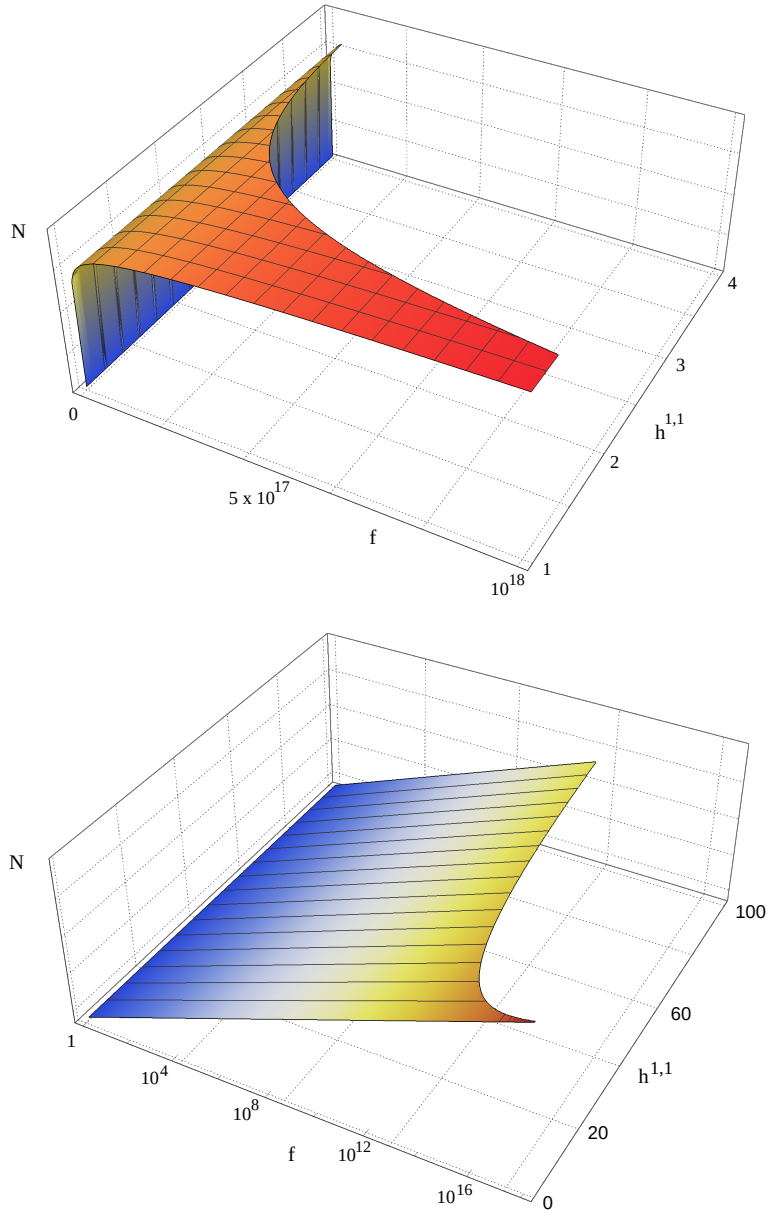

Figure 4.1: Distribution of the number of flux vacua as a function of the mean value of the axion decay constants f and $h^{1,1}$ with the constraint $f \lesssim M_p/(h^{1,1})^3$. At fixed $h^{1,1}$, $N(f) \simeq \ln(f/M_p)$. The plot on the right hand side shows a logarithmic scale for f.

4.2.2 Axion masses

Let us now compute the distribution of axion masses in the flux landscape. As in the previous section we first compute the differential of the masses and then use the known scaling of the parameters g_s, W_0 and $\mathfrak{n}$ in order to determine the distribution.

Isotropic limit

The mass spectrum of the isotropic case with SM on a blow-up cycle is summarised in (4.31). Using (4.56) which can be approximated as $df_a \simeq f_a\, dN$, the distribution of the mass of the QCD axion takes the form:

$$dm_a \simeq -\frac{m_a}{f_a}\, df_a \simeq -m_a\, dN \qquad \Rightarrow \qquad N(m_a) \sim -\ln\left(\frac{m_a}{M_p}\right). \tag{4.64}$$

On the other hand, the distributions of the masses of the two ultra-light ALPs can be easily derived by noticing that their masses can be expressed in terms of the corresponding decay constants as:

$$m_{\theta_1} \simeq M_p\, e^{-\frac{M_p}{2\sqrt{2} f_{\theta_1}}} \qquad \text{and} \qquad m_{\theta_2} \simeq M_p\, e^{-\frac{M_p}{2 f_{\theta_2}}}. \tag{4.65}$$

This result implies:

$$dm_{\theta_i} \simeq m_{\theta_i} \frac{M_p}{f_{\theta_i}} \frac{df_{\theta_i}}{f_{\theta_i}} \simeq m_{\theta_i} \ln\left(\frac{M_p}{m_{\theta_i}}\right) dN \qquad \forall\, i = 1, 2\,, \tag{4.66}$$

which yields the following distribution (neglecting subdominant logarithmic corrections):

$$N(m_{\theta_i}) \sim \ln\left(\frac{m_{\theta_i}}{M_p}\right) \qquad \forall\, i = 1, 2\,. \tag{4.67}$$

Notice that we find again a logarithmic distribution for the mass of both the QCD axion and the 2 ultra-light ALPs. However (4.64) and (4.67) have a different sign, implying that, in the QCD axion case, the type IIB flux landscape has a mild logarithmic preference for low scale masses, while the ALP case features more vacua at large mass values.

Anisotropic limit

The masses for the anisotropic geometry with SM on the bulk divisor D_1 are summarised in (4.37). As already pointed out in the previous section, this model is strongly constrained by the requirement to match the observed SM coupling. This sets the QCD axion decay constant around the GUT scale, $f_a \simeq M_{GUT}$, without a distribution. Thus the QCD axion mass would also be fixed at $m_a \simeq \Lambda^2_{QCD}/f_a \simeq 1$ neV.

The mass of the ALP θ_2 can instead take different values in the flux landscape with a distribution which is again logarithmic. This result can be easily inferred by first writing m_{θ_2} as in (4.65) and then differentiating as below:

$$dm_{\theta_2} \simeq m_{\theta_2} \frac{M_p}{f_{\theta_2}} \frac{df_{\theta_2}}{f_{\theta_2}} \simeq m_{\theta_2} \left[\ln\left(\frac{M_p}{m_{\theta_2}}\right)\right]^{3/2} dN\,, \tag{4.68}$$

where we used (4.58) approximated as:

$$\frac{df_{\theta_2}}{f_{\theta_2}} \simeq \frac{dg_s}{g_s} \simeq \sqrt{\frac{M_p}{f_{\theta_2}}}\, dN \simeq \sqrt{\ln\left(\frac{M_p}{m_{\theta_2}}\right)}\, dN\,. \tag{4.69}$$

Barring subleading logarithmic effects, (4.68) therefore implies:

$$N(m_{\theta_2}) \sim \ln\left(\frac{m_{\theta_2}}{M_p}\right). \tag{4.70}$$

This distribution, similarly to the one of f_{θ_2} derived in (4.60), holds as long as W_0 can be tuned to satisfy the condition (4.41) which keeps $\tau_1 = \alpha_{SM}^{-1}$ fixed at the right SM gauge coupling. In the case of the ALP decay constant, we estimated that its distribution is valid for $f_{\theta_2} \gtrsim 10^{12}$ GeV. Using (4.65), this gives however a lower bound for the ALP mass which can be safely ignored since it would be much smaller than today's Hubble constant: $m_{\theta_2} \gtrsim e^{-10^6} M_p \ll H_0$.

Model with arbitrary $h^{1,1}$

The mass spectrum for the model with a generic number of Kähler moduli is given in (4.51). Following the discussion of the distribution of the axion decay constants, the results for the distribution of the axion masses for the model with arbitrary $h^{1,1}$ would again be qualitatively similar to the isotropic case. Hence we expect logarithmic distributions of the form:

$$N(m_a) \sim -\ln\left(\frac{m_a}{M_p}\right) \qquad \text{and} \qquad N(m_{\theta_i}) \sim \ln\left(\frac{m_{\theta_i}}{M_p}\right) \qquad \forall\, i = 1, ..., N\,. \tag{4.71}$$

As for the case of the axion decay constants discussed above, the results of [139, 140] can be combined with ours to give an upper bound for the regime of validity of the distributions of the ALP masses as a function of $h^{1,1}$, i.e. $m_{\theta_i} \lesssim m_{\theta_i}^{\max}(h^{1,1})$.

4.2.3 Dark matter abundance

Let us now study the distribution of the axion DM abundance produced via the standard misalignment mechanism. We distinguish between the case where the DM particle is the QCD axion and the case where it is an ultra-light ALP. In the QCD axion case, the DM abundance is given by:

$$\frac{\Omega_{QCD}h^2}{0.112} \simeq 6.3 \cdot \left(\frac{f_a}{10^{12}\,\text{GeV}}\right)^{7/6} \left(\frac{\theta_{\text{in}}}{\pi}\right)^2, \tag{4.72}$$

while for the case of an ALP θ_i, it reads:

$$\frac{\Omega_{ALP}h^2}{0.112} \simeq 1.4 \cdot \left(\frac{m_{\theta_i}}{1\,\text{eV}}\right)^{1/2} \left(\frac{f_{\theta_i}}{10^{11}\,\text{GeV}}\right)^2 \left(\frac{\theta_{i,\text{in}}}{\pi}\right)^2. \tag{4.73}$$

For natural $\mathcal{O}(\pi)$ values of the initial misalignment angles θ_{in} and $\theta_{i,\text{in}}$, the QCD axion can reproduce the observed DM adundance for $f_a \simeq 10^{11}$ GeV, while an ALP would require $m_{\theta_i} \simeq 5 \cdot 10^{-21}$ eV for $f_{\theta_i} \simeq 10^{16}$ GeV (see App. B.2 for a detailed scan through the underlying parameter space and some benchmark points).

Isotropic limit and model with arbitrary $h^{1,1}$

In the isotropic case with SM on a blow-up cycle, the distribution of QCD axion DM abundance can be computed deriving (4.72) with respect to f_a and then using the result (4.56) which, at first approximation, implies $df_a \simeq f_a\, dN$. Hence we end up with:

$$d\left(\Omega_{QCD}h^2\right) = \frac{7}{6}\left(\Omega_{QCD}h^2\right)\frac{df_a}{f_a} \simeq \left(\Omega_{QCD}h^2\right) dN\,, \tag{4.74}$$

which gives:

$$N\left(\Omega_{QCD}h^2\right) \sim \ln\left(\Omega_{QCD}h^2\right) \tag{4.75}$$

This result is very important since it implies that the number of type IIB flux vacua which can reproduce the correct value of the DM abundance for $\theta_{\rm in} \sim \mathcal{O}(\pi)$ is only logarithmically suppressed with respect to what has been considered so far as the typical stringy case with $f_a \sim M_{GUT}$ and a tuned initial misalignment angle.

The isotropic case features 2 ultra-light ALPs, θ_1 and θ_2. Both of them can behave as cold DM. Noticing from (4.65) that the microscopic model sets a correlation between m_{θ_i} and f_{θ_i} of the form $m_{\theta_i} \simeq M_p\, e^{-\beta_i \frac{M_p}{f_{\theta_i}}}$ with $\beta_i \sim \mathcal{O}(1)\ \forall i = 1,2$, the distribution of the ALP DM abundance (4.73) is mainly controlled by m_{θ_i}. We can therefore derive (4.73) just with respect to m_{θ_i} and obtain:

$$d\left(\Omega_{ALP}h^2\right) = \left[\frac{1}{2}\frac{dm_{\theta_i}}{m_{\theta_i}} + 2\frac{df_{\theta_i}}{f_{\theta_i}}\right]\left(\Omega_{ALP}h^2\right) \simeq \frac{dm_{\theta_i}}{m_{\theta_i}}\left(\Omega_{ALP}h^2\right) \simeq \left(\Omega_{ALP}h^2\right) dN \quad \forall\, i = 1,2\,, \tag{4.76}$$

where we used (4.66) approximated as $dm_{\theta_i} \simeq m_{\theta_i}\, dN$. This implies for both θ_1 and θ_2:

$$N\left(\Omega_{ALP}h^2\right) \sim \ln\left(\Omega_{ALP}h^2\right). \tag{4.77}$$

Thus we realise that also the distribution of the ALP DM abundance features a logarithmic behaviour. As already explained, this result should apply also to the distribution of the DM abundance of each ultra-light ALP of the model with arbitrarily large $h^{1,1}$.

Anisotropic limit

In the anisotropic limit with the SM on the fibre divisor, the value of the QCD axion decay constant is fixed around the GUT scale once we focus just on vacua which match the SM coupling. Hence this would represent a typical stringy case which has been considered as 'anthropic' since for $f_a \sim M_{GUT} \sim 10^{16}$ GeV (4.72) would reproduce the correct DM abundance only for $\theta_{\rm in} \sim 0.001\pi$.

The DM abundance associated to the ultra-light ALP θ_2 would instead be distributed as:

$$d\left(\Omega_{ALP}h^2\right) \simeq \frac{dm_{\theta_2}}{m_{\theta_2}}\left(\Omega_{ALP}h^2\right) \simeq \left(\Omega_{ALP}h^2\right) dN \quad \Rightarrow \quad N(\Omega_{ALP}h^2) \sim \ln\left(\Omega_{ALP}h^2\right), \tag{4.78}$$

where we used $dm_{\theta_2} \simeq m_{\theta_2}\, dN$ from (4.68). Similarly to the isotropic case, we find again a logarithmic distribution with however the difference, as already pointed out, that in the anisotropic case all expressions, (4.73) included, are valid only for $f_{\theta_2} \gtrsim 10^{12}$ GeV (while we have seen that any value of m_{θ_2} is allowed).

4.2.4 Axion couplings to gauge bosons

Let us now study the distribution of the couplings between axions and gauge fields. Following the analysis of the previous sections, we first evaluate the couplings at the minimum of the scalar potential and we then determine their distribution in the flux landscape.

Isotropic limit and model with arbitrary $h^{1,1}$

We start with the couplings in the isotropic case which are summarised in (4.35). The axion couplings to visible and hidden gauge bosons feature a similar behaviour also in the model with arbitrarily many Kähler moduli, as can be seen from (4.53). Hence the results which we will obtain for the isotropic case can be directly extended to the more general case with arbitrarily large $h^{1,1}$ and SM built with a stack of D7-branes wrapped around a local del Pezzo divisor.

Interestingly, each ultra-light ALP couples in practice just to the corresponding hidden gauge fields with a coupling that is fixed at Planckian strength without a distribution in the landscape. This is a typical stringy behaviour, as expected for the imaginary part of a standard bulk modulus. On the other hand, the coupling between the QCD axion a and SM gauge fields γ is controlled by the string scale $M_s \sim M_p/\sqrt{\mathcal{V}}$ since it is inversely proportional to f_a:

$$g_{a\gamma\gamma} = \frac{\lambda_1}{\langle \tau_3 \rangle\, f_a} \sim \frac{1}{M_s}\,. \tag{4.79}$$

Thus the distribution of $g_{a\gamma\gamma}$ takes the form:

$$dg_{a\gamma\gamma} \simeq -g_{a\gamma\gamma}\,\frac{df_a}{f_a} \simeq -g_{a\gamma\gamma}\, dN \qquad \Rightarrow \qquad N(g_{a\gamma\gamma}) \sim -\ln\left(g_{a\gamma\gamma}\right). \tag{4.80}$$

where we used (4.56) approximated as $df_a \simeq f_a\, dN$. Notice the mild logarithmic preference for smaller couplings. The coupling of the QCD axion to hidden gauge bosons $\gamma_{\rm h}$ living on stacks of D7-branes wrapped around the bulk divisors D_1 and D_2, is instead weaker than Planckian since these two divisors do not intersect with the del Pezzo 4-cycle D_3:

$$g_{a\gamma_{\rm h}\gamma_{\rm h}} = \frac{\lambda_i \sqrt{\langle \tau_3 \rangle}}{\langle \mathcal{V} \rangle\, f_a} \sim \left(\frac{f_a}{M_p}\right) \frac{1}{M_p} \ll \frac{1}{M_p} \qquad \forall i = 1, 2\,. \tag{4.81}$$

Hence, using $df_a \simeq f_a\, dN \simeq g_{a\gamma_{\rm h}\gamma_{\rm h}}\, dN$, the distribution of the coupling between the QCD axion and hidden gauge bosons scales as:

$$dg_{a\gamma_{\rm h}\gamma_{\rm h}} \simeq df_a \simeq g_{a\gamma_{\rm h}\gamma_{\rm h}}\, dN \qquad \Rightarrow \qquad N(g_{a\gamma_{\rm h}\gamma_{\rm h}}) \sim \ln\left(g_{a\gamma_{\rm h}\gamma_{\rm h}}\right). \tag{4.82}$$

Contrary to the coupling to visible gauge fields, in this case the flux landscape features a logarithmic preference for larger couplings.

Anisotropic limit

The axion-gauge couplings for the anisotropic case are summarised in (4.42). Contrary to the isotropic case, the coupling of the QCD axion to visible sector gauge fields does not show a distribution since it is fixed at $1/M_p$, as typical of a string modulus. The difference with the isotropic case in this regard is due to the different topological origin of the QCD axion which in the isotropic case arises from the reduction of C_4 on a local del Pezzo 4-cycle while in the anisotropic case it is associated to the bulk divisor D_1. The behaviour of the ultra-light ALP a_2 is instead similar to the one of the 2 ALPs in the isotropic case since a_2 couples just to hidden degrees of freedom on D_2 with a fixed strength of order $1/M_p$.

In the anisotropic case, the only couplings which can take different values in the flux landscape are the couplings of the QCD axion to the gauge bosons of the hidden sectors on D_2 and D_3, which we denote respectively as γ_2 and γ_3. The coupling $g_{a\gamma_2\gamma_2}$ scales as:

$$g_{a\gamma_2\gamma_2} = \frac{\mu_2}{M_p}\frac{\langle\tau_3\rangle^{3/2}}{\langle\mathcal{V}\rangle} \sim \left(\frac{f_{\theta_2}}{M_p}\right)\frac{1}{M_p}\,. \tag{4.83}$$

As we have already estimated, in this case $10^{12}\,\text{GeV} \lesssim f_{\theta_2} \lesssim 10^{16}\,\text{GeV}$, which implies $10^{-6} \lesssim g_{a\gamma_2\gamma_2}\,M_p \lesssim 10^{-2}$. In this regime of validity, the distribution of the coupling $g_{a\gamma_2\gamma_2}$ turns out to be:

$$dg_{a\gamma_2\gamma_2} \simeq df_{\theta_2} \simeq \sqrt{g_{a\gamma_2\gamma_2}}\,dN \qquad \Rightarrow \qquad N(g_{a\gamma_2\gamma_2}) \sim \sqrt{g_{a\gamma_2\gamma_2}}\,, \tag{4.84}$$

where $df_{\theta_2} \simeq \sqrt{f_{\theta_2}}\,dN$ from (4.59). Hence the coupling of the QCD axion to hidden gauge fields on D_2 is weaker than Planckian with a mild (due to the square root) power-law preference for couplings close to $0.01/M_p$. The QCD axion is instead almost decoupled from the degrees of freedom of the hidden D7-stack wrapping D_3 since $g_{a\gamma_3\gamma_3}$ scales as:

$$g_{a\gamma_3\gamma_3} = \frac{\mu_3}{M_p}\left(\frac{m_a}{m_{\theta_3}}\right)^2 \sim \left(\frac{\Lambda^2_{QCD}}{M_{GUT}f_{\theta_2}}\right)^2\frac{\alpha^{-1}_{SM}}{M_p}\,, \tag{4.85}$$

where $m_{\theta_3} \simeq m_{3/2} \simeq \sqrt{\alpha_{SM}}\,f_{\theta_2}$ from (4.37) and (4.40), and $m_a \simeq \Lambda^2_{QCD}/M_{GUT}$. For $\alpha^{-1}_{SM} \simeq 100$ and $10^{12}\,\text{GeV} \lesssim f_{\theta_2} \lesssim 10^{16}\,\text{GeV}$, this coupling would be of order $10^{-66} \lesssim g_{a\gamma_2\gamma_2}\,M_p \lesssim 10^{-58}$, and so we can safely set it to zero in the whole flux landscape.

4.2.5 Dark radiation in Fibre Inflation

A generic feature of models where reheating occurs due to the decay of a closed string modulus is the production of ultra-light bulk axions which yield extra dark radiation [132, 133, 134, 135]. This happens also in the interesting case of type

IIB Fibre Inflation models [142, 143, 144, 145, 90, 146, 147, 148] where the CY volume takes the same form as in (4.3) and the fibre modulus τ_1 plays the role of the inflaton. The inflationary potential is generated by perturbative corrections to the Kähler potential and the CY volume is fixed around $\mathcal{V} \simeq 10^3$-10^4 by the need to reproduce the observed amplitude of the density perturbations generated by inflaton fluctuations during inflation. In order to have an efficient production of SM degrees of freedom at reheating, the SM D7-stack has to wrap the fibre divisor D_1. Hence a viable realisation of Fibre Inflation models requires to focus on the anisotropic case.

The inflaton τ_1 is the lightest Kähler modulus and its perturbative decay after the end of inflation produces SM particles together with the QCD axion θ_1 and the ultra-light ALP θ_2 which are both relativistic and yield a g_s-dependent contribution to the effective number of relativistic species $N_{\rm eff}$ [158]. One can thus exploit the known distribution of g_s to derive the distribution of extra dark radiation in the flux landscape of Fibre Inflation models. The amount of extra dark radiation is parameterised by $\Delta N_{\rm eff}$ which is determined by the ratio of the inflaton branching ratio into hidden and visible degrees of freedom [158]:

$$\Delta N_{\rm eff} = \frac{43}{7}\frac{\Gamma_{\rm hid}}{\Gamma_{\rm vis}}\left(\frac{g_*(T_{\rm dec})}{g_*(T_{\rm rh})}\right)^{1/3} \simeq \frac{0.6}{\gamma^2}\,, \tag{4.86}$$

where the parameter γ controls the coupling of the inflaton to visible sector gauge bosons and depends on the string coupling:

$$\gamma = \alpha_{_{SM}}\tau_1 = g_s^{4/3}\alpha_{_{SM}}\mathcal{V}^{2/3}\,, \tag{4.87}$$

where we have used (4.36) with $\alpha = 1$ in the the volume form (4.3). Let us stress that in Fibre Inflation models the CY volume is fixed around $\mathcal{V} \simeq 10^3$ by the need to reproduce the observed amplitude of the density perturbations generated by inflaton fluctuations during inflation. Hence in (4.87) $\mathcal{V}$ should be considered as constant. When varying g_s, this can be achieved by an appropriate choice of W_0 (see (4.8)). Moreover g_s should be varied by keeping the SM coupling fixed at its phenomenological value. Given that $\alpha_{_{SM}}$ reads:

$$\alpha_{_{SM}}^{-1} = \tau_1 - \frac{h(\mathcal{F})}{g_s} = \gamma\,\alpha_{_{SM}}^{-1} - \frac{h(\mathcal{F})}{g_s}\,, \tag{4.88}$$

where $h(\mathcal{F}) \geq 0$ is a non-negative function of the intersection numbers and the gauge flux $\mathcal{F}$ on the SM D7-brane stack, this implies that any variation of γ (by varying g_s) should be compensated by a suitable change of $h(\mathcal{F})$ by considering a different choice of $\mathcal{F}$ (if this is allowed by the discreteness of the gauge flux quanta and by tadpole cancellation). Notice that $h(\mathcal{F})$ vanishes for $\mathcal{F} = 0$, implying from (4.88) $\gamma = 1$ and $\Delta N_{\rm eff}$ fixed at $\Delta N_{\rm eff} \simeq 0.6$ [158]. However $h(\mathcal{F}) > 0$ for $\mathcal{F} \neq 0$, and so in this case $\Delta N_{\rm eff}$ features a distribution in the flux landscape due to its dependence on g_s. We can estimate the regime of validity of this distribution by setting in (4.87) $\alpha_{_{SM}}^{-1} = 25$, $\mathcal{V} = 5\cdot 10^3$ and $g_s \lesssim 0.25$ to trust perturbation theory, which gives $\Delta N_{\rm eff} \gtrsim 0.17$. We can also obtain an upper bound on $\Delta N_{\rm eff}$ by requiring $\tau_1 \geq \alpha_{_{SM}}^{-1}$ from (4.88) since $h(\mathcal{F}) > 0$. This gives $\gamma \geq 1$ from (4.87), and so $\Delta N_{\rm eff} \lesssim 0.6$.

Varying now (4.86) with respect to γ using (4.87) and $dg_s \simeq dN$, we obtain:

$$\frac{d(\Delta N_{\rm eff})}{\Delta N_{\rm eff}} \simeq -\frac{d\gamma}{\gamma} \simeq -\frac{dg_s}{g_s} \simeq -\Delta N_{\rm eff}^{3/8}\, dN \qquad \Rightarrow \qquad N(\Delta N_{\rm eff}) \sim \Delta N_{\rm eff}^{-3/8}\,. \tag{4.89}$$

which gives a power-law distribution for extra dark radiation:

$$N(\Delta N_{\rm eff}) \sim \Delta N_{\rm eff}^{-3/8} \qquad \text{for} \qquad 0.17 \lesssim \Delta N_{\rm eff} \lesssim 0.6\,. \tag{4.90}$$

Interestingly we find that the flux landscape of Fibre Inflation models features more vacua around $\Delta N_{\rm eff} \simeq 0.17$ which helps to satisfy current bounds on extra relativistic species. We stress again that this distribution is valid only for values of $\Delta N_{\rm eff}$ corresponding to values of g_s which are compatible with a choice of $h(\mathcal{F})$ that keeps α_{SM} constant.

4.3 Discussion and conclusions

In this chapter we studied the statistics of axion physics in the type IIB flux landscape focusing on the model-independent case of closed string axions coming from the dimensional reduction of C_4. We argued that a proper understanding of moduli stabilisation is crucial in order to derive the main features of the low-energy phenomenology of stringy axions.

In KKLT-like scenarios all axions are as heavy as the corresponding saxions due to non-perturbative stabilisation. If the saxion masses are larger than $\mathcal{O}(50)$ TeV in order to avoid cosmological problems, each axion is thus too heavy to behave as the QCD axion or as a very light ALP for fuzzy DM. On the contrary, moduli stabilisation schemes which rely on perturbative corrections are characterised by axion masses which are exponentially suppressed with respect to saxion masses. This singles out LVS models as the best case scenarios for analysing axion physics since they also yield an exponentially large CY volume which allows to keep the EFT under control even for a large number of Kähler moduli.

Hence we focused on an LVS model with $h^{1,1} = 4$ which is simple enough to perform moduli stabilisation in full detail but, at the same time, rich enough to show all the main features of axion physics which we consider to be valid in general for models with more Kähler moduli. We considered two regimes: (i) the isotropic limit with the SM on D7-branes wrapping a local blow-up cycle, and (ii) the anisotropic limit where the SM lives on a D7-stack wrapped around a bulk divisor. In both cases all phenomenologically interesting quantities, like axion decay constants, axion masses, contributions to the DM abundance and axion-gauge bosons couplings, feature a logarithmic distribution in the flux landscape. In the isotropic case however, the request to reproduce the correct SM gauge coupling selects a subset of the underlying parameter space where some distributions turn into a mild power-law behaviour.

Regarding the QCD axion, in the isotropic case it comes from the reduction of C_4 on a blow-up mode, whereas in the anisotropic case it is associated to a bulk cycle. In

the last case its decay constant is fixed around the GUT scale by the need to match α_{SM}. On the other hand, in the first case f_a is distributed logarithmically with just a mild preference for GUT-scale values in comparison with cases where f_a is around intermediate scales. We consider this case to be more generic in the string landscape since realisations of the QCD axion from bulk cycles require an anisotropic moduli fixing which would require a good amount of tuning for relatively large values of $\mathcal{V}$, while the case of a blow-up QCD axion can work with either isotropic or anisotropic models. We therefore conclude that what has been so far claimed to be the typical stringy situation with a GUT-scale QCD axion decay constant and a tuned initial misalignment angle to avoid DM overproduction, could be not so predominant in the flux landscape with respect to more natural cases where $f_a \sim \mathcal{O}(10^{11})$ GeV and $\theta_{\rm in} \sim \mathcal{O}(\pi)$.

On top of the QCD axion, the isotropic and anisotropic scenarios feature either 1 or 2 ultra-light ALPs. In agreement with previous studies [139, 138, 140, 141], we argued that the presence of several ultra-light ALPs is a general characteristic of 4D string models where the EFT is under control, as we have shown explicitly in a model with arbitrary $h^{1,1}$ where full moduli stabilisation can be achieved by exploiting higher derivative α' corrections following [90]. Interestingly, we found that the decay constants, the mass spectrum and the contribution to the DM abundance of all these ultra-light ALPs are also logarithmically distributed in the type IIB flux landscape.

In the previous chapter we found that the number of flux vacua is also a logarithmic function of the gravitino mass and the supersymmetry breaking scale. Moreover in App. B.3 we showed that other quantities relevant for phenomenology, as the moduli masses and the reheating temperature from moduli decay, share the same statistical properties. We are therefore tempted to argue that most, if not all, of the low-energy properties of the string theory landscape seem to obey a logarithmic distribution once moduli stabilisation is properly taken into account. Apart from the particular case of extra dark radiation in Fibre Inflation models, the only exception which we have encountered so far seems to be the supersymmetry breaking scale in KKLT scenarios which might be characterised by a power-law distribution. However its statistical significance is still unclear since this result relies on the assumption that W_0 is uniformly distributed [50] also in the exponentially small regime where however it is very hard to built explicit examples. The only ones which have been constructed so far feature $W_0 = 0$ and a flat direction at perturbative level [76, 130, 129]. The flat direction is lifted by non-perturbative physics which generates dynamically an exponentially small $W_0 \sim e^{-1/g_s}$. Exploiting the uniform distribution of the string coupling, this relation would again produce a logarithmic distribution of the gravitino mass.

It is worth stressing that these distributions follow from moduli stabilisation which applies only to corners of the string landscape where the EFT is under control thanks to supersymmetry and weak couplings. In order to judge their genericity one would have therefore to be able to control the EFT beyond the regime of validity of these approximations. Despite the difficulty to achieve this goal, scaling arguments

and approximate symmetries inherited from the 10D theory [61] could be used as a powerful guideline to shed light on larger portions of the string landscape. This top-down analysis of the statistical properties of quantities relevant for phenomenology is crucial to provide more theoretical guidance to recent bottom-up approaches to understand naturalness and string theory predictions for several observables [67, 159, 160, 161, 162, 163].

We finally comment on the fact that the relative flatness of logarithmic distributions in the string landscape might be seen at first sight as an indication of a difficulty to make sharp predictions from string theory. However a key-feature of string theory is the correlation between different low-energy phenomenological quantities due to the underlying UV framework. It is this interplay which should be used to sharpen the predictions of the string landscape. As an example, we mention the fact that in LVS models an intermediate scale QCD axion decay constant would correlate with TeV-scale soft terms and a volume mode mass around 1 MeV. Thus, in the absence of a mechanism to avoid cosmological problems associated to the presence of such a light modulus [82], a natural QCD axion DM situation with $f_a \sim \mathcal{O}(10^{11})$ GeV and $\theta_{\rm in} \sim \mathcal{O}(\pi)$ would not be viable even if the number of vacua with these features is only logarithmically suppressed with respect to the number of vacua with a GUT-scale decay constant. We leave the important study of the UV correlation between different particle physics and cosmological observables with logarithmic distributions for future work.

Chapter 5

SUPERPOTENTIAL STATISTICS

Central to the venture of string phenomenology is to carry out explicit constructions of reliable vacua which are phenomenologically viable. In this light, particularly attractive are type IIB flux compactifications [30]. Here, the complex structure moduli and axio-dilaton can be stabilised by turning on background 3-form fluxes. There are instead various scenarios for stabilising the Kähler moduli (see for example [33, 32, 66, 86, 34, 93, 90, 57, 164, 91]). The Standard Model can be realised on intersecting D-branes, branes at singularities or their F-theory generalisations [39]. Cosmic inflation can also be driven by either closed or open string moduli [165, 166]. Furthermore, the large number of possibilities for choosing flux quanta leads to a multitude of solutions which can provide a way to tune the parameters of the associated 4-dimensional effective theory [44, 167].

Our understanding of the physics of type IIB flux compactifications has been growing steadily. This often involves the discovery of a novel class of solutions which have some desirable property needed for the construction of string vacua. One such very interesting class has been discovered recently [76]. These vacua are in the large complex structure limit of the underlying Calabi-Yau of the compactification. They correspond to choices of flux quanta that yield a Gukov-Vafa-Witten superpotential [83] which, when computed using the perturbative part of the prepotential, is a degree-2 homogeneous polynomial in the complex structure moduli and the axio-dilaton. As a result, at this level, these vacua have a flat direction and the expectation value of the Gukov-Vafa-Witten superpotential vanishes along the flat direction. Therefore, these vacua have been dubbed 'perturbatively flat'. The flat direction is lifted when non-perturbative corrections to the prepotential are incorporated. With this, the Gukov-Vafa-Witten superpotential acquires a value which is exponentially small (at weak string coupling).

This discovery is particularly interesting in the context of KKLT models [33]. Defining as in [76] the vacuum expectation value of the Gukov-Vafa-Witten superpo-

tential as[1]

$$W_0 \equiv \sqrt{\frac{2}{\pi}}\,\langle e^{\mathcal{K}} \int_X G_3 \wedge \Omega \rangle\,, \tag{5.1}$$

where $\mathcal{K}$ is the Kähler potential for the complex structure moduli and axio-dilaton, G_3 is the complexified 3-form flux, and Ω the holomorphic 3-form of the underlying (orientifolded) Calabi-Yau X, controlled KKLT vacua require exponentially small values of $|W_0|$.[2] This is effectively realised in perturbatively flat vacua which feature $|W_0| \sim e^{-2\pi/(cg_s)} \ll 1$ at small string coupling $g_s \ll 1$ (with $c \in \mathbb{Q}^+$). The paper [76] presented an explicit choice of flux quanta in an orientifold of the Calabi-Yau obtained by considering a degree-18 hypersurface in $\mathbb{CP}_{[1,1,1,6,9]}$, which yielded $|W_0| \sim 10^{-8}$ (for earlier work on obtaining low values of $|W_0|$ see for example [168, 78]). Not stopping at that, an explicit example with $|W_0|$ as low as 10^{-95} was presented in [169, 170]. Here, important advances were made in developing Kähler moduli stabilisation in this context. Furthermore, [129, 171] extended the method to settings with a shrinking conifold modulus, an essential ingredient of the KKLT construction for anti-brane uplifting. The generalisation to F-theory has been considered in [172].

Perturbatively flat vacua are important also for recent LVS explicit realisations of the Standard Model with D3-branes at an orientifolded dP_5 singularity [173]. In these constructions the cancellation of all D7-charges and Freed-Witten anomalies forces the presence of a hidden D7-sector with non-zero gauge fluxes which induce a T-brane background suitable for de Sitter uplifting [92]. As can be seen from equations (5.41) and (5.46) of [173] the T-brane contribution can give a leading order Minkowski vacuum if $|W_0|$ takes a form similar to the one typical of perturbative flat vacua since $|W_0| \sim \lambda_1\, e^{-2\pi\lambda_2/g_s}$ where λ_1 and λ_2 are $\mathcal{O}(1)$ model-dependent coefficients which depend on microscopic quantities like the Calabi-Yau Euler characteristic and intersection numbers, the number of blow-up modes, gauge flux quanta and the rank of condensing gauge groups. Phenomenologically viable vacua with a de Sitter minimum and soft terms above the TeV scale can require $|W_0|$ as small as $|W_0| \sim 10^{-13}$.[3] All of these are significant developments in the direction of explicit constructions of fully reliable de Sitter vacua in string theory.

Returning to a broader discussion, phenomenological requirements will invariably lead us to specific subclasses of flux vacua (such as perturbatively flat vacua for low $|W_0|$). As we continue to examine flux vacua in detail, we will certainly discover many other interesting subclasses. Given a subclass of flux vacua, there are two important questions that are natural to ask:

- How does the subclass fit within the larger ensemble of the full set of vacua? More specifically, what can we say about the set from the point of view of the statistical approach to string phenomenology [174, 46, 50, 49, 51] (see

[1] Unless otherwise stated, in this chapter we will follow all the conventions of [76].

[2] For a general discussion on the magnitude W_0 in the context of moduli stabilisation and phenomenological implications, see [120] and references therein.

[3] Notice that very small values of $|W_0|$ are not a necessary condition for T-brane uplifting since this depends crucially on the model-dependent values of λ_1 and λ_2. In fact, [107] found explicit LVS de Sitter models with $|W_0| \sim \mathcal{O}(1-10)$.

[62, 175, 176, 177, 55, 52, 53, 54, 178, 123, 179, 180, 77, 181, 182] for studies in various settings in this context)?

- How can one carry out exhaustive searches which will allow us to have a complete understanding of the vacua in this set (and their physics)?

The goal of this work is to take the first steps and develop the methods necessary to answer the above questions in the context of perturbatively flat vacua. In the process, we hope to learn some lessons which should be applicable to the study of any subclass. Apart from the general motivation, there are interesting reasons to address both questions in the context of perturbatively flat vacua.

Usually, finding flux vacua requires solving a coupled set of equations involving the flux quanta and the complex structure moduli. In the case of perturbatively flat vacua, there is considerable simplification. As we will review below, to find vacua one just needs to solve a set of diophantine equations involving the flux quanta (once solutions to this set are found, the vacuum expectation values of the complex structure moduli are automatically determined by a simple analytic formula). Given this simplification, perturbatively flat vacua are the ideal set to look at to develop methods for exhaustive searches for flux vacua.

As already mentioned, perturbatively flat vacua provide a natural way to construct KKLT models and can be useful for effective T-brane uplifting in some LVS models. Thus, developing an understanding of how they fit into the full set of flux vacua (in the statistical context) is important for obtaining the statistical predictions for observables in these models. For instance, the analysis of [1, 3] implies that if $|W_0|$ is exponentially small in the dilaton in most vacua in a set, then the scale of supersymmetry breaking has a logarithmic distribution. The above property is true for all perturbatively flat vacua. Therefore, gaining an understanding of what fraction of the vacua at low $|W_0|$ are perturbatively flat is central to determining the distribution of the scale of supersymmetry breaking in KKLT models. The distribution of the scale of supersymmetry breaking in the landscape is of course of much interest [72, 47, 68, 183, 184, 70].

Before closing the introduction, we would like to make some comments regarding the approach that this article takes. Work on the search for flux vacua and their properties is a two step process - development of methods and then extensive numerical scan through models. The focus of the present paper is on the former. While we will make use of specific models to illustrate the methods,[4] we will not be carrying out any extensive numerical scans through models. In fact, we will often stop midway with the analysis of particular models when the necessary point regarding the methods is made. We leave detailed numerical scans of models for future work.

This chapter is organised as follows. In Sec. 5.1 we review the main ingredients of perturbatively flat vacua, while in Sec. 5.2 we discuss their statistical significance. Sec. 5.3 provides all the details of an algorithm to perform exhaustive searches for

[4]For this we will work with models with 2 complex structure moduli, keeping the numerics light.

perturbatively flat vacua for the case with 2 complex structure moduli. In Sec. 5.4 we outline instead a more general search algorithm which is valid in principle to obtain perturbatively flat vacua for examples with an arbitrarily large number of complex structure moduli. We present our conclusions and discuss our results in Sec. 5.5. Some technical details regarding our numerical search for cases with 2 complex structure moduli are summarised in App. C.1.

5.1 A brief review of perturbatively flat vacua

In this section we first recapitulate some basic material on type IIB flux compactifications and then go on to review [76]. Our discussion in the first part shall be primarily to set notation and will be quite brief. We refer the reader to [185, 186, 187, 188, 30] for further details.

As explained in the introduction, type IIB flux compactifications have an internal manifold that is conformally an orientifolded Calabi-Yau X. To describe these in the language of special geometry, one works with a symplectic basis for $H_3(X,\mathbb{Z})$, $\{A_a, B^a\}$ for $a = 1, ..., h^{1,2}_-(X)$ with $A_a \cap A_b = 0$, $A_a \cap B^b = \delta_a{}^b$, and $B^a \cap B^b = 0$, and projective coordinates on the complex structure moduli, U^a (in what follows, we will take $U^0 = 1$). The central object is the prepotential $\mathcal{F}$, which is degree-2 and homogeneous in the projective coordinates. The period vector is given by

$$\Pi = \begin{pmatrix} \int_{B^a} \Omega \\ \int_{A_a} \Omega \end{pmatrix} = \begin{pmatrix} \mathcal{F}_a \\ U^a \end{pmatrix} . \tag{5.2}$$

The flux vectors F and H are obtained by integrating the 3-form field strengths of the type IIB theory over the A_a and B_a cycles

$$F = \begin{pmatrix} \int_{B^a} F_3 \\ \int_{A_a} F_3 \end{pmatrix} , \qquad H = \begin{pmatrix} \int_{B^a} H_3 \\ \int_{A_a} H_3 \end{pmatrix} . \tag{5.3}$$

Dirac quantisation conditions require that these are integer valued. The flux superpotential, which is classically exact, is given by

$$W = \sqrt{\tfrac{2}{\pi}}\, (F - \tau H)^T \cdot \Sigma \cdot \Pi \,, \tag{5.4}$$

where

$$\Sigma = \begin{pmatrix} 0 & -1 \\ 1 & 0 \end{pmatrix} , \tag{5.5}$$

is the symplectic matrix. The tree-level Kähler potential (for the complex structure moduli and the axio-dilaton) is

$$\mathcal{K} = -\ln\left(-i\Pi^\dagger \cdot \Sigma \cdot \Pi\right) - \ln\left(-i(\tau - \bar{\tau})\right) . \tag{5.6}$$

In the large complex structure limit,[5] the prepotential is a sum of perturbative terms which are at most degree-3 and instanton corrections, i.e $\mathcal{F}(U) = \mathcal{F}_{\rm pert}(U) + \mathcal{F}_{\rm inst}(U)$

[5]For detailed studies of flux vacua in the large complex structure limit see e.g. [189, 75, 190, 191, 192, 193, 194].

with

$$\mathcal{F}_{\rm pert}(U) = -\frac{1}{3!}\,\mathcal{K}_{abc}U^aU^bU^c + \frac{1}{2}\,\mathbf{a}_{ab}U^aU^b + b_aU^a + \xi\,, \tag{5.7}$$

where $\mathcal{K}_{abc}$ are the triple intersection numbers of the mirror Calabi-Yau, $\mathbf{a}_{ab}$ and b_a are rational, and $\xi = -\frac{\zeta(3)\chi}{2(2\pi i)^3}$, with χ the Euler number of the Calabi-Yau. The instanton corrections are

$$\mathcal{F}_{\rm inst}(U) = \frac{1}{(2\pi i)^3}\sum_{\vec{q}} A_{\vec{q}}\, e^{2\pi i\vec{q}\cdot\vec{U}}\,, \tag{5.8}$$

where the sum runs over effective curves in the mirror Calabi-Yau.

Supersymmetric vacua which have $W = 0$ at the perturbative level of the prepotential and also have a flat direction were termed as perturbatively flat in [76]. The basic idea of [76] is that, when the instanton corrections are incorporated, the flat direction is lifted and W acquires an exponentially small vacuum expectation value. Furthermore, the paper provides an explicit algorithm to obtain perturbatively flat vacua, which was stated in the form of a Lemma.

The statement of the Lemma is: if there is a pair $(\vec{M},\vec{K}) \in \mathbb{Z}^n \times \mathbb{Z}^n$ satisfying $N_{\rm flux} \equiv -\frac{1}{2}\vec{M}\cdot\vec{K} \leq Q_{\rm D3}$ ($Q_{\rm D3}$ being the D3-charge tadpole bound), such that $N_{ab} \equiv \mathcal{K}_{abc}M^c$ is invertible, and $\vec{K}^T N^{-1}\vec{K} = 0$, and $\vec{p} \equiv N^{-1}\vec{K}$ lies in the Kähler cone of the mirror Calabi-Yau, and such that $\mathbf{a}_{ab}\,M^b$ and $b_a\,M^a$ take on values in integers; then there exists a choice of fluxes for which a perturbatively flat vacuum exists. The perturbative F-flatness conditions are satisfied along the 1-dimensional subspace $\vec{U} = \tau\vec{p}$, on which $W_{\rm pert}$ vanishes. The Lemma is easily verified by taking the flux vectors to be

$$F = (\vec{M}\cdot\vec{b}, \vec{M}^T\cdot\mathbf{a}, 0, \vec{M}^T) \qquad \text{and} \qquad H = (0,\vec{K}^T,0,0)\,. \tag{5.9}$$

The above choice of the flux vectors is also the most general that leads to a superpotential that is a degree-2 homogenous polynomial in the $\left(h^{1,2}_- + 1\right)$ moduli.[6] Note that this guarantees that the F-flatness conditions imply $W = 0$, and also the existence of the flat direction.

As mentioned earlier, the flat direction is lifted by the non-perturbative terms in $\mathcal{F}$. Choosing the axio-dilaton to be the coordinate along the flat direction, the superpotential which is effectively generated looks like

$$\frac{W_{\rm eff}(\tau)}{\sqrt{2/\pi}} = M^a\partial_a\mathcal{F}_{\rm inst} = \sum_{\vec{q}} \frac{A_{\vec{q}}\,\vec{M}\cdot\vec{q}}{(2\pi i)^2}\, e^{2\pi i\tau\vec{p}\cdot\vec{q}}\,. \tag{5.10}$$

The above superpotential can lead to a controlled racetrack stabilisation if the two dominant instantons (which we will call $\vec{q}_1$ and $\vec{q}_2$) satisfy $\vec{p}\cdot\vec{q}_1 \approx \vec{p}\cdot\vec{q}_2$. Furthermore, stabilisation at weak string coupling requires that there is a hierarchy between the prefactors of the instantons. This amounts to a hierarchy in the associated Gopakumar-Vafa invariants [196, 197].

[6] Degree-2 homogeneous flux superpotentials and associated flat directions in toroidal compactifications were discussed in [195].

5.2 Expectations from statistics

As discussed in the introduction of this chapter, it is of much interest to develop an understanding of how perturbatively flat vacua fit in the larger ensemble of type IIB flux vacua in the statistical sense. The question is central to understanding the distribution of the scale of supersymmetry breaking for KKLT vacua that we derived in chapter 3. Perturbatively flat vacua are supersymmetric (even after the incorporation of instanton effects in the prepotential) and have low values of $|W_0|$. The statistical properties of such vacua were derived in [50]. The number of such vacua $\mathcal{N}$ with the value of $|W_0|^2$ below λ_* is given by an integral of a density over the moduli space[7]

$$\mathcal{N}(N_{\rm flux} \leq Q_{\rm D3}, |W_0|^2 \leq \lambda_*) = \frac{(2\pi Q_{\rm D3})^{2m} \pi \lambda_*}{2(2m)!} \int_{\mathcal{M}} d^{2m}z \, \sqrt{g} \, \rho(z) \,, \tag{5.11}$$

where the density function is given by

$$\rho(z) = \frac{2\pi m}{\pi^{2m} Q_{\rm D3}} \, I(\mathcal{F}) \quad \text{for} \quad I(\mathcal{F}) = \int d^{2h^{1,2}_-} Z \, e^{-|Z|^2} |\det \begin{pmatrix} 0 & Z_J \\ Z_I & e^{\mathcal{K}} \mathcal{F}_{IJK} \bar{Z}^K \end{pmatrix}|^2, \tag{5.12}$$

with $m = h^{1,2}_- + 1$ ($h^{1,2}_-$ being the number of complex structure moduli). The $d^{2m}z$ integration runs over the $2m$-dimensional space of the complex structure moduli and the axio-dilaton and it involves its metric. $\mathcal{F}_{IJK}$ are components of triple derivatives of the prepotential expressed in a local frame. The integration variables Z_I are related to derivatives of the flux superpotential, but can be thought of as dummy integration variables for the purposes of computation of $I(\mathcal{F})$.

Now, let us turn to examining perturbatively flat vacua in this context. For this, we will exploit universal properties of these vacua. A striking property of these vacua is that for all of them, at their minima

$$\vec{U} = \tau \vec{p}, \tag{5.13}$$

where the vector $\vec{p}$ is real and has all positive entries. The real parts of $\vec{U}$ are axionic. Thus, after the axions are brought to their fundamental domain, the relations in (5.13) will continue to hold modulo factors of integers. Therefore, the solutions under consideration are contained in a subspace of the moduli space which is isomorphic to $\mathcal{M}_\tau \times (\mathbb{R}^+)^{h^{1,2}_-}$. Given that perturbatively flat vacua are a subset of the set of all solutions satisfying (5.13), a necessary criterion for them to have statistical significance is that the set of all solutions on the subspace (5.13) have statistical significance. This question can be examined from the point of view of the densities of [50]. Notice that the entire moduli space is $2\left(h^{1,2}_- + 1\right)$-dimensional, while the subspace described by (5.13) is only $\left(h^{1,2}_- + 2\right)$-dimensional. Since the subspace (5.13) is of lower dimensionality than the entire moduli space, and the densities are smooth

[7] In the discussion below, we translate the results of [50] and report them in the conventions of [76].

function on the entire moduli space, even the set of all vacua on this subspace are not expected to be of statistical significance, implying the same for perturbatively flat vacua. Hence perturbatively flat vacua are expected to be statistically sparse in the set of flux vacua with low $|W_0|$ as given by the distribution from [50] which already gives a much smaller number of vacua with respect to cases with $|W_0| \sim \mathcal{O}(1-10)$ since (5.11) is linear in λ_*, implying (at fixed $Q_{\rm D3}$) $\mathcal{N}(|W_0|^2 \leq \lambda_*)/\mathcal{N}(|W_0|^2 \leq 1) \sim \lambda_*$.

Notice that comparisons in [50] of results of explicit searches to the predictions making use of densities did show local fluctuations (such as overdensities and voids) but these were local effects not having any effect on the overall statistical predictions. It is however important to check if the distributions of [50] are peaked along the space described by (5.13). Consider the subspace in which the axio-dilaton is purely imaginary. Being on (5.13), then implies that U^a are also purely imaginary. The densities of [50] can be expressed in terms of the Kähler potential, the metric on the moduli space and triple derivatives of the prepotential $\mathcal{F}_{IJK}$. For the perturbative part of the prepotential (which dominates in the large complex structure limit), all the above quantities are independent of the real part of U^a. Thus the densities are also independent of the real part of U^a. Therefore, at fixed purely imaginary axio-dilaton, moving away from the locus (5.13) by switching on a non-zero real part of U^a does not lead to a fall in the value of the density. Similar considerations also apply when the axio-dilaton is not purely imaginary.

We would like to close this section with a cautionary remark. The diagnostics presented here relies on the fact that the basic assumption of [50] is valid, i.e. that the space of flux vacua of a given compactification can be described by smooth density functions obtained by replacing sums over flux quanta by integrals. If for some reason this fails, the diagnostics would be irrelevant. Next, we turn our discussion of setting up exhaustive searches for perturbatively flat vacua, which is crucial for developing a full understanding of their properties.

5.3 Exhaustive search with two moduli

5.3.1 The $\mathbb{CP}_{[1,1,1,6,9]}$ example

In this section we describe algorithms for carrying out exhaustive searches for perturbatively flat vacua in Calabi-Yau threefolds with 2 complex structure moduli. As mentioned in the introduction, even if this paper intends mainly to focus on methods for searches of flux vacua, for completeness we will present an explicit example in full detail. We do so by looking at the degree-18 hypersurface in $\mathbb{CP}_{[1,1,1,6,9]}$ used in [76] (studied in the context of mirror symmetry in [198]).

We begin by recalling some basic facts about the Calabi-Yau and some details of the analysis of [76]. The Calabi-Yau has 272 complex structure moduli but has a $\mathcal{G} = \mathbb{Z}_6 \times \mathbb{Z}_{18}$ symmetry. By considering $\mathcal{G}$-invariant fluxes, one is guaranteed to stabilise on the $\mathcal{G}$-symmetric locus (see [168]). Thus the stabilisation problem is

effectively reduced to a 2-moduli one. The relevant geometric data are

$$\mathcal{K}_{111} = 9\,, \quad \mathcal{K}_{112} = 3\,, \quad \mathcal{K}_{122} = 1\,, \quad \mathbf{a} = \frac{1}{2}\begin{pmatrix} 9 & 3 \\ 3 & 0 \end{pmatrix}\,, \quad \vec{b} = \frac{1}{4}\begin{pmatrix} 17 \\ 6 \end{pmatrix}\,, \tag{5.14}$$

and the instanton corrections are

$$(2\pi i)^3 \mathcal{F}_{\rm inst} = \mathcal{F}_1 + \mathcal{F}_2 + \cdots\,, \tag{5.15}$$

$$\mathcal{F}_1 = -540\, q_1 - 3\, q_2\,, \tag{5.16}$$

$$\mathcal{F}_2 = -\frac{1215}{2}\, q_1^2 + 1080\, q_1 q_2 + \frac{45}{8}\, q_2^2\,, \tag{5.17}$$

where $q_a = \exp(2\pi i U^a)$ with $a \in \{1, 2\}$. We consider the orientifold involution described in [101] which yields a D3-charge $Q_{\rm D3} = 138$.

Making use of (5.14), the condition $\vec{K}^T N^{-1} \vec{K} = 0$ gives

$$M^1 = \frac{M^2 K^2 \left(2K^1 - 3K^2\right)}{\left(K^1 - 3K^2\right)^2}\,, \tag{5.18}$$

and the flat direction is

$$\vec{U} = \tau \begin{pmatrix} p^1 \\ p^2 \end{pmatrix} = \frac{\tau\left(K^1 - 3K^2\right)}{M^2} \begin{pmatrix} -K^2/K^1 \\ 1 \end{pmatrix}\,. \tag{5.19}$$

The following choice of the vectors $(\vec{M}, \vec{K})$

$$\vec{M} = \begin{pmatrix} -16 \\ 50 \end{pmatrix}\,, \quad \vec{K} = \begin{pmatrix} 3 \\ -4 \end{pmatrix}\,, \tag{5.20}$$

meets all the conditions of the Lemma and the flat direction can be lifted by the inclusion of non-perturbative terms.

In the large complex structure limit, the Kähler potential (for the complex structure moduli and axio-dilaton) is given by

$$K = -\ln\left(i\frac{1}{6}\mathcal{K}_{abc}(U^a - \bar{U}^a)(U^b - \bar{U}^b)(U^c - \bar{U}^c) + 4i\xi\right) - \ln\left(-i(\tau - \bar{\tau})\right)\,. \tag{5.21}$$

We are interested in the locus $U^a = p^a \tau$. Furthermore, since in this limit $\mathrm{Im}(U^a) > 1$, the term involving ξ is subdominant. Thus, along this locus one has

$$\begin{aligned} K &= -\ln\left(\frac{1}{6}\mathcal{K}_{abc} p^a p^b p^c \left(-i(\tau - \bar{\tau})\right)^3 + 4i\xi\right) - \ln\left(-i(\tau - \bar{\tau})\right) \\ &\sim -\ln\left(\frac{1}{6}\mathcal{K}_{abc} p^a p^b p^c\right) - 4\ln\left(-i(\tau - \bar{\tau})\right)\,. \end{aligned} \tag{5.22}$$

The effective superpotential for stabilising the perturbatively flat direction takes the form

$$W_{\rm eff}(\tau) = c\left(e^{2\pi i p^1 \tau} + A e^{2\pi i p^2 \tau}\right) + \cdots\,, \tag{5.23}$$

where $c = \sqrt{\frac{2}{\pi}\frac{8640}{(2\pi i)^2}}$ and $A = -\frac{5}{288}$. Making use of the fluxes in (5.24), it can be easily found that $|W_0| \simeq 2 \times 10^{-8}$.

5.3.2 The algorithm

Now, we describe an algorithm for finding all perturbatively flat vacua in the $\mathbb{CP}_{[1,1,1,6,9]}$ model, which can however be easily generalised to other 2-moduli examples. The F-flatness condition is $D_\tau W_{\text{eff}} = (\partial_\tau + \partial_\tau K)\, W_{\text{eff}} = 0$. Note that the form of the Kähler potential (5.22) implies that $\partial_\tau K \propto (\text{Im}\tau)^{-1} = g_s$. Therefore, for consistent stabilisation at weak string coupling, the term involving $\partial_\tau K$ must be a small correction to the F-flatness condition. The F-flatness condition neglecting this term is

$$e^{2\pi i \tau (p^1 - p^2)} = -\frac{A p^2}{p^1}\,. \tag{5.24}$$

Let us start our search by considering the cases with $p^1 > p^2$. Now, by making use of (5.19) the condition $p^1 > p^2$ translates to

$$-\frac{K^2}{K^1} > 1\,. \tag{5.25}$$

Thus K^1 and K^2 have to be of opposite sign. Furthermore, the entire set of conditions in the Lemma have a symmetry:

$$\vec{K} \to -\vec{K} \quad \text{and} \quad \vec{M} \to -\vec{M}\,. \tag{5.26}$$

This in fact corresponds to an S-duality transformation with the centre of the group. Thus, without loss of generality, we will look at cases with $K^1 > 0$ and $K^2 < 0$. With this, the factor $(K^1 - 3K^2)$ in (5.19) is positive, implying that M^2 must be positive (so that p^2 is positive, as required by the Kähler cone condition in the Lemma). With these signs of K^1, K^2 and M^2, equation (5.18) gives the sign of M^1 to be negative. This implies that $A = M^2/(180M^1)$ has to be negative, which can be compatible with (5.24) if at the minimum $\text{Re}(\tau) = k/(p^1 - p^2) \mod \mathbb{Z}$ with $k \in \mathbb{Z}$. The above suggests the following efficient algorithm to carry out an exhaustive search for vacua:

1. Consider a rational number x between 0 and 1, express this as $x = p/q$ such that p and q are positive and have no common factors. Define the vector

$$\vec{\tilde{K}} = \begin{pmatrix} \tilde{K}^1 \\ \tilde{K}^2 \end{pmatrix} = \begin{pmatrix} p \\ -q \end{pmatrix}\,. \tag{5.27}$$

   The vector $\vec{\tilde{K}}$ will eventually be related to the vector $\vec{K}$ being searched for.

2. Now, compute the ratio

$$y = \frac{\tilde{K}^2 \left(2\tilde{K}^1 - 3\tilde{K}^2\right)}{\left(\tilde{K}^1 - 3\tilde{K}^2\right)^2}\,. \tag{5.28}$$

   Note that this is related to the ratio M^1/M^2 as given by (5.18). Express y as r/s, such that r and s have no common factors, and $s > 0$. Define

$$\vec{\tilde{M}} = \begin{pmatrix} r \\ s \end{pmatrix}\,. \tag{5.29}$$

The vector $\vec{\tilde{M}}$ will be eventually related to the vector $\vec{M}$ being searched for.

3. Check if $K_{abc}\tilde{M}^c$ is invertible or not. If it is not invertible, discard x and start again with a new one. If it is invertible, then proceed further.

4. Compute the values
$$\alpha \mathbf{a} \,.\, \vec{\tilde{M}} \quad \text{and} \quad \alpha \vec{b} \,.\, \vec{\tilde{M}} \,, \tag{5.30}$$
for $\alpha = 1, 2, 4$. Determine the minimum value of α for which the above quantities are integer valued. Call this $\hat{\alpha}$. Note that they certainly must be integer valued for the case of $\alpha = 4$, given the form of $\mathbf{a}$ and $\vec{b}$ in equation (5.14).

5. Consider the quantity
$$-\frac{1}{2}\hat{\alpha}\vec{\tilde{M}} \,.\, \vec{\tilde{K}} \,. \tag{5.31}$$
If this does not satisfy the D3-tadpole bound, then discard x and move to another x. If it lies in the allowed range, we have a solution satisfying all conditions of the Lemma with
$$\vec{M} = \hat{\alpha}\vec{\tilde{M}} \quad \text{and} \quad \vec{K} = \vec{\tilde{K}} \,. \tag{5.32}$$
Also, for *any* positive integer β such that $-\frac{1}{2}\beta\hat{\alpha}\vec{\tilde{M}}.\tilde{K}$ satisfies the D3-tadpole bound, we have solutions
$$\vec{M} = \hat{\alpha}\beta_1\vec{\tilde{M}} \quad \text{and} \quad \vec{K} = \beta_2\vec{\tilde{K}} \,, \tag{5.33}$$
where β_1 and β_2 are positive and provide a factorisation of β.

6. To scan through all x, note that the signs of K^a and M^a (with our working assumption of $K^1 > 0$) are such that $M^1K^1 < 0$ and $M^2K^2 < 0$. Thus both terms contribute with a *positive* sign to the inner product $-\frac{1}{2}\vec{M}.\vec{K}$. Therefore, *the maximum value* of $|K^2|$ necessary to carry out an exhaustive search is $2Q_{\rm D3} = 2 \times 138$ (as higher values would violate the D3-tadpole condition). This bound on $|K^2|$ implies that we need to consider only those x for which $q \leq 2Q_{\rm D3}$. Reduced rationals between 0 and 1 with a fixed upper bound on the denominator are given by the Farey sequence. Thus an exhaustive search is carried out by selecting x from the set $\text{Farey}_{2Q_{\rm D3}}$.

7. Scan through the solutions obtained in this way, checking that non-perturbative effects lead to stabilisation at weak string coupling. Discard the ones that do not satisfy this condition.

8. Enlarge the solution list by considering the solutions obtained by the above process and then generating the solutions related to them by the S-duality symmetry
$$\vec{K} \to -\vec{K} \quad \text{and} \quad \vec{M} \to -\vec{M} \,. \tag{5.34}$$

9. Finally, run the same algorithm considering the possibility of $p^1 \leq p^2$.

Carrying out the search using the above algorithm, after S-duality identification, we find that there exist only 2 solutions which satisfy the conditions of the Lemma, although one of them does not have a very low value of $|W_0|$ since it features just $|W_0| \simeq 0.3$. We report these in Tab. 5.1 along with the associated value of $|W_0|$, after stabilisation by non-perturbative effects (the second entry in the table is the solution reported in [76]). We conclude that the $\mathbb{CP}_{[1,1,1,6,9]}$ model essentially features only 1 perturbatively flat solution with very low $|W_0|$.

$\vec{M}^T$	$\vec{K}^T$	$\vec{b}.\vec{M}$	$(\mathbf{a}.\vec{M})^T$	N_{flux}	τ	$\lvert W_0\rvert$
(32, -98)	(-1, 2)	-11	(-3, 48)	114	4.884 i	0.2871
(16, -50)	(-3, 4)	-7	(-3, 24)	124	6.855 i	2.048×10^{-8}

Table 5.1: All perturbatively flat vacua for the $\mathbb{CP}_{[1,1,1,6,9]}$ example.

5.3.3 General treatment of 2-moduli case

In this section we will present a general discussion of the cases with 2 complex structure moduli. A key-feature of the algorithm in Sec. 5.3.2 was the bound on the range of the elements of the vectors $\vec{M}$ and $\vec{K}$. First we show that this follows from general considerations. The definition $\vec{p} = N^{-1}\vec{K}$, together with the equation $\vec{K}^T N^{-1}\vec{K} = 0$ implies

$$\vec{K}^T \vec{p} = 0\,. \tag{5.35}$$

The requirement that $\vec{p}$ lies in the Kähler cone, then implies that K^1 and K^2 have opposite signs. By making use of the definition of $\vec{p}$ again, the equation $\vec{K}^T N^{-1}\vec{K}$ can alternatively be written as

$$p^a p^b K_{abc} M^c = 0\,. \tag{5.36}$$

The requirement that $\vec{p}$ lies in the Kähler cone implies also that $\tilde{p}_c \equiv p^a p^b K_{abc}$ has positive entries. Thus the vector $\vec{M}$ satisfies an equation similar to $\vec{K}$, i.e.

$$\vec{M}^T \vec{\tilde{p}} = 0\,. \tag{5.37}$$

Therefore, M^1 and M^2 have to have different signs.

Now, if K^1 and M^1 have the same sign, then so would K^2 and M^2. And this would imply a negative value for $N_{\text{flux}} = -\frac{1}{2}\vec{M}.\vec{K}$, which is impossible for imaginary self dual fluxes.[8] Thus viable solutions feature K^1 and M^1 of opposite sign. This

[8] Any fluxes that solve the conditions being imposed are imaginary self dual from the 10-dimensional perspective (see e.g. [30]).

implies that both terms contributing to the $N_{\rm flux}$ inner product have to be positive. Thus, an exhaustive search can be carried out by considering the range

$$|M^a| \leq 2Q_{\rm D3} \quad \text{and} \quad |K^a| \leq 2Q_{\rm D3}\,, \tag{5.38}$$

which is the same as for the $\mathbb{CP}_{[1,1,1,6,9]}$ example, obtained by using slightly different considerations. As an example, we have carried out the analysis for the Calabi-Yau embedded in $\mathbb{CP}_{[1,1,2,2,2]}$ discussed in [199]. To gain a model-independent picture, we treat $Q_{\rm D3}$ as a free parameter. The results are summarised in Tab. 5.2.

$Q_{\rm D3}$	Number of perturbatively flat vacua
50	37
100	128
250	531
500	1445

Table 5.2: Number of perturbatively flat vacua in the $\mathbb{CP}_{[1,1,2,2,2]}$ model taking $Q_{\rm D3}$ as a free parameter. The reported numbers are before imposing any of the following 3 requirements: stabilisation at weak string coupling, low $|W_0|$, S-duality identification.

All these solutions can potentially correspond to perturbatively flat vacua but these numbers would be reduced by the following 3 requirements which have still to be imposed: (*i*) dilaton stabilisation at weak string coupling by instanton effects; (*ii*) a value of $|W_0|$ which is indeed very small (i.e. not of order $|W_0| \simeq 0.3$ as for 1 solution in the $\mathbb{CP}_{[1,1,1,6,9]}$ example); (*iii*) possible equivalences between solutions via S-duality. Given that these numbers are still small to be attractive in the context of a landscape, we do not push the analysis further.

It is important to note that the key-element in obtaining the bounds in (5.38) was the sign correlations between the elements in $\vec{M}$ and $\vec{K}$. While the arguments in the first part of this section hold for any number of moduli, it is easy to see that the sign correlations need not hold when there are more than 2 moduli. To remedy this, we will discuss a more general method in Sec. 5.4.

5.3.4 Comparison with statistics

Let us compare our results with the statistical expectations of [50]. For $h^{1,2}_{-} = 2$, (5.11) yields

$$\mathcal{N}(N_{\rm flux} \leq Q_{\rm D3}, |W_0|^2 \leq \lambda_*) = \left(\frac{2^6\pi^4}{5!}\right) Q_{\rm D3}^5 \lambda_* \int_{\mathcal{M}} d^6z \sqrt{g}\, e^{2\mathcal{K}} \mathcal{F}_{abc}\bar{\mathcal{F}}^{abc}\,, \tag{5.39}$$

where the indices of $\mathcal{F}$ have been converted to tangent bundle ones. For the $\mathbb{CP}_{[1,1,1,6,9]}$ example discussed in Sec. 5.3.1, carrying out the integration over the large complex structure patch one finds

$$\mathcal{N}(N_{\rm flux} \leq Q_{\rm D3} = 138, |W_0|^2 \leq \lambda_*) \simeq 3 \times 10^{12} \lambda_*\,. \tag{5.40}$$

As pointed out in [76], this predicts the lowest value of $|W_0|$ being of order 6×10^{-7}, close to what was found. On the other hand, the same formula predicts $\mathcal{O}(10^8)$ vacua for $|W_0| \lesssim 0.01$, even if our exhaustive search has shown that there is only 1 vacuum with such a feature, in agreement with the argument presented in Sec. 5.2.[9] We therefore conclude that in the $\mathbb{CP}_{[1,1,1,6,9]}$ model, perturbatively flat vacua are interesting examples to show explicitly the existence of vacua with very low $|W_0|$, but they do not possess any tuning freedom in the value of $|W_0|$. Given the argument presented in Sec. 5.3.3, we expect this conclusion to hold for all cases with 2 complex structure moduli. Notice, for example, that in the $\mathbb{CP}_{[1,1,2,2,2]}$ model the number of perturbatively flat vacua summarised in Tab. 5.2 is also much less than as predicted by the $Q_{\rm D3}^5$ scaling of (5.39). Models with more than 2 complex structure moduli require a refined analysis for exhaustive searches which we outline in the next section, although the analysis of Sec. 5.2 indicates that they should still be statistically sparse.

Let us close this section by stressing that a key-assumption in the derivation of the results of [50], is a high density of flux vacua allowing for the sums over integer fluxes to be converted to integrals. Our results indicate that for the $\mathbb{CP}_{[1,1,1,6,9]}$ model, under these circumstances, there are many more vacua at low $|W_0|$ that remain to be discovered.

5.4 A more general search algorithm

The key to carry out exhaustive searches is isolating the region in the flux vector space which contains all perturbatively flat vacua. Once such a region is obtained, one can carry out numerical searches in this region to obtain all solutions (if the region is not too large). In this section we present a general method to isolate such regions which is in principle valid for examples with an arbitrary large number of complex structure moduli. Here, we will discuss the method and leave its detailed numerical implementation for future work.[10]

Central to our arguments will be certain properties of $N_{\rm flux}$. Recall that the quantity $-\frac{1}{2}\vec{M}.\vec{K}$ is equal to the contribution of the fluxes to the D3-charge

$$N_{\rm flux} = -\frac{1}{2}\,\vec{M}.\vec{K} = \frac{1}{(2\pi)^4\alpha'^2}\int_X H_3 \wedge F_3\,, \tag{5.41}$$

where the integration is over the Calabi-Yau X. The fluxes of interest to us correspond to an imaginary self dual G_3, i.e.

$$*\,\frac{H_3}{g_s} = -\left(F_3 - C_0 H_3\right). \tag{5.42}$$

[9] In this context, we would like to mention that the values of $|W_0|$ obtained after stabilisation crucially depend on the hierarchy in the Gopakumar-Vafa invariants. However, the densities of [50] in the moduli space in the large complex structure limit have mild sensitivity to this. This is in keeping with the arguments of Sec. 5.2 which suggest that perturbatively flat vacua are a small fraction of the vacua at low $|W_0|$.

[10] Our preliminary analysis indicates that the numerics can be quite involved when one considers models with more than 2 moduli.

Thus (see e.g. [200])

$$\int_X H_3 \wedge F_3 = \frac{1}{3! g_s} \int_X d^6y \sqrt{g_6}\, H_3^2 \,. \tag{5.43}$$

This is the usual argument given to show that N_{flux} is positive semi-definite. Here we list two consequences that are important for our arguments:

(a) Equation (5.43) implies that the only way for N_{flux} to vanish is $H_3 = 0$. Equation (5.42) then implies that $F_3 = 0$. Translating this in terms of the vectors $\vec{M}$ and $\vec{K}$, one learns that, for consistent solutions, $N_{\text{flux}} = 0$ only if $\vec{M} = \vec{K} = 0$.

(b) The derivation of (5.43) does not make use of flux integrality. Thus, the conclusions of the above point remain valid even when one considers fluxes which do not obey the Dirac quantisation conditions (we will do so as an intermediate step in our analysis).

Now, returning to finding the solutions to the conditions of the Lemma, let us think of carrying out a search by scanning through the vectors $\vec{M}$ and $\vec{K}$, by starting from the origin and progressively going through points with larger and larger $|\vec{M}|$ and $|\vec{K}|$. We would like to obtain upper bounds on the values of $|\vec{M}|$ and $|\vec{K}|$ which can possibly yield solutions to the conditions of the Lemma. For this, we write the D3-tadpole condition as

$$-\frac{1}{2}|\vec{M}||\vec{K}|\epsilon \leq Q_{\text{D3}} \,, \tag{5.44}$$

where ϵ is the cosine of the angle between the vectors $\vec{M}$ and $\vec{K}$. Since both $|\vec{M}|$ and $|\vec{K}|$ are bounded from below, the only way $|\vec{M}|$ or $|\vec{K}|$ (or both) can be large is if $|\epsilon|$ is small. While in general the cosine of the angle between two vectors in $\mathbb{Z}^n$ can be arbitrarily small, our interest is only in vectors that satisfy the conditions of the Lemma (i.e. provide consistent solutions to the type IIB equations of motion). We begin by defining

$$\hat{m} = \frac{\vec{M}}{|\vec{M}|} \,, \qquad \hat{k} = \frac{\vec{K}}{|\vec{K}|} \qquad \text{and} \qquad \hat{\mathbf{n}}_{ab} = K_{abc} m^c \,. \tag{5.45}$$

The vectors $\vec{m}$ and $\vec{k}$ lie on the unit sphere and the integrality condition of the fluxes is now that the ratio of any two components of the vectors is rational. The equation constraining the vectors in the Lemma becomes

$$\hat{k}^T\, \hat{\mathbf{n}}\, \hat{k} = 0 \,. \tag{5.46}$$

We will consider the equation (5.46) as an equation over *real* variables $\vec{m}$ and $\vec{k}$ (taking values on the unit sphere). Furthermore, we will demand that the vector $\hat{p} = \hat{\mathbf{n}}^{-1}\, \hat{k}$ lies in the Kähler cone of the mirror Calabi-Yau. With the variables taking on values over reals, the solution space can be studied using standard numerical

methods. A lower bound on $|\epsilon|$ can be obtained by numerically searching for the minimum (or infimum) of $|\hat{m}.\hat{k}|$ in the solution space. Once such a bound is obtained, an exhaustive search can be carried out by scanning through

$$0 < |\vec{M}|, |\vec{K}| \leq \frac{2Q_{\rm D3}}{|\epsilon|_{\rm inf}} \,. \tag{5.47}$$

We note that a bound so obtained is conservative, due to the expansion of the domain of the variables to the reals.

Next, we would like to discuss some aspects of the minimisation problem at hand. As we have reviewed above, as long as one is in the physically allowed region of the moduli space, $N_{\rm flux}$ is always greater than zero, i.e. $|\epsilon| > 0$. Thus there are two possibilities for the infimum of $|\epsilon|$: either it is a positive number or it is equal to zero. In the former case, an exhaustive search can be carried by considering $|\vec{M}|$ and $|\vec{K}|$ in the range (5.47).

The later case (in which $|\epsilon|$ takes on arbitrarily small values) is more subtle. In this case, there would be a point with $|\epsilon| = 0$ as a limit point of points in the solution space. Since all points in the physically allowed region must have $|\epsilon| > 0$, the limit point must lie in the boundary of the physical region. Typically, as one approaches the boundary, one loses control over the effective field theory or encounters phenomenological challenges. Taking this into consideration will lead to an effective $|\epsilon|_{\rm inf}$ which can be used to determine a region to carry out exhaustive searches.[11]

To illustrate the method in a concrete setting, we consider the 39 Calabi-Yau threefolds with 2 Kähler moduli[12] constructed by Kreuzer and Skarke in [201] and listed (along with the intersection numbers) in Table 11 of [91]. In all these cases we have followed the above described procedure to determine $|\epsilon|_{\rm inf}$. For 22 of them, $|\epsilon|_{\rm inf}$ does not take values close to zero, implying a strong bound on the region where all solutions are contained. We record the associated values of $|\epsilon|_{\rm inf}$ for them in Tab. 3 in App. C.1.

On the other hand, in the remaining 17, the numerics yield very low values of $|\epsilon|_{\rm inf}$. Thus these models might seem to be more promising to find a larger number of perturbatively flat vacua (from the perspective of the present algorithm). However, as we discuss below, most of the would-be solutions would not be ideal for phenomenological applications. In fact, in these cases we find a solution to the equations with $|\epsilon| = 0$ on the boundary of the Kähler cone, i.e. $\hat{p}^b = 0$ for some b. The definition of $\hat{\mathbf{n}}$ in (5.45) together with the definition of $\hat{p}$ implies that $\vec{p} = \hat{p}\,\frac{|\vec{K}|}{|\vec{M}|}$. Thus we have the relation

$$\vec{U} = \hat{p}\,\frac{|\vec{K}|}{|\vec{M}|}\,\tau \,. \tag{5.48}$$

[11] In principle, there can be situations where there are no good reasons to exclude a region of arbitrary small ϵ. In such a case, one would need to carry out a more extensive search along vectors $\vec{m}$ and $\vec{k}$ in this region.

[12] The mirrors have 2 complex structure moduli. Of course, our analysis in Sec. 6.3 already provides regions for exhaustive searches for these. The goal here is to obtain the analogous regions from the algorithm presented in this section. We will proceed without worrying about issues that can arise from orientifolding.

Being in the large complex structure limit requires $\mathrm{Im}(U^c) > 1\ \forall c$. In the limit where $\hat{p}^b \to 0$ for one of the b,[13] this can be achieved by either $|\vec{K}|/|\vec{M}| \gg 1$ or $\mathrm{Im}(\tau) \gg 1$. However both cases are problematic for the following reasons. $|\vec{K}|/|\vec{M}| \gg 1$ will induce large hierarchies in the vector $\vec{p}$, making it unsuited for racetrack stabilisation at small string coupling. On the other hand, $\mathrm{Im}(\tau) = g_s^{-1}$ cannot become too small without inducing phenomenological problems. In fact, in type IIB compactifications the Standard Model can either be realised on D3- or D7-branes. In the first case, the strength of the gauge couplings is set by g_s, and in the second by the Einstein frame volume of the 4-cycle wrapped by the D7-stack (which we denote as $\mathrm{Re}(T_{\mathrm{SM}})$). In the scenario at hand, however Kähler moduli stabilisation [170] gives

$$\frac{4\pi}{g_{\mathrm{SM}}^2} = \mathrm{Re}(T_{\mathrm{SM}}) \simeq \frac{1}{2\pi} \ln |W_0|^{-1} \sim \frac{1}{g_s}\,. \tag{5.49}$$

Thus, irrespective of how the Standard Model is realised, in perturbatively flat vacua the strength of its gauge couplings is always determined by g_s.[14] This effectively sets a lower bound on the range of interest for g_s (for instance one can demand $10^{-3} \lesssim g_s \lesssim 0.1$). Thus, the regions of small ϵ should be effectively avoided, implying that also the remaining 17 models are not expected to produce a large number of perturbatively flat vacua which are phenomenologically viable.

Before closing this section, we note that the key-aspect of the algorithm has been that, by determining the minimum value of the angle between the flux vectors, one can isolate a region by scanning through which exhaustive searches can be carried out. It will be interesting to see if the same considerations can be used in other settings.

5.5 Conclusion and discussion

In this chapter we have developed exhaustive search algorithms to find perturbatively flat vacua. The 2-moduli case has been discussed in detail and an algorithm applicable to any number of moduli has been presented. Detailed numerical scans going through specific models (including ones with higher number of complex structure moduli) is subject of future studies.

In Sec. 5.2 we have also examined perturbatively flat vacua as part of the entire ensemble of vacua at low $|W_0|$ from the point of view of a statistical approach. We found that they are statistically sparse when compared to the expectation from the distribution of low values of $|W_0|$ from [50]. This expectation has been confirmed in Sec. 5.3 by our numerical searches for cases with 2 complex structure moduli. In particular, for the $\mathbb{CP}_{[1,1,1,6,9]}$ model we found that there is only 1 perturbatively flat

[13] In none of the 17 cases both $\hat{p}^1$ and $\hat{p}^2$ tend to zero.

[14] Notice that in the string frame $\mathrm{Re}(T_{\mathrm{SM}})|_{\mathrm{str}} = g_s \mathrm{Re}(T_{\mathrm{SM}}) \sim \mathcal{O}(1)$, implying that one should consider all perturbative and non-perturbative α' corrections at string tree-level, except when $|W_0| \ll 1$ for those which come from 10-dimensional terms proportional to G_3^{2n} with $n > 1$ [202]. However, as shown in [170], these α' effects should induce just a subdominant shift of the KKLT minimum for $|W_0| \ll 1$.

solution with $|W_0| \lesssim 0.01$ (featuring $|W_0| \sim 10^{-8}$), while [50] would predict around $\mathcal{O}(10^8)$ flux vacua. We argued that similar considerations apply to all other 2-moduli cases. We therefore conclude that this set by itself does not provide tuning freedom for phenomenological applications. Using the general algorithm outlined in Sec. 5.4, it would be interesting in the future to perform a detailed search for cases with more than 2 complex structure moduli, although one expects them to be statistically sparse from the analysis of Sec. 5.3. Let us just mention here that, as one goes to higher values of $h^{1,2}_-$, one can expect more solutions. However, the analysis of [49] implies that with higher values of $h^{1,2}_-$ the vacua in the large complex structure limit give a lower contribution to the statistics. This poses an interesting challenge for achieving statistical tuning in phenomenological applications. Furthermore, one can expect that the numerics required to obtain all vacua explicitly should become harder as one goes up in the number of complex structure moduli.

Let us also stress that our analysis in Sec. 5.3 relied heavily on the specific form of the vacuum expectation values of the complex structure moduli (equation (5.13) which is specific to the vacua of [76]) but in principle there can be other families of vacua featuring $W = 0$ at perturbative level. An interesting question is to develop diagnostic methods to study the statistical significance of the vacua of [76] in general. Let us touch upon this briefly. For all such vacua, the instanton effects that give W_0 a non-zero value would also be responsible for giving the perturbatively flat direction a mass. Thus a universal property is a modulus (in the subspace spanned by the complex structure moduli and the axio-dilaton) with a low mass, more specifically a mass proportional to a positive power of $|W_0|$. Given this, one can ask whether there is a correlation between low $|W_0|$ and a modulus of low mass. This question can be addressed by examining the bosonic mass matrix of Sec. 3.2 of [50] (for which we refer the reader to the paper, as when presented in full glory the formulae are quite involved and we will only need some general features of the matrix for our discussion). If one of the masses scales as $|W_0|^k$ (for some positive k), then the determinant of the mass matrix would scale as $|W_0|^{2k}$, i.e. it would vanish in the $W_0 \to 0$ limit. On the other hand, taking $W_0 \to 0$ (which is equal to X in the notation of [50]) is not a sufficient condition for the vanishing of the determinant. This indicates that the correlation is not universal, and so that there should exist another set of vacua with $W = 0$ at perturbative level but with no flat directions. This observation agrees with the analysis of [61] based on scale invariance of the 10-dimensional tree-level type IIB action. One family of the two original scaling symmetries is broken spontaneously by the vacuum expectation value of the dilaton, resulting in a massless Goldstone boson in 4 dimensions which can be identified with τ. Non-zero background fluxes can act as explicit symmetry breaking parameters (like non-zero quark masses in chiral perturbation theory), and can lift this flat direction. However, $W = 0$ is not enough to guarantee no explicit breaking, and so no flat direction, since also derivatives of W should vanish.

Let us close by pointing out that, given a model, the statistical significance of any family of perturbatively flat vacua can be determined by the cut in the integration range of the flux variable Z^I (of [50]) put by the requirement of a low mass (at $|W_0|$

below a certain value). We hope to return to this question in the future.

Part III

DARK MATTER FROM STRING THEORY

Chapter 6

SUPERHEAVY DARK MATTER

While there are various lines of evidence for the existence of dark matter (DM) in the universe [203], the nature of DM remains a major problem at the interface of cosmology and particle physics. Weakly interacting massive particles (WIMPs) have long been a promising candidate and the focus of most direct, indirect and collider searches. In an attractive scenario, called the 'WIMP miracle', the DM relic abundance is obtained via thermal freeze-out in a radiation dominated (RD) universe for the nominal value of the DM annihilation rate $\langle\sigma_{\rm ann}v\rangle = 3\times10^{-26}$ cm^3 s^{-1}. This scenario, however, has been coming under increasing scrutiny by recent experiments, namely the Fermi-LAT results from observations of dwarf spheroidal galaxies [204] and newly discovered Milky Way satellites [205]. A recent analysis [206] has specifically ruled out thermal DM with a mass below 20 GeV in a model-independent way (unless there is P-wave annihilation or co-annihilation). Masses up to 100 GeV can be excluded if specific annihilation channels are considered.

The situation is different if the universe is not RD at the time of DM freeze-out [207]. This typically happens in non-standard thermal histories where the universe is not in a RD phase from inflationary reheating all the way to Big Bang nucleosynthesis (BBN) [208]. An important example is an epoch of early matter domination (EMD) driven by a component whose equation of state is the same as matter. This is a generic feature of early universe models arising from string theory constructions [209, 210, 211]. In this context, a string modulus is displaced from the minimum of its potential during inflation. Due to its long lifetime, the modulus dominates the energy density and gives rise to a period of EMD in the post-inflationary history. The modulus eventually decays and a RD universe is established prior to BBN. Various production mechanisms during EMD can yield the correct DM abundance for both $\langle\sigma_{\rm ann}v\rangle < 3\times10^{-26}$ cm^3 s^{-1} and $\langle\sigma_{\rm ann}v\rangle > 3\times10^{-26}$ cm^3 s^{-1} [212].

Furthermore, the DM relic abundance can be completely decoupled from $\langle\sigma_{\rm ann}v\rangle$ if its main source is direct production from the decay of the component that drives an EMD phase [213]. In this scenario, the relic abundance depends on the branching fraction for decay to DM (hence the 'branching scenario' [214]) and the yield from the decay of the matter-like component. Non-thermal production of supersymmetric DM

via the branching scenario has been studied in explicit string theory constructions where the volume modulus drives an epoch of EMD just before the onset of BBN [215]. A successful realization along these lines seems to be challenging for two reasons. First, the branching fraction of the volume modulus to DM is such that the correct abundance can be obtained for DM $\sim \mathcal{O}(10)$ GeV. Second, the decay of the volume modulus typically produces dark radiation (DR) in addition to DM, and avoiding an excess of DR severely constrains the branching scenario [128].

However, in this chapter we shall show that the branching scenario could instead arise very generically in 4D string models with superheavy WIMPs. Several scenarios of supersymmetry breaking and inflation have already been realized in the context of string theory. Combining low-energy supersymmetry with successful inflationary model building is notoriously hard to achieve [184]. The main reason is that the requirement of obtaining density perturbations of the correct size tends to fix the inflationary scale at relatively high energies. In turn, masses of the supersymmetric particles are also generically pushed to large values, typically at an intermediate scale around $10^{10} - 10^{11}$ GeV. A possible way to reconcile inflation with low-energy supersymmetry is to sequester the visible sector from the source of supersymmetry breaking in the bulk of the extra dimensions. Sequestered models, however, require a very specific brane configuration and Kähler metric for matter fields [216, 65]. This solution therefore is not very generic. We note that we have seen in the previous chapters that high scale supersymmetry is a generic feature of the string landscape regardless of inflation.

Though the thermal DM scenario is known to overproduce superheavy WIMPs [217], the DM abundance may be diluted by epochs of EMD driven by string moduli. Hence two generic features of string compactifications, high-scale supersymmetry breaking and late time epochs of modulus domination, can successfully accommodate superheavy WIMPs with a mass around $10^{10} - 10^{11}$ GeV. Incidentally, if such a DM candidate is unstable and has the right coupling to neutrinos, its decay into very energetic neutrinos could provide a tantalizing explanation of the ultra-high-energy cosmic rays recently observed by IceCube and ANITA [218].

We will illustrate this general picture by presenting an explicit model that involves two periods of EMD. The first one is driven by inflaton oscillations at the end of which the inflaton mainly decays to DR in a hidden sector, and produces superheavy DM via its tiny coupling to the visible sector. A second stage of EMD is driven by the volume modulus, which is dominantly coupled to the visible sector and is lighter than the DM. As a result, this second EMD phase only dilutes the abundance of DM and DR produced in inflaton decay down to observationally acceptable values.

This chapter is organized as follows. In Sec. 6.1 we briefly review the branching scenario for DM production. In Sec. 6.2 we discuss a successful framework for production of superheavy DM via the branching scenario. In Sec. 6.3 we introduce an explicit string theory model for realizing this scenario. In Sec. 6.4 we identify the allowed parameter space of this model for a successful inflation and a correct DM abundance, and we present numerical results for the post-inflationary evolution for a benchmark point. We conclude in Sec. 6.5, and discuss generalized scenarios that

involve more than one modulus in App. D.1.

6.1 Branching scenario: a brief review

Let us consider a post-inflationary history that includes an EMD era driven by coherent oscillations or non-relativistic quanta of a long-lived scalar field φ with mass m_φ and decay width Γ_φ. The continuous decay of φ feeds radiation (assuming that decay products thermalize immediately) during the period that it dominates the energy density of the universe. The decay of φ completes when the Hubble expansion rate is $H \simeq \Gamma_\varphi$, at which time the universe enters a RD phase. The resulting reheat temperature is $T_{\rm R} = (90/\pi^2 g_{*,{\rm R}})^{1/4}(\Gamma_\varphi M_{\rm P})^{1/2}$, where $g_{*,{\rm R}}$ is the number of relativistic degrees of freedom at $T = T_{\rm R}$.

The energy densities of φ and radiation, denoted by ρ_φ and $\rho_{\rm R}$ respectively, and the number density n_χ of DM particles χ are found by solving the following system of Boltzmann equations:

$$\begin{aligned} \dot{\rho}_{\rm R} + 4H\rho_{\rm R} &= \Gamma_\varphi \rho_\varphi \,, \\ \dot{\rho}_\varphi + 3H\rho_\varphi &= -\Gamma_\varphi \rho_\varphi \,, \\ \dot{n}_\chi + 3Hn_\chi &= \langle\sigma_{\rm ann} v\rangle \left(n_{\chi,{\rm eq}}^2 - n_\chi^2\right) + {\rm Br}_\chi \Gamma_\varphi n_\varphi \,. \end{aligned} \tag{6.1}$$

The first term on the right-hand side (RHS) of the last equation accounts for DM annihilation and inverse annihilation from the thermal bath ($\langle\sigma_{\rm ann} v\rangle$ denotes the thermally-averaged annihilation/inverse annihilation rate). The second term accounts for direct production of DM from φ decay [219] (where ${\rm Br}_\chi$ is the number of DM particles produced per φ decay). Freeze-out/in of DM happens during the EMD epoch if $T_{\rm f} > T_{\rm R}$, where $T_{\rm f} \simeq m_\chi/20$ in the case of freeze-out and $T_{\rm f} \simeq m_\chi/4$ for freeze-in [220, 221].

Assuming that freeze-out/in production is subdominant, the main contribution to the DM relic density comes from direct production at $H \simeq \Gamma_\varphi$, and the number density of DM particles at this time is given by:

$$n_\chi \simeq {\rm Br}_\chi n_\varphi = \frac{3\Gamma_\varphi^2 M_{\rm P}^2}{m_\varphi}\, {\rm Br}_\chi \,. \tag{6.2}$$

The comoving number density of DM follows this expression, hence the name 'branching scenario' [213, 214], provided that residual annihilation of DM particles to the thermal bath is inefficient. This will be the case if $\langle\sigma_{\rm ann} v\rangle n_\chi < \Gamma_\varphi$, where n_χ is substituted from (6.2). Otherwise, partial annihilation will somewhat reduce the DM number density leading to the so-called 'annihilation scenario' of DM production [210, 222, 223, 224]. The annihilation scenario can only be successful if $\langle\sigma_{\rm ann} v\rangle > 3 \times 10^{-26}$ cm^3 s^{-1}, which happens to be the case for weak-scale Wino and Higgsino DM. For small values of $\langle\sigma_{\rm ann} v\rangle$, as in the case of Bino DM or for $m_\chi \gtrsim 100$ TeV, only the branching scenario can yield the correct DM abundance.

After normalizing n_χ in (6.2) by the entropy density $s = 2\pi^2 g_{*,\mathrm{R}} T_\mathrm{R}^3/45$ at $T = T_\mathrm{R}$, the DM relic abundance in the branching scenario is found to be:

$$\frac{n_\chi}{s} = \frac{3T_\mathrm{R}}{4m_\varphi}\,\mathrm{Br}_\chi\,. \tag{6.3}$$

Here $3T_\mathrm{R}/4m_\varphi$ is the yield factor that is related to dilution due to entropy released by φ decay. In order for the branching scenario to work, this must match the observed value:

$$\left(\frac{n_\chi}{s}\right)_\mathrm{obs} \simeq 4.2\times 10^{-10}\left(\frac{1\,\mathrm{GeV}}{m_\chi}\right)\,. \tag{6.4}$$

A natural question is if the branching scenario can be successfully realized in explicit particle physics models of the early universe. This issue has been discussed in the context of type IIB string compactifications where φ is the volume modulus [215]. In this case, we have $T_\mathrm{R}/m_\varphi \simeq (m_\varphi/M_\mathrm{P})^{1/2}$. Also, for supersymmetric DM, three-body decays of φ result in a lower bound $\mathrm{Br}_\chi \gtrsim \mathcal{O}(10^{-3})$. Considering that $T_\mathrm{R} \gtrsim 3$ MeV (corresponding to $m_\varphi \gtrsim 50$ TeV) is required for BBN, (6.3) and (6.4) imply that the correct DM abundance can be obtained for $m_\chi \lesssim \mathcal{O}(10)$ GeV. Moreover, avoiding excessive production of DR, which typically accompanies DM production in string compactifications [132, 225, 135, 158], seems to favor the annihilation scenario [128].

6.2 Branching scenario and superheavy DM

In this Section we lay down a framework for production of superheavy DM via the branching scenario. To overcome the challenges mentioned in Sec. 6.1, we invoke two epochs of EMD driven by the inflaton and a modulus field respectively, as in generic string models. We also consider constraints from the cosmic microwave background (CMB) on such a scenario. In Sec. 6.3 we shall present an explicit type IIB string model that successfully realizes this scenario (see also App. D.1 for another explicit string model which realizes this scenario with an additional epoch of moduli domination).

6.2.1 Scenario with an epoch of modulus domination

The scenario we consider involves two periods of EMD driven by the inflaton σ and a modulus field ϕ in succession. Both of these fields behave as the field φ described in Sec. 6.1. The inflaton σ is responsible for inflation at the end of which the Hubble expansion rate is H_inf. The inflaton mass at the minimum of its potential is m_σ and its couplings to the visible and hidden sectors are $c_\mathrm{vis}/M_\mathrm{P}$ and $c_\mathrm{hid}/M_\mathrm{P}$ respectively where $c_\mathrm{vis} \ll c_\mathrm{hid}$. We will also assume that there is no stable non-relativistic particle in the hidden sector, so that the inflaton decay into hidden sector degrees of freedom just produces DR. Therefore, the inflaton decay rate into DR dominates over the one into visible sector particles since $\Gamma_{\sigma\to\mathrm{DR}} \simeq c_\mathrm{hid}^2 m_\sigma^3/M_\mathrm{P}^2 \gg \Gamma_{\sigma\to\mathrm{vis}} \simeq c_\mathrm{vis}^2 m_\sigma^3/M_\mathrm{P}^2$. We will also denote the total inflaton decay width as $\Gamma_\sigma = \Gamma_{\sigma\to\mathrm{vis}} + \Gamma_{\sigma\to\mathrm{DR}}$.

The modulus ϕ has mass $m_\phi < m_\sigma$. Its coupling to the visible sector is $d_{\rm vis}/M_{\rm P}$, while its coupling to the hidden sector is $d_{\rm hid}/M_{\rm P}$ with $d_{\rm vis} \gg d_{\rm hid}$. We will assume again that the modulus decay into the hidden sector produces just DR. This gives $\Gamma_{\phi\to{\rm vis}} \simeq d_{\rm vis}^2 m_\phi^3/M_{\rm P}^2 \gg \Gamma_{\phi\to{\rm DR}} \simeq d_{\rm hid}^2 m_\phi^3/M_{\rm P}^2$. The total modulus decay width is instead $\Gamma_\phi = \Gamma_{\phi\to{\rm vis}} + \Gamma_{\phi\to{\rm DR}}$. We assume that $m_\phi < m_\chi$ so that ϕ decay to DM is kinematically forbidden. The modulus acquires a displacement ϕ_0 from the minimum of its potential during inflation.

Below, we summarize the important stages of the post-inflationary history in this scenario in chronological order:

1- $\Gamma_\sigma \lesssim H < H_{\rm inf}$: The universe is in an EMD phase driven by inflaton oscillations about the minimum of its potential. ϕ also starts oscillating at this stage and $\rho_\phi = (\phi_0/M_{\rm P})^2 \rho_\sigma$. The inflaton decay completes at $H \simeq \Gamma_\sigma$ and mainly populates the hidden sector.

2- $H_{\rm D} \lesssim H < \Gamma_\sigma$: The universe is in a RD phase at this stage. The modulus oscillations behave like matter, and hence ρ_ϕ is redshifted more slowly than $\rho_{\rm R}$. As a result, ϕ starts to dominate at $H_{\rm D} \simeq (\phi_0/M_{\rm P})^4 \Gamma_\sigma$, which is the onset of a second phase of EMD.

3- $\Gamma_\phi \lesssim H < H_{\rm D}$: The universe is in a modulus-driven EMD epoch during this stage. The modulus decay completes when the Hubble expansion rate is $H \simeq \Gamma_\phi$ and reheats the visible sector. This results in the formation of a RD universe prior to the onset of BBN.

The inflaton decay to the visible and hidden sectors produces DM and DR respectively. Given that $m_\chi > m_\phi$, the modulus decay dilutes both abundances and reproduces some amount of DR in the hidden sector. The number density of DM particles directly produced by the inflaton decay at $H \simeq \Gamma_\phi$ is:

$$n_\chi \simeq n_\sigma \, {\rm Br}_\chi \, \left(\frac{a_\sigma}{a_{\rm D}}\right)^3 \left(\frac{a_{\rm D}}{a_\phi}\right)^3 , \tag{6.5}$$

where $n_\sigma = 3\Gamma_\sigma^2 M_{\rm P}^2/m_\sigma$ is the inflaton number density at the end of stage 1, $(a_\sigma/a_{\rm D})^3 = (H_{\rm D}/\Gamma_\sigma)^{3/2}$ is the number density redshift during stage 2, and $(a_{\rm D}/a_\phi)^3 = (\Gamma_\phi/H_{\rm D})^2$ is the number density redshift during stage 3.

If DM is the lightest R-parity odd particle in the visible sector, we have:

$${\rm Br}_\chi \simeq \frac{\Gamma_{\sigma\to{\rm vis}}}{\Gamma_\sigma} \, {\rm Br}_{\rm vis,odd} \, . \tag{6.6}$$

The first factor on the RHS of this expression is the fraction of σ quanta that decay to the visible sector. The second factor is the ratio of the number of R-parity odd particles (which subsequently decay to DM) to the total number of particles in the visible sector produced per σ decay. In the explicit example that we discuss later, the σ decay into the visible sector mainly occurs through two-body decays to gauge fields. Two-body decays to R-parity odd particles are highly suppressed, but they are produced via three-body decays including one gauge field and two gauginos resulting in ${\rm Br}_{\rm vis,odd} \simeq 10^{-3}$ (which is essentially a phase space factor) [214].

Therefore, after normalizing n_χ by the entropy density s, we find:

$$\frac{n_\chi}{s} \simeq \frac{3}{4} \times 10^{-3} \, \frac{1}{Y_\phi^2} \, \frac{\Gamma_{\sigma\to\mathrm{vis}}}{\Gamma_\sigma} \, \frac{\Gamma_\phi}{\Gamma_{\phi\to\mathrm{vis}}} \, \frac{T_\mathrm{R}}{m_\sigma} \,, \tag{6.7}$$

where:

$$T_\mathrm{R} = \left(\frac{90}{\pi^2 g_{*,\mathrm{R}}} \, \frac{\Gamma_{\phi\to\mathrm{vis}}}{\Gamma_\phi} \right)^{1/4} \sqrt{\Gamma_\phi M_\mathrm{P}} \,, \tag{6.8}$$

with $g_{*,\mathrm{R}}$ denoting the number of relativistic degrees of freedom in the visible sector at $T = T_\mathrm{R}$, and $Y_\phi \equiv \phi_0/M_\mathrm{P}$.

Regarding DR, its energy density at $H \simeq \Gamma_\phi$ is:

$$\rho_\mathrm{DR} \simeq \rho_\sigma \, \frac{\Gamma_{\sigma\to\mathrm{DR}}}{\Gamma_\sigma} \left(\frac{a_\sigma}{a_\mathrm{D}} \right)^4 \left(\frac{a_\mathrm{D}}{a_\phi} \right)^4 + \rho_\phi \, \frac{\Gamma_{\phi\to\mathrm{DR}}}{\Gamma_\phi} \,, \tag{6.9}$$

where $\rho_\sigma \simeq 3\Gamma_\sigma^2 M_\mathrm{P}^2$, $(a_\sigma/a_\mathrm{D})^4 = (H_\mathrm{D}/\Gamma_\sigma)^2$ is the energy density redshift during stage 2, $(a_\mathrm{D}/a_\phi)^4 = (\Gamma_\phi/H_\mathrm{D})^{8/3}$ is the energy density redshift during stage 3, and $\rho_\phi \simeq 3\Gamma_\phi^2 M_\mathrm{P}^2$. Hence, the final fractional energy density of DR is given by:

$$\frac{\rho_\mathrm{DR}}{\rho_\mathrm{R}} \simeq \frac{1}{Y_\phi^{8/3}} \left(\frac{\Gamma_\phi}{\Gamma_\sigma} \right)^{2/3} \frac{\Gamma_{\sigma\to\mathrm{DR}}}{\Gamma_\sigma} \, \frac{\Gamma_\phi}{\Gamma_{\phi\to\mathrm{vis}}} + \frac{\Gamma_{\phi\to\mathrm{DR}}}{\Gamma_{\phi\to\mathrm{vis}}} \,. \tag{6.10}$$

This ratio must be small enough to satisfy the observational constraints on the DR abundance.

6.2.2 Constraints from CMB

Inflation is the dominant paradigm for generating the almost scale-invariant perturbations. The number of e-foldings between the time when perturbations of a given wavelength exit the horizon and the end of inflation depends on the scale of inflation as well as the post-inflationary thermal history. One or more periods of EMD change the number of e-foldings from that in a standard thermal history.

In the scenario discussed in Sec. 6.2.1, the number of e-foldings of inflation between the time when the pivot scale $k_* = 0.05$ Mpc^{-1} left the horizon and the end of inflation can be written as [226, 227]:

$$N_\mathrm{e} \simeq 57 + \frac{1}{4} \ln r - \frac{1}{4} N_\mathrm{reh} - \frac{1}{4} N_\phi, \tag{6.11}$$

where r is the tensor-to-scalar ratio and:

$$\begin{aligned} N_\mathrm{reh} &\simeq \frac{2}{3} \ln \left(\frac{H_\mathrm{inf}}{\Gamma_\sigma} \right) \,, \\ N_\phi &\simeq \frac{2}{3} \ln \left(\frac{H_\mathrm{D}}{\Gamma_\phi} \right) \simeq \frac{2}{3} \ln \left(Y_\phi^4 \frac{\Gamma_\sigma}{\Gamma_\phi} \right) \,. \end{aligned} \tag{6.12}$$

Here $N_{\rm reh}$ and N_ϕ denote the duration of EMD phases from inflationary reheating and modulus domination (stages 1 and 3 above) respectively. This results in:

$$N_{\rm e} \simeq 57 + \frac{1}{4}\ln r - \frac{1}{6}\ln\left(Y_\phi^4 \frac{H_{\rm inf}}{\Gamma_\phi}\right). \tag{6.13}$$

In important universality classes of inflation, the scalar spectral index $n_{\rm s}$ is related to $N_{\rm e}$ through a simple relation [228]:

$$n_{\rm s} = 1 - \frac{a}{N_{\rm e}}. \tag{6.14}$$

For example, in the Starobinsky model and Higgs inflation, as well as the specific model of string inflation that we will discuss later, $a = 2$. This then leads to:

$$N_{\rm e} = \frac{2}{1 - n_{\rm s}}. \tag{6.15}$$

This implies that:

$$N_{\rm e} \gtrsim \frac{2}{1 - n_{\rm s,min}}, \tag{6.16}$$

where $n_{\rm s,min}$ is the minimum value in the 2σ region allowed by Planck data [229]. For a given model of inflation where $H_{\rm inf}$ is known, this in turn sets an upper bound on $Y_\phi^4\Gamma_\phi^{-1}$ through (6.13).

On the other hand, for known inflaton parameters m_σ and Γ_σ, (6.7) and (6.10) result in a lower bound on $Y_\phi^4\Gamma_\phi^{-1}$ in order not to overproduce DM and DR in our scenario.

Therefore, obtaining the correct abundance of DM (while avoiding an excessive production of DR) and getting an acceptable value of $n_{\rm s}$ constrain the epoch of modulus domination in opposite ways.[1] This can be understood intuitively as follows. While diluting the abundance of DM and DR produced from inflaton decay to acceptable levels requires a long enough bout of modulus domination, satisfying the lower bound on $n_{\rm s}$ limits the duration of that period from above.

6.3 A string model with an epoch of modulus domination

In this Section we shall present an explicit string model which successfully realizes inflation and superheavy DM via the branching scenario with an epoch of modulus domination.

[1] The implications of CMB constraints for non-thermal DM in low-scale supersymmetry has been studied in [230].

6.3.1 The setup

We consider a type IIB model with 3 Kähler moduli $T_i = \tau_i + \mathrm{i}c_i$, $i = 1, ..., 3$ and a Calabi-Yau volume of the form:

$$\mathcal{V} = \tau_{\rm big}^{3/2} - \tau_{\rm vis}^{3/2} - \tau_{\rm inf}^{3/2} \,. \tag{6.17}$$

The visible sector is realized via a stack of D7-branes wrapped around the 4-cycle whose volume is controlled by $\tau_{\rm vis}$, while inflation is driven by the modulus $\tau_{\rm inf}$ as in Kähler moduli inflation [231]. A hidden sector lives instead on a stack of D7-branes wrapped around the 4-cycle whose volume is given by $\tau_{\rm inf}$.

The structure of the effective supergravity theory is determined by the Kähler potential K and the superpotential W. K is given by:

$$K = -2\ln\left(\mathcal{V} + \frac{\xi}{2g_s^{3/2}}\right), \tag{6.18}$$

where g_s is the string coupling and ξ is an $\mathcal{O}(1)$ coefficient which controls α' corrections [232] beyond the tree-level expression. W instead reads:

$$W = W_0 + A_{\rm vis}\, e^{-a_{\rm vis}T_{\rm vis}} + A_{\rm inf}\, e^{-a_{\rm inf}T_{\rm inf}} \,, \tag{6.19}$$

where $W_0 \sim \mathcal{O}(10-100)$ is the tree-level contribution, while the terms proportional to $A_{\rm vis}$ and $A_{\rm inf}$ are non-perturbative effects [233] (all A's and a's are expected to be $\mathcal{O}(1)$ constants).

Moduli stabilization produces a typical LVS minimum [234] at exponentially large volume in string units, $\mathcal{V} \simeq \tau_{\rm big}^{3/2} \sim e^{1/g_s}$, while the two blow-up modes are fixed at smaller values $\tau_{\rm vis} \sim \tau_{\rm inf} \sim 1/g_s \sim \mathcal{O}(10)$, where we take the string coupling in the perturbative regime $g_s \lesssim 0.1$. Notice that $\tau_{\rm vis}$ sets the value of the visible sector gauge coupling $\alpha_{\rm vis}^{-1} = 4\pi g_{\rm vis}^{-2} = \tau_{\rm vis} \sim \mathcal{O}(10)$ which turns out to be in the appropriate phenomenological regime.

Moduli stabilization proceeds as follows: at leading order in a $1/\mathcal{V}$ expansion, non-perturbative corrections to W combined with α' corrections to K stabilize $\mathcal{V}$, $\tau_{\rm vis}$, $c_{\rm vis}$, $\tau_{\rm inf}$ and $c_{\rm inf}$, leaving 1 flat direction parameterized by the axion $c_{\rm big}$.[2] This axion turns out to be ultra-light since it receives a tiny mass due to additional $T_{\rm big}$-dependent non-perturbative corrections to W. Thus $c_{\rm big}$ plays the role of hidden sector dark radiation. This system admits a non-supersymmetric AdS minimum which can however be uplifted to dS via several possible mechanisms (anti D3-branes [235], T-branes [92], non-perturbative effects at singularities [93], non-zero F-terms of the complex structure moduli [57]).

[2] More precisely $\tau_{\rm vis}$ should be fixed by perturbative corrections to K [34] due to the interplay between chirality and non-perturbative effects [151]. However this detail is almost irrelevant for the phenomenological implications of our model.

6.3.2 Moduli mass spectrum

The determination of the moduli mass spectrum and couplings to both visible and hidden sector fields requires first to go to canonically normalized fields. Following the notation of Sec. 6.2, we will denote them as: (*i*) σ for $\tau_{\rm inf}$ since this modulus plays the role of the inflaton; (*ii*) ϕ for $\tau_{\rm big}$ since this modulus will give rise to an EMD epoch after the end of inflation; and (*iii*) $a_{\rm DR}$ for the closed string axion $c_{\rm big}$ which behaves as dark radiation. Defining:

$$\epsilon \equiv \frac{W_0}{\mathcal{V}} \ll 1 \qquad \text{and} \qquad \kappa \equiv \frac{g_s}{8\pi} \ll 1\,, \tag{6.20}$$

the mass spectrum of the relevant moduli around the minimum becomes [236, 237] (see [238] for the correct normalization factor κ):

$$\begin{aligned} m_\sigma^2 &\simeq \kappa\,\epsilon^2\,(\ln\epsilon)^2\;M_{\rm P}^2 \\ m_\phi^2 &\simeq \frac{\epsilon\, m_\sigma^2}{g_s^{3/2} W_0\,|\,(\ln\epsilon)^3\,|} \ll m_\sigma^2 \quad \text{for} \quad \epsilon \ll 1 \\ m_{a_{\rm DR}}^2 &\simeq \kappa\, e^{-2\mathcal{V}^{2/3}}\, M_{\rm P}^2 \sim 0\,. \end{aligned} \tag{6.21}$$

This setup allows to realize Kähler moduli inflation [231] where the inflaton is σ since this modulus becomes much lighter than $H \simeq m_\phi$ as soon as it is displaced from its minimum. $\tau_{\rm vis}$, $c_{\rm vis}$, and $c_{\rm inf}$ are heavy spectator fields which do not get displaced during inflation since their mass is of the same order of the mass of σ around the minimum, and so it is much larger than H. On the other hand, all the other moduli get displaced from their minimum during inflation. We shall focus just on ϕ since the axion $a_{\rm DR}$ remains almost massless and behaves as a source of extra dark radiation. We shall also denote the displacement of the canonically normalized light Kähler modulus as $\phi_0 = Y_\phi\, M_{\rm P}$. Explicit computations have shown that $Y_\phi \simeq 0.01 - 0.1$ [211]. Due to this displacement during inflation, ϕ gives rise to a period of modulus domination. Moreover supersymmetry is broken due to non-zero F-terms of the Kähler moduli which generate a gravitino mass $m_{3/2}$ together with gaugino and scalar masses of order [95]:

$$m_{3/2} = \sqrt{\kappa}\,\epsilon\, M_{\rm P}\,, \qquad m_0 \simeq M_{1/2} \simeq \frac{m_{3/2}}{|\ln\epsilon|}\,. \tag{6.22}$$

Taking the DM mass of the same order as the soft terms, $m_\chi \simeq m_0 \simeq M_{1/2}$, we realize that:

$$m_\phi^2 \simeq \frac{\epsilon\,|\ln\epsilon|}{g_s^{3/2} W_0}\, m_\chi^2 \ll m_\chi^2 \quad \text{for} \quad \epsilon \ll 1\,, \tag{6.23}$$

which ensures that DM cannot be reproduced from the decay of the light modulus ϕ.

Notice that in order to avoid any cosmological moduli problem, the mass of ϕ has to be $m_\phi \gtrsim \mathcal{O}(50)$ TeV. Using (6.21) and setting $g_s \simeq 0.1$ and $1 \lesssim W_0 \lesssim 100$, this gives the bound $5 \times 10^{-9} - 10^{-8} \lesssim \epsilon \ll 1$ which, when translated in terms of the overall volume, becomes $1 \ll \mathcal{V} \lesssim 10^8 - 5 \times 10^9$. This, in turn, produces a

scenario of superheavy DM since it sets a lower bound on the DM mass of order $m_\chi \gtrsim 10^{10} - 10^{11}$ GeV. As we shall see in the Sec. 6.4, values of $\mathcal{V}$ below $10^8 - 5 \times 10^9$ are also required to generate, during inflation, the observed value of the amplitude of the density perturbations.

6.3.3 Hidden sector configuration

Let us comment a bit more on the configuration of the hidden sector D7-stack wrapping $\tau_{\rm inf}$. This has to provide a non-perturbative contribution to the superpotential which generates the inflationary potential, and be such that the inflaton decay into the hidden sector produces just relativistic degrees of freedom without additional contributions to the DM abundance. This dark radiation component is subsequently diluted by the decay of the lightest modulus. If the hidden sector is a supersymmetric $SU(N_c)$ theory with N_f flavors, it would confine if $N_f < N_c$. The corresponding scale of strong dynamics Λ can be shown to be above the inflaton mass, $m_\sigma < \Lambda$ [236], and so σ cannot decay into glueballs (gg), 'gluinoballs' ($\tilde{g}\tilde{g}$), and 'glueballinos' ($g\tilde{g}$) since they all develop a mass of order Λ. Hence we need to discard the pure SYM case. For $N_f > 0$ with soft supersymmetry breaking terms, squarks and quarks form scalar and fermionic condensates which all develop a mass of order $m_0 \simeq M_{1/2} \ll m_\sigma$ [239], except for pion-like mesons which are exactly massless in the absence of a supersymmetric quark mass term in W. Therefore σ could decay into these heavy condensates but some of them would be stable in the absence of EW interactions. We conclude that the hidden sector cannot be a simple $SU(N_c)$ theory with N_f flavors. The best configuration for the hidden sector is instead a copy of the visible sector, i.e. an MSSM-like hidden sector, with however 3 differences with respect to the visible sector: (*i*) the scale of strong dynamics Λ is much higher than in ordinary QCD; (*ii*) R-parity is not conserved so that hidden protons are unstable; (*iii*) the mass of the hidden electrons is very small so that they are still relativistic, like neutrinos. In this scenario, all hidden degrees of freedom produced from the inflaton decay eventually decay into hidden massless gauge bosons or hidden relativistic matter fermions.

A final requirement is the absence of any leakage of energy between hidden and visible sector degrees of freedom due to kinetic mixing between $U(1)$s or a possible moduli portal. The first option can be avoided by construction if the hidden gauge group does not contain any Abelian $U(1)$ factor.[3] On the other hand, a moduli portal between the two sectors could be created by the volume modulus ϕ. However, we expect this effect to be negligible since, as we shall see in Sec. 6.3.4, this field couples only with Planckian strength to both sectors, and so any leakage would be proportional to $(1/M_{\rm P})^4$.

[3]Even in the presence of a $U(1)$ kinetic mixing, we expect the mixing parameter to be very small due to the geometric separation between $\tau_{\rm vis}$ and $\tau_{\rm hid}$ [240].

6.3.4 Moduli couplings and decay rates

Due to the geometric separation in the extra dimensions between $\tau_{\rm vis}$ (which supports the visible sector D7 stack) and $\tau_{\rm inf}$ (which supports a hidden sector D7 stack), the coupling of the canonically normalized inflaton σ to hidden sector gauge bosons is much stronger than the one to visible sector gauge fields [236]:

$$\mathcal{L} \supset -\frac{1}{4}\frac{c_{\rm hid}}{M_{\rm P}}\,\sigma\,F^{\rm hid}_{\mu\nu}F^{\mu\nu}_{\rm hid} - \frac{1}{4}\frac{c_{\rm vis}}{M_{\rm P}}\,\sigma\,F^{\rm vis}_{\mu\nu}F^{\mu\nu}_{\rm vis}\,, \tag{6.24}$$

with:

$$c_{\rm hid} \simeq g_s^{3/4}\sqrt{\mathcal{V}} \gg 1 \qquad \text{and} \qquad c_{\rm vis} \simeq c_{\rm hid}^{-1}\,. \tag{6.25}$$

Notice that the interactions in (6.24) provide the main contributions to the inflaton decay rate to both visible and hidden degrees of freedom. In fact, since $m_0 \simeq M_{1/2} \ll m_\sigma$, the inflaton decay into supersymmetric partners is mass suppressed. The same consideration applies to the inflaton decay into both visible and hidden sector matter fermions. The decay rate into Higgses is also mass suppressed except for the case of a Giudice-Masiero interaction in K which we assume to be absent.[4] This implies the following important relation for the determination of the DM abundance using (6.7):

$$\frac{\Gamma_{\sigma\to\rm vis}}{\Gamma_\sigma} = \frac{N_g}{N_g^{\rm hid}}\frac{1}{c_{\rm hid}^4}\frac{1}{\left(1+\frac{N_g}{N_g^{\rm hid}}\frac{1}{c_{\rm hid}^4}\right)} \simeq \frac{N_g}{N_g^{\rm hid}}\frac{1}{g_s^3\,\mathcal{V}^2} \ll 1\,, \tag{6.26}$$

where we included also the number of visible and hidden sector gauge bosons denoted respectively as N_g and $N_g^{\rm hid}$. For an MSSM-like visible sector we have $N_g = 12$ while $N_g^{\rm hid}$ is a model-dependent parameter which can also be larger than N_g.

On the other hand the light modulus ϕ can decay to:

- Hidden sector gauge bosons:

$$\mathcal{L} \supset -\frac{1}{4}\frac{\lambda_{\rm hid}}{M_{\rm P}}\,\phi\,F^{\rm hid}_{\mu\nu}F^{\mu\nu}_{\rm hid}\,, \qquad \lambda_{\rm hid} \simeq \frac{1}{|\ln\epsilon|}$$

- Dark radiation bulk axions:

$$\mathcal{L} \supset \lambda_{\rm DR}\,\frac{m_\phi^2}{M_{\rm P}}\,\phi\,a_{\rm DR}\,a_{\rm DR}\,, \qquad \lambda_{\rm DR} \simeq \frac{1}{\sqrt{6}}$$

- Visible sector gauge bosons:

$$\mathcal{L} \supset -\frac{1}{4}\frac{\lambda_{\rm vis}}{M_{\rm P}}\,\phi\,F^{\rm vis}_{\mu\nu}F^{\mu\nu}_{\rm vis}\,, \qquad \lambda_{\rm vis} \simeq \frac{1}{|\ln\epsilon|}$$

[4] Including a Giudice-Masiero coupling between σ and Higgs degrees of freedom would not modify our results qualitatively.

- Visible sector Higgs h^0 and would-be Goldstone bosons G^0 and $G^\pm$ [135]:

$$\mathcal{L} \supset c\,\frac{m_\phi^2}{M_{\rm P}}\,\phi\left[(h^0)^2+(G^0)^2+({\rm Re}G^+)^2+({\rm Im}G^+)^2\right]$$

  with $c = Z/(2\sqrt{6})$ where Z is an $\mathcal{O}(1)$ parameter controlling Giudice-Masiero contributions to the Kähler potential of the form $K \supset \frac{Z}{\tau_b}(H_u H_d + {\rm h.c.})$ [132].

For $\epsilon \ll 1$, the decay rate of ϕ into both hidden and visible gauge bosons is suppressed. On the other hand, the decay of ϕ into ultra-light bulk axions could give rise to extra dark radiation which needs to be in agreement with present observational bounds [241]. This sets a lower bound on Z of order (neglecting DR from inflaton decay since this is diluted by the decay of ϕ) [135]:

$$\Delta N_{\rm eff} \simeq 3\,\frac{\Gamma_{\phi\to{\rm DR}}}{\Gamma_{\phi\to{\rm vis}}} = \frac{3}{Z^2} \lesssim 0.75 \quad \text{for} \quad Z \gtrsim 2\,. \tag{6.27}$$

Therefore the ratio $\Gamma_\phi/\Gamma_{\phi\to{\rm vis}}$ which appears in (6.7) for the final DM abundance looks like:

$$\frac{\Gamma_\phi}{\Gamma_{\phi\to{\rm vis}}} = 1+\frac{1}{Z^2} \lesssim 1.25\,, \tag{6.28}$$

and the reheating temperature $T_{\rm R}$ in (6.8) can be derived from the following decay width:

$$\Gamma_\phi = \frac{1+Z^2}{48\pi}\,\frac{m_\phi^3}{M_{\rm P}^2}\,. \tag{6.29}$$

Finally, the remaining quantities which are crucial to derive the fractional energy density of DR using (6.10) are:

$$\begin{aligned}\Gamma_\sigma &= N_g^{\rm hid}\,\frac{c_{\rm hid}^2}{64\pi}\left(1+\frac{N_g}{N_g^{\rm hid}}\frac{1}{c_{\rm hid}^4}\right)\frac{m_\sigma^3}{M_{\rm P}^2}\\ &\simeq N_g^{\rm hid}\,\frac{c_{\rm hid}^2}{64\pi}\,\frac{m_\sigma^3}{M_{\rm P}^2}\,,\end{aligned} \tag{6.30}$$

and:

$$\frac{\Gamma_{\sigma\to{\rm DR}}}{\Gamma_\sigma} = \left(1+\frac{N_g}{N_g^{\rm hid}}\frac{1}{c_{\rm hid}^4}\right)^{-1} \simeq 1\,. \tag{6.31}$$

6.3.5 Consistency of the branching scenario

In this paper we are considering a branching scenario for DM production from inflaton decay. This is generically the case for superheavy WIMP DM since the corresponding annihilation rate would be too small to realize the so-called non-thermal annihilation scenario. However the computation of the DM relic density relies on the assumption that the standard thermal freeze-out mechanism cannot occur. This is true if the visible sector reheating temperature after the inflaton decay $T_{\rm R,inf}^{\rm vis}$ is below $T_{\rm f}$, where

$T_{\rm f} \simeq m_\chi/20$ in the case of freeze-out (and $T_{\rm f} \simeq m_\chi/4$ for freeze-in). We shall now show that this is indeed the case in our model.

In standard supersymmetric scenarios, the LSP mass is expected to be of order the soft mass. As we have already seen, the DM mass is therefore slightly below the inflaton mass, $m_\chi \simeq m_\sigma/(\ln\epsilon)^2 < m_\sigma$. Notice that this feature is not a peculiarity of our model but it is a generic characteristic of string compactifications since, whenever the 4-cycle supporting the visible sector is stabilized in the geometric regime, the visible sector is always not sequestered from the source of supersymmetry breaking in the bulk. Thus the soft terms, and the DM mass, turn out to be of the same order as the gravitino mass, which sets also the order of magnitude of the mass of generic moduli (up to possible $|\ln\epsilon|$ suppression factors).

Therefore we shall consider $T_{\rm f} \simeq m_\sigma/[20\,(\ln\epsilon)^2]$. On the other hand, the visible sector reheating temperature reads:

$$\begin{aligned} T_{\rm R,inf}^{\rm vis} &= \left(\frac{40 N_g N_g^{\rm hid}}{\pi^2 g_*}\right)^{1/4} \sqrt{\frac{c_{\rm vis} c_{\rm hid}}{64\pi}}\, m_\sigma \sqrt{\frac{m_\sigma}{M_{\rm P}}} \\ &\simeq \frac{m_\chi}{20}\,(\ln\epsilon)^2 \sqrt{\frac{m_\sigma}{M_{\rm P}}}\,, \end{aligned} \tag{6.32}$$

where we used $c_{\rm hid} \simeq c_{\rm vis}^{-1}$, and $N_g^{\rm hid} \simeq N_g = 12$. Hence we obtain $T_{\rm R,inf}^{\rm vis} < T_{\rm f}$ provided that:

$$\frac{T_{\rm R,inf}^{\rm vis}}{T_{\rm f}} \simeq (\ln\epsilon)^2 \sqrt{\frac{m_\sigma}{M_{\rm P}}} \simeq \kappa^{1/4}\,|\ln\epsilon|^{5/2}\,\sqrt{\epsilon} < 1\,. \tag{6.33}$$

This is indeed the case for $\epsilon \ll 1$ and $\kappa \ll 1$, which guarantees the consistency of the branching scenario. This will be confirmed in Sec. 6.4.2 which presents a numerical analysis of the cosmological evolution of our model.

6.4 Cosmology of the string model

In this Section we shall first determine the values of the microscopic parameters which give the right amplitude of the density perturbations and the correct DM abundance, finding a DM mass around 10^{10}-10^{11} GeV. We shall then perform a numerical analysis of the cosmological evolution of our string model with an epoch of modulus domination.

6.4.1 Inflationary observables and DM abundance

Let us derive the allowed DM mass range in a single modulus cosmology. We achieve a rather precise prediction by imposing a combination of observational and geometrical constraints. We start with the expression for the number of e-foldings between horizon exit and the end of inflation [211]:

$$N_{\rm e} \simeq 57 + \frac{1}{4}\ln r - \frac{1}{4}N_{\rm reh} - \frac{1}{4}N_\phi + \frac{1}{4}\ln\left(\frac{\rho_{\sigma,\rm start}}{\rho_{\sigma,\rm end}}\right). \tag{6.34}$$

Here r is the tensor-to-scalar ratio, $N_{\rm reh}$ is the duration of the reheating period due to the inflaton σ, and N_ϕ is the duration of the EMD epoch due to the modulus ϕ. Note that we have set the equation-of-state parameter w equal to zero during inflationary reheating. Also $\rho_{\sigma,\rm start}$ is the energy density at horizon exit, while $\rho_{\sigma,\rm end}$ is the energy density at the end of inflation. Let us rewrite (6.34) in terms of fundamental parameters. The duration of the reheating period is:

$$N_{\rm reh} \simeq \frac{2}{3}\ln\left(\frac{H_{\sigma,\rm end}}{\Gamma_\sigma}\right), \tag{6.35}$$

where $H_{\sigma,\rm end}$ is the Hubble rate at the end of inflation, which is given by [211]:

$$H_{\sigma,\rm end} \simeq \sqrt{\frac{3}{2}\frac{\kappa}{(2\pi)^{3/2}W_0}}\,\epsilon^{3/2}|\ln\epsilon|^{3/4}\,M_{\rm P}\,. \tag{6.36}$$

Combining (6.36) with the inflaton decay rate (6.30) gives:

$$N_{\rm reh} \simeq \frac{2}{3}\ln\left(\sqrt{\frac{3}{2}\frac{512^2\pi^4}{(2\pi)^{3/2}}}\frac{\mathcal{V}^{1/2}}{N_g^{\rm hid}W_0^2 g_s^{5/2}\,|\ln\epsilon|^{9/4}}\right). \tag{6.37}$$

The duration of modulus domination is given by:

$$\begin{aligned} N_\phi &\simeq \frac{2}{3}\ln\left(Y_\phi^4\frac{\Gamma_\sigma}{\Gamma_\phi}\right) \\ &\simeq \frac{2}{3}\ln\left(\frac{3}{4}\frac{N_g^{\rm hid}}{1+Z^2}\,Y_\phi^4\,g_s^{15/4}\,\mathcal{V}^{5/2}\,|\ln\epsilon|^{9/2}\right). \end{aligned} \tag{6.38}$$

Following again [211], the tensor-to-scalar ratio can be expressed as:

$$r \simeq 16\times 3.7\times 10^6\left(\frac{3}{2}\frac{|\ln\epsilon|^{3/2}}{(2\pi)^{3/2}}\right)\frac{g_s}{16\pi}\frac{W_0^2}{\mathcal{V}^3}\,. \tag{6.39}$$

Noting that the amplitude of the density perturbations can be written as $A_s = \frac{2}{3\pi^2 r}\frac{\rho_{\sigma,\rm start}}{M_{\rm P}^4}$, we get:

$$N_{\rm e} \simeq 60.1 - \frac{1}{6}\ln\left(\frac{Y_\phi^4\,\mathcal{V}^{15/2}}{5g_s^{1/4}W_0^5\,|\ln\epsilon|^{9/4}}\right), \tag{6.40}$$

where we have set $Z=2$ and used $\ln(10^{10}A_s) = 3.044$ [229]. To proceed further, we need the relation between the inflaton $\tau_{\rm inf}$, the volume $\mathcal{V}$, and the number of e-foldings $N_{\rm e}$ that matches the observed value of A_s. This reads [211]:

$$\tau_{\rm inf} \simeq 1.15\times 10^{-11}\frac{1}{2\pi g_s^2}\left(\frac{\mathcal{V}}{W_0\,|\ln\epsilon|^{3/4}\,N_{\rm e}}\right)^4. \tag{6.41}$$

Given that $\tau_{\rm inf}$ describes the volume of a local 4-cycle, we have to impose the geometrical constraint $\mathcal{V}^{2/3} \simeq \tau_b \gg \tau_{\rm inf}$ which guarantees that the effective field theory is under control. We can implement this constraint as $\mathcal{V}^{2/3} \simeq \lambda\, \tau_{\rm inf}$, where $\lambda \gg 1$ is a tunable parameter that determines the hierarchy between the overall volume $\mathcal{V}$ and the volume of the blow-up mode $\tau_{\rm inf}$. This gives us the final expression:

$$\mathcal{V}^{2/3} \simeq \lambda \left(\frac{\alpha^{1/4} \mathcal{V}}{g_s^{1/2} W_0 \, |\ln \epsilon|^{3/4} \, N_{\rm e}} \right)^4 , \tag{6.42}$$

with $\alpha = 1.15 \times 10^{-11} \frac{1}{2\pi}$ and $N_{\rm e}$ given in (6.40).

Let us briefly summarize the procedure that we shall follow to derive the DM mass corresponding to the observed DM abundance:

- We extract from (6.42) W_0 as a function of $\mathcal{V}$. This step encodes in $W_0(\mathcal{V})$ the information of the amplitude of the density perturbations and the geometrical relation between $\mathcal{V}^{2/3}$ and $\tau_{\rm inf}$. We also set a natural bound on W_0 by constraining it to be in the range $\mathcal{O}(1 - 10^3)$.

- We perform this step for different values of the underlying parameters g_s, Y_ϕ, and λ, choosing the discrete parameter space to be $g_s \in [10^{-3}, 0.1]$, $Y_\phi \in [0.01, 1]$, and $\lambda \in [10, 10^4]$. We start with 1444 initial combinations.

- We extract the value of $\mathcal{V}$ by matching the expressions for the observed and predicted DM abundances. We perform this step for each of the 1444 initial parameter combinations.

- We compute the DM mass for those parameter combinations that allow for the correct DM abundance.

In Fig. 6.1 we present all data points in the $(W_0, \mathcal{V})$ plane which reproduce the observed amplitude of the density perturbations, respect our geometrical constraints, and yield the correct DM abundance. Approximately 72% of our initial parameter space leads to a consistent solution. Notice that, although each point corresponds to different values of g_s, Y_ϕ, and λ, the resulting DM mass is always in the range 10^{10}-10^{11} GeV, giving a robust prediction which is almost independent of the variation of the underlying parameters.

The accumulation around the origin and the jet-like structures in the distribution of the data points can be understood from Fig. 6.2 where we split the points shown in Fig. 6.1 into two sets with, respectively, $g_s = 0.001 - 0.009$ and $g_s = 0.01 - 0.1$. Moreover black dots correspond to $\lambda = 10^4$, red to $\lambda = 10^3$, blue to $\lambda = 10^2$, and green to $\lambda = 10$. The plot for smaller values of g_s shows clearly that the four jet structures correspond to different values of λ. This behavior is a direct consequence of (6.42) which implies that λ determines the slope of the function $W_0(\mathcal{V})$. On the other hand, the plot for larger values of g_s features a larger density at smaller values

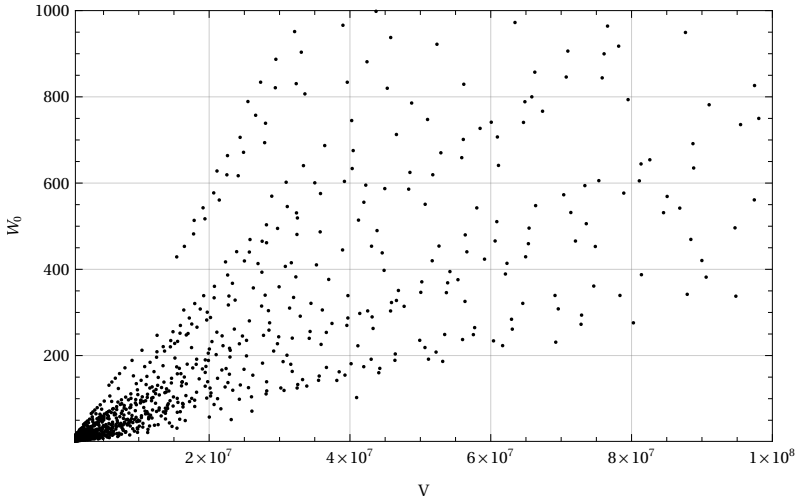

Figure 6.1: Points in the $(W_0, \mathcal{V})$ plane which reproduce the observed amplitude of the density perturbations and DM abundance.

of W_0 and $\mathcal{V}$. This behavior is a consequence of the consistency of the branching scenario. In fact, in order for (6.26) to hold, smaller values of the volume must lead to an increase in g_s. It is worth mentioning also that around 71% of the data points correspond to $g_s \in [0.01, 0.1]$, whereas 29% of the acceptable parameter space correspond to $g_s \in [10^{-3}, 0.01]$.

In Fig. 6.3 we present a similar analysis, this time splitting all data points from Fig. 6.1 into two sets, depending on the value of the misalignment Y_ϕ. We observe again the same jet structure depending on the value of the parameter λ. An important observation here is the slight rotation of the data-point cone towards the W_0 axis if we increase Y_ϕ. This behavior is mainly driven by the DM abundance constraint formulated in (6.7). The abundance scales like $\sim {Y_\phi}^{-2}\mathcal{V}^{-13/4}$. Hence, in order to match the right abundance, a smaller volume must be compensated by a larger misalignment Y_ϕ.

Understanding the behavior of our data set as a function of the underlying parameters is important in order to understand the distribution of the scalar spectral index n_s. For each point in Fig. 6.1, we calculated the resulting value of n_s. All obtained values are within the 2- and 3σ range [229], as can be seen from Fig. 6.4.

In Fig. 6.4 each black dot corresponds to a scalar spectral index within the 2σ range, i.e. $0.9565 < n_s < 0.9733$, while each red dot has n_s in the 3σ range, i.e. $0.9523 < n_s < 0.9775$, but outside 2σ. By comparing the two distributions, we see that the data points corresponding to 2σ seem to be accumulating at the origin and their cone is slightly rotated towards the volume axis. From this observation we conclude that phenomenologically more acceptable values of n_s drive the string coupling g_s to larger values and the misalignment Y_ϕ to smaller ones.

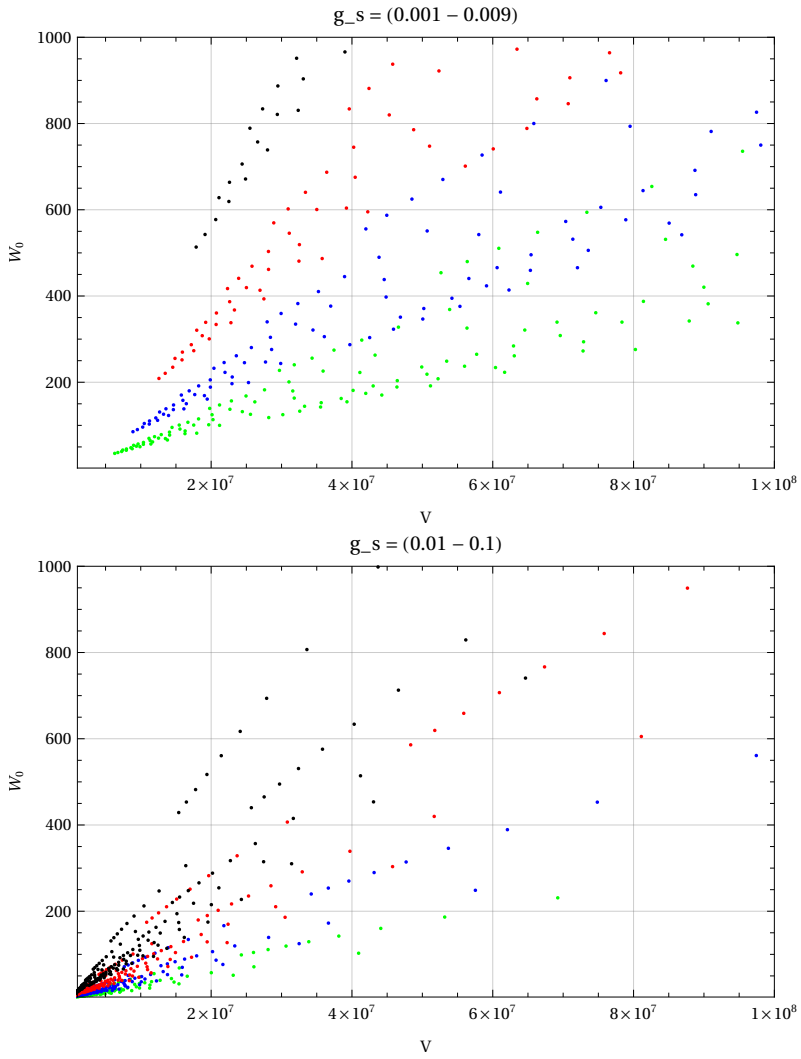

Figure 6.2: Selected data points for different values of g_s and λ. Around 29% of the data points are in the lower g_s regime, while around 71% are in the upper regime. Black points correspond to $\lambda = 10^4$, red to $\lambda = 10^3$, blue to $\lambda = 10^2$, and green to $\lambda = 10$.

A crucial observation is that the parameter values in our data set naturally respect the relation between the volume and the underlying model parameters at the minimum of the scalar potential [234]:

$$\langle \mathcal{V} \rangle \simeq \frac{3\sqrt{\langle \tau_{\rm inf} \rangle}|W_0|}{4 a_{\rm inf} A_{\rm inf}} e^{a_{\rm inf}\langle \tau_{\rm inf}\rangle}, \quad \langle \tau_{\rm inf} \rangle \simeq \frac{1}{g_s}\left(\frac{\xi}{2}\right)^{2/3},$$

for natural $\mathcal{O}(1)$ values of the microscopic parameters $a_{\rm inf}$, $A_{\rm inf}$ and ξ.

In Sec. 6.4.2 we shall perform a more in-depth numerical analysis of the cosmological evolution, using the benchmark parameters listed in Tab. 6.1.

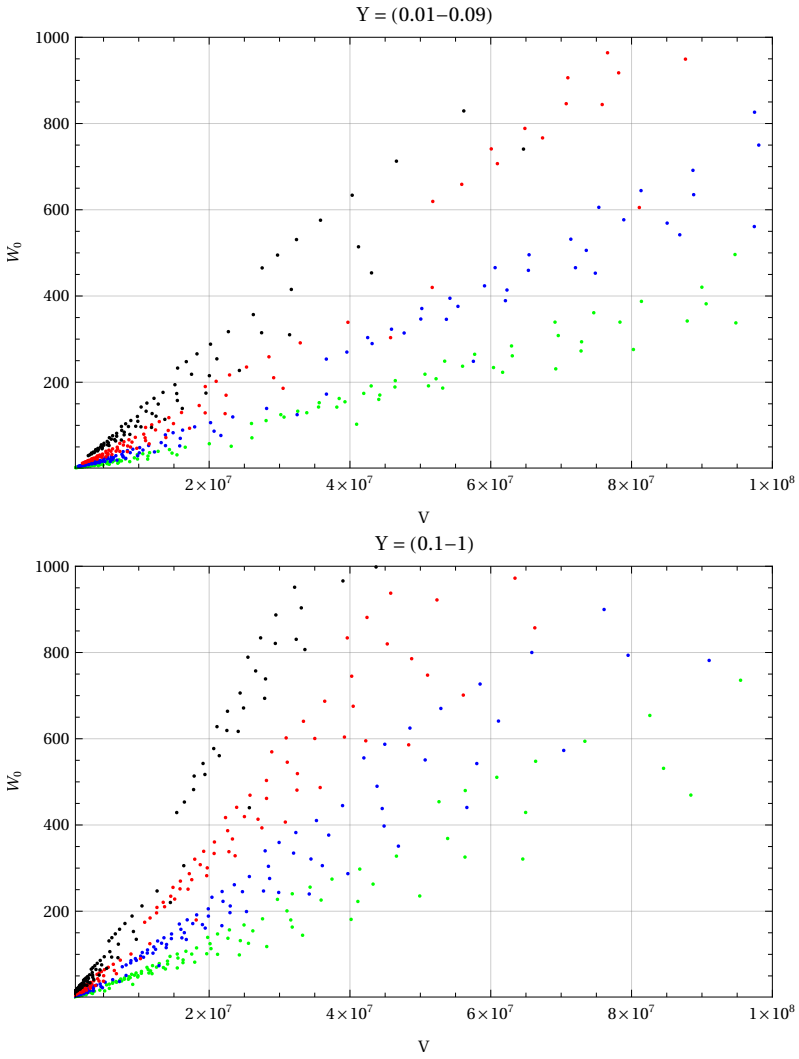

Figure 6.3: Selected data points for different values of Y_ϕ and λ. Around 42% of the data points are in the lower Y_ϕ regime, while around 58% are in the upper regime. Black points correspond to $\lambda = 10^4$, red to $\lambda = 10^3$, blue to $\lambda = 10^2$, and green to $\lambda = 10$.

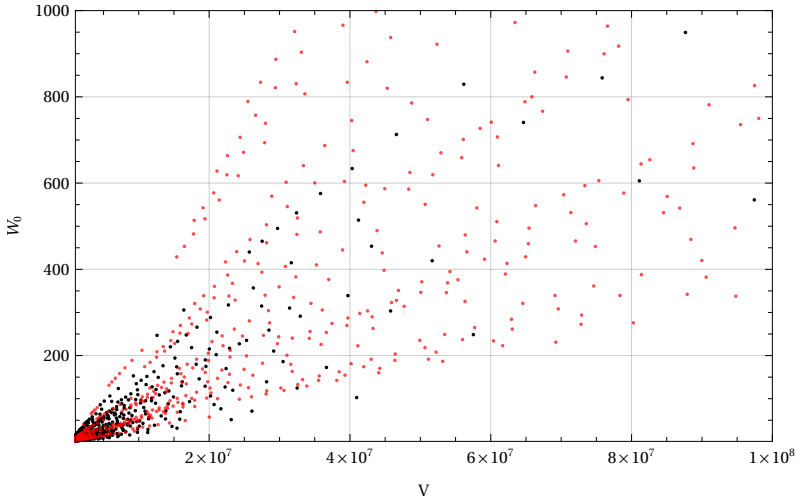

Figure 6.4: Scalar spectral index coloring of the entire data set. Black dots correspond to $n_{\rm s}$ within the 2σ range, while red dots have $n_{\rm s}$ within 3σ (but outside 2σ).

W_0	39.1
$\mathcal{V}$	8.4×10^6
N_e	47.4
$N_{\rm reh}$	3.7
N_ϕ	16.4
$n_{\rm s}$	0.9578
m_σ	8.7×10^{12}GeV
m_ϕ	3.9×10^{8}GeV
$m_{3/2}$	7.1×10^{11}GeV
m_χ	5.8×10^{10}GeV
$c_{\rm hid}$	514.7

Table 6.1: Microscopic parameters W_0 and $\mathcal{V}$, the resulting e-folding numbers, $n_{\rm s}$, mass scales, and inflaton coupling to hidden degrees of freedom $c_{\rm hid}$ at a benchmark point that gives the right amplitude of the density perturbations and the correct DM abundance. The input parameters are $g_s = 0.1$, $Y_\phi = 0.01$, $\lambda = 10^3$, $N_g^{\rm hid} = 12$, and $Z = 2$.

6.4.2 Numerical analysis of cosmological evolution

We perform a numerical analysis of the cosmological evolution of our scenario by solving the coupled set of Boltzmann equations for the various cosmological components (see App. D.1 for a scenario with two moduli). We begin the numerical evolution at $H \simeq H_{\rm inf}$, with both σ and ϕ oscillating, and other components highly subdominant. The Boltzmann equations for our single-modulus scenario are as

follows:

$$\frac{d\rho_\sigma}{dt} + 3H\rho_\sigma = -\Gamma_\sigma\,\rho_\sigma\,, \tag{6.43}$$

$$\frac{d\rho_\phi}{dt} + 3H\rho_\phi = -\Gamma_\phi\,\rho_\phi\,, \tag{6.44}$$

$$\frac{d\rho_{\rm DR}}{dt} + 4H\rho_{\rm DR} = \Gamma_{\sigma\to{\rm DR}}\rho_\sigma + \Gamma_{\phi\to{\rm DR}}\rho_\phi\,, \tag{6.45}$$

$$\frac{d\rho_{\rm R}}{dt} + 4H\rho_{\rm R} = \Gamma_{\sigma\to{\rm vis}}\rho_\sigma + \Gamma_{\phi\to{\rm vis}}\rho_\phi\,, \tag{6.46}$$

$$\frac{dn_\chi}{dt} + 3Hn_\chi = {\rm Br}_\chi\Gamma_\sigma\left(\frac{\rho_\sigma}{m_\sigma}\right) + \langle\sigma_{\rm ann}v\rangle\left(n^2_{\chi,{\rm eq}} - n^2_\chi\right), \tag{6.47}$$

where the Hubble rate H is given by the sum of all energy density components, and the various decay rates are given in (6.26), (6.29) and (6.30) using the benchmark values of Tab. 6.1. $\langle\sigma_{\rm ann}v\rangle$ denotes the thermally averaged rate for χ production from/annihilation to the thermal bath with the average energy per χ particle approximated as $\langle E_\chi\rangle \approx \sqrt{m_\chi^2 + 9T_{\rm vis}^2}$ [220]. Here, we take $\langle\sigma_{\rm ann}v\rangle \approx \alpha_\chi^2/m_\chi^2$ with $\alpha_\chi \sim 0.1$. This happens to be the case, for example, for Higgsino and Wino DM [242]. However, because thermal production is subdominant in our scenarios, the exact form of $\langle\sigma_{\rm ann}v\rangle$, including possible temperature dependence, is not really important. For typical DM masses in our scenarios, $m_\chi \sim 10^{10}$-10^{11} GeV, we obtain values of $\langle\sigma_{\rm ann}v\rangle$ in the freeze-in regime. Finally, the DM equilibrium number density, relevant for thermal production, is given by:

$$n_{\chi,{\rm eq}} = \frac{g_\chi}{(2\pi)^3}\int\frac{d^3p}{e^{E(p)/T_{\rm vis}}\pm 1}\,. \tag{6.48}$$

A sample numerical solution of (6.43)-(6.47) is shown in Fig. 6.5. As the evolution proceeds, DM, dark radiation, and ordinary radiation are continually produced by inflaton decay until $H \simeq \Gamma_\sigma$, at which point inflaton decay completes. This begins an era of hidden-radiation domination which lasts until the light modulus ϕ overcomes the energy density of hidden radiation. From here until the time when $H \simeq \Gamma_\phi$, we have a period of EMD driven by the modulus, which is then followed by the standard period of radiation domination once the modulus decay completes.

The DM abundance is set by the inflaton decay at $H \simeq \Gamma_\sigma$ and simply redshifts through the remaining cosmological history. For typical values of the parameters in our scenario, the maximum visible sector temperature established during inflationary reheating is smaller than the DM mass, such that thermal production of DM occurs on the Boltzmann tail of the equilibrium distribution, rendering the thermal contribution irrelevant.[5] Fig. 6.6 shows the visible sector temperature as a function of the scale

[5]Freeze-in production of DM from the visible sector thermal bath is quite sensitive to the DM mass, and can dominate over the branching contribution from inflaton decay if the DM mass is lowered below the range in our scenario.

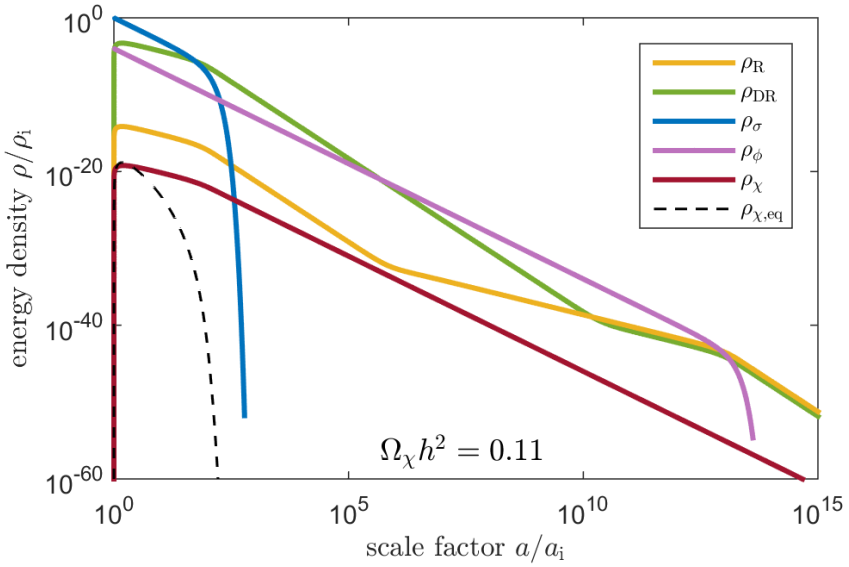

Figure 6.5: Numerical evolution of the system in (6.43)-(6.47). Curves depict the energy densities as functions of scale factor in our scenario. Numerical values of the underlying parameters correspond to the benchmark values given in Tab. 6.1. DM is primarily produced from inflaton decay, with a negligible thermal contribution, establishing the observed relic abundance.

factor for the cosmological history shown in Fig. 6.5, where we have assumed a smooth function for the temperature dependence of the relativistic degrees of freedom in the visible sector.

One comment is in order at this point. Our calculation of freeze-in production of DM in (6.47) assumes instantaneous thermalization of inflaton decay products in the visible sector. In fact, it holds as long as the visible sector reaches thermal equilibrium at a temperature $T > T_f$. However, due to the small number density of inflaton decay products in the visible sector, thermalization may be significantly delayed (for example, see [243, 244]). If $T < T_f$ at the time of thermalization, then thermal production of DM will be completely negligible. Before thermal equilibrium is established, DM production from inflaton decay products is kinematically possible due to their typical mass hierarchy $m_\sigma \gg m_\chi$ [245, 246, 247, 248]. However, by conservation of energy, the number density of these particles is much smaller than what it would be in thermal equilibrium. We have checked that DM production during thermalization is a few orders of magnitude smaller than that from direct inflaton decay, for the parameters shown in Tab. 6.1, even if the visible sector is not thermalized until $H \simeq \Gamma_\sigma$.

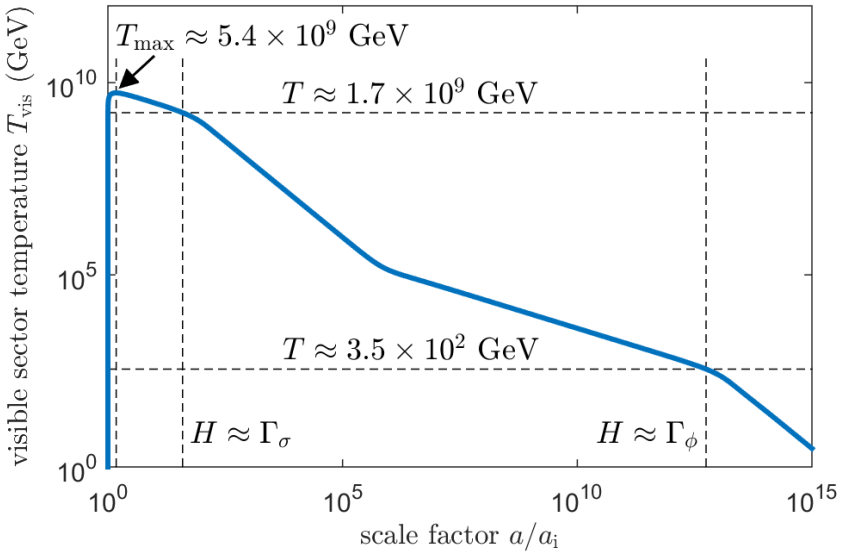

Figure 6.6: Evolution of the visible sector temperature as a function of scale factor in the cosmological history of Fig. 6.5.

6.5 Conclusions

In this chapter we have argued that two generic features of string compactifications, a high supersymmetry breaking scale (which is favored by both statistical arguments [50, 1] and by the requirement of a viable inflationary model building [184]) and the presence of light moduli which drive epochs of EMD [209, 210, 211], lead typically to superheavy WIMP DM with mass around the intermediate scale. This scenario has not received significant attention so far because DM with a mass in the 10^{10}-10^{11} GeV range is inevitably overproduced in a standard thermal history. However, if DM is produced non-thermally from the decay of the inflaton and it is subsequently diluted by the decay of long-lived string moduli which are so light that their decay does not reproduce DM, one can obtain the observed abundance in this so-called branching scenario even for very large DM masses. This does not just account for the non-observation of supersymmetry and WIMPs at colliders, but it may also provide a natural explanation of the origin of ultra-high-energy cosmic rays recently observed by IceCube and ANITA, if DM is unstable and has the right coupling to neutrinos [218].

We illustrated this general picture by presenting two explicit 4D string models which lead to superheavy WIMP DM. The first model is described in Sec. 6.3 and features a single epoch of modulus domination, while App. D.1 gives all the details of a different model with two epochs of EMD driven by two different light moduli. It turns out that in both cases the observed DM abundance can be obtained for a mass around 10^{10}-10^{11} GeV. The main virtue of both models is the possibility to follow their entire cosmological evolution from inflation to the final reheating (due to the decay of the lightest modulus) that establishes a RD universe before the onset of

BBN. This can be achieved by focusing on type IIB LVS string models where the exponentially large volume of the extra dimensions allows to keep control over the 4D low-energy effective field theory. Hence all moduli masses and couplings to both visible and hidden sector degrees of freedom can be computed in detail. Moreover one can build 4D models which can realize inflation, supersymmetry breaking and a chiral MSSM-like visible sector on D-branes (see [104, 105, 106, 75, 144, 107] for explicit Calabi-Yau models with all these features).

We followed the entire cosmological evolution in both models using analytical and numerical tools. This allowed us to combine various constraints coming from both theoretical and phenomenological considerations. Interestingly, we derived the ranges of the microscopic parameters in a regime where geometrical constraints on the underlying extra-dimensional construction are respected, which yield the observed DM abundance as well as the correct value of inflationary observables, namely the amplitude of the density perturbations and the scalar spectral index.

Future investigations could include more formal aspects as well as more phenomenological implications of our findings. From the formal point of view, it would be very interesting to investigate how generic superheavy WIMP DM is from the string landscape point of view, for example comparing this scenario to the case of fuzzy DM [131] which has also been claimed to be a natural outcome of string models due to the ubiquitous presence of ultra-light axions [124, 249, 126, 127]. On the other hand, from the phenomenological side, it is crucial to understand how a superheavy DM could be detected in actual observations, for example establishing in more detail the possible connection of our results with the production of very energetic cosmic rays from DM decay. We leave all these intriguing possibilities for future work.

Part IV

CONCLUSION

Let us conclude by summarizing what we have done in this thesis and highlighting the main results.

- In Sec. 1 of this work we gave a brief introduction to the standard model of particle physics and the standard model of cosmology. We highlighted the tensions of these models such as the cosmological constant problem, the hierarchy problem, the matter/anti-matter asymmetry and the nature of dark matter and dark energy. We finished with a short introduction to concepts beyond the standard models such as string theory, compactification, supersymmetry and inflation in Sec. 2.

- In Sec. 3 we studied the statistical distribution of the supersymmetry breaking scale in the type IIB flux landscape. First, we reviewed the seminal work of [50] in Sec. 3.1.1 and highlighted the importance of Kähler moduli stabilisation in this context. Since Kähler moduli are not stabilised by fluxes at tree-level but rather via higher order corrections, it was believed that their stabilization would only contribute small corrections to the leading order solution coming from the S and U-moduli. However, it turns out that the tree-level superpotential does not dependent on the Kähler moduli. The resulting vacuum is unstable due to a run-away behavior of the volume mode $\mathcal{V}$. A stable solution requires the F-terms of the S and U-moduli to vanish, making the F-terms of the Kähler moduli the object that determines the supersymmetry breaking scale.
  We continued by briefly summarizing 3 different approaches to Kähler moduli stabilisation: KKLT which uses only non-perturbative effects, LVS which combines perturbative and non-perturbative corrections and a stabilisation procedure that uses only perturbative effects.
  In Sec. 3.2 we present the different scaling behaviors of the gravitino mass for the 3 different stabilisation mechanisms. In the case of LVS we find that the distribution of the gravitino mass is given by

$$\rho_{\text{LVS}}(m_{3/2}) \sim \frac{1}{\mathfrak{n} m_{3/2}^2}\left[\ln\left(\frac{M_p}{m_{3/2}}\right)\right]^{-2}. \tag{6.49}$$

  Whereas for KKLT we find

$$\rho_{\text{KKLT}}(m_{3/2}) \sim \frac{1}{M_p^2}\left(\frac{\mathfrak{n}^3|\ln W_0|^3}{g_s}\right) \sim \text{const.}, \tag{6.50}$$

  and for the puerly perturbative case we obtain

$$\rho_{\text{pert}}(m_{3/2}) \sim \frac{1}{M_p^2}\left(\frac{m_{3/2}}{M_p}\right)^{\frac{k-7}{3}}. \tag{6.51}$$

  We see that in LVS the gravitino mass scales logarithmically, whereas in KKLT and in the puerly perturbative case we obtain a power-law scaling. The reason for the different scalings is due to the fact that different no-scale breaking

effects used to fix the Kähler moduli lead to a different dependence of $m_{3/2}$ on the flux-dependent microscopic parameters, whose distribution ultimately governs the statistics of the soft terms.

- In Sec. 4 we continued our investigation of the statistical properties of the flux landscape and focused on axion physics. Here, we focused on the model-independent case of closed string axions originating from the dimensional reduction of C_4. First, we introduced an appropriate model where we chose $h^{1,1} = 4$ and a fibered underlying geometry. We distinguished between two geometric limiting cases, the istoropic limit with the SM located on a local cycle and the anisotropic limit with the SM located on a bulk cycle. Then, we presented a detailed discussion of moduli stabilisation in the LVS setting and derived the axion mass spectrum, decay constants and axion-photon couplings for both limiting cases. In Sec. 4.1.6 we presented an analysis for models with arbitrary values of $h^{1,1}$. In Sec. 4.2 we built upon the results from Sec. 3 and studied the distribution of various axion physics related quantities in the type IIB flux landscape. To this end we expressed the relevant quantities in terms of the underlying flux-dependent parameters and used our knowledge about their distribution. In the isotropic case we found for the decay constants feature a logarithmic scaling of the form

$$N(f_a) \sim \ln\left(\frac{f_a}{M_p}\right), \tag{6.52}$$

$$N(f_{\theta_i}) \sim \ln\left(\frac{f_{\theta_i}}{M_p}\right), \quad i = 1, 2. \tag{6.53}$$

In the anisotropic limit the QCD axion decay constant is fixed around the GUT scale due to the requirement of matching the correct SM gauge coupling. For the ALP θ_2 we found instead

$$N(f_{\theta_2}) \sim \sqrt{\frac{f_{f_{\theta_2}}}{M_{GUT}}}. \tag{6.54}$$

Interestingly, for the ALP decay constant we obtain a power-law distribution which, however, prefers higher scales only mildly, similar to a logarithmic distribution.
In the next section we presented the scaling properties of models with arbitrary $h^{1,1}$. In this case we expect a logarithmic distribution as in the isotropic scenario. However, these distributions hold only at fixed $h^{1,1}$ when moving in the Kähler moduli space by varying microscopic parameters after the decay constants are written in terms of them due to moduli stabilisation.
Finally, we investigated the distribution of the axion mass spectrum in both geometric regimes. Again, we find a logarithmic scaling for the mass spectrum (except for the QCD axion in the anisotropic limit).
We continued our discussion by analysing the distribution of the dark matter

abundance which is assumed to be produced via the standard misalignment mechanism. For natural values of the misalignment angle π we can identify the decay constants which reproduce the observed dark matter abundance. The QCD axion can reproduce the DM abundance for $f_a \simeq 10^{11}$ GeV, while an ALP would require $m_{\theta_i} \simeq 5 \cdot 10^{-21}$ eV for $f_{\theta_i} \simeq 10^{16}$ GeV.
We finisehd this section with a discussion of the axion-photon coupling and the distribution of dark radiation. In the isotropic case the axion-photon couplings featured again a logarithmic distribution. However, when the coupling was volume suppressed or enhanced, the resulting distribution had a positive or negative prefactor, respectively. Therefore, the landscape showed a mild logarithmic preference for smaller couplings when they were volume enhanced and a mild logarithmic preference for larger couplings when they were volume suppressed. In the anisotropic case the coupling of the QCD axion to the visible sector did not exhibit a distribution since it is fixed at $1/M_p$. The ultra-light ALP a_2 turned out to be similar to one of the 2 ALPs in the isotropic case since a_2 couples just to hidden degrees of freedom. The only couplings in the anisotropic case that showed a different behavior were the couplings of the QCD axion to the gauge bosons of the hidden sectors on D_2 and D_3. In this case we found a mild square root scaling.
Finally, we analyzed the distribution of the amount of dark radiation, which we found to be power-law distributed.

- In Sec. 5 we shifted our focus from LVS to KKLT and investigated the distribution of the Gukov-Vafa-Witten superpotential. First, we gave a brief review of perturbatively flat vacua in Sec. 5.1 and discussed the results of [76]. Then, we compared the results with the expectation from standard statistical studies of the landscape in 5.2 and discussed the question how this newly found class of vacua fit in the overall set of solutions. We found that perturbatively flat vacua are statistically sparse when compared to the expectation from the distribution of low values of $|W_0|$ from [50].
  Finally, in Sec. 5.3 we present our algorithm for finding perturbatively flat vacua in Calabi-Yau 3-folds with 2 complex structure moduli and compute an upper bound for the number of perturbatively flat vacua for the model $\mathbb{CP}_{[1,1,2,2,2]}$ for different values of Q_{D3}. For the case of $\mathbb{CP}_{[1,1,1,6,9]}$ we find only one solution which is in agreement with our discussion in Sec. 5.2.
  In Sec. 5.4 we present a general search algorithm. The idea is to isolate the region in the flux vector space which contains all perturbatively flat vacua. Once such a region is obtained, one can carry out numerical searches in this region in order to obtain all solutions.

- In Sec. 6 we presented an application of the considerations from the previous sections. Motivated by the logarithmic preference for higher scale supersymmetry breaking, we discussed the application of a specific type IIB model to inflation and early universe physics.
  In Sec. 6.1 we gave a brief review of the branching scenario for dark matter

production. Then, in Sec. 6.2, we presented a non-standard scenario for the early universe evolution combined with the branching scenario, which together can accommodate superheavy dark matter. In Sec. 6.3 we introduced a specific type IIB model that can realize the previously discussed ideas. Finally, in Sec. 6.4 we studied the introduced model in detail and discussed the resulting cosmological picture. In particular, we computed the number of e-foldings between horizon exit and the end of inflation and combined the result with observational constraints. We combined the resulting expressions with a grid of values for the underlying model parameters and computed for each combination the resulting dark matter mass. Interestingly, the predicted mass range is rather narrow and is for all parameter combinations $m_\chi \simeq 10^{10} - 10^{11}$ GeV. Finally, we performed a numerical evolution of the full set of Boltzmann equations and compared our result with the semi-analytical result.

In this work we discussed the importance of Kähler moduli stabilisation and its importance for a consistent and successful understanding of the statistical properties of the type IIB flux landscape. We observed a predominant preference for logarithmic probability distributions if the stabilisation mechanism is based on the Large Volume Scenario and a power-law distribution in the case of KKLT.
Which behavior is more descriptive of the true nature of the landscape remains an open question since it depends on the ratio of LVS and KKLT vacua. However, since the LVS approach requires less fine-tuning, it enjoys a larger parameter space. One might argue, that the large parameter space is an indication that LVS solutions are more abundant and the majority of phenomenological observables feature a logarithmic distribution in the flux landscape.
This observation implies that the possibility to observe new physics at lower energies is larger than what was believed, since higher energy scales are only mildly prefered. However, given the results we have seen in this thesis, one could also argue that string theory does not make any sharp predictions in the low-energy theory. This is due to the appearance of the logarithmic distribution which is almost flat. However, consistency of the UV theory and the mechanism of moduli stabilisation impose strong correlations among the observables of the effective 4-dimensional theory. Therefore, in order to obtain more definitive predictions from our analysis one should investigate these correlations and identify phenomenologicaly allowed and possibly prohibited ranges in parameter space. For instance, we have seen that a gravitino mass at the TeV-scale correlates with an axion decay constant at the intermediate scale, whereas a gravitino mass at the intermediate scale corresponds to a decay constant at the GUT scale. For a future line of research it would be important to study these correlations in more detail and find correlations related to different ares of physics such as inflation, reheating or the cosmological moduli problem. Combining these correlations with observational constraints would narrow down the range of the allowed parameter space and be a step towards a clear prediction from string theory.

Appendix A

Supersymmetry Statistics

A.1 Distribution of the string coupling

In this appendix we discuss the distribution of g_s in type IIB flux compactifications. This has been studied in [46, 50], and we follow here their analysis to obtain an understanding of the distribution in the region of our interest, i.e. low values of g_s. As in [46, 50], we will carry out a detailed numerical analysis for the simple tractable case of rigid Calabi-Yaus, and use these results to develop intuition for general Calabi-Yaus.

For rigid Calabi-Yaus, the τ modulus ($\tau = a + \frac{i}{g_s}$, where g_s is the dilaton and a its axionic partner), has a linear superpotential:

$$W = A\tau + B\,, \tag{A.1}$$

the 'fluxes' $A = a_1 + ia_2$ and $B = b_1 + ib_2$ take values in $\mathbb{Z} + i\mathbb{Z}$. The tadpole cancellation condition is:

$$\mathrm{Im}(A^* B) = L \equiv \mathrm{Det}(X) = L\,, \tag{A.2}$$

where X is the matrix:

$$X = \begin{pmatrix} a_1 & a_2 \\ b_1 & b_2 \end{pmatrix}. \tag{A.3}$$

The form of the tadpole condition in (A.2) makes it manifest that the tadpole cancellation condition has an $SL(2,\mathbb{Z})$ symmetry, i.e. transformations of the form:

$$X \to X' = MX\,, \tag{A.4}$$

map solutions to solutions, with M $\in SL(2,\mathbb{Z})$. Taking the matrix M to be:

$$M = \begin{pmatrix} p & q \\ r & s \end{pmatrix},$$

the explicit form of the the transformation is given by:

$$\begin{pmatrix} a_1' & a_2' \\ b_1' & b_2' \end{pmatrix} = \begin{pmatrix} p & q \\ r & s \end{pmatrix} \cdot \begin{pmatrix} a_1 & a_2 \\ b_1 & b_2 \end{pmatrix} = \begin{pmatrix} pa_1 + qb_1 & pa_2 + qb_2 \\ ra_1 + sb_1 & ra_2 + sb_2 \end{pmatrix}. \tag{A.5}$$

Now, let us come to the vacua. They are supersymmetric:

$$DW = 0 \leftrightarrow \bar{\tau} = -\frac{B}{A} \implies \tau = \frac{-b_1 + ib_2}{a_1 - ia_2}\,. \tag{A.6}$$

Note that under the above described $SL(2,\mathbb{Z})$ transformation:

$$\tau \to \tau' = \frac{-b_1' + ib_2'}{a_1' - ia_2'} = \frac{s\tau - r}{-q\tau + p}\,. \tag{A.7}$$

This is an $SL(2,\mathbb{Z})$ action on τ associated with the matrix Y given by:[1]

$$Y = \begin{pmatrix} s & -r \\ -q & p \end{pmatrix} \tag{A.8}$$

Therefore, given the $SL(2,\mathbb{Z})$ symmetry of type IIB, the action does not generate physically distinct solutions.[2] In fact, solutions related by this symmetry should be considered as equivalent.

The above described gauge symmetry is crucial to understand the solution space. Firstly, we can use the $SL(2,\mathbb{Z})$ symmetry to set $a_2 = 0$. This implies:

$$\tau = -\frac{b_1}{a_1} + i\frac{b_2}{a_1}\,. \tag{A.9}$$

Also, the tadpole condition reduces to:

$$a_1 b_2 = L\,. \tag{A.10}$$

Requiring $\mathrm{Im}(\tau) > 0$, yields:

$$\frac{b_2}{a_1} > 0 \implies \frac{b_2^2}{a_1 b_2} \implies \frac{b_2^2}{L} \implies L > 0\,. \tag{A.11}$$

Thus, we have the condition $L = a_1 b_2$ with $L > 0$. Hence, a_1 and b_2 have to be integers which divide L with $L > 0$. To see what values b_1 can take, we need to examine the residual $SL(2,\mathbb{Z})$ invariance. The residual $SL(2,\mathbb{Z})$ transformations correspond to transformations which maintain the condition $a_2 = 0$, from (A.5) we see that this implies that $q = 0$. Thus the $SL(2,\mathbb{Z})$ matrix must take the form:

$$\begin{pmatrix} 1 & 0 \\ r & 1 \end{pmatrix} \tag{A.12}$$

[1]The fact that Y is an element of $SL(2,\mathbb{Z})$ follows from the fact that its determinant is the same as the one of M.

[2]There is another $SL(2,\mathbb{Z})$ symmetry of the equation (A.2). This involves taking $X \to X.N$, where N is an $SL(2,\mathbb{Z})$ matrix. It is easy to see that such transformations do not correspond to $SL(2,\mathbb{Z})$ transformations of τ. In this case, $a_i \to a_l N_{lk}$ and $b_j \to b_l N_{lj}$. Thus we can start with a point with $a_1, b_1 \neq 0$ and $a_2, b_2 = 0$ (i.e. τ on the real axis) and map it to a point where $a_1, a_2, b_1, b_2 \neq 0$. Thus a point on the real line can get mapped to a point in the interior of the upper half plane. Thus, this does not correspond to an $SL(2,\mathbb{Z})$ transformation of τ. Hence, this cannot be thought of as a 'gauge' transformation.

where r is an integer.[3] Now the action of an $SL(2,\mathbb{Z})$ matrix of the form (A.12) takes b_1 to:

$$b_1 \to r a_1 + b_1 \,. \tag{A.13}$$

This implies that b_1 takes the values $0, 1, ...|a_1 - 1|$. In summary, the analysis of [46, 50] implies that vacua are characterised by:

1. An integer a_1 which divides L.
2. For every such integer b_1 takes the values $0, 1, ...|a_1 - 1|$.
3. $b_2 = \frac{L}{a_1}$
4. The value of τ is given by:

$$\tau = -\frac{b_1}{a_1} + i\frac{b_2}{a_1} \tag{A.14}$$

To get the distribution in the fundamental domain one takes the value of τ obtained from (A.14) and maps it to the fundamental domain of $SL(2,\mathbb{Z})$. This involves the repeated action of the generators:

$$T : \tau \to \tau + 1, \qquad S : \tau \to -\frac{1}{\tau} \,. \tag{A.15}$$

The algorithm to bring a general point which is outside the fundamental domain to inside the fundamental domain is as follows: First, by repeated action of T (or T^{-1}) the point is brought to the region $-\frac{1}{2} \leq Re(\tau) < \frac{1}{2}$. If this process also brings the point to inside the fundamental domain, then the algorithm terminates. Otherwise, one acts with the generator S. If this does not bring the point inside the fundamental domain one iterates the process of repeated action of T (or T^{-1}) and a single action of S (if needed) until the point is mapped to the fundamental domain.

Now, let us come to our discussion of the distribution of g_s. Note that the characterisation of inequivalent solutions implies that the values of imaginary part of τ as obtained in (A.14) are bounded by:

$$\frac{1}{L} \leq \mathrm{Im}(\tau) \leq \mathrm{L} \,. \tag{A.16}$$

It is easy to check that this condition is preserved by the algorithm to bring the points inside the fundamental domain. Thus the lowest value of g_s is $\frac{1}{L}$. We have carried out detailed numerical studies to probe the distribution for small values of g_s (in the region of phenomenological interest). First, we present the results of our numerics for $L = 100$. The distribution of τ in the fundamental domain is shown in Fig. A.1 and the distribution of g_s is shown in Fig. A.2. The results are consistent with that of [50].

[3] Note that $\begin{pmatrix} 1 & 0 \\ r & 1 \end{pmatrix} \equiv \begin{pmatrix} -1 & 0 \\ -r & -1 \end{pmatrix}$ Hence we do not have to mod out by matrices of the form in the RHS of the equivalence.

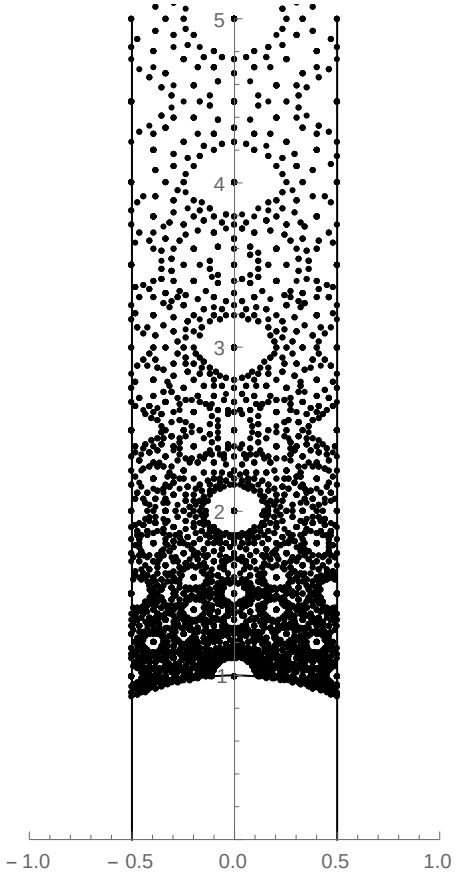

Figure A.1: Values of τ for $L = 100$.

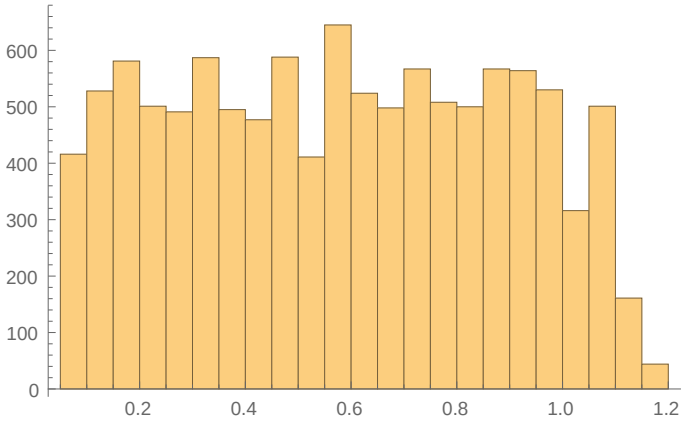

Figure A.2: Distribution of g_s for $L = 100$.

The plot in Fig. A.2 shows that the distribution is roughly uniform for $g_s > 0.01$. Next we present our results for $L = 500$. The distribution of the number of vacua as a function of g_s is shown in Fig. A.3 and A.4. Again for $g_s > 0.002$, the distribution is uniform. We studied the cases with $L = 150, 400$ and obtained similar results. Our results clearly indicate that for rigid Calabi-Yaus, $\rho(g_s)$ is uniform in the region of interest in Sec. 3.2.

From our numerics, we observe that the basic reason for the uniform distribution is the following: As L is increased, generically the number of its divisors increases and as a result the number of points given by (A.14) increases. The first step in the algorithm to bring the points given by (A.14) to the fundamental domain is to act on them repeatedly by T (or T^{-1}) so as to bring them to the strip $\frac{1}{2} \leq \tau < \frac{1}{2}$. For large L, we find that even just after this first step the region of phenomenological interest is uniformly populated with the number of points of the same order as the final answer (i.e the number of points after all points are brought to the fundamental domain). Note that in (A.14):

$$\text{Im}(\tau) = \frac{L}{a_1^2}\,,$$

where a_1 divides L. Thus, for the points given by (A.14), the number of points with $\text{Im}(\tau) > 1$ is equal to the number of points with $\text{Im}(\tau) < 1$. This is essentially the reason why after the first step in the algorithm the number of points is of the same order as in the final answer. For large L, with the increase in the number of divisors, there are more and more points in the region of interest and the spacing between them becomes uniform.

Now, let us turn to the case of general Calabi-Yaus. The exact characterisation of the vacua (the analogue of equation (A.14)) is not available, and a complete numerical analysis remains challenging[4] and is beyond the scope of the present work. Here, we will use our results for the case of rigid Calabi-Yaus to develop intuition for the distribution of g_s in case of general Calabi-Yaus (the basic philosophy shall be the same as that advocated in [44]). As described in the previous paragraph, the basic reason for the uniform distribution in the case of rigid Calabi-Yaus is that with increase in L, generically the number of vacua increases and the solutions are more and more uniformly spaced. This leads to the uniform distribution of g_s. For general Calabi-Yaus, the value of the dilaton is set by the ratio of flux quanta associated with the 3-form fluxes H_3 and F_3. As the number of 3-cycles increases, one can expect the same phenomenon – the number of vacua increases and the spacing between the values of the dilaton in these solutions decreases and the distribution function for the dilaton becomes uniform. Note that we found a uniform distribution in the case of rigid Calabi-Yaus, where the number of fluxes is only four. For a general Calabi-Yau with large number of cycles, the solutions are certainly expected to be more uniformly spaced, corresponding to a uniform distribution of the dilaton.

[4]For recent progress in this direction see e.g [77, 78]

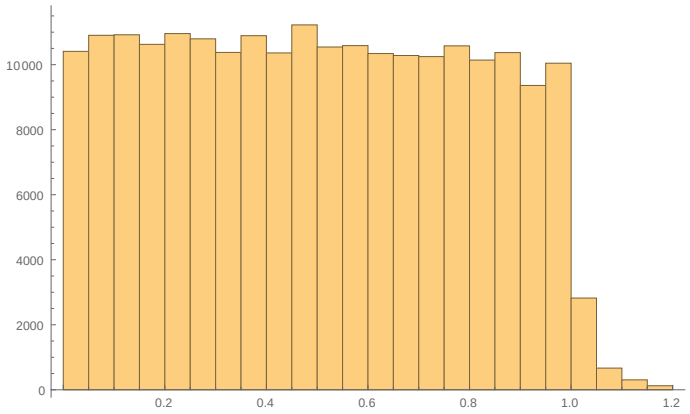

Figure A.3: Distribution of g_s for $L = 500$.

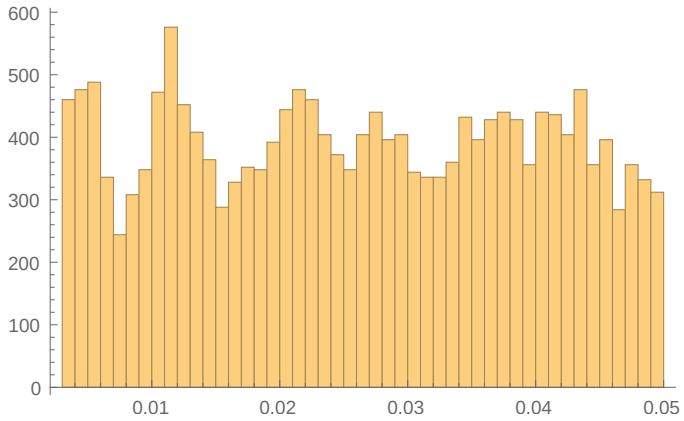

Figure A.4: Distribution for small g_s with L=500.

A.2 Soft terms in LVS and KKLT

In this section we briefly summarise the structure of the soft masses in KKLT and LVS with matter fields located on D3/D7 branes. The general expressions for the soft masses are given by:

$$M_a = \frac{1}{2}\frac{F^i \partial_i f_a}{Re(f_a)} \tag{A.17}$$

$$m_\alpha^2 = m_{3/2}^2 + V_0 - F^{\bar{i}} F^j \partial_{\bar{i}} \partial_j \ln(\tilde{K}_\alpha) \tag{A.18}$$

$$A_{\alpha\beta\gamma} = F^i \left(K_i + \partial_i \ln(Y_{\alpha\beta\gamma}) - \partial_i \ln(\tilde{K}_\alpha \tilde{K}_\beta \tilde{K}_\gamma) \right), \tag{A.19}$$

where $Y_{\alpha\beta\gamma}$ are the Yukawa couplings, $\tilde{K}_\alpha$ is the Kähler matter metric and the F-terms are given by $F^i = e^{K/2} K^{i\bar{j}} D_{\bar{j}} \bar{W}$. In the following table we summarise the soft supersymmetry breaking terms in both KKLT and LVS for matter living on D3 and D7 branes [87].

In the last table we collect the soft masses that come from anomaly mediation. Note that anomaly mediation plays no rôle in LVS but is important in KKLT. Let us compute the variation of the soft masses. In the case of KKLT the variation of

D3	KKLT	LVS
$M_{1/2}$	$\frac{3}{2}\frac{1}{a\mathcal{V}^{2/3}}m_{3/2}$	$\frac{3}{4}\frac{\xi}{g_s^{3/2}\mathcal{V}}m_{3/2}$
m_0^2	$(1-3\omega)\,m_{3/2}^2$	$\frac{5}{8}\frac{\xi}{g_s^{3/2}\mathcal{V}}m_{3/2}^2$
$A_{\alpha\beta\gamma}$	$-(1-s\partial_s\log(Y_{\alpha\beta\gamma}))\,\frac{3}{2}\frac{1}{a\mathcal{V}^{2/3}}m_{3/2}$	$-(1-s\partial_s\log(Y_{\alpha\beta\gamma}))\,\frac{3}{4}\frac{\xi}{g_s^{3/2}\mathcal{V}}m_{3/2}$

D7	KKLT	LVS
$M_{1/2}$	$\frac{1}{a\mathcal{V}^{2/3}}m_{3/2}$	$m_{3/2}$
m_α^2	$(1-3\omega)\,m_{3/2}^2$	$\frac{1}{3}m_{3/2}^2$
$A_{\alpha\beta\gamma}$	$-\frac{3}{2}s\partial_s\log(Y_{\alpha\beta\gamma})\,\frac{1}{a\mathcal{V}^{2/3}}m_{3/2}$	$-m_{3/2}$

Anomaly	KKLT	LVS
M_a	$-\frac{g_a^2 b_a}{16\pi^2}m_{3/2}$	$-\frac{g_a^2 b_a}{16\pi^2}M_{1/2}$
m_i^2	$\sum_a \frac{g_a^4 C_a(i) b_a}{(16\pi^2)^2}m_{3/2}^2$	$\sum_a \frac{g_a^4 C_a(i) b_a}{(16\pi^2)^2}m_0^2$
$A_{\alpha\beta\gamma}$	$Y_{\alpha\beta\gamma}\sum_{m=\alpha,\beta,\gamma}\sum_a \frac{C_a(m)}{b_a}M_a$	$Y_{\alpha\beta\gamma}\sum_{m=\alpha,\beta,\gamma}\sum_a \frac{g_a^2 C_a(m)}{16\pi^2}A_{\alpha\beta\gamma}$

Table A.1: Soft masses for KKLT/LVS with standard model fields realized on D3/D7 branes. Here g_a is the gauge coupling, the parameter b_a is defined as $b_a = 3T_G - T_R$, with the Casimir invariant T_G in the adjoint representation, the Dynkin index T_R and the quadratic Casimir invariants in the fundamental representation $C_a(i)$. The parameter ω is a function of the coefficients of the Kähler matter metrics.

the gaugino mass scales as:

$$dM_{1/2} \sim \left(\frac{g_a^2 b_a}{16\pi^2}\right)^2 \frac{g_s}{\mathfrak{n}^3|\ln W_0|^3}\frac{M_p^2}{M_{1/2}}dN\,, \tag{A.20}$$

which implies a scaling for the number of states:

$$N_{KKLT}(M_{1/2}) \sim \left(\frac{M_{1/2}}{M_p}\right)^2\,. \tag{A.21}$$

This functional dependence holds for all soft masses for D3 and D7 branes. In LVS the gaugino mass at the minimum of the potential scales as:

$$M_{1/2} = \frac{3}{4}\sqrt{8\pi}\frac{c_1^2}{|W_0|\mathfrak{n}^2}e^{-\frac{2c_2}{g_s\mathfrak{n}}}\,. \tag{A.22}$$

Performing the variation gives us:

$$dM_{1/2} \sim \mathfrak{n}M_{1/2}\ln\left(\frac{M_p}{M_{1/2}}\right)^2 dN\,. \tag{A.23}$$

Ignoring subleading logarithmic corrections, this implies a scaling:

$$N_{LVS}(M_{1/2}) \sim \ln\left(\frac{M_{1/2}}{M_p}\right), \tag{A.24}$$

which is again true for all soft masses for D3 and D7 branes. In summary our conclusion for the distribution of the soft terms in KKLT and LVS vacua is:

$$\boxed{N_{KKLT} \sim \left(\frac{M_{\rm soft}}{M_p}\right)^2} \tag{A.25}$$

and:

$$\boxed{N_{LVS} \sim \ln\left(\frac{M_{\rm soft}}{M_p}\right)}\,. \tag{A.26}$$

Appendix B

Axion Statistics

B.1 Canonical normalisation

In this appendix we shall perform the canonical normalisation of the axion fields.

B.1.1 A single axion

Let us start with the simple case with a single closed string modulus $T = \tau + \mathrm{i}\theta$ where it is easy to identify the correct definition of the axion decay constant and periodicity. We start with the following Lagrangian:

$$\mathcal{L} = K_{T\bar{T}}\partial_\mu\theta\partial^\mu\theta - \frac{1}{4}\mathrm{Re}(f)\, F_b^{\mu\nu}F^b_{\mu\nu} - \frac{1}{4}\mathrm{Im}(f)\, F_b^{\mu\nu}\tilde{F}^b_{\mu\nu} + \Lambda^4\cos\left(\frac{2\pi}{\mathfrak{n}}\theta\right), \tag{B.1}$$

where b is a non-Abelian index and the gauge kinetic function is given by $f = T/(2\pi)$. Expressing $\mathcal{L}$ in terms of the canonically normalised axion $a = \sqrt{2K_{T\bar{T}}}\,\theta$ and Yang-Mills field strength $G^b_{\mu\nu} = \sqrt{\mathrm{Re}(f)}\, F^{\mu\nu}_b$, we end up with:

$$\mathcal{L} = \frac{1}{2}\partial_\mu a\partial^\mu a - \frac{1}{4}G_b^{\mu\nu}G^b_{\mu\nu} - \frac{\alpha_b}{4}\frac{a}{\sqrt{2K_{T\bar{T}}}}\, G_b^{\mu\nu}\tilde{G}^b_{\mu\nu} + \Lambda^4\cos\left(\frac{2\pi}{\mathfrak{n}}\frac{a}{\sqrt{2K_{T\bar{T}}}}\right), \tag{B.2}$$

where we used the fact that $\tau = \alpha_b^{-1}$. This expression suggests the definition of the axion decay constant f_a as (inserting the appropriate power of M_p):

$$f_a \equiv \left(\frac{\mathfrak{n}}{2\pi}\right)\sqrt{2K_{T\bar{T}}}\, M_p\,, \tag{B.3}$$

since $\mathcal{L}$ would simplify to the standard expression:

$$\mathcal{L} = \frac{1}{2}\partial_\mu a\partial^\mu a - \frac{1}{4}G_b^{\mu\nu}G^b_{\mu\nu} - \frac{a}{f_a}\frac{\mathfrak{n}\alpha_b}{8\pi}\, G_b^{\mu\nu}\tilde{G}^b_{\mu\nu} + \Lambda^4\cos\left(\frac{a}{f_a}\right). \tag{B.4}$$

B.1.2 A more general case with 3 axions

Without loss of generality we shall consider the volume form (4.3) with $\tau_4 = 0$. The Kähler metric and its inverse take the following form at leading order in a large-$\mathcal{V}$

expansion:

$$\mathcal{K} = \begin{pmatrix} \frac{1}{4\tau_1^2} & \frac{\gamma_3}{4}\frac{\tau_3^{3/2}}{\tau_1^{3/2}\tau_2^2} & -\frac{3\gamma_3}{8}\frac{\sqrt{\tau_3}}{\tau_1^{3/2}\tau_2} \\ \frac{\gamma_3}{4}\frac{\tau_3^{3/2}}{\tau_1^{3/2}\tau_2^2} & \frac{1}{2\tau_2^2} & -\frac{3\gamma_3}{4}\frac{\sqrt{\tau_3}}{\sqrt{\tau_1}\tau_2^2} \\ -\frac{3\gamma_3}{8}\frac{\sqrt{\tau_3}}{\tau_1^{3/2}\tau_2} & -\frac{3\gamma_3}{4}\frac{\sqrt{\tau_3}}{\sqrt{\tau_1}\tau_2^2} & \frac{3\gamma_3}{8}\frac{1}{\sqrt{\tau_3\tau_1}\tau_2} \end{pmatrix}, \tag{B.5}$$

and:

$$\mathcal{K}^{-1} = \begin{pmatrix} 4\tau_1^2 & 4\gamma_3\sqrt{\tau_1}\tau_3^{3/2} & 4\tau_1\tau_3 \\ 4\gamma_3\sqrt{\tau_1}\tau_3^{3/2} & 2\tau_2^2 & 4\tau_2\tau_3 \\ 4\tau_1\tau_3 & 4\tau_2\tau_3 & \frac{8}{3\gamma_3}\sqrt{\tau_3\tau_1}\tau_2 \end{pmatrix}. \tag{B.6}$$

Let us now consider the isotropic and anisotropic limits separately.

Isotropic limit

In the isotropic limit θ_1 and θ_2 are essentially massless while θ_3 develops a potential via QCD instantons of the form $V(\theta_3) = -\Lambda_{QCD}^4 \cos(2\pi\theta_3)$. Hence the only non-zero entry of the axionic Hessian is $V_{33} = (2\pi)^2\Lambda_{QCD}^4$. Multiplying the inverse Kähler metric (B.6) by the axionic Hessian we find the mass-squared matrix $\mathcal{M}^2 = \frac{1}{2}\mathcal{K}^{-1}V_{ij}$ which becomes:

$$\mathcal{M}^2 = \begin{pmatrix} 0 & 0 & 2\tau_1\tau_3 \\ 0 & 0 & 2\tau_2\tau_3 \\ 0 & 0 & \frac{4}{3\gamma_3}\sqrt{\tau_3\tau_1}\tau_2 \end{pmatrix} (2\pi)^2\Lambda_{QCD}^4 . \tag{B.7}$$

The eigenvalues of $\mathcal{M}^2$ are (reinstating appropriate powers of M_p):

$$m_1^2 = 0\,, \qquad m_2^2 = 0\,, \qquad m_3^2 = \frac{4}{3\gamma_3}\sqrt{\tau_3\tau_1}\tau_2(2\pi)^2\frac{\Lambda_{QCD}^4}{M_p^2}\,, \tag{B.8}$$

and the corresponding eigenvectors read:

$$\vec{v}_1 = \begin{pmatrix} 1 \\ 0 \\ 0 \end{pmatrix} \frac{\mathfrak{n}_1}{2\pi}\frac{M_p}{f_1}\,, \qquad \vec{v}_2 = \begin{pmatrix} 0 \\ 1 \\ 0 \end{pmatrix} \frac{\mathfrak{n}_2}{2\pi}\frac{M_p}{f_2}\,, \qquad \vec{v}_3 = \begin{pmatrix} \frac{3\gamma_3}{2}\frac{\sqrt{\tau_3\tau_1}}{\tau_2} \\ \frac{3\gamma_3}{2}\sqrt{\frac{\tau_3}{\tau_1}} \\ 1 \end{pmatrix} \frac{M_p}{2\pi f_3}\,, \tag{B.9}$$

where f_1, f_2 and f_3 are the axion decay constants which can be obtained by requiring $\vec{v}_i^{\,T}\mathcal{K}\vec{v}_j = \frac{1}{2}\delta_{ij}$. We find (at leading order in a large-$\mathcal{V}$ approximation):

$$f_1 = \frac{\mathfrak{n}_1}{2\pi}\frac{M_p}{\sqrt{2}\tau_1}\,, \qquad f_2 = \frac{\mathfrak{n}_2}{2\pi}\frac{M_p}{\tau_2}\,, \qquad f_3 = \frac{\sqrt{3\alpha\gamma_3}}{4\pi}\frac{M_p}{\tau_3^{1/4}\sqrt{\mathcal{V}}}\,. \tag{B.10}$$

Therefore the QCD axion mass in (B.8) can correctly be written also as $m_3 = \Lambda_{QCD}^2/f_3$. Moreover the original axions θ_i's can be expressed in terms of the canonically

normalised axions a_i's as:

$$\begin{aligned}\theta_1 &= \frac{\mathfrak{n}_1}{2\pi}\frac{a_1}{f_1} + \frac{3\gamma_3}{4\pi}\frac{\sqrt{\tau_3\tau_1}}{\tau_2}\frac{a_3}{f_3}\,,\\ \theta_2 &= \frac{\mathfrak{n}_2}{2\pi}\frac{a_2}{f_2} + \frac{3\gamma_3}{4\pi}\sqrt{\frac{\tau_3}{\tau_1}}\frac{a_3}{f_3}\,,\\ \theta_3 &= \frac{1}{2\pi}\frac{a_3}{f_3}\,.\end{aligned} \tag{B.11}$$

Anisotropic limit

In the anisotropic limit θ_3 develops a potential via non-perturbative corrections to W, θ_2 is essentially massless while θ_1 becomes massive via QCD instantons. Hence the axionic Hessian at the minimum takes the form:

$$V_{ij} = \begin{pmatrix} (2\pi)^2\Lambda_{QCD}^4 & 0 & 0\\ 0 & 0 & 0\\ 0 & 0 & 3\alpha\mathfrak{a}_3^2\tau_3^{3/2}\frac{W_0^2}{\mathcal{V}^3}\end{pmatrix}. \tag{B.12}$$

Thus the mass-squared matrix $\mathcal{M}^2 = \frac{1}{2}\mathcal{K}^{-1}V_{ij}$ now becomes:

$$\mathcal{M}^2 = \begin{pmatrix} 8\pi^2\tau_1^2\Lambda_{QCD}^4 & 0 & 6\alpha\mathfrak{a}_3^2\tau_1\tau_3^{5/2}\frac{W_0^2}{\mathcal{V}^3}\\ 8\gamma_3\pi^2\sqrt{\tau_1}\tau_3^{3/2}\Lambda_{QCD}^4 & 0 & 6\mathfrak{a}_3^2\tau_3^{5/2}\tau_1^{-1/2}\frac{W_0^2}{\mathcal{V}^2}\\ 8\pi^2\tau_1\tau_3\Lambda_{QCD}^4 & 0 & 4\mathfrak{a}_3^2\gamma_3^{-1}\tau_3^2\frac{W_0^2}{\mathcal{V}^2}\end{pmatrix}. \tag{B.13}$$

The leading order expressions of the eigenvalues of $\mathcal{M}^2$ are (inserting suitable powers of M_p):

$$m_1^2 = 8\pi^2\tau_1^2\frac{\Lambda_{QCD}^4}{M_p^2}\,,\qquad m_2^2 = 0\,,\qquad m_3^2 = \frac{4\mathfrak{a}_3^2\tau_3^2}{\gamma_3}\left(\frac{W_0}{\mathcal{V}}\right)^2 M_p^2\,, \tag{B.14}$$

and the corresponding eigenvectors read:

$$\vec{v}_1 = \begin{pmatrix} 1\\ -\frac{\gamma_3}{2}\left(\frac{\tau_3}{\tau_1}\right)^{3/2}\\ -\frac{\gamma_3\mathfrak{n}_3^2}{2}\frac{\tau_1}{\tau_3}\frac{\mathcal{V}^2}{W_0^2}\Lambda_{QCD}^4\end{pmatrix}\frac{\mathfrak{n}_1}{2\pi}\frac{M_p}{f_1}\,,\qquad \vec{v}_2 = \begin{pmatrix}0\\1\\0\end{pmatrix}\frac{\mathfrak{n}_2}{2\pi}\frac{M_p}{f_2}\,,\qquad \vec{v}_3 = \begin{pmatrix}\frac{3\alpha\gamma_3}{2}\frac{\sqrt{\tau_3}\tau_1}{\mathcal{V}}\\ \frac{3\gamma_3}{2}\sqrt{\frac{\tau_3}{\tau_1}}\\ 1\end{pmatrix}\frac{\mathfrak{n}_3}{2\pi}\frac{M_p}{f_3}\,, \tag{B.15}$$

where f_1, f_2 and f_3 are the axion decay constants which can be obtained by requiring $\vec{v}_i^{\,T}\mathcal{K}\vec{v}_j = \frac{1}{2}\delta_{ij}$. We obtain (at leading order in a large-$\mathcal{V}$ approximation):

$$f_1 = \frac{1}{2\sqrt{2}\pi}\frac{M_p}{\tau_1}\,,\qquad f_2 = \frac{\mathfrak{n}_2}{2\pi}\frac{M_p}{\tau_2}\,,\qquad f_3 = \frac{\mathfrak{n}_3\sqrt{3\alpha\gamma_3}}{4\pi}\frac{M_p}{\tau_3^{1/4}\sqrt{\mathcal{V}}}\,. \tag{B.16}$$

Therefore the QCD axion mass in (B.14) can correctly be written also as $m_1 = \Lambda_{QCD}^2/f_1$. Moreover the original axions θ_i's can be expressed in terms of the canonically

normalised axions a_i's as:

$$\begin{aligned}
\theta_1 &= \frac{1}{2\pi}\frac{a_1}{f_1} + \frac{3\alpha\mathfrak{n}_3\gamma_3}{4\pi}\frac{\sqrt{\tau_3}\tau_1}{\mathcal{V}}\frac{a_3}{f_3}\,, \\
\theta_2 &= -\frac{\gamma_3}{4\pi}\left(\frac{\tau_3}{\tau_1}\right)^{3/2}\frac{a_1}{f_1} + \frac{\mathfrak{n}_2}{2\pi}\frac{a_2}{f_2} + \frac{3\mathfrak{n}_3\gamma_3}{4\pi}\sqrt{\frac{\tau_3}{\tau_1}}\frac{a_3}{f_3}\,, \\
\theta_3 &= -\frac{1}{2\pi}\frac{\tau_3}{\tau_1}\left(\frac{m_1}{m_3}\right)^2\frac{a_1}{f_1} + \frac{\mathfrak{n}_3}{2\pi}\frac{a_3}{f_3}\,.
\end{aligned} \tag{B.17}$$

B.2 Benchmark points for ALP dark matter

In this appendix we present some benchmark points for ALP DM generated by the misalignment mechanism. In this case the DM relic abundance is given by (4.73). We focus on the bulk axion θ_2 which behaves as an ultra-light ALP for both the isotropic and the anisotropic case. Its mass and decay constant can be written in terms of the underlying parameters as:

$$m_{\theta_2} = \sqrt{\frac{1}{2}\mathcal{K}_{22}^{-1}V_{\theta_2\theta_2}} = \frac{4\pi}{\alpha\mathfrak{n}_2^{3/2}}\sqrt{g_sA_2W_0}\sqrt{\frac{\tau_2}{\tau_1}}\,e^{-\frac{\pi}{\mathfrak{n}_2}\tau_2}\,M_p\,, \qquad f_{\theta_2} = \frac{\mathfrak{n}_2}{2\pi}\frac{M_p}{\tau_2}\,. \tag{B.18}$$

In the isotropic case $\tau_1 = \tau_2$, while in the anisotropic limit $\tau_1 = g_s^2\,\tau_2 = \alpha_{SM}^{-1}$. After writing τ_1 in terms of τ_2, τ_2 can in turn be expressed as a function of the microscopic parameters using (4.8) with $\mathcal{V} \simeq \alpha\sqrt{\tau_1}\tau_2$. The expression (4.73) for the ALP DM abundance becomes then just a function of 9 UV parameters: g_s, W_0, $\mathfrak{n}_2$, $\mathfrak{n}_4$, A_2, A_4, α, ξ and $\theta_{2,\text{in}}$. In what follows we shall restrict our numerical search for benchmark examples to a 4D subregion of this parameter space by focusing on natural values $A_2 = A_4 = 1$ and $\theta_{2,\text{in}} = \pi$. Moreover we shall set the topological quantities $\alpha = 1/6$ and $\xi = 0.46$ as in the explicit toric constructions of [143]. In Tables B.1 and B.2 we present some benchmark points which reproduce the observed DM abundance for different values of W_0, g_s, $\mathfrak{n}_2$ and $\mathfrak{n}_4$, for the isotropic and anisotropic cases respectively.

$\mathfrak{n}_2$	$\mathfrak{n}_4$	g_s	W_0	τ_2	m_{θ_2} (eV)	f_{θ_2} (GeV)
1	1	0.250	$2.05 \cdot 10^{-11}$	32.39	$2.62 \cdot 10^{-21}$	$1.18 \cdot 10^{16}$
1	1	0.100	$4.46 \cdot 10^{-32}$	24.97	$1.02 \cdot 10^{-21}$	$1.53 \cdot 10^{16}$
1	1	0.075	$1.58 \cdot 10^{-43}$	20.97	$4.79 \cdot 10^{-22}$	$1.82 \cdot 10^{16}$
1	10	0.250	3.66	36.36	$4.29 \cdot 10^{-21}$	$1.05 \cdot 10^{16}$
1	10	0.100	$2.08 \cdot 10^{-2}$	35.42	$3.87 \cdot 10^{-21}$	$1.08 \cdot 10^{16}$
1	10	0.075	$1.32 \cdot 10^{-3}$	34.96	$3.61 \cdot 10^{-21}$	$1.09 \cdot 10^{16}$
10	1	0.250	$6.32 \cdot 10^{-10}$	318.47	$2.54 \cdot 10^{-21}$	$1.20 \cdot 10^{16}$
10	1	0.100	$1.37 \cdot 10^{-30}$	244.35	$9.70 \cdot 10^{-22}$	$1.56 \cdot 10^{16}$
10	1	0.075	$4.81 \cdot 10^{-42}$	204.47	$4.35 \cdot 10^{-22}$	$1.87 \cdot 10^{16}$
10	10	0.250	113.2	358.27	$4.00 \cdot 10^{-21}$	$1.07 \cdot 10^{16}$
10	10	0.100	0.643	348.90	$3.62 \cdot 10^{-21}$	$1.09 \cdot 10^{16}$
10	10	0.075	$4.07 \cdot 10^{-2}$	344.27	$3.37 \cdot 10^{-21}$	$1.11 \cdot 10^{16}$

Table B.1: Benchmark points which match the observed ALP DM abundance for the isotropic case setting $A_2 = A_4 = 1$, $\theta_{\text{in},2} = \pi$, $\alpha = 1/6$ and $\xi = 0.46$.

$\mathfrak{n}_2$	$\mathfrak{n}_4$	g_s	W_0	τ_2	m_{θ_2} (eV)	f_{θ_2} (GeV)
1	1	0.833	0.108	36.03	$4.53 \cdot 10^{-21}$	$1.06 \cdot 10^{16}$
1	10	0.822	48.93	37.00	$4.61 \cdot 10^{-21}$	$1.03 \cdot 10^{16}$
6	1	0.352	$1.11 \cdot 10^{-6}$	201.66	$3.06 \cdot 10^{-21}$	$1.14 \cdot 10^{16}$
6	10	0.339	47.88	217.80	$4.36 \cdot 10^{-21}$	$1.05 \cdot 10^{16}$
10	1	0.277	$4.05 \cdot 10^{-9}$	325.35	$2.82 \cdot 10^{-21}$	$1.17 \cdot 10^{16}$
10	10	0.263	36.15	360.61	$4.22 \cdot 10^{-21}$	$1.06 \cdot 10^{16}$
30	1	0.168	$1.06 \cdot 10^{-16}$	883.67	$1.79 \cdot 10^{-21}$	$1.30 \cdot 10^{16}$
30	10	0.153	9.75	1063.23	$3.88 \cdot 10^{-21}$	$1.08 \cdot 10^{16}$

Table B.2: Benchmark points which match the observed ALP DM abundance for the anisotropic case setting $A_2 = A_4 = 1$, $\theta_{\text{in},2} = \pi$, $\alpha = 1/6$ and $\xi = 0.46$. All benchmark points satisfy the phenomenological constraint $\tau_1 = \alpha_{SM}^{-1} = 25$.

Notice that in both cases the typical values of the mass and the decay constant are respectively $m_{\theta_2} \simeq 5 \cdot 10^{-21}$ eV and $f_{\theta_2} \simeq 10^{16}$ GeV. In the isotropic case we have chosen $\mathfrak{n}_2$, $\mathfrak{n}_4$ and g_s freely (focusing on values of g_s which keep perturbation theory under control) and we have derived the value of W_0 which matches the observed DM abundance. Notice that natural $\mathcal{O}$(1-10) values of W_0 require $\mathfrak{n}_4 \gtrsim 10$ since from (4.8) $\tau_2 \sim W_0^{2/3}\, e^{k/\mathfrak{n}_4}$ for an appropriate k, and so $\mathfrak{n}_4 \sim \mathcal{O}(1)$ would give a value of τ_2 which is too large to match $\Omega_{ALP} h^2 \simeq 0.112$ due to the exponential suppression $m_{\theta_2} \sim e^{-\frac{\pi}{\mathfrak{n}_2}\tau_2}\, M_p$ in (B.18). This relation explains also why larger values of τ_2 correspond to larger values of $\mathfrak{n}_2$. Let us finally stress that in the anisotropic case we have chosen freely only $\mathfrak{n}_2$ and $\mathfrak{n}_4$ since g_s is fixed by the phenomenological constraint $\tau_1 = g_s^2\, \tau_2 = \alpha_{SM}^{-1} = 25$. As can be seen from Table B.2, this condition tends to push the string coupling close to 1 unless $\mathfrak{n}_2 \gtrsim 10$ since $g_s^2 \tau_2 = 25$ can be satisfied for $g_s \simeq 0.1$ only for large values of τ_2 which, as we have already pointed out, need large values of $\mathfrak{n}_2$.

B.3 Other distributions relevant for phenomenology

In this appendix we shall show that other phenomenologically interesting quantities feature also a logarithmic distribution in the type IIB flux landscape.

B.3.1 Moduli masses

Let us investigate the distribution of moduli masses in the flux landscape. For all cases, the isotropic and anisotropic cases with $h^{1,1} = 4$ and the model with arbitrarily large $h^{1,1}$, the mass of each Kähler modulus scales with the CY volume as:

$$m_{\tau_i} \simeq \frac{W_0}{\mathcal{V}^{p_i}} M_p \qquad \text{with} \quad p_i > 0 \quad \forall i = 1, ..., h^{1,1}. \tag{B.19}$$

Following the same logic as in Sec. 4.2, we find again a logarithmic distribution for each m_{τ_i} since these masses are controlled by the exponentially large volume $\mathcal{V}$:

$$N(m_{\tau_i}) \sim \ln\left(\frac{m_{\tau_i}}{M_p}\right), \qquad \forall i = 1, ..., h^{1,1}. \tag{B.20}$$

For the anisotropic case one has just to make sure that the bound $g_s \gtrsim 0.01$ (coming from the ability to tune W_0 to satisfy (4.41)) does not set a lower bound on m_{τ_i} for the regime of validity of the distribution (B.20). However this bound is negligible since combining (4.8) with (4.41) one would find $m_{3/2} \gtrsim 10^{-45}\, M_p \simeq 10^{-16}$ eV for $g_s \gtrsim 0.01$.

B.3.2 Reheating temperature

Using the moduli masses we can study the distribution of the reheating temperature coming from moduli decay [158, 236]. The reheating temperature due to the perturbative decay of the i-th Kähler modulus is given by [158]:

$$T_{\text{rh},i} = \left(\frac{40 c_{\text{vis}} c_{\text{tot}}}{\pi^2 g_*(T_{\text{rh}})}\right)^{1/4} \sqrt{\Gamma_{\tau_i} M_p}\,, \tag{B.21}$$

where c_{vis} and c_{vis} control the strength the interaction of the modulus τ_i with the visible and the hidden sector respectively, $c_{\text{tot}} = c_{\text{vis}} + c_{\text{hid}}$, and the decay rate Γ_{τ_i} looks like:

$$\Gamma_{\tau_i} = \frac{1}{48\pi} \frac{m_{\tau_i}^3}{M_p^2}\,. \tag{B.22}$$

Thus using (B.20) we obtain again a logarithmic distribution for all cases:

$$T_{\text{rh},i} \sim m_{\tau_i} \sqrt{\frac{m_{\tau_i}}{M_p}} \quad \Rightarrow \quad \frac{dT_{\text{rh},i}}{T_{\text{rh},i}} \sim \frac{dm_{\tau_i}}{m_{\tau_i}} \quad \Rightarrow \quad N(T_{\text{rh}}) \sim \ln\left(\frac{T_{\text{rh}}}{M_p}\right). \tag{B.23}$$

Appendix C

Superpotential Statistics

C.1 2-moduli examples data

As discussed in Sec. 5.4, our numerical analysis has shown that in 22 of the 39 2-moduli examples in the Kreuzer-Skarke list, $|\epsilon|_{\text{inf}}$ does not take values close to zero. This by itself gives a strong bound on the region where all possible solutions to the Lemma are contained (without the need of imposing requirements such as validity of the effective field theory or phenomenological viability). We list these models in Tab. C.1 together with the associated values of $|\epsilon|_{\text{inf}}$ and the values of $\vec{m}$ and $\vec{k}$ at which the infimum is attained.

Model	$\vec{m}^T$	$\vec{k}^T$	$\lvert\epsilon\rvert_{\text{inf}}$
$M_{2,2}$	$(-0.186, 0.982)$	$(-0.399, 0.917)$	0.9751
$M_{2,3}$	$(-0.966, 0.257)$	$(-0.746, 0.666)$	0.8919
$M_{2,4}$	$(-0.966, 0.257)$	$(-0.746, 0.666)$	0.8919
$M_{2,5}$	$(-0.966, 0.257)$	$(-0.746, 0.666)$	0.8919
$M_{2,7}$	$(-0.967., 0.253)$	$(-0.778, 0.628)$	0.9114
$M_{2,13}$	$(-0.143, 0.989)$	$(-0.297, 0.955)$	0.9870
$M_{2,18}$	$(-0.132, 0.991)$	$(-0.272, 0.962)$	0.9897
$M_{2,19}$	$(-0.186, 0.982)$	$(-0.399, 0.917)$	0.9750
$M_{2,21}$	$(0.966, -0.257)$	$(0.746, -0.666)$	0.8919
$M_{2,22}$	$(-0.896, 0.438)$	$(-0.695, 0.709)$	0.9336
$M_{2,23}$	$(-0.896, 0.438)$	$(-0.695, 0.709)$	0.9336
$M_{2,24}$	$(-0.896, 0.438)$	$(-0.695, 0.709)$	0.9336
$M_{2,25}$	$(-0.186, 0.982)$	$(-0.399, 0.917)$	0.9752
$M_{2,26}$	$(-0.969, 0.243)$	$(-0.816, 0.577)$	0.9321
$M_{2,27}$	$(-0.969, 0.247)$	$(-0.599, 0.801)$	0.7784
$M_{2,28}$	$(-0.969, 0.247)$	$(-0.599, 0.801)$	0.7784
$M_{2,29}$	$(-0.969, 0.247)$	$(-0.599, 0.801)$	0.7784
$M_{2,35}$	$(-0.993, 0.114)$	$(-0.972, 0.233)$	0.9927
$M_{2,36}$	$(-0.186, 0.982)$	$(-0.399, 0.917)$	0.9752
$M_{2,37}$	$(-0.186, 0.982)$	$(-0.399, 0.917)$	0.9752
$M_{2,38}$	$(-0.186, 0.982)$	$(-0.399, 0.917)$	0.9752
$M_{2,39}$	$(-0.970, 0.243)$	$(-0.577, 0.817)$	0.7581

Table C.1: 22 2-moduli examples from the Kreuzer-Skarke list in which $\lvert\epsilon\rvert_{\text{inf}}$ does not take values close to zero. For each model, we show the associated values of $\lvert\epsilon\rvert_{\text{inf}}$ and the values of $\vec{m}$ and $\vec{k}$ at which the infimum is attained.

Appendix D

Superheavy Dark Matter

D.1 Superheavy DM in a scenario with two moduli

String compactifications are in general characterized by a large number of moduli and by a leading order no-scale structure that makes some of them (in general more than one) lighter than expected, i.e. $m_\phi \ll m_{3/2}$ [61]. Hence one might expect to have several epochs of modulus domination in the post-inflationary history. One could have either multiple eras of EMD separated by intermediate phases of RD (if there is a hierarchy among the initial displacements of the moduli), or a single extended EMD epoch (if the initial displacements of all moduli are of the same order). In what follows we shall investigate the features of this general scenario by focusing on the illustrative example with two light moduli.

D.2 Branching scenario with two epochs of EMD

Let us present a branching scenario that involves two moduli ϕ_1 and ϕ_2. The two moduli have masses m_{ϕ_1} and m_{ϕ_2} with $m_{\phi_2} \lesssim m_{\phi_1}$. They mainly decay to the visible sector with respective couplings $c_1/M_{\rm P}$ and $c_2/M_{\rm P}$, leading to decay widths $\Gamma_{\phi_1\to\rm vis} \simeq c_1^2 m_{\phi_1}^3/M_{\rm P}^2$ and $\Gamma_{\phi_2\to\rm vis} \simeq c_2^2 m_{\phi_2}^3/M_{\rm P}^2$ (we assume that their decays to hidden sector particles are suppressed and produce just a small amount of DR). Assuming that $m_{\phi_1} < m_\chi$, the decay of ϕ_1 and ϕ_2 to DM will be kinematically forbidden. Therefore their decay only dilutes the abundance of DM and DR produced from the inflaton decay. The initial displacements of ϕ_1 and ϕ_2 from the minimum of their potential are $\phi_{1,0}$ and $\phi_{2,0}$ respectively. We assume $\phi_{1,0} \gtrsim \phi_{2,0}$ so that each modulus can dominate the energy density of the universe for a period of time.

The important stages of the post-inflationary history in this scenario (in chronological order) are as follows:

1- $\Gamma_\sigma \lesssim H < H_{\rm inf}$: The universe is in an EMD phase driven by inflaton oscillations about the minimum of its potential. Both moduli also start oscillating at this stage with respective energy densities $\rho_{\phi_1} = (\phi_{1,0}/M_{\rm P})^2\rho_\sigma$ and $\rho_{\phi_2} = (\phi_{2,0}/M_{\rm P})^2\rho_\sigma$. The

inflaton decay completes at $H \simeq \Gamma_\sigma$ mainly populating the hidden sector.

2- $H_{\rm D,1} \lesssim H < \Gamma_\sigma$: The universe is in a RD phase at this stage. Moduli oscillations behave like matter, and hence $\rho_{\phi_{1,2}}$ redshifted more slowly than $\rho_{\rm R}$. Since $\rho_{\phi_1} > \rho_{\phi_2}$, ϕ_1 starts to dominate at $H_{\rm D,1} \simeq (\phi_{1,0}/M_{\rm P})^4 \Gamma_\sigma$, which is the onset of a second phase of EMD.

3- $\Gamma_{\phi_1} \lesssim H < H_{\rm D,1}$: The universe is in an EMD epoch that is driven by ϕ_1 during this stage. Decay of ϕ_1 completes when the Hubble expansion rate is $H \simeq \Gamma_{\phi_1}$ (Γ_{ϕ_1} denotes the total decay rate of ϕ_1) and reheats the visible sector. This leads to the formation of a RD universe.

4- $H_{\rm D,2} \lesssim H < \Gamma_{\phi_1}$: The universe is in an intermediate RD phase during this stage. Since ρ_{ϕ_2} is redshifted more slowly than $\rho_{\rm R}$, ϕ_2 starts to dominate when the Hubble expansion rate is $H_{\rm D,2} \simeq (\phi_{2,0}/\phi_{1,0})^4 \Gamma_{\phi_1}$, which is the onset of another epoch of EMD.

5- $\Gamma_{\phi_2} \lesssim H < H_{\rm D,2}$: The universe is in a third phase of EMD that is driven by ϕ_2. The decay of ϕ_2 completes when the Hubble expansion rate is $H \simeq \Gamma_{\phi_2}$ (Γ_{ϕ_2} is the total decay rate of ϕ_2), at which time the universe enters the final RD phase prior to the onset of BBN.

One point to note is that $H_{\rm D,2} \simeq \Gamma_{\phi_1}$ if $\phi_{2,0} \simeq \phi_{1,0}$. In this case, ϕ_2 dominates the energy density of the universe as soon as the decay of ϕ_1 completes. Stage 4 above thus effectively disappears and there is a direct transition from the first EMD era (stage 3) to the second one (stage 5), implying a single extended epoch of EMD driven by the two moduli ϕ_1 and ϕ_2.[1]

Let us now estimate the relic abundance of DM in this scenario. The number density of DM particles at $H \simeq \Gamma_{\phi_2}$ is given by:

$$n_\chi \simeq n_\sigma \, {\rm Br}_\chi \left(\frac{a_\sigma}{a_{\rm D,1}}\right)^3 \left(\frac{a_{\rm D,1}}{a_{\phi_1}}\right)^3 \left(\frac{a_{\phi_1}}{a_{\rm D,2}}\right)^3 \left(\frac{a_{\rm D,2}}{a_{\phi_2}}\right)^3 . \tag{D.1}$$

This is similar to (6.5) for the case with a single epoch of modulus domination. The last two terms on the RHS, which are new, account for the dilution of the number density in stages 4 and 5 above respectively. After using the scaling of a with time in stages 4 and 5 above, and normalizing n_χ by the entropy density s at $H \simeq \Gamma_{\phi_2}$, we find:

$$\frac{n_\chi}{s} \simeq \frac{3}{4} \times 10^{-3} \, \frac{1}{Y_{\phi_2}^2} \, \frac{\Gamma_{\sigma\to{\rm vis}}}{\Gamma_\sigma} \, \frac{\Gamma_{\phi_2}}{\Gamma_{\phi_2\to{\rm vis}}} \, \frac{T_{\rm R,2}}{m_\sigma} , \tag{D.2}$$

where:

$$T_{\rm R,2} = \left(\frac{90}{\pi^2 g_{*,{\rm R},2}} \, \frac{\Gamma_{\phi_2\to{\rm vis}}}{\Gamma_{\phi_2}}\right)^{1/4} \sqrt{\Gamma_{\phi_2} M_{\rm P}} , \tag{D.3}$$

with $g_{*,{\rm R},2}$ denoting the number of relativistic degrees of freedom in the visible sector at $T = T_{\rm R,2}$, and $Y_{\phi_2} \equiv \phi_{2,0}/M_{\rm P}$. The energy density of DR at $H \simeq \Gamma_{\phi_2}$ is given by

[1] This is an example of the two-field EMD scenario studied in [250].

(assuming that no DR is produced from ϕ_1 decay):

$$\begin{aligned}\rho_{\rm DR} &\simeq \rho_\sigma \frac{\Gamma_{\sigma\to{\rm DR}}}{\Gamma_\sigma}\left(\frac{a_\sigma}{a_{\rm D,1}}\right)^4\left(\frac{a_{\rm D,1}}{a_{\phi_1}}\right)^4\left(\frac{a_{\phi_1}}{a_{\rm D,2}}\right)^4\left(\frac{a_{\rm D,2}}{a_{\phi_2}}\right)^4 \\ &+ \rho_{\phi_2}\frac{\Gamma_{\phi_2\to{\rm DR}}}{\Gamma_{\phi_2}}. \end{aligned} \tag{D.4}$$

This is similar to (6.9) with two additional terms on the RHS that account for the energy density redshift in stages 4 and 5 respectively. Thus the fractional energy density of DR is given by:

$$\frac{\rho_{\rm DR}}{\rho_{\rm R}} \simeq \frac{1}{Y_{\phi_2}^{8/3}}\left(\frac{\Gamma_{\phi_2}}{\Gamma_\sigma}\right)^{2/3}\frac{\Gamma_{\sigma\to{\rm DR}}}{\Gamma_\sigma}\frac{\Gamma_{\phi_2}}{\Gamma_{\phi_2\to{\rm vis}}} + \frac{\Gamma_{\phi_2\to{\rm DR}}}{\Gamma_{\phi_2\to{\rm vis}}}\,. \tag{D.5}$$

Some comments are in order at this point. It is seen from (D.2) and (D.5) that final abundance of DM and DR in the two modulus scenario depends only on the initial amplitude and decay width of the second modulus ϕ_2. This can be understood as follows. For fixed Y_{ϕ_2}, varying $Y_{\phi_1} \equiv \phi_{1,0}/M_{\rm P}$ (as long as $Y_{\phi_1} \gtrsim Y_{\phi_2}$) affects the two epochs of modulus domination in opposite ways. Increasing (decreasing) Y_{ϕ_1} makes stage 4 longer (shorter) and stage 3 shorter (longer) by the same factor. A similar thing happens by decreasing (increasing) Γ_{ϕ_1} with Γ_{ϕ_2} fixed (as long as $\Gamma_{\phi_1} \gtrsim \Gamma_{\phi_2}$). As a result, the combined dilution factor from two epochs of modulus domination does not depend on the parameters of ϕ_1.

That said, it is helpful to compare the DM and DR abundance with the previous scenario when there is one epoch of modulus domination. We can rewrite (D.2) in terms of (6.7) as follows (in the limit where the production of DR from the decay of the lightest modulus is completely negligible):

$$\left.\frac{n_\chi}{s}\right|_2 = \left.\frac{n_\chi}{s}\right|_1 \left(\frac{Y_{\phi_1}}{Y_{\phi_2}}\right)^2 \left(\frac{T_{\rm R,2}}{T_{\rm R,1}}\right)\,. \tag{D.6}$$

Similarly, (D.5) can be written in terms of (6.10):

$$\left.\frac{\rho_{\rm DR}}{\rho_{\rm R}}\right|_2 = \left.\frac{\rho_{\rm DR}}{\rho_{\rm R}}\right|_1 \left(\frac{Y_{\phi_1}}{Y_{\phi_2}}\right)^{4/3}\left(\frac{\Gamma_{\phi_2}}{\Gamma_{\phi_1}}\right)^{2/3}\,. \tag{D.7}$$

It is seen from (D.6) and (D.7) that the maximum dilution in the scenario with two moduli is achieved for $Y_{\phi_2} \simeq Y_{\phi_1}$ and $m_{\phi_2} \ll m_{\phi_1}$.[2] As pointed out earlier, in this case there is a single extended epoch of EMD consisting of stages 3 and 5 that are not separated by an intermediate RD phase.

[2]Note that $T_{\rm R,2}/T_{\rm R,1} \propto (\Gamma_{\phi_2}/\Gamma_{\phi_1})^{1/2} \propto (m_{\phi_2}/m_{\phi_1})^{3/2}$.

D.3 A string model with two epochs of modulus domination

D.3.1 The setup

We now focus on a type IIB model which can allow for two epochs of modulus domination. This model shares the same features with the model discussed in Sec. 6.3 but it also gives rise to novel phenomenological properties. The Calabi-Yau volume now takes the form:

$$\mathcal{V} = \sqrt{\tau_{\rm vis}}\tau_{\rm big} - \tau_{\rm np}^{3/2} - \tau_{\rm inf}^{3/2} \,, \tag{D.8}$$

where again $\tau_{\rm inf}$ drives inflation and it is wrapped by a hidden sector D7 stack as in the model presented in Sec. 6.3. However now the second blow-up mode, here denoted as $\tau_{\rm np}$, is just responsible for generating non-perturbative effects needed for moduli stabilization but it does not support the visible sector stack of D7 branes.[3] In fact, in this model the requirement to avoid dark radiation overproduction from the decay of the lightest modulus forces the visible D7 stack to be wrapped around the 4-cycle whose volume is controlled by $\tau_{\rm vis}$ [158].

In this case the 4D low-energy supergravity theory is determined by the following Kähler potential:

$$K = -2\ln\left(\mathcal{V} + \frac{\xi}{2g_s^{3/2}}\right) + K_{g_s} \,, \tag{D.9}$$

where K_{g_s} denotes string loop corrections [99, 36, 37] which have been shown to be $\mathcal{V}$-suppressed with respect to the leading α' correction proportional to ξ [232]. The superpotential instead looks like:

$$W = W_0 + A_{\rm np}\, e^{-a_{\rm np}T_{\rm np}} + A_{\rm inf}\, e^{-a_{\rm inf}T_{\rm inf}} \,. \tag{D.10}$$

As in Sec. 6.3, at leading order in $1/\mathcal{V} \ll 1$, non-perturbative corrections to W combined with α' corrections to K produce an LVS minimum with 5 stabilized moduli: $\mathcal{V} \simeq \sqrt{\tau_{\rm vis}}\tau_{\rm big} \sim e^{1/g_s}$, $\tau_{\rm np} \sim \tau_{\rm inf} \sim 1/g_s \sim \mathcal{O}(10)$ together with the 2 corresponding axions $c_{\rm np}$ and $c_{\rm inf}$. However at this level of approximation there are still 3 flat directions which can be parameterized by $\tau_{\rm vis}$, $c_{\rm vis}$, and $c_{\rm big}$. The visible sector modulus $\tau_{\rm vis}$ is fixed at subleading order by the string loop contribution to the Kähler potential K_{g_s} at [142]:

$$\tau_{\rm vis} \simeq g_s^{4/3}\, \lambda_{\rm loop}\, \mathcal{V}^{2/3} \,, \tag{D.11}$$

where $\lambda_{\rm loop}$ is a tunable combination of the coefficients of g_s corrections to K. Notice that the requirement of reproducing the observed value of the visible sector gauge coupling, $\alpha_{\rm vis}^{-1} = 4\pi g_{\rm vis}^{-2} = \tau_{\rm vis} \sim \mathcal{O}(10-100)$, leads necessarily to an anisotropic

[3] $\tau_{\rm np}$ instead supports a pure SYM hidden sector which generates gaugino condensation at a scale larger than the inflaton mass, so that the decay of σ into heavy condensates on $\tau_{\rm np}$ is kinematically forbidden.

shape of the extra dimensions since the exponentially large Calabi-Yau volume $\mathcal{V} \simeq \sqrt{\tau_{\rm vis}}\tau_{\rm big}$ is now controlled by 2 cycles but with $\tau_{\rm big} \sim e^{1/g_s} \gg \tau_{\rm vis} \sim 1/g_s$. Finally, the two axions $c_{\rm vis}$ and $c_{\rm big}$ receive tiny masses due to additional $T_{\rm vis}$- and $T_{\rm big}$-dependent non-perturbative corrections to W. Thus both $c_{\rm vis}$ and $c_{\rm big}$ are in general ultra-light and play the role of hidden sector dark radiation.

D.3.2 Moduli mass spectrum

The mass spectrum of the relevant moduli around the minimum becomes:

$$\begin{aligned} m_\sigma^2 &\simeq \kappa\,\epsilon^2\,(\ln\epsilon)^2\;M_{\rm P}^2 \\ m_{\phi_1}^2 &\simeq \frac{\epsilon\, m_\sigma^2}{g_s^{3/2} W_0\,|\,(\ln\epsilon)^3\,|} \ll m_\sigma^2 \quad \text{for} \quad \epsilon \ll 1 \\ m_{\phi_2}^2 &\simeq \frac{\epsilon^{1/3}\, g_s^{5/6} |\ln\epsilon|\, m_{\phi_1}^2}{W_0^{1/3}\sqrt{\lambda_{\rm loop}}} < m_{\phi_1}^2 \quad \text{for} \quad \epsilon, g_s \ll 1 \\ m_{a_{\rm DR_1}}^2 &\sim m_{a_{\rm DR_2}}^2 \sim 0\,, \end{aligned} \tag{D.12}$$

where σ, ϕ_1, ϕ_2, $a_{\rm DR_1}$, and $a_{\rm DR_1}$ are the canonically normalized fields corresponding respectively to $\tau_{\rm inf}$, $\tau_{\rm big}$, $\tau_{\rm vis}$, $c_{\rm big}$, and $c_{\rm vis}$.

As in Sec. 6.3, σ plays the role of the inflaton. This field, when displaced from its minimum, becomes exponentially lighter than the Hubble constant during inflation which is set by the mass of ϕ_1: $H \simeq m_{\phi_1}$. The 3 fields $\tau_{\rm np}$, $c_{\rm inf}$, and $c_{\rm np}$ are instead heavy spectator fields, while ϕ_1 and ϕ_2 get displaced from their minimum during inflation, and so give rise to 2 epochs of EMD. On the other hand, the 2 ultra-light axions $a_{\rm DR_1}$ and $a_{\rm DR_2}$ yield extra contributions to $N_{\rm eff}$. Moreover the gravitino mass and the soft terms are still given by (6.22). Hence for $m_\chi \simeq m_0 \simeq M_{1/2}$, we conclude that DM cannot be reproduced from the decay of any of the 2 light moduli since:

$$m_{\phi_2}^2 < m_{\phi_1}^2 \simeq \frac{\epsilon\,|\ln\epsilon|}{g_s^{3/2} W_0}\, m_\chi^2 \ll m_\chi^2 \quad \text{for} \quad \epsilon \ll 1\,. \tag{D.13}$$

Requiring $m_{\phi_2} \gtrsim \mathcal{O}(50)$ TeV in order to avoid any cosmological moduli problem together with $\tau_{\rm vis} \sim \mathcal{O}(100)$ in order to reproduce the observed value of the visible sector gauge coupling, corresponds to $1 \ll \mathcal{V} \lesssim 5\times 10^7 - 10^9$ for $g_s \simeq 0.1$ and $1 \lesssim W_0 \lesssim 100$. Therefore DM is necessarily superheavy since $m_\chi \gtrsim 10^{11}$ GeV. Notice that values of the overall volume below $5\times 10^7 - 10^9$ are also required to match inflationary observables like the amplitude of primordial fluctuations [231].

D.3.3 Moduli couplings and decay rates

The configuration of the hidden sector D7-stack wrapped around $\tau_{\rm inf}$ is the same as the one described in Sec. 6.3.3. Moreover, also the couplings of the inflaton σ to hidden and visible gauge bosons are still given by (6.25). Hence the ratio $\Gamma_{\sigma\to\rm vis}/\Gamma_\sigma$ is also still given by (6.26) and the inflaton decay width Γ_σ takes the same form as (6.30).

On the other hand the light modulus ϕ_1 decays mainly into visible sector gauge bosons with decay rate [236, 158]:

$$\Gamma_{\phi_1} \simeq \Gamma_{\phi_1 \to \text{vis}} = \gamma^2 \frac{N_g}{96\pi} \frac{m_{\phi_1}^3}{M_{\text{P}}^2} = \frac{\gamma^2}{8\pi} \frac{m_{\phi_1}^3}{M_{\text{P}}^2} \quad \text{for} \quad N_g = 12\,, \tag{D.14}$$

where $\gamma \geq 1$ is a microscopic parameter which depends on the gauge flux on the visible sector D7-stack (in particular $\gamma = 1$ for a fluxless D7-stack while $\gamma > 1$ for non-zero gauge fluxes) [158]. The decay of ϕ_1 produces also axionic dark radiation which is however suppressed for $\gamma > 1$ and gets diluted by the decay of ϕ_2. In what follows we shall therefore neglect $\Gamma_{\phi_1 \to \text{DR}}$.

The final modulus to decay is ϕ_2 whose main decay channels are [158]:

- Dark radiation bulk axions:

$$\Gamma_{\phi_2 \to \text{DR}} = \frac{5}{96\pi} \frac{m_{\phi_2}^3}{M_{\text{P}}^2}\,, \tag{D.15}$$

- Visible sector gauge bosons:

$$\Gamma_{\phi_2 \to \text{vis}} = \gamma^2 \frac{N_g}{48\pi} \frac{m_{\phi_2}^3}{M_{\text{P}}^2} = \frac{\gamma^2}{4\pi} \frac{m_{\phi_2}^3}{M_{\text{P}}^2}\,, \tag{D.16}$$

  where we have set again $N_g = 12$.

The amount of axionic dark radiation produced from ϕ_2 decay is controlled by the underlying parameter γ:

$$\Delta N_{\text{eff}} \simeq 3\, \frac{\Gamma_{\phi_2 \to \text{DR}}}{\Gamma_{\phi_2 \to \text{vis}}} \simeq \frac{0.6}{\gamma^2}\,, \tag{D.17}$$

showing how for $\gamma \geq 1$ this model naturally satisfies present observational bounds since it yields $\Delta N_{\text{eff}} \lesssim 0.6$.

The relevant quantities to compute the final DM abundance using (D.2) and (D.3) can be derived from the decay widths (D.15) and (D.16) and read:

$$\frac{\Gamma_{\phi_2}}{\Gamma_{\phi_2 \to \text{vis}}} = 1 + \frac{5}{24\gamma^2}\,, \tag{D.18}$$

and:

$$T_{\text{R},2} \simeq 0.16\gamma \left(1 + \frac{5}{24\gamma^2}\right)^{1/4} m_{\phi_2} \sqrt{\frac{m_{\phi_2}}{M_{\text{P}}}}\,. \tag{D.19}$$

Notice that the decay rates (D.15) and (D.16), together with the inflaton decay width (6.30), also determine, via (D.5), the fractional energy density of DR.

D.4 Inflationary observables and DM abundance

As in Sec. 6.4, we start analyzing the cosmology of the model with two moduli by presenting the expression for the total number of e-foldings:

$$N_{\rm e} \simeq 57 + \frac{1}{4}\left[\ln r - N_{\rm reh} - N_{\phi_1} - N_{\phi_2} + \ln\left(\frac{\rho_{\sigma,\rm start}}{\rho_{\sigma,\rm end}}\right)\right],$$

where $N_{\rm reh}$ is the duration of the reheating epoch after the end of inflation, while N_{ϕ_1} and N_{ϕ_2} denote respectively the number of e-foldings of the two EMD eras driven by the light moduli ϕ_1 and ϕ_2, which look like:

$$N_{\phi_1} \simeq \frac{2}{3}\ln\left(Y_{\phi_1}^4\frac{\Gamma_\sigma}{\Gamma_{\phi_1}}\right) \quad , \quad N_{\phi_2} \simeq \frac{2}{3}\ln\left(\left(\frac{Y_{\phi_2}}{Y_{\phi_1}}\right)^4\frac{\Gamma_{\phi_1}}{\Gamma_{\phi_2}}\right).$$

By rewriting $N_{\rm e}$ in terms of fundamental parameters, we obtain:

$$N_{\rm e} \simeq 58.88 - \frac{1}{6}\ln\left(\frac{Y_{\phi_2}^4\mathcal{V}^8}{W_0^5 g_s^{3/2}\left|\ln\epsilon\right|^{3/2}}\right), \tag{D.20}$$

where we have set $\gamma = 1$. Notice that the total number of e-foldings does not depend on the initial misalignment value of the first modulus.

As in the single modulus scenario, we obtain W_0 as a function of $\mathcal{V}$ by combining two constraints coming from the amplitude of the primordial scalar fluctuations and the geometrical requirement to have the volume of blow-up modes hierarchically smaller than the overall internal volume. Following the same procedure as in Sec. 6.4, we then extract the value of $\mathcal{V}$ from matching the observed DM abundance. Finally, this value of the volume fixes the DM mass for every combination of the underlying parameters. Interestingly, all data points correspond to a DM mass in the same range as in the single modulus case, $m_\chi \simeq 10^{10}$-10^{11}GeV, with a bias towards smaller values (65% of the data points result in $m_\chi \simeq 10^{10}$GeV).

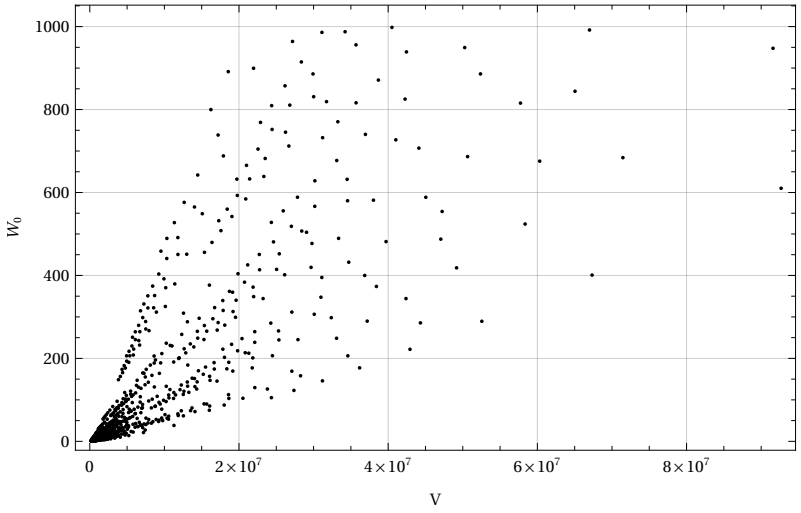

Figure D.1: Points in the $(W_0, \mathcal{V})$ plane which match the observed amplitude of the density perturbations and DM abundance.

In Fig. D.1 we present the points in the $(W_0,\ \mathcal{V})$ plane which satisfy all our theoretical and phenomenological conditions. Note that 65% of the initial parameter set reproduces the correct DM abundance. Moreover we were not able to obtain values of $n_{\rm s}$ within the 2σ range, as each point in Fig. D.1 corresponds to $n_{\rm s}$ at the lower end of the 3σ range. The qualitative behavior of the underlying parameters g_s, Y_{ϕ_2}, and λ is the same as in the single modulus case. Tab. D.1 shows a representative choice of the parameters used to perform a numerical study of the full cosmological evolution in this scenario.

W_0	20.4
$\mathcal{V}$	3×10^6
$N_{\rm e}$	44.4
$N_{\rm reh}$	4.4
N_{ϕ_1}	14.8
N_{ϕ_2}	3.9
$n_{\rm s}$	0.9550
m_σ	1.1×10^{13}GeV
m_{ϕ_1}	7.7×10^{8}GeV
m_{ϕ_2}	8.3×10^{7}GeV
$m_{3/2}$	8.9×10^{11}GeV
m_χ	7.3×10^{10}GeV
$c_{\rm hid}$	332.0

Table D.1: Microscopic parameters W_0 and $\mathcal{V}$, the resulting e-folding numbers, $n_{\rm s}$, mass scales, and inflaton coupling to hidden degrees of freedom $c_{\rm hid}$ at a benchmark point that gives the right amplitude of the density perturbations and the correct DM abundance. The input parameters are $g_s = 0.1$, $Y_{\phi_1} = Y_{\phi_2} = 0.01$, $\lambda = 10^3$, $N_g^{\rm hid} = 12$, and $\gamma = 1$.

D.5 Numerical analysis of cosmological evolution

We obtain the numerical evolution of energy densities for the scenario with two moduli. As in Sec. 6.4.2, we begin the evolution at $H \simeq H_{\rm inf}$ with both σ and ϕ_1 oscillating. Though ϕ_2 begins oscillating shortly after this time, its energy density is subdominant and its initial evolution can be approximated as a matter component without altering the overall evolution. The other energy density components are again highly suppressed initially. The Boltzmann equations for this scenario are (neglecting the tiny production of DR from the decay of ϕ_1):

$$\frac{d\rho_\sigma}{dt} + 3H\rho_\sigma = -\Gamma_\sigma\,\rho_\sigma\,, \tag{D.21}$$

$$\frac{d\rho_{\phi_1}}{dt} + 3H\rho_{\phi_1} = -\Gamma_{\phi_1}\,\rho_{\phi_1}\,, \tag{D.22}$$

$$\frac{d\rho_{\phi_2}}{dt} + 3H\rho_{\phi_2} = -\Gamma_{\phi_2}\,\rho_{\phi_2}\,, \tag{D.23}$$

$$\frac{d\rho_{\rm DR}}{dt} + 4H\rho_{\rm DR} = \Gamma_{\sigma\to{\rm DR}}\rho_\sigma + \Gamma_{\phi_2\to{\rm DR}}\rho_{\phi_2}\,, \tag{D.24}$$

$$\frac{d\rho_{\rm R}}{dt} + 4H\rho_{\rm R} = \Gamma_{\sigma\to{\rm vis}}\rho_\sigma + \Gamma_{\phi_1\to{\rm vis}}\rho_{\phi_1} + \Gamma_{\phi_2\to{\rm vis}}\rho_{\phi_2}\,, \tag{D.25}$$

$$\frac{dn_\chi}{dt} + 3Hn_\chi = {\rm Br}_\chi\Gamma_\sigma\left(\frac{\rho_\sigma}{m_\sigma}\right) + \langle\sigma_{\rm ann}v\rangle\left(n_{\chi,{\rm eq}}^2 - n_\chi^2\right)\,. \tag{D.26}$$

A sample numerical solution is shown in Fig. D.2 for the becnhmark point in Tab.

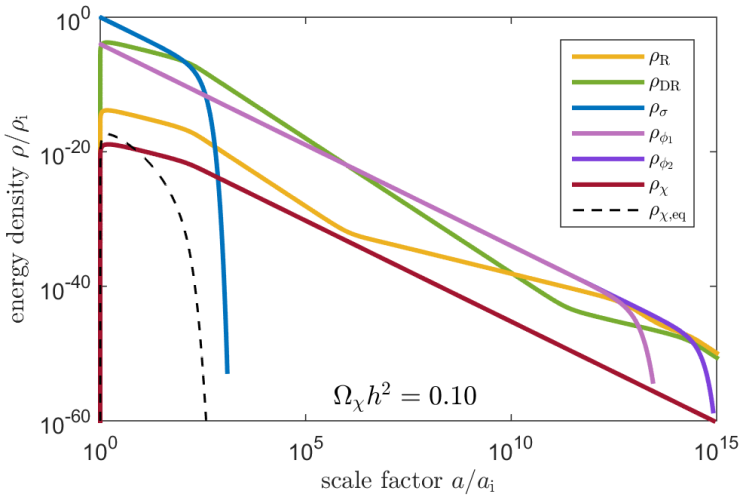

Figure D.2: Energy density evolution of the various components as functions of scale factor in the two-moduli scenario for the benchmark point in Tab. D.1.

D.1. The cosmological evolution is very similar to the one-modulus case. The effect of the second, lighter, modulus is to extend the EMD period to lower temperatures. Because the two moduli start with equal misalignments, we have a single extended period of EMD with a brief period of substantial radiation while the lighter modulus dominates, instead of two EMD periods separated by a RD phase. Fig. D.3 shows the visible sector temperature as a function of the scale factor, where we have taken the temperature dependence of the relativistic degrees of freedom into account.

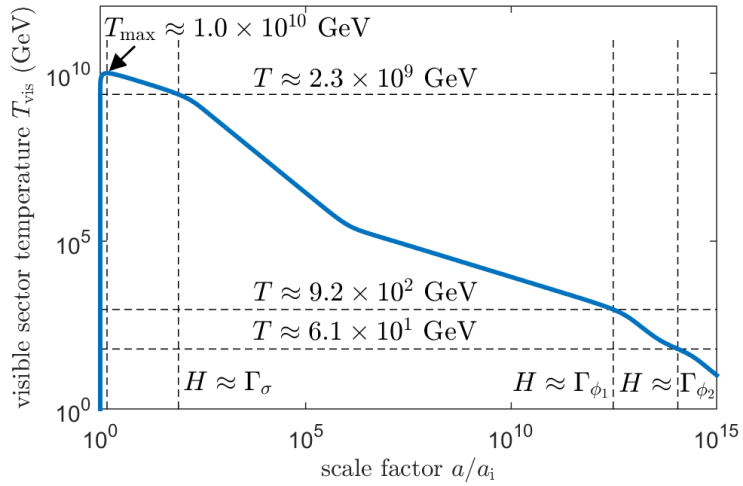

Figure D.3: Visible sector temperature as a function of scale factor in the scenario with two moduli.

Bibliography

[1] I. Broeckel, M. Cicoli, A. Maharana, K. Singh, and K. Sinha, "Moduli Stabilisation and the Statistics of SUSY Breaking in the Landscape," *JHEP* **10** (2020) 015, arXiv:2007.04327 [hep-th].

[2] R. Allahverdi, I. Broeckel, M. Cicoli, and J. K. Osiński, "Superheavy dark matter from string theory," *JHEP* **02** (2021) 026, arXiv:2010.03573 [hep-ph].

[3] I. Broeckel, M. Cicoli, A. Maharana, K. Singh, and K. Sinha, "Moduli stabilisation and the statistics of axion physics in the landscape," 2021.

[4] I. Broeckel, M. Cicoli, A. Maharana, K. Singh, and K. Sinha, "On the Search for Low W_0," arXiv:2108.04266 [hep-th].

[5] D. Hanneke, S. Fogwell Hoogerheide, and G. Gabrielse, "Cavity control of a single-electron quantum cyclotron: Measuring the electron magnetic moment," *Phys. Rev. A* **83** (May, 2011) 052122. https://link.aps.org/doi/10.1103/PhysRevA.83.052122.

[6] T. Aoyama, M. Hayakawa, T. Kinoshita, and M. Nio, "Tenth-order electron anomalous magnetic moment: Contribution of diagrams without closed lepton loops," *Physical Review D* **91** no. 3, (Feb, 2015) . http://dx.doi.org/10.1103/PhysRevD.91.033006.

[7] **LIGO Scientific Collaboration and Virgo Collaboration** Collaboration, B. P. Abbott, R. Abbott, T. D. Abbott, M. R. Abernathy, F. Acernese, K. Ackley, C. Adams, T. Adams, P. Addesso, R. X. Adhikari, V. B. Adya, C. Affeldt, M. Agathos, K. Agatsuma, N. Aggarwal, O. D. Aguiar, L. Aiello, A. Ain, P. Ajith, B. Allen, A. Allocca, P. A. Altin, S. B. Anderson, W. G. Anderson, K. Arai, M. A. Arain, M. C. Araya, C. C. Arceneaux, J. S. Areeda, N. Arnaud, K. G. Arun, S. Ascenzi, G. Ashton, M. Ast, S. M. Aston, P. Astone, P. Aufmuth, C. Aulbert, S. Babak, P. Bacon, M. K. M. Bader, P. T. Baker, F. Baldaccini, G. Ballardin, S. W. Ballmer, J. C. Barayoga, S. E. Barclay, B. C. Barish, D. Barker, F. Barone, B. Barr, L. Barsotti, M. Barsuglia, D. Barta, J. Bartlett, M. A. Barton, I. Bartos, R. Bassiri, A. Basti, J. C. Batch, C. Baune, V. Bavigadda, M. Bazzan, B. Behnke, M. Bejger, C. Belczynski, A. S. Bell, C. J. Bell, B. K. Berger,

J. Bergman, G. Bergmann, C. P. L. Berry, D. Bersanetti, A. Bertolini, J. Betzwieser, S. Bhagwat, R. Bhandare, I. A. Bilenko, G. Billingsley, J. Birch, R. Birney, O. Birnholtz, S. Biscans, A. Bisht, M. Bitossi, C. Biwer, M. A. Bizouard, J. K. Blackburn, C. D. Blair, D. G. Blair, R. M. Blair, S. Bloemen, O. Bock, T. P. Bodiya, M. Boer, G. Bogaert, C. Bogan, A. Bohe, P. Bojtos, C. Bond, F. Bondu, R. Bonnand, B. A. Boom, R. Bork, V. Boschi, S. Bose, Y. Bouffanais, A. Bozzi, C. Bradaschia, P. R. Brady, V. B. Braginsky, M. Branchesi, J. E. Brau, T. Briant, A. Brillet, M. Brinkmann, V. Brisson, P. Brockill, A. F. Brooks, D. A. Brown, D. D. Brown, N. M. Brown, C. C. Buchanan, A. Buikema, T. Bulik, H. J. Bulten, A. Buonanno, D. Buskulic, C. Buy, R. L. Byer, M. Cabero, L. Cadonati, G. Cagnoli, C. Cahillane, J. C. Bustillo, T. Callister, E. Calloni, J. B. Camp, K. C. Cannon, J. Cao, C. D. Capano, E. Capocasa, F. Carbognani, S. Caride, J. C. Diaz, C. Casentini, S. Caudill, M. Cavaglià, F. Cavalier, R. Cavalieri, G. Cella, C. B. Cepeda, L. C. Baiardi, G. Cerretani, E. Cesarini, R. Chakraborty, T. Chalermsongsak, S. J. Chamberlin, M. Chan, S. Chao, P. Charlton, E. Chassande-Mottin, H. Y. Chen, Y. Chen, C. Cheng, A. Chincarini, A. Chiummo, H. S. Cho, M. Cho, J. H. Chow, N. Christensen, Q. Chu, S. Chua, S. Chung, G. Ciani, F. Clara, J. A. Clark, F. Cleva, E. Coccia, P.-F. Cohadon, A. Colla, C. G. Collette, L. Cominsky, M. Constancio, A. Conte, L. Conti, D. Cook, T. R. Corbitt, N. Cornish, A. Corsi, S. Cortese, C. A. Costa, M. W. Coughlin, S. B. Coughlin, J.-P. Coulon, S. T. Countryman, P. Couvares, E. E. Cowan, D. M. Coward, M. J. Cowart, D. C. Coyne, R. Coyne, K. Craig, J. D. E. Creighton, T. D. Creighton, J. Cripe, S. G. Crowder, A. M. Cruise, A. Cumming, L. Cunningham, E. Cuoco, T. D. Canton, S. L. Danilishin, S. D'Antonio, K. Danzmann, N. S. Darman, C. F. Da Silva Costa, V. Dattilo, I. Dave, H. P. Daveloza, M. Davier, G. S. Davies, E. J. Daw, R. Day, S. De, D. DeBra, G. Debreczeni, J. Degallaix, M. De Laurentis, S. Deléglise, W. Del Pozzo, T. Denker, T. Dent, H. Dereli, V. Dergachev, R. T. DeRosa, R. De Rosa, R. DeSalvo, S. Dhurandhar, M. C. Díaz, L. Di Fiore, M. Di Giovanni, A. Di Lieto, S. Di Pace, I. Di Palma, A. Di Virgilio, G. Dojcinoski, V. Dolique, F. Donovan, K. L. Dooley, S. Doravari, R. Douglas, T. P. Downes, M. Drago, R. W. P. Drever, J. C. Driggers, Z. Du, M. Ducrot, S. E. Dwyer, T. B. Edo, M. C. Edwards, A. Effler, H.-B. Eggenstein, P. Ehrens, J. Eichholz, S. S. Eikenberry, W. Engels, R. C. Essick, T. Etzel, M. Evans, T. M. Evans, R. Everett, M. Factourovich, V. Fafone, H. Fair, S. Fairhurst, X. Fan, Q. Fang, S. Farinon, B. Farr, W. M. Farr, M. Favata, M. Fays, H. Fehrmann, M. M. Fejer, D. Feldbaum, I. Ferrante, E. C. Ferreira, F. Ferrini, F. Fidecaro, L. S. Finn, I. Fiori, D. Fiorucci, R. P. Fisher, R. Flaminio, M. Fletcher, H. Fong, J.-D. Fournier, S. Franco, S. Frasca, F. Frasconi, M. Frede, Z. Frei, A. Freise, R. Frey, V. Frey, T. T. Fricke, P. Fritschel, V. V. Frolov, P. Fulda, M. Fyffe, H. A. G. Gabbard, J. R. Gair, L. Gammaitoni, S. G. Gaonkar, F. Garufi, A. Gatto, G. Gaur, N. Gehrels, G. Gemme, B. Gendre, E. Genin, A. Gennai, J. George, L. Gergely, V. Germain, A. Ghosh, A. Ghosh, S. Ghosh, J. A.

Giaime, K. D. Giardina, A. Giazotto, K. Gill, A. Glaefke, J. R. Gleason, E. Goetz, R. Goetz, L. Gondan, G. González, J. M. G. Castro, A. Gopakumar, N. A. Gordon, M. L. Gorodetsky, S. E. Gossan, M. Gosselin, R. Gouaty, C. Graef, P. B. Graff, M. Granata, A. Grant, S. Gras, C. Gray, G. Greco, A. C. Green, R. J. S. Greenhalgh, P. Groot, H. Grote, S. Grunewald, G. M. Guidi, X. Guo, A. Gupta, M. K. Gupta, K. E. Gushwa, E. K. Gustafson, R. Gustafson, J. J. Hacker, B. R. Hall, E. D. Hall, G. Hammond, M. Haney, M. M. Hanke, J. Hanks, C. Hanna, M. D. Hannam, J. Hanson, T. Hardwick, J. Harms, G. M. Harry, I. W. Harry, M. J. Hart, M. T. Hartman, C.-J. Haster, K. Haughian, J. Healy, J. Heefner, A. Heidmann, M. C. Heintze, G. Heinzel, H. Heitmann, P. Hello, G. Hemming, M. Hendry, I. S. Heng, J. Hennig, A. W. Heptonstall, M. Heurs, S. Hild, D. Hoak, K. A. Hodge, D. Hofman, S. E. Hollitt, K. Holt, D. E. Holz, P. Hopkins, D. J. Hosken, J. Hough, E. A. Houston, E. J. Howell, Y. M. Hu, S. Huang, E. A. Huerta, D. Huet, B. Hughey, S. Husa, S. H. Huttner, T. Huynh-Dinh, A. Idrisy, N. Indik, D. R. Ingram, R. Inta, H. N. Isa, J.-M. Isac, M. Isi, G. Islas, T. Isogai, B. R. Iyer, K. Izumi, M. B. Jacobson, T. Jacqmin, H. Jang, K. Jani, P. Jaranowski, S. Jawahar, F. Jiménez-Forteza, W. W. Johnson, N. K. Johnson-McDaniel, D. I. Jones, R. Jones, R. J. G. Jonker, L. Ju, K. Haris, C. V. Kalaghatgi, V. Kalogera, S. Kandhasamy, G. Kang, J. B. Kanner, S. Karki, M. Kasprzack, E. Katsavounidis, W. Katzman, S. Kaufer, T. Kaur, K. Kawabe, F. Kawazoe, F. Kéfélian, M. S. Kehl, D. Keitel, D. B. Kelley, W. Kells, R. Kennedy, D. G. Keppel, J. S. Key, A. Khalaidovski, F. Y. Khalili, I. Khan, S. Khan, Z. Khan, E. A. Khazanov, N. Kijbunchoo, C. Kim, J. Kim, K. Kim, N.-G. Kim, N. Kim, Y.-M. Kim, E. J. King, P. J. King, D. L. Kinzel, J. S. Kissel, L. Kleybolte, S. Klimenko, S. M. Koehlenbeck, K. Kokeyama, S. Koley, V. Kondrashov, A. Kontos, S. Koranda, M. Korobko, W. Z. Korth, I. Kowalska, D. B. Kozak, V. Kringel, B. Krishnan, A. Królak, C. Krueger, G. Kuehn, P. Kumar, R. Kumar, L. Kuo, A. Kutynia, P. Kwee, B. D. Lackey, M. Landry, J. Lange, B. Lantz, P. D. Lasky, A. Lazzarini, C. Lazzaro, P. Leaci, S. Leavey, E. O. Lebigot, C. H. Lee, H. K. Lee, H. M. Lee, K. Lee, A. Lenon, M. Leonardi, J. R. Leong, N. Leroy, N. Letendre, Y. Levin, B. M. Levine, T. G. F. Li, A. Libson, T. B. Littenberg, N. A. Lockerbie, J. Logue, A. L. Lombardi, L. T. London, J. E. Lord, M. Lorenzini, V. Loriette, M. Lormand, G. Losurdo, J. D. Lough, C. O. Lousto, G. Lovelace, H. Lück, A. P. Lundgren, J. Luo, R. Lynch, Y. Ma, T. MacDonald, B. Machenschalk, M. MacInnis, D. M. Macleod, F. Magaña Sandoval, R. M. Magee, M. Mageswaran, E. Majorana, I. Maksimovic, V. Malvezzi, N. Man, I. Mandel, V. Mandic, V. Mangano, G. L. Mansell, M. Manske, M. Mantovani, F. Marchesoni, F. Marion, S. Márka, Z. Márka, A. S. Markosyan, E. Maros, F. Martelli, L. Martellini, I. W. Martin, R. M. Martin, D. V. Martynov, J. N. Marx, K. Mason, A. Masserot, T. J. Massinger, M. Masso-Reid, F. Matichard, L. Matone, N. Mavalvala, N. Mazumder, G. Mazzolo, R. McCarthy, D. E. McClelland, S. McCormick, S. C. McGuire, G. McIntyre, J. McIver, D. J. McManus, S. T. McWilliams, D. Meacher, G. D.

Meadors, J. Meidam, A. Melatos, G. Mendell, D. Mendoza-Gandara, R. A. Mercer, E. Merilh, M. Merzougui, S. Meshkov, C. Messenger, C. Messick, P. M. Meyers, F. Mezzani, H. Miao, C. Michel, H. Middleton, E. E. Mikhailov, L. Milano, J. Miller, M. Millhouse, Y. Minenkov, J. Ming, S. Mirshekari, C. Mishra, S. Mitra, V. P. Mitrofanov, G. Mitselmakher, R. Mittleman, A. Moggi, M. Mohan, S. R. P. Mohapatra, M. Montani, B. C. Moore, C. J. Moore, D. Moraru, G. Moreno, S. R. Morriss, K. Mossavi, B. Mours, C. M. Mow-Lowry, C. L. Mueller, G. Mueller, A. W. Muir, A. Mukherjee, D. Mukherjee, S. Mukherjee, N. Mukund, A. Mullavey, J. Munch, D. J. Murphy, P. G. Murray, A. Mytidis, I. Nardecchia, L. Naticchioni, R. K. Nayak, V. Necula, K. Nedkova, G. Nelemans, M. Neri, A. Neunzert, G. Newton, T. T. Nguyen, A. B. Nielsen, S. Nissanke, A. Nitz, F. Nocera, D. Nolting, M. E. N. Normandin, L. K. Nuttall, J. Oberling, E. Ochsner, J. O'Dell, E. Oelker, G. H. Ogin, J. J. Oh, S. H. Oh, F. Ohme, M. Oliver, P. Oppermann, R. J. Oram, B. O'Reilly, R. O'Shaughnessy, C. D. Ott, D. J. Ottaway, R. S. Ottens, H. Overmier, B. J. Owen, A. Pai, S. A. Pai, J. R. Palamos, O. Palashov, C. Palomba, A. Pal-Singh, H. Pan, Y. Pan, C. Pankow, F. Pannarale, B. C. Pant, F. Paoletti, A. Paoli, M. A. Papa, H. R. Paris, W. Parker, D. Pascucci, A. Pasqualetti, R. Passaquieti, D. Passuello, B. Patricelli, Z. Patrick, B. L. Pearlstone, M. Pedraza, R. Pedurand, L. Pekowsky, A. Pele, S. Penn, A. Perreca, H. P. Pfeiffer, M. Phelps, O. Piccinni, M. Pichot, M. Pickenpack, F. Piergiovanni, V. Pierro, G. Pillant, L. Pinard, I. M. Pinto, M. Pitkin, J. H. Poeld, R. Poggiani, P. Popolizio, A. Post, J. Powell, J. Prasad, V. Predoi, S. S. Premachandra, T. Prestegard, L. R. Price, M. Prijatelj, M. Principe, S. Privitera, R. Prix, G. A. Prodi, L. Prokhorov, O. Puncken, M. Punturo, P. Puppo, M. Pürrer, H. Qi, J. Qin, V. Quetschke, E. A. Quintero, R. Quitzow-James, F. J. Raab, D. S. Rabeling, H. Radkins, P. Raffai, S. Raja, M. Rakhmanov, C. R. Ramet, P. Rapagnani, V. Raymond, M. Razzano, V. Re, J. Read, C. M. Reed, T. Regimbau, L. Rei, S. Reid, D. H. Reitze, H. Rew, S. D. Reyes, F. Ricci, K. Riles, N. A. Robertson, R. Robie, F. Robinet, A. Rocchi, L. Rolland, J. G. Rollins, V. J. Roma, J. D. Romano, R. Romano, G. Romanov, J. H. Romie, D. Rosińska, S. Rowan, A. Rüdiger, P. Ruggi, K. Ryan, S. Sachdev, T. Sadecki, L. Sadeghian, L. Salconi, M. Saleem, F. Salemi, A. Samajdar, L. Sammut, L. M. Sampson, E. J. Sanchez, V. Sandberg, B. Sandeen, G. H. Sanders, J. R. Sanders, B. Sassolas, B. S. Sathyaprakash, P. R. Saulson, O. Sauter, R. L. Savage, A. Sawadsky, P. Schale, R. Schilling, J. Schmidt, P. Schmidt, R. Schnabel, R. M. S. Schofield, A. Schönbeck, E. Schreiber, D. Schuette, B. F. Schutz, J. Scott, S. M. Scott, D. Sellers, A. S. Sengupta, D. Sentenac, V. Sequino, A. Sergeev, G. Serna, Y. Setyawati, A. Sevigny, D. A. Shaddock, T. Shaffer, S. Shah, M. S. Shahriar, M. Shaltev, Z. Shao, B. Shapiro, P. Shawhan, A. Sheperd, D. H. Shoemaker, D. M. Shoemaker, K. Siellez, X. Siemens, D. Sigg, A. D. Silva, D. Simakov, A. Singer, L. P. Singer, A. Singh, R. Singh, A. Singhal, A. M. Sintes, B. J. J. Slagmolen, J. R. Smith, M. R. Smith, N. D. Smith, R. J. E.

Smith, E. J. Son, B. Sorazu, F. Sorrentino, T. Souradeep, A. K. Srivastava, A. Staley, M. Steinke, J. Steinlechner, S. Steinlechner, D. Steinmeyer, B. C. Stephens, S. P. Stevenson, R. Stone, K. A. Strain, N. Straniero, G. Stratta, N. A. Strauss, S. Strigin, R. Sturani, A. L. Stuver, T. Z. Summerscales, L. Sun, P. J. Sutton, B. L. Swinkels, M. J. Szczepańczyk, M. Tacca, D. Talukder, D. B. Tanner, M. Tápai, S. P. Tarabrin, A. Taracchini, R. Taylor, T. Theeg, M. P. Thirugnanasambandam, E. G. Thomas, M. Thomas, P. Thomas, K. A. Thorne, K. S. Thorne, E. Thrane, S. Tiwari, V. Tiwari, K. V. Tokmakov, C. Tomlinson, M. Tonelli, C. V. Torres, C. I. Torrie, D. Töyrä, F. Travasso, G. Traylor, D. Trifirò, M. C. Tringali, L. Trozzo, M. Tse, M. Turconi, D. Tuyenbayev, D. Ugolini, C. S. Unnikrishnan, A. L. Urban, S. A. Usman, H. Vahlbruch, G. Vajente, G. Valdes, M. Vallisneri, N. van Bakel, M. van Beuzekom, J. F. J. van den Brand, C. Van Den Broeck, D. C. Vander-Hyde, L. van der Schaaf, J. V. van Heijningen, A. A. van Veggel, M. Vardaro, S. Vass, M. Vasúth, R. Vaulin, A. Vecchio, G. Vedovato, J. Veitch, P. J. Veitch, K. Venkateswara, D. Verkindt, F. Vetrano, A. Viceré, S. Vinciguerra, D. J. Vine, J.-Y. Vinet, S. Vitale, T. Vo, H. Vocca, C. Vorvick, D. Voss, W. D. Vousden, S. P. Vyatchanin, A. R. Wade, L. E. Wade, M. Wade, S. J. Waldman, M. Walker, L. Wallace, S. Walsh, G. Wang, H. Wang, M. Wang, X. Wang, Y. Wang, H. Ward, R. L. Ward, J. Warner, M. Was, B. Weaver, L.-W. Wei, M. Weinert, A. J. Weinstein, R. Weiss, T. Welborn, L. Wen, P. Weßels, T. Westphal, K. Wette, J. T. Whelan, S. E. Whitcomb, D. J. White, B. F. Whiting, K. Wiesner, C. Wilkinson, P. A. Willems, L. Williams, R. D. Williams, A. R. Williamson, J. L. Willis, B. Willke, M. H. Wimmer, L. Winkelmann, W. Winkler, C. C. Wipf, A. G. Wiseman, H. Wittel, G. Woan, J. Worden, J. L. Wright, G. Wu, J. Yablon, I. Yakushin, W. Yam, H. Yamamoto, C. C. Yancey, M. J. Yap, H. Yu, M. Yvert, A. Zadrożny, L. Zangrando, M. Zanolin, J.-P. Zendri, M. Zevin, F. Zhang, L. Zhang, M. Zhang, Y. Zhang, C. Zhao, M. Zhou, Z. Zhou, X. J. Zhu, M. E. Zucker, S. E. Zuraw, and J. Zweizig, "Observation of gravitational waves from a binary black hole merger," *Phys. Rev. Lett.* **116** (Feb, 2016) 061102. `https://link.aps.org/doi/10.1103/PhysRevLett.116.061102`.

[8] **Event Horizon Telescope** Collaboration, K. Akiyama *et al.*, "First M87 Event Horizon Telescope Results. I. The Shadow of the Supermassive Black Hole," *Astrophys. J. Lett.* **875** (2019) L1, `arXiv:1906.11238 [astro-ph.GA]`.

[9] Y. Fukuda, T. Hayakawa, E. Ichihara, K. Inoue, K. Ishihara, H. Ishino, Y. Itow, T. Kajita, J. Kameda, S. Kasuga, and et al., "Evidence for oscillation of atmospheric neutrinos," *Physical Review Letters* **81** no. 8, (Aug, 1998) 1562–1567. `http://dx.doi.org/10.1103/PhysRevLett.81.1562`.

[10] **Supernova Cosmology Project** Collaboration, S. Perlmutter *et al.*, "Measurements of Ω and Λ from 42 high redshift supernovae," *Astrophys. J.* **517** (1999) 565–586, `arXiv:astro-ph/9812133`.

[11] A. G. Riess, A. V. Filippenko, P. Challis, A. Clocchiatti, A. Diercks, P. M. Garnavich, R. L. Gilliland, C. J. Hogan, S. Jha, R. P. Kirshner, and et al., "Observational evidence from supernovae for an accelerating universe and a cosmological constant," *The Astronomical Journal* **116** no. 3, (Sep, 1998) 1009–1038. http://dx.doi.org/10.1086/300499.

[12] F. Halzen and A. Martin, *Quarks & Leptons: An introductory course in modern particle physics*. John Wiley & Sons, New York, USA, 1984.

[13] D. J. Griffiths, *Introduction to elementary particles; 2nd rev. version*. Physics textbook. Wiley, New York, NY, 2008. https://cds.cern.ch/record/111880.

[14] S. M. Carroll, "TASI lectures: Cosmology for string theorists," in *Theoretical Advanced Study Institute in Elementary Particle Physics (TASI 99): Strings, Branes, and Gravity*, pp. 437–492. 5, 1999. arXiv:hep-th/0011110.

[15] D. Baumann, "Primordial Cosmology," *PoS* **TASI2017** (2018) 009, arXiv:1807.03098 [hep-th].

[16] A. Liddle, *An Introduction to Modern Cosmology*. Wiley, 2003. https://books.google.de/books?id=zZg3AQAAIAAJ.

[17] C. S. Wu, E. Ambler, R. W. Hayward, D. D. Hoppes, and R. P. Hudson, "Experimental test of parity conservation in beta decay," *Phys. Rev.* **105** (Feb, 1957) 1413–1415. https://link.aps.org/doi/10.1103/PhysRev.105.1413.

[18] G. Aad, T. Abajyan, B. Abbott, J. Abdallah, S. Abdel Khalek, A. Abdelalim, O. Abdinov, R. Aben, B. Abi, M. Abolins, and et al., "Observation of a new particle in the search for the standard model higgs boson with the atlas detector at the lhc," *Physics Letters B* **716** no. 1, (Sep, 2012) 1–29. http://dx.doi.org/10.1016/j.physletb.2012.08.020.

[19] E. Hubble, "A relation between distance and radial velocity among extra-galactic nebulae," *Proceedings of the National Academy of Sciences* **15** no. 3, (1929) 168–173, https://www.pnas.org/content/15/3/168.full.pdf.

[20] **Planck** Collaboration, N. Aghanim *et al.*, "Planck 2018 results. VI. Cosmological parameters," *Astron. Astrophys.* **641** (2020) A6, arXiv:1807.06209 [astro-ph.CO]. [Erratum: Astron.Astrophys. 652, C4 (2021)].

[21] L. E. Ibanez and A. M. Uranga, *String theory and particle physics: An introduction to string phenomenology*. Cambridge University Press, 2, 2012.

[22] K. Becker, M. Becker, and J. H. Schwarz, *String theory and M-theory: A modern introduction*. Cambridge University Press, 12, 2006.

[23] J. Polchinski, *String theory. Vol. 1: An introduction to the bosonic string*. Cambridge Monographs on Mathematical Physics. Cambridge University Press, 12, 2007.

[24] J. Polchinski, *String theory. Vol. 2: Superstring theory and beyond*. Cambridge Monographs on Mathematical Physics. Cambridge University Press, 12, 2007.

[25] D. Baumann, "Inflation," in *Theoretical Advanced Study Institute in Elementary Particle Physics: Physics of the Large and the Small*, pp. 523–686. 2011. arXiv:0907.5424 [hep-th].

[26] L. Anguelova, V. Calo, and M. Cicoli, "LARGE Volume String Compactifications at Finite Temperature," *JCAP* **10** (2009) 025, arXiv:0904.0051 [hep-th].

[27] S. Coleman and J. Mandula, "All possible symmetries of the s matrix," *Phys. Rev.* **159** (Jul, 1967) 1251–1256. https://link.aps.org/doi/10.1103/PhysRev.159.1251.

[28] R. Haag, J. T. Łopuszański, and M. F. Sohnius, "All possible generators of supersymmetries of the s-matrix," *Nuclear Physics* **88** (1975) 257–274.

[29] M. Duff, B. Nilsson, and C. Pope, "Kaluza-klein supergravity," *Physics Reports* **130** no. 1, (1986) 1–142. https://www.sciencedirect.com/science/article/pii/0370157386901638.

[30] S. B. Giddings, S. Kachru, and J. Polchinski, "Hierarchies from fluxes in string compactifications," *Phys. Rev. D* **66** (2002) 106006, arXiv:hep-th/0105097.

[31] J. Polchinski and A. Strominger, "New vacua for type II string theory," *Phys. Lett. B* **388** (1996) 736–742, arXiv:hep-th/9510227.

[32] V. Balasubramanian, P. Berglund, J. P. Conlon, and F. Quevedo, "Systematics of moduli stabilisation in Calabi-Yau flux compactifications," *JHEP* **03** (2005) 007, arXiv:hep-th/0502058.

[33] S. Kachru, R. Kallosh, A. D. Linde, and S. P. Trivedi, "De Sitter vacua in string theory," *Phys. Rev. D* **68** (2003) 046005, arXiv:hep-th/0301240.

[34] M. Cicoli, J. P. Conlon, and F. Quevedo, "General Analysis of LARGE Volume Scenarios with String Loop Moduli Stabilisation," *JHEP* **10** (2008) 105, arXiv:0805.1029 [hep-th].

[35] D. G. Cerdeno and C. Munoz, "An introduction to supergravity," *PoS* **CORFU98** (1998) 011.

[36] M. Berg, M. Haack, and E. Pajer, "Jumping Through Loops: On Soft Terms from Large Volume Compactifications," *JHEP* **09** (2007) 031, arXiv:0704.0737 [hep-th].

[37] M. Cicoli, J. P. Conlon, and F. Quevedo, "Systematics of String Loop Corrections in Type IIB Calabi-Yau Flux Compactifications," *JHEP* **01** (2008) 052, arXiv:0708.1873 [hep-th].

[38] H. Baer, V. Barger, S. Salam, D. Sengupta, and K. Sinha, "Midi-review: Status of weak scale supersymmetry after LHC Run 2 and ton-scale noble liquid WIMP searches," arXiv:2002.03013 [hep-ph].

[39] A. Maharana and E. Palti, "Models of Particle Physics from Type IIB String Theory and F-theory: A Review," *Int. J. Mod. Phys. A* **28** (2013) 1330005, arXiv:1212.0555 [hep-th].

[40] F. Denef, M. R. Douglas, and S. Kachru, "Physics of String Flux Compactifications," *Ann. Rev. Nucl. Part. Sci.* **57** (2007) 119–144, arXiv:hep-th/0701050.

[41] M. Grana, "Flux compactifications in string theory: A Comprehensive review," *Phys. Rept.* **423** (2006) 91–158, arXiv:hep-th/0509003.

[42] E. Silverstein, "TASI / PiTP / ISS lectures on moduli and microphysics," in *Theoretical Advanced Study Institute in Elementary Particle Physics (TASI 2003): Recent Trends in String Theory*, pp. 381–415. 5, 2004. arXiv:hep-th/0405068.

[43] A. R. Frey, "Warped strings: Selfdual flux and contemporary compactifications," phd thesis, 8, 2003.

[44] R. Bousso and J. Polchinski, "Quantization of four form fluxes and dynamical neutralization of the cosmological constant," *JHEP* **06** (2000) 006, arXiv:hep-th/0004134.

[45] J. L. Feng, J. March-Russell, S. Sethi, and F. Wilczek, "Saltatory relaxation of the cosmological constant," *Nucl. Phys. B* **602** (2001) 307–328, arXiv:hep-th/0005276.

[46] S. Ashok and M. R. Douglas, "Counting flux vacua," *JHEP* **01** (2004) 060, arXiv:hep-th/0307049.

[47] M. R. Douglas, "Statistical analysis of the supersymmetry breaking scale," arXiv:hep-th/0405279.

[48] M. R. Douglas, "Basic results in vacuum statistics," *Comptes Rendus Physique* **5** (2004) 965–977, arXiv:hep-th/0409207.

[49] F. Denef, M. R. Douglas, and B. Florea, "Building a better racetrack," *JHEP* **06** (2004) 034, arXiv:hep-th/0404257.

[50] F. Denef and M. R. Douglas, "Distributions of flux vacua," *JHEP* **05** (2004) 072, arXiv:hep-th/0404116.

[51] F. Denef and M. R. Douglas, "Distributions of nonsupersymmetric flux vacua," *JHEP* **03** (2005) 061, arXiv:hep-th/0411183.

[52] A. Giryavets, S. Kachru, and P. K. Tripathy, "On the taxonomy of flux vacua," *JHEP* **08** (2004) 002, arXiv:hep-th/0404243.

[53] A. Misra and A. Nanda, "Flux vacua statistics for two-parameter Calabi-Yau's," *Fortsch. Phys.* **53** (2005) 246–259, arXiv:hep-th/0407252.

[54] J. P. Conlon and F. Quevedo, "On the explicit construction and statistics of Calabi-Yau flux vacua," *JHEP* **10** (2004) 039, arXiv:hep-th/0409215.

[55] B. S. Acharya, F. Denef, and R. Valandro, "Statistics of M theory vacua," *JHEP* **06** (2005) 056, arXiv:hep-th/0502060.

[56] M. R. Douglas and S. Kachru, "Flux compactification," *Rev. Mod. Phys.* **79** (2007) 733–796, arXiv:hep-th/0610102.

[57] D. Gallego, M. C. D. Marsh, B. Vercnocke, and T. Wrase, "A New Class of de Sitter Vacua in Type IIB Large Volume Compactifications," *JHEP* **10** (2017) 193, arXiv:1707.01095 [hep-th].

[58] E. Cremmer, S. Ferrara, C. Kounnas, and D. V. Nanopoulos, "Naturally Vanishing Cosmological Constant in N=1 Supergravity," *Phys. Lett. B* **133** (1983) 61.

[59] J. R. Ellis, A. Lahanas, D. V. Nanopoulos, and K. Tamvakis, "No-Scale Supersymmetric Standard Model," *Phys. Lett. B* **134** (1984) 429.

[60] C. Burgess, A. Font, and F. Quevedo, "Low-Energy Effective Action for the Superstring," *Nucl. Phys. B* **272** (1986) 661–676.

[61] C. Burgess, M. Cicoli, D. Ciupke, S. Krippendorf, and F. Quevedo, "UV Shadows in EFTs: Accidental Symmetries, Robustness and No-Scale Supergravity," arXiv:2006.06694 [hep-th].

[62] F. Marchesano, G. Shiu, and L.-T. Wang, "Model building and phenomenology of flux-induced supersymmetry breaking on D3-branes," *Nucl. Phys. B* **712** (2005) 20–58, arXiv:hep-th/0411080.

[63] R. Blumenhagen, J. Conlon, S. Krippendorf, S. Moster, and F. Quevedo, "SUSY Breaking in Local String/F-Theory Models," *JHEP* **09** (2009) 007, arXiv:0906.3297 [hep-th].

[64] J. P. Conlon, A. Maharana, and F. Quevedo, "Towards Realistic String Vacua," *JHEP* **05** (2009) 109, arXiv:0810.5660 [hep-th].

[65] L. Aparicio, M. Cicoli, S. Krippendorf, A. Maharana, F. Muia, and F. Quevedo, "Sequestered de Sitter String Scenarios: Soft-terms," *JHEP* **11** (2014) 071, arXiv:1409.1931 [hep-th].

[66] M. Berg, M. Haack, and B. Kors, "On volume stabilization by quantum corrections," *Phys. Rev. Lett.* **96** (2006) 021601, arXiv:hep-th/0508171.

[67] H. Baer, V. Barger, H. Serce, and K. Sinha, "Higgs and superparticle mass predictions from the landscape," *JHEP* **03** (2018) 002, arXiv:1712.01399 [hep-ph].

[68] M. Dine, E. Gorbatov, and S. D. Thomas, "Low energy supersymmetry from the landscape," *JHEP* **08** (2008) 098, arXiv:hep-th/0407043.

[69] M. Dine, "The Intermediate scale branch of the landscape," *JHEP* **01** (2006) 162, arXiv:hep-th/0505202.

[70] M. Dine, D. O'Neil, and Z. Sun, "Branches of the landscape," *JHEP* **07** (2005) 014, arXiv:hep-th/0501214.

[71] M. Dine, "Supersymmetry, naturalness and the landscape," in *10th International Symposium on Particles, Strings and Cosmology (PASCOS 04 and Pran Nath Fest)*, pp. 249–263. 10, 2004. arXiv:hep-th/0410201.

[72] L. Susskind, "Supersymmetry breaking in the anthropic landscape," arXiv:hep-th/0405189.

[73] T. Banks, M. Dine, and E. Gorbatov, "Is there a string theory landscape?," *JHEP* **08** (2004) 058, arXiv:hep-th/0309170.

[74] O. DeWolfe, A. Giryavets, S. Kachru, and W. Taylor, "Enumerating flux vacua with enhanced symmetries," *JHEP* **02** (2005) 037, arXiv:hep-th/0411061.

[75] M. Cicoli, D. Klevers, S. Krippendorf, C. Mayrhofer, F. Quevedo, and R. Valandro, "Explicit de Sitter Flux Vacua for Global String Models with Chiral Matter," *JHEP* **05** (2014) 001, arXiv:1312.0014 [hep-th].

[76] M. Demirtas, M. Kim, L. Mcallister, and J. Moritz, "Vacua with Small Flux Superpotential," *Phys. Rev. Lett.* **124** no. 21, (2020) 211603, arXiv:1912.10047 [hep-th].

[77] P. Betzler and E. Plauschinn, "Type IIB flux vacua and tadpole cancellation," *Fortsch. Phys.* **67** no. 11, (2019) 1900065, arXiv:1905.08823 [hep-th].

[78] A. Cole, A. Schachner, and G. Shiu, "Searching the Landscape of Flux Vacua with Genetic Algorithms," *JHEP* **11** (2019) 045, arXiv:1907.10072 [hep-th].

[79] G. Coughlan, W. Fischler, E. W. Kolb, S. Raby, and G. G. Ross, "Cosmological Problems for the Polonyi Potential," *Phys. Lett. B* **131** (1983) 59–64.

[80] T. Banks, D. B. Kaplan, and A. E. Nelson, "Cosmological implications of dynamical supersymmetry breaking," *Phys. Rev. D* **49** (1994) 779–787, arXiv:hep-ph/9308292.

[81] B. de Carlos, J. Casas, F. Quevedo, and E. Roulet, "Model independent properties and cosmological implications of the dilaton and moduli sectors of 4-d strings," *Phys. Lett. B* **318** (1993) 447–456, arXiv:hep-ph/9308325.

[82] G. Kane, K. Sinha, and S. Watson, "Cosmological Moduli and the Post-Inflationary Universe: A Critical Review," *Int. J. Mod. Phys. D* **24** no. 08, (2015) 1530022, arXiv:1502.07746 [hep-th].

[83] S. Gukov, C. Vafa, and E. Witten, "CFT's from Calabi-Yau four folds," *Nucl. Phys. B* **584** (2000) 69–108, arXiv:hep-th/9906070. [Erratum: Nucl.Phys.B 608, 477–478 (2001)].

[84] T. W. Grimm and J. Louis, "The Effective action of N = 1 Calabi-Yau orientifolds," *Nucl. Phys. B* **699** (2004) 387–426, arXiv:hep-th/0403067.

[85] H. Jockers, *The Effective Action of D-branes in Calabi-Yau Orientifold Compactifications*. PhD thesis, Hamburg U., Inst. Theor. Phys. II, 2005. arXiv:hep-th/0507042.

[86] A. Westphal, "de Sitter string vacua from Kahler uplifting," *JHEP* **03** (2007) 102, arXiv:hep-th/0611332.

[87] L. Aparicio, F. Quevedo, and R. Valandro, "Moduli Stabilisation with Nilpotent Goldstino: Vacuum Structure and SUSY Breaking," *JHEP* **03** (2016) 036, arXiv:1511.08105 [hep-th].

[88] K. Choi, A. Falkowski, H. P. Nilles, and M. Olechowski, "Soft supersymmetry breaking in KKLT flux compactification," *Nucl. Phys. B* **718** (2005) 113–133, arXiv:hep-th/0503216.

[89] M. Cicoli, C. Burgess, and F. Quevedo, "Anisotropic Modulus Stabilisation: Strings at LHC Scales with Micron-sized Extra Dimensions," *JHEP* **10** (2011) 119, arXiv:1105.2107 [hep-th].

[90] M. Cicoli, D. Ciupke, S. de Alwis, and F. Muia, "α' Inflation: moduli stabilisation and observable tensors from higher derivatives," *JHEP* **09** (2016) 026, arXiv:1607.01395 [hep-th].

[91] S. AbdusSalam, S. Abel, M. Cicoli, F. Quevedo, and P. Shukla, "A Systematic Approach to Kähler Moduli Stabilisation," arXiv:2005.11329 [hep-th].

[92] M. Cicoli, F. Quevedo, and R. Valandro, "De Sitter from T-branes," *JHEP* **03** (2016) 141, arXiv:1512.04558 [hep-th].

[93] M. Cicoli, A. Maharana, F. Quevedo, and C. Burgess, "De Sitter String Vacua from Dilaton-dependent Non-perturbative Effects," *JHEP* **06** (2012) 011, arXiv:1203.1750 [hep-th].

[94] J. P. Conlon, F. Quevedo, and K. Suruliz, "Large-volume flux compactifications: Moduli spectrum and D3/D7 soft supersymmetry breaking," *JHEP* **08** (2005) 007, arXiv:hep-th/0505076.

[95] J. P. Conlon, S. S. Abdussalam, F. Quevedo, and K. Suruliz, "Soft SUSY Breaking Terms for Chiral Matter in IIB String Compactifications," *JHEP* **01** (2007) 032, arXiv:hep-th/0610129.

[96] M. Cicoli, S. De Alwis, A. Maharana, F. Muia, and F. Quevedo, "De Sitter vs Quintessence in String Theory," *Fortsch. Phys.* **67** no. 1-2, (2019) 1800079, arXiv:1808.08967 [hep-th].

[97] K. Becker, M. Becker, M. Haack, and J. Louis, "Supersymmetry breaking and alpha-prime corrections to flux induced potentials," *JHEP* **06** (2002) 060, arXiv:hep-th/0204254.

[98] G. von Gersdorff and A. Hebecker, "Kahler corrections for the volume modulus of flux compactifications," *Phys. Lett. B* **624** (2005) 270–274, arXiv:hep-th/0507131.

[99] M. Berg, M. Haack, and B. Kors, "String loop corrections to Kahler potentials in orientifolds," *JHEP* **11** (2005) 030, arXiv:hep-th/0508043.

[100] J. J. Blanco-Pillado, K. Sousa, M. A. Urkiola, and J. M. Wachter, "Complete Mass Spectrum of Type-IIB Flux Vacua at Large Complex Structure," arXiv:2007.10381 [hep-th].

[101] J. Louis, M. Rummel, R. Valandro, and A. Westphal, "Building an explicit de Sitter," *JHEP* **10** (2012) 163, arXiv:1208.3208 [hep-th].

[102] A. Grassi, J. Halverson, J. Shaneson, and W. Taylor, "Non-Higgsable QCD and the Standard Model Spectrum in F-theory," *JHEP* **01** (2015) 086, arXiv:1409.8295 [hep-th].

[103] D. R. Morrison and W. Taylor, "Non-Higgsable clusters for 4D F-theory models," *JHEP* **05** (2015) 080, arXiv:1412.6112 [hep-th].

[104] M. Cicoli, C. Mayrhofer, and R. Valandro, "Moduli Stabilisation for Chiral Global Models," *JHEP* **02** (2012) 062, arXiv:1110.3333 [hep-th].

[105] M. Cicoli, S. Krippendorf, C. Mayrhofer, F. Quevedo, and R. Valandro, "D-Branes at del Pezzo Singularities: Global Embedding and Moduli Stabilisation," *JHEP* **09** (2012) 019, arXiv:1206.5237 [hep-th].

[106] M. Cicoli, S. Krippendorf, C. Mayrhofer, F. Quevedo, and R. Valandro, "D3/D7 Branes at Singularities: Constraints from Global Embedding and Moduli Stabilisation," *JHEP* **07** (2013) 150, arXiv:1304.0022 [hep-th].

[107] M. Cicoli, I. Garcìa-Etxebarria, C. Mayrhofer, F. Quevedo, P. Shukla, and R. Valandro, "Global Orientifolded Quivers with Inflation," *JHEP* **11** (2017) 134, arXiv:1706.06128 [hep-th].

[108] I. Affleck, M. Dine, and N. Seiberg, "Supersymmetry Breaking by Instantons," *Phys. Rev. Lett.* **51** (1983) 1026.

[109] **ATLAS** Collaboration, M. Aaboud *et al.*, "Search for squarks and gluinos in final states with jets and missing transverse momentum using 36 fb^{-1} of $\sqrt{s} = 13$ TeV pp collision data with the ATLAS detector," *Phys. Rev. D* **97** no. 11, (2018) 112001, arXiv:1712.02332 [hep-ex].

[110] **ATLAS, CMS** Collaboration, T. A. Vami, "Searches for gluinos and squarks," *PoS* **LHCP2019** (2019) 168, arXiv:1909.11753 [hep-ex].

[111] **ATLAS** Collaboration, "Search for direct top squark pair production in the 3-body decay mode with a final state containing one lepton, jets, and missing transverse momentum in $\sqrt{s} = 13$TeV pp collision data with the ATLAS detector,".

[112] **CMS** Collaboration, A. M. Sirunyan *et al.*, "Search for direct top squark pair production in events with one lepton, jets, and missing transverse momentum at 13 TeV with the CMS experiment," *JHEP* **05** (2020) 032, arXiv:1912.08887 [hep-ex].

[113] R. Barbieri and G. Giudice, "Upper Bounds on Supersymmetric Particle Masses," *Nucl. Phys. B* **306** (1988) 63–76.

[114] H. Baer, V. Barger, S. Salam, H. Serce, and K. Sinha, "LHC SUSY and WIMP dark matter searches confront the string theory landscape," *JHEP* **04** (2019) 043, arXiv:1901.11060 [hep-ph].

[115] H. Baer, V. Barger, and M. Savoy, "Upper bounds on sparticle masses from naturalness or how to disprove weak scale supersymmetry," *Phys. Rev. D* **93** no. 3, (2016) 035016, arXiv:1509.02929 [hep-ph].

[116] S. Weinberg, "Anthropic Bound on the Cosmological Constant," *Phys. Rev. Lett.* **59** (1987) 2607.

[117] V. Agrawal, S. M. Barr, J. F. Donoghue, and D. Seckel, "Viable range of the mass scale of the standard model," *Phys. Rev. D* **57** (1998) 5480–5492, arXiv:hep-ph/9707380.

[118] H. Baer, V. Barger, P. Huang, A. Mustafayev, and X. Tata, "Radiative natural SUSY with a 125 GeV Higgs boson," *Phys. Rev. Lett.* **109** (2012) 161802, arXiv:1207.3343 [hep-ph].

[119] H. Baer, V. Barger, P. Huang, D. Mickelson, A. Mustafayev, and X. Tata, "Radiative natural supersymmetry: Reconciling electroweak fine-tuning and the Higgs boson mass," *Phys. Rev. D* **87** no. 11, (2013) 115028, arXiv:1212.2655 [hep-ph].

[120] M. Cicoli, J. P. Conlon, A. Maharana, and F. Quevedo, "A Note on the Magnitude of the Flux Superpotential," *JHEP* **01** (2014) 027, arXiv:1310.6694 [hep-th].

[121] A. Saltman and E. Silverstein, "A New handle on de Sitter compactifications," *JHEP* **01** (2006) 139, arXiv:hep-th/0411271.

[122] O. DeWolfe and S. B. Giddings, "Scales and hierarchies in warped compactifications and brane worlds," *Phys. Rev. D* **67** (2003) 066008, arXiv:hep-th/0208123.

[123] A. Hebecker and J. March-Russell, "The Ubiquitous throat," *Nucl. Phys. B* **781** (2007) 99–111, arXiv:hep-th/0607120.

[124] P. Svrcek and E. Witten, "Axions In String Theory," *JHEP* **06** (2006) 051, arXiv:hep-th/0605206.

[125] J. P. Conlon, "The QCD axion and moduli stabilisation," *JHEP* **05** (2006) 078, arXiv:hep-th/0602233.

[126] A. Arvanitaki, S. Dimopoulos, S. Dubovsky, N. Kaloper, and J. March-Russell, "String Axiverse," *Phys. Rev. D* **81** (2010) 123530, arXiv:0905.4720 [hep-th].

[127] M. Cicoli, M. Goodsell, and A. Ringwald, "The type IIB string axiverse and its low-energy phenomenology," *JHEP* **10** (2012) 146, arXiv:1206.0819 [hep-th].

[128] R. Allahverdi, M. Cicoli, B. Dutta, and K. Sinha, "Correlation between Dark Matter and Dark Radiation in String Compactifications," *JCAP* **10** (2014) 002, arXiv:1401.4364 [hep-ph].

[129] M. Demirtas, M. Kim, L. Mcallister, and J. Moritz, "Conifold Vacua with Small Flux Superpotential," arXiv:2009.03312 [hep-th].

[130] R. Álvarez-García, R. Blumenhagen, M. Brinkmann, and L. Schlechter, "Small Flux Superpotentials for Type IIB Flux Vacua Close to a Conifold," arXiv:2009.03325 [hep-th].

[131] L. Hui, J. P. Ostriker, S. Tremaine, and E. Witten, "Ultralight scalars as cosmological dark matter," *Phys. Rev. D* **95** no. 4, (2017) 043541, arXiv:1610.08297 [astro-ph.CO].

[132] M. Cicoli, J. P. Conlon, and F. Quevedo, "Dark radiation in LARGE volume models," *Phys. Rev. D* **87** no. 4, (2013) 043520, arXiv:1208.3562 [hep-ph].

[133] T. Higaki and F. Takahashi, "Dark Radiation and Dark Matter in Large Volume Compactifications," *JHEP* **11** (2012) 125, arXiv:1208.3563 [hep-ph].

[134] A. Hebecker, P. Mangat, F. Rompineve, and L. T. Witkowski, "Dark Radiation predictions from general Large Volume Scenarios," *JHEP* **09** (2014) 140, arXiv:1403.6810 [hep-ph].

[135] M. Cicoli and F. Muia, "General Analysis of Dark Radiation in Sequestered String Models," *JHEP* **12** (2015) 152, arXiv:1511.05447 [hep-th].

[136] M. Cicoli, J. P. Conlon, M. C. D. Marsh, and M. Rummel, "3.55 keV photon line and its morphology from a 3.55 keV axionlike particle line," *Phys. Rev. D* **90** (2014) 023540, arXiv:1403.2370 [hep-ph].

[137] M. Cicoli, V. A. Diaz, V. Guidetti, and M. Rummel, "The 3.5 keV Line from Stringy Axions," *JHEP* **10** (2017) 192, arXiv:1707.02987 [hep-th].

[138] M. Demirtas, C. Long, L. McAllister, and M. Stillman, "The Kreuzer-Skarke Axiverse," *JHEP* **04** (2020) 138, arXiv:1808.01282 [hep-th].

[139] V. M. Mehta, M. Demirtas, C. Long, D. J. Marsh, L. Mcallister, and M. J. Stott, "Superradiance Exclusions in the Landscape of Type IIB String Theory," arXiv:2011.08693 [hep-th].

[140] V. M. Mehta, M. Demirtas, C. Long, D. J. E. Marsh, L. McAllister, and M. J. Stott, "Superradiance in String Theory," arXiv:2103.06812 [hep-th].

[141] J. Halverson, C. Long, B. Nelson, and G. Salinas, "Towards string theory expectations for photon couplings to axionlike particles," *Phys. Rev. D* **100** no. 10, (2019) 106010, arXiv:1909.05257 [hep-th].

[142] M. Cicoli, C. P. Burgess, and F. Quevedo, "Fibre Inflation: Observable Gravity Waves from IIB String Compactifications," *JCAP* **03** (2009) 013, arXiv:0808.0691 [hep-th].

[143] M. Cicoli, F. Muia, and P. Shukla, "Global Embedding of Fibre Inflation Models," *JHEP* **11** (2016) 182, arXiv:1611.04612 [hep-th].

[144] M. Cicoli, D. Ciupke, V. A. Diaz, V. Guidetti, F. Muia, and P. Shukla, "Chiral Global Embedding of Fibre Inflation Models," *JHEP* **11** (2017) 207, arXiv:1709.01518 [hep-th].

[145] M. Cicoli, D. Ciupke, C. Mayrhofer, and P. Shukla, "A Geometrical Upper Bound on the Inflaton Range," *JHEP* **05** (2018) 001, arXiv:1801.05434 [hep-th].

[146] M. Cicoli and E. Di Valentino, "Fitting string inflation to real cosmological data: The fiber inflation case," *Phys. Rev. D* **102** no. 4, (2020) 043521, arXiv:2004.01210 [astro-ph.CO].

[147] C. P. Burgess, M. Cicoli, S. de Alwis, and F. Quevedo, "Robust Inflation from Fibrous Strings," *JCAP* **05** (2016) 032, arXiv:1603.06789 [hep-th].

[148] M. Cicoli, F. G. Pedro, and G. Tasinato, "Poly-instanton Inflation," *JCAP* **12** (2011) 022, arXiv:1110.6182 [hep-th].

[149] M. Cicoli, M. Kreuzer, and C. Mayrhofer, "Toric K3-Fibred Calabi-Yau Manifolds with del Pezzo Divisors for String Compactifications," *JHEP* **02** (2012) 002, arXiv:1107.0383 [hep-th].

[150] C. Crinò, F. Quevedo, and R. Valandro, "On de Sitter String Vacua from Anti-D3-Branes in the Large Volume Scenario," arXiv:2010.15903 [hep-th].

[151] R. Blumenhagen, S. Moster, and E. Plauschinn, "Moduli Stabilisation versus Chirality for MSSM like Type IIB Orientifolds," *JHEP* **01** (2008) 058, arXiv:0711.3389 [hep-th].

[152] R. Minasian and G. W. Moore, "K theory and Ramond-Ramond charge," *JHEP* **11** (1997) 002, arXiv:hep-th/9710230.

[153] D. S. Freed and E. Witten, "Anomalies in string theory with D-branes," *Asian J. Math.* **3** (1999) 819, arXiv:hep-th/9907189.

[154] H. Jockers and J. Louis, "D-terms and F-terms from D7-brane fluxes," *Nucl. Phys. B* **718** (2005) 203–246, arXiv:hep-th/0502059.

[155] M. Haack, D. Krefl, D. Lust, A. Van Proeyen, and M. Zagermann, "Gaugino Condensates and D-terms from D7-branes," *JHEP* **01** (2007) 078, arXiv:hep-th/0609211.

[156] D. Ciupke, J. Louis, and A. Westphal, "Higher-Derivative Supergravity and Moduli Stabilization," *JHEP* **10** (2015) 094, arXiv:1505.03092 [hep-th].

[157] T. W. Grimm, K. Mayer, and M. Weissenbacher, "Higher derivatives in Type II and M-theory on Calabi-Yau threefolds," *JHEP* **02** (2018) 127, arXiv:1702.08404 [hep-th].

[158] M. Cicoli and G. A. Piovano, "Reheating and Dark Radiation after Fibre Inflation," *JCAP* **02** (2019) 048, arXiv:1809.01159 [hep-th].

[159] H. Baer, V. Barger, S. Salam, and D. Sengupta, "String landscape guide to soft SUSY breaking terms," *Phys. Rev. D* **102** no. 7, (2020) 075012, arXiv:2005.13577 [hep-ph].

[160] H. Baer, V. Barger, S. Salam, and D. Sengupta, "Landscape Higgs boson and sparticle mass predictions from a logarithmic soft term distribution," *Phys. Rev. D* **103** no. 3, (2021) 035031, arXiv:2011.04035 [hep-ph].

[161] H. Baer, V. Barger, S. Salam, and H. Serce, "Sparticle and Higgs boson masses from the landscape: dynamical versus spontaneous supersymmetry breaking," arXiv:2103.12123 [hep-ph].

[162] H. Baer, V. Barger, D. Sengupta, and R. W. Deal, "Distribution of supersymmetry μ parameter and Peccei-Quinn scale f_a from the landscape," arXiv:2104.03803 [hep-ph].

[163] H. Baer, V. Barger, and H. Serce, "Anomalous muon magnetic moment, supersymmetry, naturalness, LHC search limits and the landscape," arXiv:2104.07597 [hep-ph].

[164] I. Antoniadis, Y. Chen, and G. K. Leontaris, "Perturbative moduli stabilisation in type iib/f-theory framework," *The European Physical Journal C* **78** no. 9, (Sep, 2018) . http://dx.doi.org/10.1140/epjc/s10052-018-6248-4.

[165] M. Cicoli and F. Quevedo, "String moduli inflation: an overview," *Classical and Quantum Gravity* **28** no. 20, (Oct, 2011) 204001. http://dx.doi.org/10.1088/0264-9381/28/20/204001.

[166] D. Baumann and L. McAllister, "Inflation and string theory," 2014.

[167] L. Susskind, "The Anthropic landscape of string theory," arXiv:hep-th/0302219.

[168] A. Giryavets, S. Kachru, P. K. Tripathy, and S. P. Trivedi, "Flux compactifications on Calabi-Yau threefolds," *JHEP* **04** (2004) 003, arXiv:hep-th/0312104.

[169] M. Demirtas, M. Kim, L. McAllister, J. Moritz, and A. Rios-Tascon, "A cosmological constant that is too small," 2021.

[170] M. Demirtas, M. Kim, L. McAllister, J. Moritz, and A. Rios-Tascon, "Small cosmological constants in string theory," 2021.

[171] R. Álvarez-García, R. Blumenhagen, M. Brinkmann, and L. Schlechter, "Small flux superpotentials for type iib flux vacua close to a conifold," *Fortschritte der Physik* **68** no. 11-12, (Oct, 2020) 2000088. http://dx.doi.org/10.1002/prop.202000088.

[172] Y. Honma and H. Otsuka, "Small flux superpotential in f-theory compactifications," *Physical Review D* **103** no. 12, (Jun, 2021) . http://dx.doi.org/10.1103/PhysRevD.103.126022.

[173] M. Cicoli, I. G. Etxebarria, F. Quevedo, A. Schachner, P. Shukla, and R. Valandro, "The standard model quiver in de sitter string compactifications," 2021.

[174] M. R. Douglas, "The statistics of string/m theory vacua," *Journal of High Energy Physics* **2003** no. 05, (May, 2003) 046–046. http://dx.doi.org/10.1088/1126-6708/2003/05/046.

[175] K. R. Dienes, "Statistics on the heterotic landscape: Gauge groups and cosmological constants of four-dimensional heterotic strings," *Physical Review D* **73** no. 10, (May, 2006) . http://dx.doi.org/10.1103/PhysRevD.73.106010.

[176] F. Gmeiner, R. Blumenhagen, G. Honecker, D. Lüst, and T. Weigand, "One in a billion: Mssm-like d-brane statistics," *Journal of High Energy Physics* **2006** no. 01, (Jan, 2006) 004–004. http://dx.doi.org/10.1088/1126-6708/2006/01/004.

[177] M. R. Douglas and W. Taylor, "The landscape of intersecting brane models," *Journal of High Energy Physics* **2007** no. 01, (Jan, 2007) 031–031. http://dx.doi.org/10.1088/1126-6708/2007/01/031.

[178] O. DeWolfe, "Enhanced symmetries in multiparameter flux vacua," *Journal of High Energy Physics* **2005** no. 10, (Oct, 2005) 066–066. http://dx.doi.org/10.1088/1126-6708/2005/10/066.

[179] D. Martínez-Pedrera, D. Mehta, M. Rummel, and A. Westphal, "Finding all flux vacua in an explicit example," *Journal of High Energy Physics* **2013** no. 6, (Jun, 2013) . http://dx.doi.org/10.1007/JHEP06(2013)110.

[180] J. Halverson and F. Ruehle, "Computational complexity of vacua and near-vacua in field and string theory," *Physical Review D* **99** no. 4, (Feb, 2019) . http://dx.doi.org/10.1103/PhysRevD.99.046015.

[181] I. Bena, J. Blaback, M. Grana, and S. Lüst, "Algorithmically solving the tadpole problem," 2021.

[182] S. Krippendorf, R. Kroepsch, and M. Syvaeri, "Revealing systematics in phenomenologically viable flux vacua with reinforcement learning," 2021.

[183] N. Arkani-Hamed, S. Dimopoulos, and S. Kachru, "Predictive landscapes and new physics at a TeV," arXiv:hep-th/0501082.

[184] R. Kallosh and A. Linde, "Landscape, the scale of susy breaking, and inflation," *Journal of High Energy Physics* **2004** no. 12, (Dec, 2004) 004–004. http://dx.doi.org/10.1088/1126-6708/2004/12/004.

[185] S. Hosono, A. Klemm, and S. Theisen, "Lectures on mirror symmetry," *Lecture Notes in Physics* 235–280. http://dx.doi.org/10.1007/3-540-58453-6_13.

[186] A. Klemm, "Topological string theory on Calabi-Yau threefolds," *PoS* **RTN2005** (2005) 002.

[187] G. Curio, A. Klemm, D. Lüst, and S. Theisen, "On the vacuum structure of type ii string compactifications on calabi–yau spaces with h-fluxes," *Nuclear Physics B* **609** no. 1-2, (Aug, 2001) 3–45. http://dx.doi.org/10.1016/S0550-3213(01)00285-1.

[188] K. Dasgupta, G. Rajesh, and S. Sethi, "M-theory, orientifolds and g-flux," *Journal of High Energy Physics* **1999** no. 08, (Aug, 1999) 023–023. http://dx.doi.org/10.1088/1126-6708/1999/08/023.

[189] T. D. Dimofte, "Type iib flux vacua at large complex structure," *Journal of High Energy Physics* **2008** no. 09, (Sep, 2008) 064–064. http://dx.doi.org/10.1088/1126-6708/2008/09/064.

[190] M. C. D. Marsh and K. Sousa, "Universal properties of type iib and f-theory flux compactifications at large complex structure," *Journal of High Energy Physics* **2016** no. 3, (Mar, 2016) . http://dx.doi.org/10.1007/JHEP03(2016)064.

[191] Y. Honma and H. Otsuka, "On the flux vacua in f-theory compactifications," *Physics Letters B* **774** (Nov, 2017) 225–228. http://dx.doi.org/10.1016/j.physletb.2017.09.062.

[192] T. W. Grimm, C. Li, and I. Valenzuela, "Asymptotic flux compactifications and the swampland," *Journal of High Energy Physics* **2020** no. 6, (Jun, 2020) . http://dx.doi.org/10.1007/JHEP06(2020)009.

[193] J. J. Blanco-Pillado, K. Sousa, M. A. Urkiola, and J. M. Wachter, "Universal class of type-iib flux vacua with analytic mass spectrum," *Physical Review D* **103** no. 10, (May, 2021) . http://dx.doi.org/10.1103/PhysRevD.103.106006.

[194] F. Marchesano, D. Prieto, and M. Wiesner, "F-theory flux vacua at large complex structure," 2021.

[195] A. Hebecker, P. Henkenjohann, and L. T. Witkowski, "Flat monodromies and a moduli space size conjecture," *Journal of High Energy Physics* **2017** no. 12, (Dec, 2017) . http://dx.doi.org/10.1007/JHEP12(2017)033.

[196] R. Gopakumar and C. Vafa, "M theory and topological strings. 1.," arXiv:hep-th/9809187.

[197] R. Gopakumar and C. Vafa, "M theory and topological strings. 2.," arXiv:hep-th/9812127.

[198] P. Candelas, A. Font, s. Katz, and D. R. Morrison, "Mirror symmetry for two-parameter models — ii," *Nuclear Physics B* **429** no. 3, (Nov, 1994) 626–674. http://dx.doi.org/10.1016/0550-3213(94)90155-4.

[199] P. Candelas, X. de la Ossa, A. Font, S. Katz, and D. R. Morrison, "Mirror symmetry for two-parameter models (i)," *Nuclear Physics B* **416** no. 2, (Mar, 1994) 481–538. http://dx.doi.org/10.1016/0550-3213(94)90322-0.

[200] S. Kachru, M. Schulz, and S. P. Trivedi, "Moduli stabilization from fluxes in a simple iib orientifold," *Journal of High Energy Physics* **2003** no. 10, (Oct, 2003) 007–007. http://dx.doi.org/10.1088/1126-6708/2003/10/007.

[201] M. Kreuzer and H. Skarke, "Complete classification of reflexive polyhedra in four-dimensions," *Adv. Theor. Math. Phys.* **4** (2002) 1209–1230, arXiv:hep-th/0002240.

[202] M. Cicoli, F. Quevedo, R. Savelli, A. Schachner, and R. Valandro, "Systematics of the α' expansion in f-theory," 2021.

[203] G. Bertone, D. Hooper, and J. Silk, "Particle dark matter: evidence, candidates and constraints," *Physics Reports* **405** no. 5-6, (Jan, 2005) 279–390. http://dx.doi.org/10.1016/j.physrep.2004.08.031.

[204] M. Ackermann, A. Albert, B. Anderson, W. Atwood, L. Baldini, G. Barbiellini, D. Bastieri, K. Bechtol, R. Bellazzini, E. Bissaldi, and et al., "Searching for dark matter annihilation from milky way dwarf spheroidal galaxies with six years of fermi large area telescope data," *Physical Review Letters* **115** no. 23, (Nov, 2015) . http://dx.doi.org/10.1103/PhysRevLett.115.231301.

[205] A. Albert, B. Anderson, K. Bechtol, A. Drlica-Wagner, M. Meyer, M. Sánchez-Conde, L. Strigari, M. Wood, T. M. C. Abbott, F. B. Abdalla, and et al., "Searching for dark matter annihilation in recently discovered milky way satellites withfermi-lat," *The Astrophysical Journal* **834** no. 2, (Jan, 2017) 110. http://dx.doi.org/10.3847/1538-4357/834/2/110.

[206] R. K. Leane, T. R. Slatyer, J. F. Beacom, and K. C. Ng, "Gev-scale thermal wimps: Not even slightly ruled out," *Physical Review D* **98** no. 2, (Jul, 2018) . http://dx.doi.org/10.1103/PhysRevD.98.023016.

[207] M. Kamionkowski and M. S. Turner, "Thermal relics: Do we know their abundances?," *Phys. Rev. D* **42** (Nov, 1990) 3310–3320. https://link.aps.org/doi/10.1103/PhysRevD.42.3310.

[208] R. Allahverdi, M. A. Amin, A. Berlin, N. Bernal, C. T. Byrnes, M. S. Delos, A. L. Erickcek, M. Escudero, D. G. Figueroa, K. Freese, and et al., "The first three seconds: a review of possible expansion histories of the early universe," *The Open Journal of Astrophysics* **4** no. 1, (Jan, 2021) . http://dx.doi.org/10.21105/astro.2006.16182.

[209] G. Kane, K. Sinha, and S. Watson, "Cosmological moduli and the post-inflationary universe: A critical review," *International Journal of Modern Physics D* **24** no. 08, (Jul, 2015) 1530022. http://dx.doi.org/10.1142/S0218271815300220.

[210] B. S. Acharya, K. Bobkov, G. Kane, J. Shao, S. Watson, and P. Kumar, "Non-thermal dark matter and the moduli problem in string frameworks," *Journal of High Energy Physics* **2008** no. 06, (Jun, 2008) 064–064. http://dx.doi.org/10.1088/1126-6708/2008/06/064.

[211] M. Cicoli, K. Dutta, A. Maharana, and F. Quevedo, "Moduli vacuum misalignment and precise predictions in string inflation," *Journal of Cosmology and Astroparticle Physics* **2016** no. 08, (Aug, 2016) 006–006. http://dx.doi.org/10.1088/1475-7516/2016/08/006.

[212] H. Baer, K.-Y. Choi, J. E. Kim, and L. Roszkowski, "Dark matter production in the early universe: Beyond the thermal wimp paradigm," *Physics Reports* **555** (Feb, 2015) 1–60. http://dx.doi.org/10.1016/j.physrep.2014.10.002.

[213] G. Gelmini and P. Gondolo, "Neutralino with the right cold dark matter abundance in (almost) any supersymmetric model," *Physical Review D* **74** no. 2, (Jul, 2006) . http://dx.doi.org/10.1103/PhysRevD.74.023510.

[214] R. Allahverdi, B. Dutta, and K. Sinha, "Cladogenesis: Baryon-dark matter coincidence from branchings in moduli decay," *Physical Review D* **83** no. 8, (Apr, 2011) . http://dx.doi.org/10.1103/PhysRevD.83.083502.

[215] R. Allahverdi, M. Cicoli, B. Dutta, and K. Sinha, "Nonthermal dark matter in string compactifications," *Physical Review D* **88** no. 9, (Nov, 2013) . http://dx.doi.org/10.1103/PhysRevD.88.095015.

[216] R. Blumenhagen, J. Conlon, S. Krippendorf, S. Moster, and F. Quevedo, "Susy breaking in local string/f-theory models," *Journal of High Energy Physics* **2009** no. 09, (Sep, 2009) 007–007. http://dx.doi.org/10.1088/1126-6708/2009/09/007.

[217] K. Griest and M. Kamionkowski, "Unitarity limits on the mass and radius of dark-matter particles," *Phys. Rev. Lett.* **64** (Feb, 1990) 615–618. https://link.aps.org/doi/10.1103/PhysRevLett.64.615.

[218] L. Heurtier, Y. Mambrini, and M. Pierre, "Dark matter interpretation of the anita anomalous events," *Physical Review D* **99** no. 9, (May, 2019) . http://dx.doi.org/10.1103/PhysRevD.99.095014.

[219] M. Kawasaki, T. Moroi, and T. Yanagida, "Constraint on the reheating temperature from the decay of the polonyi field," *Physics Letters B* **370** no. 1-2, (Mar, 1996) 52–58. http://dx.doi.org/10.1016/0370-2693(95)01546-9.

[220] G. F. Giudice, E. W. Kolb, and A. Riotto, "Largest temperature of the radiation era and its cosmological implications," *Physical Review D* **64** no. 2, (Jun, 2001) . http://dx.doi.org/10.1103/PhysRevD.64.023508.

[221] A. L. Erickcek, "The dark matter annihilation boost from low-temperature reheating," *Physical Review D* **92** no. 10, (Nov, 2015) . http://dx.doi.org/10.1103/PhysRevD.92.103505.

[222] T. Moroi and L. Randall, "Wino cold dark matter from anomaly mediated susy breaking," *Nuclear Physics B* **570** no. 1-2, (Mar, 2000) 455–472. http://dx.doi.org/10.1016/S0550-3213(99)00748-8.

[223] B. S. Acharya, G. Kane, S. Watson, and P. Kumar, "A Non-thermal WIMP Miracle," *Phys. Rev. D* **80** (2009) 083529, arXiv:0908.2430 [astro-ph.CO].

[224] B. Dutta, L. Leblond, and K. Sinha, "Mirage in the Sky: Non-thermal Dark Matter, Gravitino Problem, and Cosmic Ray Anomalies," *Phys. Rev. D* **80** (2009) 035014, arXiv:0904.3773 [hep-ph].

[225] T. Higaki and F. Takahashi, "Dark radiation and dark matter in large volume compactifications," *Journal of High Energy Physics* **2012** no. 11, (Nov, 2012) . http://dx.doi.org/10.1007/JHEP11(2012)125.

[226] A. R. Liddle and S. M. Leach, "How long before the end of inflation were observable perturbations produced?," *Physical Review D* **68** no. 10, (Nov, 2003) . http://dx.doi.org/10.1103/PhysRevD.68.103503.

[227] T. Rehagen and G. B. Gelmini, "Low reheating temperatures in monomial and binomial inflationary potentials," 2015.

[228] D. Roest, "Universality classes of inflation," *Journal of Cosmology and Astroparticle Physics* **2014** no. 01, (Jan, 2014) 007–007. http://dx.doi.org/10.1088/1475-7516/2014/01/007.

[229] Y. Akrami, F. Arroja, M. Ashdown, J. Aumont, C. Baccigalupi, M. Ballardini, A. J. Banday, R. B. Barreiro, N. Bartolo, and et al., "Planck2018 results," *Astronomy & Astrophysics* **641** (Sep, 2020) A10. http://dx.doi.org/10.1051/0004-6361/201833887.

[230] R. Allahverdi, K. Dutta, and A. Maharana, "Constraining non-thermal dark matter by cmb," *Journal of Cosmology and Astroparticle Physics* **2018** no. 10, (Oct, 2018) 038–038. http://dx.doi.org/10.1088/1475-7516/2018/10/038.

[231] J. P. Conlon and F. Quevedo, "Kähler moduli inflation," *Journal of High Energy Physics* **2006** no. 01, (Jan, 2006) 146–146. http://dx.doi.org/10.1088/1126-6708/2006/01/146.

[232] K. Becker, M. Becker, M. Haack, and J. Louis, "Supersymmetry breaking and alpha'-corrections to flux induced potentials," *Journal of High Energy Physics* **2002** no. 06, (Jun, 2002) 060–060. http://dx.doi.org/10.1088/1126-6708/2002/06/060.

[233] R. Blumenhagen, M. Cvetič, S. Kachru, and T. Weigand, "d-brane instantons in type ii orientifolds," *Annual Review of Nuclear and Particle Science* **59** no. 1, (Nov, 2009) 269–296. http://dx.doi.org/10.1146/annurev.nucl.010909.083113.

[234] V. Balasubramanian, P. Berglund, J. P. Conlon, and F. Quevedo, "Systematics of moduli stabilisation in calabi-yau flux compactifications," *Journal of High Energy Physics* **2005** no. 03, (Mar, 2005) 007–007. http://dx.doi.org/10.1088/1126-6708/2005/03/007.

[235] S. Kachru, R. Kallosh, A. Linde, and S. P. Trivedi, "de sitter vacua in string theory," *Physical Review D* **68** no. 4, (Aug, 2003) . http://dx.doi.org/10.1103/PhysRevD.68.046005.

[236] M. Cicoli and A. Mazumdar, "Reheating for Closed String Inflation," *JCAP* **09** (2010) 025, arXiv:1005.5076 [hep-th].

[237] M. Cicoli and A. Mazumdar, "Inflation in string theory: A graceful exit to the real world," *Physical Review D* **83** no. 6, (Mar, 2011) . http://dx.doi.org/10.1103/PhysRevD.83.063527.

[238] C. P. Burgess, M. Cicoli, M. Gómez-Reino, F. Quevedo, G. Tasinato, and I. Zavala, "Non-standard primordial fluctuations and nongaussianity in string inflation," *Journal of High Energy Physics* **2010** no. 8, (Aug, 2010) . http://dx.doi.org/10.1007/JHEP08(2010)045.

[239] S. P. Martin and J. D. Wells, "Chiral symmetry breaking and effective lagrangians for softly broken supersymmetric qcd," *Physical Review D* **58** no. 11, (Nov, 1998) . http://dx.doi.org/10.1103/PhysRevD.58.115013.

[240] M. Cicoli, M. Goodsell, J. Jaeckel, and A. Ringwald, "Testing string vacua in the lab: from a hidden cmb to dark forces in flux compactifications," *Journal of High Energy Physics* **2011** no. 7, (Jul, 2011) . http://dx.doi.org/10.1007/JHEP07(2011)114.

[241] N. Aghanim, Y. Akrami, M. Ashdown, J. Aumont, C. Baccigalupi, M. Ballardini, A. J. Banday, R. B. Barreiro, N. Bartolo, and et al., "Planck 2018 results," *Astronomy & Astrophysics* **641** (Sep, 2020) A6. http://dx.doi.org/10.1051/0004-6361/201833910.

[242] N. Arkani-Hamed, S. Dimopoulos, G. Giudice, and A. Romanino, "Aspects of split supersymmetry," *Nuclear Physics B* **709** no. 1-2, (Mar, 2005) 3–46. http://dx.doi.org/10.1016/j.nuclphysb.2004.12.026.

[243] K. Harigaya and K. Mukaida, "Thermalization after/during reheating," *Journal of High Energy Physics* **2014** no. 5, (May, 2014) . http://dx.doi.org/10.1007/JHEP05(2014)006.

[244] K. Mukaida and M. Yamada, "Thermalization process after inflation and effective potential of scalar field," *Journal of Cosmology and Astroparticle Physics* **2016** no. 02, (Feb, 2016) 003–003. http://dx.doi.org/10.1088/1475-7516/2016/02/003.

[245] R. Allahverdi and M. Drees, "Thermalization after inflation and production of massive stable particles," *Physical Review D* **66** no. 6, (Sep, 2002) . http://dx.doi.org/10.1103/PhysRevD.66.063513.

[246] K. Harigaya, M. Kawasaki, K. Mukaida, and M. Yamada, "Dark matter production in late time reheating," *Physical Review D* **89** no. 8, (Apr, 2014) . http://dx.doi.org/10.1103/PhysRevD.89.083532.

[247] M. A. Garcia and M. A. Amin, "Prethermalization production of dark matter," *Physical Review D* **98** no. 10, (Nov, 2018) . http://dx.doi.org/10.1103/PhysRevD.98.103504.

[248] K. Harigaya, K. Mukaida, and M. Yamada, "Dark matter production during the thermalization era," *Journal of High Energy Physics* **2019** no. 7, (Jul, 2019) . http://dx.doi.org/10.1007/JHEP07(2019)059.

[249] M. Cicoli, K. Dutta, and A. Maharana, "N-flation with hierarchically light axions in string compactifications," *Journal of Cosmology and Astroparticle Physics* **2014** no. 08, (Aug, 2014) 012–012. http://dx.doi.org/10.1088/1475-7516/2014/08/012.

[250] R. Allahverdi and J. K. Osiński, "Nonthermal dark matter from modified early matter domination," *Physical Review D* **99** no. 8, (Apr, 2019) . http://dx.doi.org/10.1103/PhysRevD.99.083517.